Dispersion approach to real and virtual Compton scattering

Dissertation

zur Erlangung des Grades ”Doktor der Naturwissenschaften”
am Fachbereich Physik der Johannes Gutenberg-Universität
in Mainz

Mikhail Gorchtein
geboren in Pskov

Institut für Kernphysik
Johannes Gutenberg-Universität Mainz

Mainz 2002

FOREWORD

It is probably due to the nature of human mind that already in antique the thinkers tried to deduce the world from a simple system of basic elements and principles. One of the first such systems, widely accepted in the ancient world, used earth, water, air and fire as such basic elements. Plants can be understood as consisting of these ingredients because they grow on earth, need water, air and the warmth of the sun; as well, the animals can, since they eat plants (or other animals) to survive. Though this system operated with the elements which are well known in the everyday life, earth and water are different in different places on the Earth and may change with the time, and these elements cannot be understood as objects but as symbols of four different ideal substances, i.e., this system was metaphysical rather than physical. However, these four basic elements correspond to the four aggregate states of matter, solid, fluid, gaseous and plasma.

Much less recognized at those times was the atomic hypothesis of Demokritas who supposed that everything in the world consists of unchangeable and indivisible (= "atomos") particles. All the diversity of the properties of objects comes about only due to a specific constellation of these atoms in each case. Actually, this picture shifts the classification problem from the term "elements" to the term "constellations" or, in modern language, interactions, since it is a wild variety of interactions of the atoms that causes the dazzling array of findings, as by Demokritas. However, at that time, there was no evidence for the very existence of these mysterious atoms, which also excluded that their properties and interactions could be determined. Though this theory was forgotten for a long time, it served later as the first building block of modern science. [1]

It was not before the early 19th century that the term "atom" was firmly accepted by nature scientists. Though the atomic theory proved to be fruitful in numerous applications, at that time, the properties of the atoms could not be accessed experimentally. The atoms were therefore understood as Newton's matter points interacting by means of mechanical forces.

The necessary tool to investigate the structure of matter was found in the end of the 19th century with the discovery of radioactivity. The birth of nuclear physics 1910 was due to Rutherford's famous experiment, where α-particles were scattered on a thin gold foil. The observation showed the presence of strong scattering centers within atoms, and these centers were called nuclei. In further experiments, Rutherford found that the nucleus of the lightest hydrogen atom has a fundamental meaning as being contained within the heavier nuclei. This particle was called proton (greek "protos"= the first) and was believed to be the finally found elementary (i.e., structureless) building block of matter.

1933, the experiment of W. Frisch and O. Stern showed an anomalously large value of the magnetic moment of the proton, as compared to that predicted by the Dirac equation for a pointlike particle. This indicated that the proton is not pointlike but has an internal structure. Since then, the structure of the nucleon (the proton and the neutron, discovered in 1930) has a central role in the quest to understand the structure of mat-

[1] strictly speaking, the modern term "atom" carries a different meaning than that of Demokritas: nowaday, one calls atoms the smallest particles which have the properties of a corresponding chemical element, whereas the atoms of Demokritas are closer to the term "elementary particle"

ter.

In 1964, Gell-Mann published his quark model which represented the nucleon as an entity consisting of three quarks, spin-1/2 particles with fractional charge, and held together by the strong force. This allowed to bring systematics in vast amount of nucleon and meson resonances which bewildered physicists in the 60's. Five years later, the existence of the hypothetical quarks was revealed experimentally by means of the deep inelastic electron scattering off a proton target at SLAC. The pointlike quarks are behaving as free particles at very short distances (asymptotic freedom) but the interaction between them increases with the distance. As a consequence, it is not possible to separate the quarks to large distances such that they would stay confined within a hadron. The remaining challenge of hadronic physics is to understand how the complicated bound state of quarks and gluons (which mediate the interaction between two quarks) arises from the underlying field theory, quantum chromodynamics (QCD). For this investigation, one can use the electromagnetic interaction as a probe.

From classical electrodynamics, one knows that in a system of electric charges put into a weak constant electric field, the charges get displaced from their positions such that the electric field inside the system is weakened. The measure of the response of a system to this external field, the so called polarizability of a system, characterizes and quantitatively describes the forces which hold the charges together. In the early 1960's, the idea of polarizabilities was applied to the scattering of very low-energy photons off the nucleon (low energy Compton scattering) and the polarizabilities α *(electric) and* β *(magnetic) were introduced. The application of dispersion relation methods to low energy Compton scattering led to a relation between the polarizabilities and the excitation spectrum of the nucleon (Baldin sum rule). Thus, together with the nucleon mass, charge and magnetic moment, the polarizabilities are fundamental characteristics of the nucleon and its internal structure. To improve our understanding of the strong interactions at low energy, where QCD cannot yet be solved, precision experiments to measure quantities like nucleon polarizabilities are extremely helpful.*

Contents

Chapter 1

Overview

In recent years, new precision experiments have become possible with the high luminosity accelerator facilities at MAMI and JLab, supplying physicists with precise data sets for different hadronic reactions in the intermediate energy region, such as pion photo- and electroproduction, real and virtual Compton scattering *etc.* The present work is dedicated to developing a tool to extract the nucleon polarizabilities from these precise Compton data, making use of the detailed knowledge of pion photoproduction by means of dispersion relations (DR). In order to minimize the model dependence of such extraction, we confront our *subtracted* DR formalism with the already existing unsubtracted one [L'vo 81, L'vo 97]. Furthermore, we develop a DR formalism for virtual Compton scattering (radiative electron scattering off the nucleon) in which the concept of the polarizabilities obtains its natural generalization to the case of a virtual initial photon. For the first time, we obtain DR predictions for four of the six generalized polarizabilities and provide the experimentalists with the tool to extract the other two from the experiment with minimum model dependence.

The outline of this work is as follows. In Chapter 2, a historical survey to dispersion relations will be given, starting from classical electrodynamics and extending the consideration further to low energy Compton scattering. Finally, these ideas will be applied to an arbitrary hadronic reaction, and analytical properties of its invariant amplitudes will be determined by means of the Mandelstam plot and double integral representation. Illustration of this formalism for the example of $\pi\pi$-scattering will complete this Chapter.

Chapter 3 is dedicated to the dispersion relations for real Compton scattering (RCS). Due to the presence of the poles in the t-channel, it will be shown that two of the six invariant amplitudes describing Compton scattering, have to be subtracted. In order to calculate the subtraction functions, we suggest to use the t-channel DR which take account of the $\gamma\gamma \to \pi\pi \to N\bar{N}$ process. Applying subtraction also to the t-channel DRs, we finally obtain the formalism which involves only two free parameters, the backward polarizabilities $\alpha - \beta$ and γ_π. We further compare the predictions for the RCS observables within the presented formalism with the existing data and investigate the sensitivity to changes of the values for the polarizabilities, and study the model dependence of the presented formalism by confronting its predictions with

those of the unsubtracted DRs of [L'vo 97].

Chapter 4 generalizes the DR approach to the case of VCS. After a short introduction and definition of kinematics, the low energy theorem for VCS and the generalized polarizabilities (GPs) of the nucleon of Refs. [Gui 95], [Dre 97] will be considered. To extend the DR formalism for VCS, we will choose the appropriate invariant tensor basis, consider the properties of the invariant amplitudes and elaborate the DRs in this basis. It will be shown that also for VCS, two of the polarizabilities cannot be described by the dispersion integrals in the *s*-channel alone. Within the unsubtracted DR formalism, we show that the four spin-dependent GPs can be calculated directly and compare our DR predictions with the results obtained within different models.

The values of the two scalar GPs, $\alpha(Q^2)$ and $\beta(Q^2)$, cannot be calculated in our formalism and are used as free parameters. These values should then be obtained from a fit to the VCS data. Alternatively, we suggest a dipole parametrization of their Q^2-dependence, which involves two mass scales Λ_α and Λ_β. Using this parametrization, we will present our DR predictions for the VCS observables in the kinematics of the recent VCS experiments, and investigate the sensitivity of the cross sections to the parameters Λ_α and Λ_β. Before concluding this Chapter, we also study the double polarization observables for VCS.

Chapter 2

Introduction to dispersion relations

2.1 Classical theory of dispersion

In classical electrodynamics, the spreading of light in matter is described by the set of Maxwell equations. If the electromagnetic field is affected by the presence of some material with the dielectric constant ε and, e.g., the magnetic susceptibility $\mu = 0$, the differential equation for the fields $\vec{E}(\vec{x},t)$, $\vec{D}(\vec{x},t)$ with given boundary conditions can be stated. The whole information on the problem can be expressed in terms of the Green function
[Jac 83]:

$$\vec{D}(\vec{x},t) \;=\; \vec{E}(\vec{x},t) + \int_{-\infty}^{\infty} \vec{E}(\vec{x},t-\tau)G(\tau)d\tau \tag{2.1}$$

The field $\vec{D}(\vec{x},t)$ is introduced such that its Fourier transform
$\vec{D}(\vec{x},\omega) = \frac{1}{2\pi}\int e^{i\omega t}\vec{D}(\vec{x},t)dt$ is, by definition, a smooth function in the whole space,

$$\vec{D}(\vec{x},\omega) \;=\; \varepsilon(\omega)\vec{E}(\vec{x},\omega)\;. \tag{2.2}$$

The dependence of the dielectric constant on the frequency is called dispersion. The solution of the two equations gives us the following relation between the Green function and the dielectric constant:

$$\varepsilon(\omega) \;=\; 1 + \int_{-\infty}^{\infty} d\tau e^{i\omega\tau}G(\tau) \tag{2.3}$$

The crucial role in the problem is played by *Causality*, i.e. the fact that the signal in matter can only be transferred with velocity $v \leq c$ with c the velocity of light in the vacuum. This implies that $G(\tau) = 0$ for $\tau < 0$. We assume that the Green function possesses the necessary asymptotic behaviour that the integral in Eq. (2.3) converges. This integral representation of the dielectricity constant means that it is an analytic function of ω in the upper half of the *complex* ω-plane (though only real positive values of frequency make physical sense).

For an analytic function, Cauchy's theorem can be applied. We construct the contour to run from $-R$ to R along the real axis of ω and close it with the semi-circle of radius R in the upper half plane,

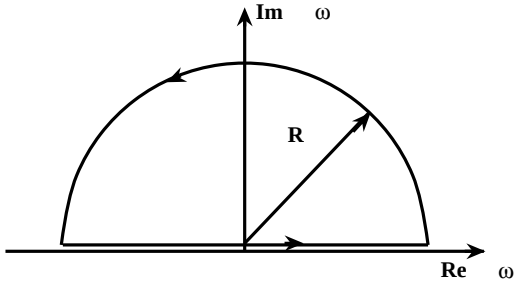

Figure 2.1: Cauchy contour for dielectric constant

$$\varepsilon(\omega) - 1 \;=\; \frac{1}{2\pi i}\oint \frac{\varepsilon(\omega')-1}{\omega'-\omega-i\varepsilon}d\omega' \,. \tag{2.4}$$

If $R \to \infty$, the complex exponential in Eq.(2.3) leads to vanishing of the integral over the semi-circle, and the same representation of $\varepsilon(\omega)$ relates the integral over the negative values of ω to the physical range:

$$\varepsilon(-\omega) \;=\; \varepsilon^*(\omega^*) \,. \tag{2.5}$$

Noting also that $\frac{1}{\omega'-\omega-i\varepsilon} = \mathcal{P}\frac{1}{\omega'-\omega} + i\pi\delta(\omega'-\omega)$, one obtains two relations between the real and imaginary parts of ε:

$$\begin{aligned} \mathrm{Re}\,[\varepsilon(\omega)] &= 1 + \frac{2}{\pi}\mathcal{P}\int_0^\infty d\omega' \frac{\omega'\,\mathrm{Im}\,[\varepsilon(\omega')]}{\omega'^2-\omega^2} \\ \mathrm{Im}\,[\varepsilon(\omega)] &= -\frac{2\omega}{\pi}\mathcal{P}\int_0^\infty d\omega' \frac{\mathrm{Re}\,[\varepsilon(\omega')]-1}{\omega'^2-\omega^2} \end{aligned} \tag{2.6}$$

The imaginary part $\mathrm{Im}\,\varepsilon(\omega)$ corresponds to the absorption of light since

$$\begin{aligned} \frac{k'}{k} &= \sqrt{\varepsilon\mu} \\ \vec{D}(\vec{x},t) &= \vec{D}_0 e^{i(\vec{k}'\vec{x}-\omega t)} \;=\; \vec{D}_0 e^{i(\mathrm{Re}\,k'x-\omega t)}\cdot e^{-\mathrm{Im}\,k'x} \,, \end{aligned} \tag{2.7}$$

and the real part is responsible for the scattering. In optics, instead of the dielectricity constant one normally uses the index of refraction $n(\omega) = \sqrt{\varepsilon\mu}$. The dispersion relation (DR) between the real and imaginary parts of $n(\omega)$ was independently obtained by Kramers [Kra 27] and Kronig [Kro 26]. The dispersion relation had to be subtracted at $\omega = 0$ to take out the contribution of a free particle:

$$\mathrm{Re}\,n(\omega) - n(0) \;=\; \frac{2\omega^2}{\pi}\mathcal{P}\int_0^\infty d\omega' \frac{\mathrm{Im}n(\omega')}{\omega'(\omega'^2-\omega^2)} \tag{2.8}$$

If the absorption spectrum for the studied material can be measured experimentally, the scattering properties of the material are then unambiguously determined by

the subtracted dispersion relation of Kramers and Kronig. It should be stressed that no assumptions about the material and its dielectric constant were made for this derivation. The fact that the real and imaginary parts of the index of refraction are not independent follows directly from causality stated in terms of the Green function.
The coherent forward scattering amplitude is defined by

$$n(\omega) \;=\; 1 + \frac{2\pi c^2}{\omega^2} N\, f(\omega)\,, \tag{2.9}$$

which describes scattering on a system of scattering centers whose density in the material is denoted by N. Classical electrodynamics also gives a model independent limit for the scattering of electromagnetic waves of very low energy on a free particle of charge e and mass m. This is the Thomson limit:

$$f^{Thomson}(\omega = 0) \;=\; -\frac{\alpha_{em}}{m}(\varepsilon'^{*} \cdot \varepsilon)\,, \tag{2.10}$$

where $\alpha_{em} = e^2/(4\pi\varepsilon_0\hbar c) \approx 1/137$ is the fine structure constant and ε and ε' are the polarization vectors of the incoming and outgoing waves, respectively. The corresponding cross section is given for Thomson scattering just by the squared amplitude,

$$\frac{d\sigma}{d\Omega_{Lab}} \;=\; r_0^2\,|\varepsilon'^{*} \cdot \varepsilon|^2\,, \tag{2.11}$$

where $r_0 = \alpha_{em}\frac{\hbar}{mc} = 2.82 \times 10^{-13} cm$ is the classical electron radius. For an unpolarized cross section, one obtains the so-called Thomson formula,

$$\frac{d\sigma}{d\Omega_{Lab}} \;=\; r_0^2\,\frac{1}{2}(1 + \cos^2\Theta)\,, \tag{2.12}$$

describing the intensity of light, scattered by the free particle at the angle Θ. The integration of this formula gives the total cross section

$$\sigma_T \;=\; \frac{8\pi}{3} r_0^2\,. \tag{2.13}$$

This formula holds, however, only for very small frequencies, i.e.

$$\hbar\omega \ll mc^2 \qquad \text{or} \qquad \lambda \gg \lambda_{Compton}\,, \tag{2.14}$$

with $\lambda_{Compton} = \frac{2\pi r_0}{\alpha_{em}}$ the Compton wavelength.

It was observed experimentally by Compton that the frequency of the scattered light ω' is angular dependent. This dependence is given by the well known Compton formula,

$$\omega' \;=\; \frac{\omega}{1 + \frac{\hbar\omega}{mc^2}(1 - \cos\Theta)}\,, \tag{2.15}$$

which follows from the two body kinematics in the lab frame. To correct the cross section, the recoil factor $\frac{\omega'}{\omega}$ should be introduced:

$$\frac{d\sigma}{d\Omega_{Lab}} \;=\; \left(\frac{\omega'}{\omega}\right)^2 r_0^2\,|\varepsilon'^{*} \cdot \varepsilon|^2\,. \tag{2.16}$$

This result describes the scattering of light off the spinless particle with charge e and mass m.

The electron, being a fermion, is described by the relativistic Dirac equation, which leads to further corrections absorbed in the Klein-Nishina formula [Kle 29],

$$\left(\frac{d\sigma}{d\Omega_{Lab}}\right)^{KN} = \frac{1}{2} r_0^2 \left(\frac{\omega'}{\omega}\right)^2 \left[\frac{\omega'}{\omega} + \frac{\omega}{\omega'} - \sin^2\Theta\right] , \tag{2.17}$$

which gives the Thomson formula as $\omega \to 0$ ($\omega' \to \omega$). This is the correct result in the leading order of the perturbation theory for Compton scattering off leptons (e, μ, τ), which can be considered as point-like Dirac particles.

The measurement of the magnetic moment of the proton by O. Stern and collaborators [Ste 21] showed that it differs from the value predicted by the Dirac equation, the nuclear magneton $\mu_N = e\hbar/2Mc$, where $M = 938.273$ MeV/c^2 is the mass of the proton.

The fact that the nucleon has an anomalous magnetic moment, results in the Powell cross section [Pow 49]:

$$\left(\frac{d\sigma}{d\Omega_{Lab}}\right)^{Powell} = \frac{1}{2} \left(\frac{\alpha_{em}\hbar}{Mc}\right)^2 \left(\frac{\omega'}{\omega}\right)^2 \left[\frac{\omega'}{\omega} + \frac{\omega}{\omega'} - \sin^2\Theta + \frac{\omega\omega'}{M^2} C(\cos\Theta)\right] , \tag{2.18}$$

where $C(\cos\Theta)$ is the correction due to the anomalous magnetic moment κ:

$$\begin{aligned} C(\cos\Theta) &= a_0 + a_1\cos\Theta + a_2\cos^2\Theta , \\ a_0 &= 2\kappa + \frac{9}{2}\kappa^2 + 3\kappa^3 + \frac{3}{4}\kappa^4 , \\ a_1 &= -4\kappa - 5\kappa^2 - 2\kappa^3 , \\ a_2 &= 2\kappa + \frac{1}{2}\kappa^2 - \kappa^3 - \frac{1}{4}\kappa^4 . \end{aligned} \tag{2.19}$$

We note in particular that in the forward direction only the correction terms $O(\kappa^4)$ contribute,

$$\left(\frac{d\sigma}{d\Omega_{Lab}}\right)^{Powell} (\Theta = 0) = \left(\frac{\alpha_{em}\hbar}{Mc}\right)^2 \left[1 + \frac{1}{4}\frac{\omega^2}{M^2}\kappa^4\right] , \tag{2.20}$$

which is the basis of the GDH sum rule [Ger 65].

2.2 Low energy forward Compton scattering, dispersion relations and sum rules

We introduce the Compton scattering amplitude by the following definition:

$$F \;=\; -\frac{i}{2M}\frac{1}{4\pi}T_{fi}\,. \tag{2.21}$$

In terms of F, the lab cross section reads

$$\left(\frac{d\sigma}{d\Omega}\right)_{Lab} \;=\; \frac{1}{64\pi^2M^2}\left(\frac{\omega'}{\omega}\right)^2|T_{fi}|^2 \;=\; \left(\frac{\omega'}{\omega}\right)^2|F(\omega,\Theta)|^2\,, \tag{2.22}$$

with ω and ω' the incoming and outgoing photon energies, respectively. In the forward direction, the amplitude F has only two components,

$$F(\omega,\Theta=0) \;=\; \chi'^{+}(s')\left\{f(\omega)\,(\varepsilon'^{*}\cdot\varepsilon)+g(\omega)\,i\vec{\sigma}\cdot[\varepsilon'^{*}\times\varepsilon]\right\}\chi(s)\,, \tag{2.23}$$

where χ and χ' are Pauli spinors of the initial and final nucleons, respectively.

At low photon energies, Low showed [Low 54] that the static properties of the nucleon, i.e. its charge e, mass M and anomalous magnetic moment κ govern the scattering, resulting in the Powell cross section of Eq.(2.18).

All the possible excitations of the nucleon show up only at relative order $O(\omega^2)$. This statement, based on gauge invariance and crossing symmetry, is the content of the Low Energy Theorem (LET).
In the relativistic formulation, gauge invariance reads

$$q^{\mu}H_{\mu\nu} = q'^{\nu}H_{\mu\nu} = 0 \tag{2.24}$$

and forbids any negative power of energy in the Low Energy Expansion (LEX) of the Compton tensor of Eq.(3.13).

Crossing invariance

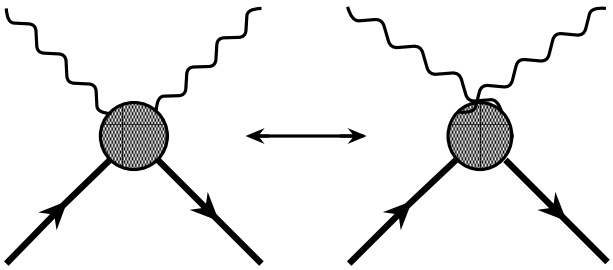

Figure 2.2: Direct and crossed Compton diagrams

The crossing symmetry, which will be discussed in more detail in Section 2.4 requires $H_{\mu\nu}(q,q') = H_{\nu\mu}(-q',-q)$. As a consequence of the crossing symmetry, the spin-independent (f) and the spin-dependent (g) scattering amplitudes have the following crossing behaviour:

$$f(-\omega) = f(\omega) \qquad g(-\omega) = -g(\omega) \tag{2.25}$$

The leading terms of f and g in the LEX can be calculated in Born approximation, where the coupling of the photon to the nucleon is considered to be pointlike:

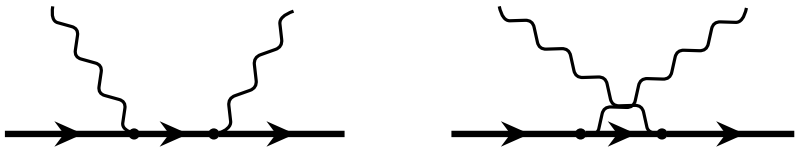

Figure 2.3: Born contributions to Compton scattering

The Feynman rules for these two diagramms give the following expression for the invariant amplitude:

$$\begin{aligned} T^{Born} &= -e^2 \varepsilon'^{*}_{\nu} \varepsilon_{\mu} \\ &\quad \bar{N}'(p',s') \left\{ \left(\gamma^{\nu} - i\kappa\sigma^{\nu\alpha} \frac{q'_{\alpha}}{2M} \right) \frac{i}{\not{p} + \not{q} - M} \left(\gamma^{\mu} + i\kappa\sigma^{\mu\beta} \frac{q_{\beta}}{2M} \right) \right. \\ &\quad \left. + \left(\gamma^{\mu} + i\kappa\sigma^{\mu\beta} \frac{q_{\beta}}{2M} \right) \frac{i}{\not{p} - \not{q}' - M} \left(\gamma^{\nu} - i\kappa\sigma^{\nu\alpha} \frac{q'_{\alpha}}{2M} \right) \right\} N(p,s) \end{aligned} \tag{2.26}$$

At forward scattering angle this formula reduces to two terms,

$$\mathcal{M}^{Born}(\omega, \Theta = 0) = \frac{ie^2}{M\omega} \left[(\varepsilon'^{*}\varepsilon) \bar{N}' \not{q} N + \omega \frac{\kappa^2}{4M} \bar{N}' (\not{\varepsilon}' \not{\varepsilon} - \not{\varepsilon} \not{\varepsilon}') \not{q} N \right] . \tag{2.27}$$

Recalling the relation between $\mathcal{M}$ and F, we can write at leading order

$$\begin{aligned} f(\omega) &= -\frac{\alpha_{em}}{M} + O(\omega^2) \\ g(\omega) &= -\frac{\alpha_{em}\kappa^2}{2M^2}\omega + O(\omega^3) , \end{aligned} \tag{2.28}$$

where the unknown higher order contributions of relative order ω^2 come from the nucleon excitation spectrum. As we see, we again obtain the familiar Thomson term as a model independent low energy limit in terms of charge and mass only. The leading term in the expansion of g is the correction to the Thomson term due to the anomalous magnetic moment κ. Performing the calculation with the Born amplitude of Eq.(2.26) at arbitrary angle leads to the Powell cross section of Eq.(2.18).

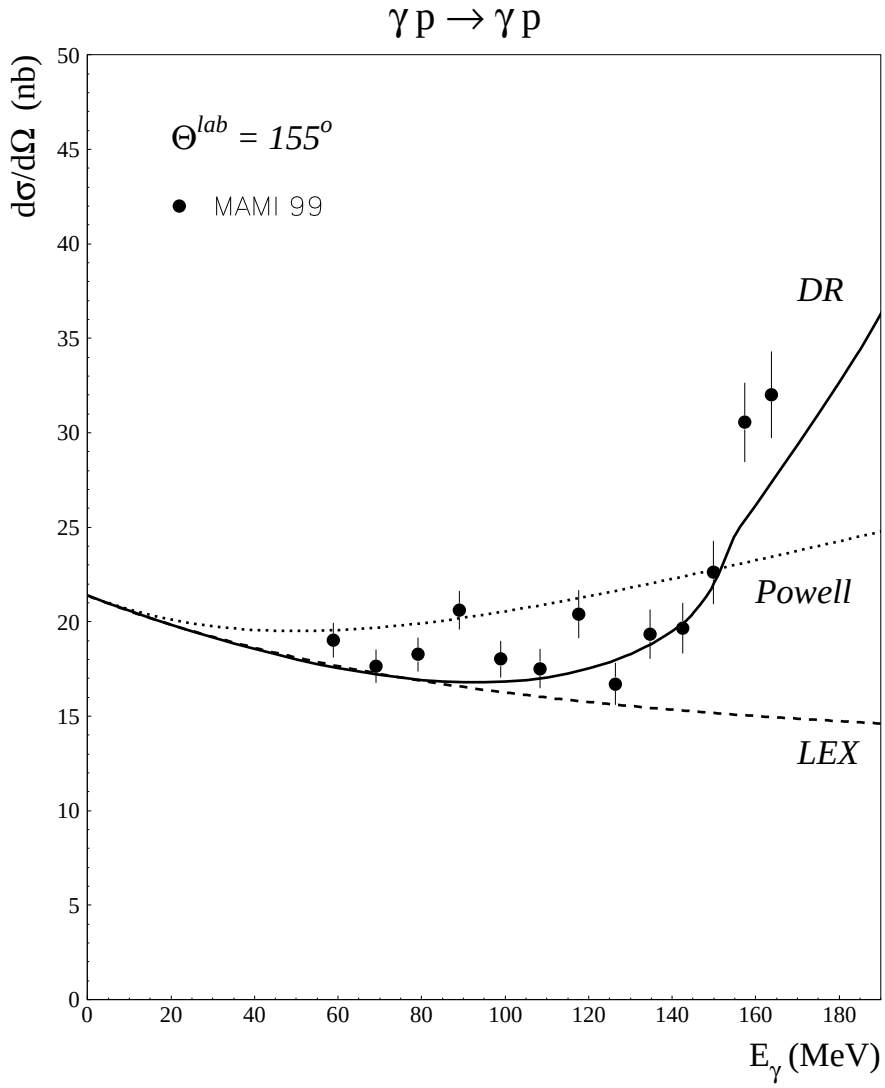

Figure 2.4: Compton differential cross section at 155^o lab scattering angle. Comparison of Born, LEX and full calculations with the low energy data of Ref.[Olm 01] is shown.

This result, however, fails to describe the experimental cross section already at low energy. The discrepancy is due to (unknown) effects of the internal structure of the nucleon. In the case of forward scattering, e.g., these effects can be effectively absorbed in the constants parametrizing the two next-to-leading order corrections in the LEX Eq.(2.28) [Pet 61],[Pet 81]:

$$\begin{aligned} f(\omega) &= -\frac{\alpha_{em}}{M} + (\alpha+\beta)\omega^2 + O(\omega^4) \\ g(\omega) &= -\frac{\alpha_{em}\kappa^2}{2M^2}\omega + \gamma_0\omega^3 + O(\omega^5)\,. \end{aligned} \tag{2.29}$$

In this way, the nucleon polarizabilities appear in the forward Compton scattering, whereby α is the electric polarizability, β the magnetic susceptibility, and γ_0 is the forward spin polarizability, a combination of the vector or spin polarizabilities introduced

by Ragusa [Rag 93].

2.3 Sum rules

In the following, similar ideas as those introduced by Kramers and Kronig in the classical theory, will be applied to a quantised system. We recall that the key point in the derivation of the Kramers-Kronig relation was causality, the consequence of the finite speed of signal transfer, $v \leq c$, with c the speed of light in vacuum. In relativistic quantum mechanics, this is equivalent to the statement that two measurements of an observable at two different space-time points *can not interfere*, provided these points are separated by a space-like interval. Mathematically, this fact requires the vanishing of the commutator of electromagnetic field operators taken at two such points:

$$[\mathcal{A}^{\mu}(x), \mathcal{A}^{\nu}(y)] \; = \; 0 \;\; , \;\; \text{if} \quad (x-y)^2 \; < \; 0 \tag{2.30}$$

In one of the basic works on dispersion relations by Gell-Mann, Goldberger and Thirring [Gel 54], it was shown that this microscopic causality condition necessarily leads to analyticity of the forward scattering amplitude in the upper half-plane of the complex energy ω. By means of Cauchy's theorem, this results in a constraint between the real and imaginary parts of the amplitude through DR. Constructing the Cauchy contour in the upper half-plane of the energy, we obtain two different DR for f and g due to their different crossing behaviour:

$$\begin{aligned} \mathrm{Re}\, f(\omega) - f(0) &= \frac{2\omega^2}{\pi} \mathcal{P} \int_{thr}^{\infty} d\omega' \frac{\mathrm{Im} f(\omega')}{\omega'(\omega'^2 - \omega^2)} \\ \mathrm{Re} g(\omega) &= \frac{2\omega}{\pi} \mathcal{P} \int_{thr}^{\infty} d\omega' \frac{\mathrm{Im} g(\omega')}{\omega'^2 - \omega^2} \; . \end{aligned} \tag{2.31}$$

The first (subtracted) DR is exactly the result of Kramers and Kronig. The second DR is left unsubtracted, though its convergence is still under discussion.
The unitarity of the S-matrix implies a bound on the imaginary part of the scattering amplitude due to the conservation of probability. In the case of forward Compton scattering, this principle leads to the *Optical Theorem*:

$$\mathrm{Im} F(\omega, \Theta = 0) \; = \; \frac{\omega}{4\pi} \sigma_{tot} \; , \tag{2.32}$$

where σ_{tot} is the total photoabsorption cross section. To "decode" this relation for the amplitudes f and g, we have to consider spin. Let us consider the case of a circularly polarized photon (spin along positive or negative z-direction, assumed to coincide with the photon three-momentum direction, i.e. positive or negative helicity) and a target proton, also polarized along the z-axis. Then, depending on the relative polarization of the incoming (or outgoing) particles, we can distinguish two cases:

Figure 2.5: Helicity channels for forward Compton scattering

Denoting the total cross section for the two helicity channels by $\sigma_{\frac{1}{2}}$ and $\sigma_{\frac{3}{2}}$, we specify the optical theorem for the Compton amplitude with definite helicity,

$$\mathrm{Im}\, F_{\frac{1}{2},\frac{3}{2}}(\omega,\Theta=0) \;=\; \frac{\omega}{4\pi}\sigma_{\frac{1}{2},\frac{3}{2}}\,. \tag{2.33}$$

Calculating $F_{\frac{1}{2},\frac{3}{2}}$ with helicity spinors and polarization vectors as specified in Subsection (A.1), we find

$$F_{\frac{1}{2}} \;=\; f+g \qquad F_{\frac{3}{2}} \;=\; f-g\,, \tag{2.34}$$

and hence the optical theorem for f and g,

$$\begin{aligned} \mathrm{Im}\, f &= \frac{\omega}{4\pi}\sigma_{tot}\,, \\ \mathrm{Im} g &= \frac{\omega}{8\pi}\left[\sigma_{\frac{1}{2}}-\sigma_{\frac{3}{2}}\right]\,, \end{aligned} \tag{2.35}$$

with $\sigma_{tot} \equiv \frac{1}{2}(\sigma_{\frac{1}{2}}+\sigma_{\frac{3}{2}})$.

The DR for F now take the form

$$\begin{aligned} \mathrm{Re}\, f(\omega) - f(0) &= \frac{\omega^2}{2\pi^2}\mathcal{P}\int_{\omega_{thr}}^{\infty} d\omega' \frac{\sigma_{tot}}{\omega'^2-\omega^2}\,, \\ \mathrm{Re}\, g(\omega) &= \frac{\omega}{4\pi^2}\mathcal{P}\int_{\omega_{thr}}^{\infty} d\omega' \frac{(\sigma_{\frac{1}{2}}-\sigma_{\frac{3}{2}})\omega'}{\omega'^2-\omega^2}\,. \end{aligned} \tag{2.36}$$

The integrals extend from the threshold of pion-photoproduction, ω_{thr}, to infinite energy. In principle, higher order electromagnetic corrections lead to absorption also below this threshold, but since these effects are of order $O(\alpha_{em})$, we shall neglect them completely.

As our main interest is the low energy limit for the amplitude F, we expand the integrand in Eq. (2.36) in a geometrical series for small ω and compare this expansion for the amplitudes f and g with the LEX :

$$-\frac{\alpha_{em}}{M}+(\alpha+\beta)\omega^2+O(\omega^4) \;=\; -\frac{\alpha_{em}}{M}+\omega^2\frac{1}{2\pi}\int_{thr}^{\infty} d\omega'\frac{\sigma_{tot}}{\omega'^2}+O(\omega^4) \tag{2.37}$$

$$-\frac{\alpha_{em}\kappa^2}{2M^2}\omega+\gamma_0\omega^3+O(\omega^5) \;=\; \frac{\omega}{4\pi^2}\int_{thr}^{\infty} d\omega'\frac{\sigma_{\frac{1}{2}}-\sigma_{\frac{3}{2}}}{\omega'}+\frac{\omega^3}{4\pi^2}\int_{thr}^{\infty} d\omega'\frac{\sigma_{\frac{1}{2}}-\sigma_{\frac{3}{2}}}{\omega'^3}+O(\omega^5) \tag{2.38}$$

We now identify the coefficients of the same powers of energy. Starting with Eq. (2.37), we see why the subtraction in the DR for f was necessary: otherwise, we would have to identify the negative Thomson term with the (positive!) integral over the photoabsorption cross section,

$$-\frac{\alpha_{em}}{M} \neq \frac{1}{2\pi}\int_{thr}^{\infty} d\omega' \, \sigma_{tot} \, . \tag{2.39}$$

The solution of this problem is that the latter integral diverges, because at very high energies the cross section slowly increases as $\sigma_{tot} \sim \omega^{\alpha_P - 1}$, with $\alpha_P = 1.08$ the experimental parameter identified in Regge theory with the so-called Pomeron exchange. Incidentally, also the purely electromagnetic cross section leads to a divergence, i.e., Eq.(2.39) would not apply to any charged particle.
The term in ω^2 provides Baldin sum rule [Bal 60],

$$(\alpha+\beta) = \frac{1}{2\pi}\int_{thr}^{\infty} d\omega \frac{\sigma_{tot}}{\omega'^2} \, , \tag{2.40}$$

which states that the sum of the scalar polarizabilities be always positive.
From the DR Eq.(2.38) for g, we have

$$-\frac{\alpha_{em}\kappa^2}{2M^2} = \frac{1}{4\pi^2}\int_{thr}^{\infty} d\omega' \frac{\sigma_{\frac{1}{2}} - \sigma_{\frac{3}{2}}}{\omega'} \, , \tag{2.41}$$

the Gerasimov-Drell-Hearn (GDH) sum rule [Ger 65], which relates the value of the anomalous magnetic moment of the nucleon with the integral over the helicity cross section difference. The values $\kappa_p = 1.79$ for the proton, and $\kappa_n = -1.91$ for the neutron [PDG 01] are known to excellent precision and hence provide a very good check for the theoretical investigations.
Furthermore, the hypothesis of convergence of the unsubtracted DR for g bases on the assumption that the Pomeron does not couple to the spin, i.e. contributes equally to $\sigma_{\frac{1}{2}}$ and $\sigma_{\frac{3}{2}}$ and therefore drops out of the GDH integral. In recent years, new precise experiments with circularly polarized photon beams and linearly polarized targets became possible (Mainz, Bonn, JLab). The value for the GDH integral has been measured at MAMI for 200 MeV$\leq \omega \leq$800 MeV and the value over the measured range supplemented with theoretical estimates for the remaining integration range is in good agreement with the value of κ_p for the proton. The analysis for the GDH experiment on the neutron is much more complicated since no free neutron target exists. Theoretical analysis for the GDH on the neutron [MAID] is at present not consistent with the value of the sum rule. However, to confirm the assumption of convergence of the GDH integral experimentally, one has to go to substantially higher energies. Preliminary data exist now also at the higher energies from the experiment at ELSA (Bonn).

The last and best convergent sum rule follows from the term $[\omega^3]$ in (2.38) and was first derived by Gell-Mann, Goldberger and Thirring:

$$\gamma_0 = \frac{1}{4\pi^2}\int_{thr}^{\infty} d\omega' \frac{\sigma_{\frac{1}{2}} - \sigma_{\frac{3}{2}}}{\omega'^3} \, , \tag{2.42}$$

which defines the forward spin polarizability in terms of helicity cross sections.

2.4 Analytical properties of the invariant amplitudes

As we have seen for forward Compton scattering, causality necessarily leads to analyticity of the forward scattering amplitude as function of energy. This result was generalized to the case of finite scattering angles but sufficiently small momentum transfer by a number of authors, e.g. [Bog 56], [Cap 56], [Dys 58], [Jos 57], [Oeh 55], [Sal 56], [Sal 56a]. These investigations have made it possible to construct the DR in energy at fixed momentum transfer. Along with analyticity, the principle of "physicalness" of singularities of the invariant amplitude as function of energy led to useful relations between the imaginary (absorptive) and the real parts of the invariant amplitude. The natural question arises, however, whether the scattering amplitude is an analytic function of momentum transfer, too. The simultaneous analyticity in both energy and momentum transfer has unfortunately never been strictly proven. However, with or without the necessary proof, to capitalize the simultaneous analyticity of the scattering amplitude in all its variables, one needs information about the singularities in both energy and momentum transfer. For this, Mandelstam proposed [Man 58] the following method.

2.4.1 s, t and u-reaction channels

Let us consider a general process of the type $1(p_1) + 2(p_2) \to 3(p_3) + 4(p_4)$ and discuss the general structure of its scattering amplitude.

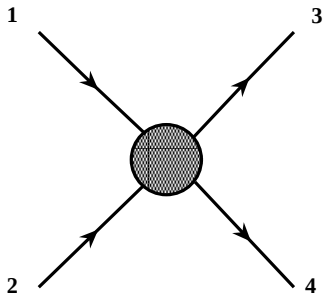

Figure 2.6: General scattering process 1 + 2 → 3 + 4

From the four momenta of the particles one can construct the three invariant Mandelstam variables in the standard way,

$$\begin{aligned} s &= (p_1 + p_2)^2 \\ u &= (p_2 - p_3)^2 \\ t &= (p_1 - p_3)^2 \,. \end{aligned} \tag{2.43}$$

The energy-momentum conservation $p_1 + p_2 = p_3 + p_4$ fixes the sum of the invariant variables to the sum of the masses squared,

$$s + u + t = M_1^2 + M_2^2 + M_3^2 + M_4^2 \,, \tag{2.44}$$

so that only two of the three variables are independent. We first consider the simplest case of four identical spinless particles (for example, $\pi-\pi$ scattering). In the center-of-momentum frame, $\vec{p}_1+\vec{p}_2=\vec{p}_3+\vec{p}_4=0$, thus

$$\begin{aligned} s &= (E_1^{cm}+E_2^{cm})^2 \\ u &= -4\vec{q}_{cm}{}^2\cos^2\frac{\Theta_{cm}}{2} \\ t &= -4\vec{q}_{cm}{}^2\sin^2\frac{\Theta_{cm}}{2}\,. \end{aligned} \tag{2.45}$$

Such scattering process is described in terms of one invariant amplitude, which is defined by factorizing out the four-momentum conserving δ-function from the S-matrix element,

$$< f\,|\,S-1\,|\,i> = i(2\pi)^4\,\delta^4(p_1+p_2-p_3-p_4)\,A(s,t,u)\,. \tag{2.46}$$

The amplitude A is a Lorentz-invariant function of its arguments. Eq.(2.46) defines this amplitude for those values of the variables s, t and u that can physically correspond to the scattering process, i.e. s, the square of the total c.m. energy W, should be larger than some positive threshold value, and t should be such that the cosine of the scattering angle lies between -1 and 1. Our aim is to continue the function $A(s,t,u)$ into the unphysical region and to define it for arbitrary values of s, t and u, or in other words, to define a more general function on the whole plane, which reduces to the physical amplitude whenever the variables take on physical values.

By definition, one calls the process under consideration *the s-channel process*, with the s-variable the square of the total energy in the center of mass frame. As a first step, we define the *crossing operation*, or "partial" CP-transformation which interchanges an incoming particle with an outgoing one. The first possibility is

$$\begin{aligned} 1\,(p_1) &\rightarrow \overline{1}\,(-p_1)\,, \\ 3\,(p_3) &\rightarrow \overline{3}\,(-p_3)\,, \end{aligned} \tag{2.47}$$

which corresponds to the scattering of the antiparticle $\overline{3}\,(-p_3)$ off particle $2\,(p_2)$ with $\overline{1}\,(-p_1)$ and $4\,(p_4)$ in the outgoing channel. Another process, related to the basic one by the crossing transformation, reads

$$\begin{aligned} 2\,(p_2) &\rightarrow \overline{2}\,(-p_2)\,, \\ 3\,(p_3) &\rightarrow \overline{3}\,(-p_3)\,, \end{aligned} \tag{2.48}$$

If constructing the Mandelstam variables for these new processes, one immediately finds for the first transformation, that the crossing interchanges the variables s and u of the s-channel reaction and leaves t unchanged, and that the second transformation interchanges s and t. Since in the reactions of Eqs. (2.47) and (2.48) the square of the total c.m. energy is given by u and t, respectively, one calls these processes u- or t-channels with respect to the s-channel. The other two possible crossing transformations are trivial in the sense that the corresponding reactions are just time reversed t or

u-channel processes.
The idea of Mandelstam was to combine these three processes by defining a more general function on the whole plane, which reduces to the physical scattering amplitude for the s, t or u-process in the corresponding regions, accessible for each physical reaction.

2.4.2 Mandelstam representation

In each channel, the analyticity of the amplitude $A(s,t,u)$ in energy can be stated as a consequence of causality. Studying the singularity structure of the Feynman graphs, Cutkosky [Cut 60] and Landau [Lan 59] showed that two types of physical singularities are possible:
A single pole if a single particle in the intermediate state can go on-shell, causing the denominator of the corresponding Feynman propagator to vanish, and a branch cut, provided two or more on-shell particles in the intermediate state can be produced.

Another type, the anomalous singularity, occurs if the scattering takes place on a compound object, consisting of two or more particles bound together, for instance the deuteron as a system of p and n, or Λ as a system of a nucleon and a pion.

Since no anomalous contributions appear in Compton scattering, as well as in $\pi\pi$-scattering, they will be left out of consideration.

This allows us to write down three one-dimensional DRs at fixed momentum transfer,

$$\begin{aligned}
A(s,t,u) &= \frac{1}{\pi}\int_{s_{thr}}^{\infty} ds' \frac{A(s',t,u)}{s'-s-i\varepsilon} + \frac{1}{\pi}\int_{-\infty}^{u_{thr}} ds' \frac{A(s',t,u)}{s'-s-i\varepsilon}\,, \\
A(u,t,s) &= \frac{1}{\pi}\int_{u_{thr}}^{\infty} du' \frac{A(u',t,s)}{u'-u-i\varepsilon} + \frac{1}{\pi}\int_{-\infty}^{s_{thr}} du' \frac{A(u',t,s)}{u'-u-i\varepsilon}\,, \\
A(t,s,u) &= \frac{1}{\pi}\int_{t_{thr}}^{\infty} dt' \frac{A(t',s,u)}{t'-t-i\varepsilon} + \frac{1}{\pi}\int_{-\infty}^{u_{thr}} dt' \frac{A(t',s,u)}{t'-t-i\varepsilon}\,,
\end{aligned} \tag{2.49}$$

where s_{thr}, u_{thr} and t_{thr} correspond to the threshold energy for the respective reaction channel. The infinitesimal imaginary part in each denominator reflects the fact that the analyticity is stated in the upper half of the complex plane of s (u, t, correspondingly). To indicate the channel in which the DR is written, the order of the arguments was interchanged. The first variable then denotes the energy in the respective channel and the second one the momentum transfer. For the first DR, the integration runs along a line at constant-t with two contributions from the s and u-channels, and analogously for the other two DRs. Assuming now analyticity in momentum transfer and applying Cauchy's theorem once more, one finds a general prescription for the analytical continuation of the invariant amplitude into the whole plane,

$$\begin{aligned}
A(s,t,u) &= \frac{1}{\pi}\int_{s_{thr}}^{\infty} ds' \frac{\rho_s(s')}{s'-s} + \frac{1}{\pi}\int_{u_{thr}}^{\infty} du' \frac{\rho_u(u')}{u'-u} + \frac{1}{\pi}\int_{t_{thr}}^{\infty} dt' \frac{\rho_t(t')}{t'-t} \\
&+ \frac{1}{\pi^2}\int_{s_{thr}}^{\infty}\int_{u_{thr}}^{\infty} ds'\,du' \frac{\rho_{su}(s',u')}{(s'-s)(u'-u)}
\end{aligned}$$

$$+ \quad \frac{1}{\pi^2}\int_{s_{thr}}^{\infty}\int_{t_{thr}}^{\infty} ds'dt' \frac{\rho_{st}(s',t')}{(s'-s)(t'-t)}$$

$$+ \quad \frac{1}{\pi^2}\int_{u_{thr}}^{\infty}\int_{t_{thr}}^{\infty} du'dt' \frac{\rho_{ut}(u',t')}{(u'-u)(t'-t)} \,. \tag{2.50}$$

Here, each denominator, e.g., $\frac{1}{s'-s}$ should be understood as $\frac{1}{s'-s-i\varepsilon}$. The functions ρ_s, ρ_t, ρ_u are due to intermediate states in the indicated channel alone, whereas ρ_{st}, ρ_{su}, ρ_{ut} are the spectral functions which are finite in the (unphysical) kinematical regions where the intermediate states are energetically possible in two channels at the same time.

This double integral representation contains more information than the one-dimensional DRs. If we recall that $\frac{1}{s'-s-i\varepsilon} = \mathcal{P}\frac{1}{s'-s} + i\pi\delta(s'-s)$, we obtain for the imaginary part of A:

$$A_s(s,t,u) \;=\; \rho_s(s,t,u) + \frac{1}{\pi}\int dt' \frac{\rho_{st}}{t'-t} + \frac{1}{\pi}\int du' \frac{\rho_{su}}{u'-u} \,, \tag{2.51}$$

which is purely real in the physical region of the s-channel reaction, and is complex otherwise. The DR of Eq.(2.51) represents the generalized unitarity relation, which obtains additional contributions from the (unphysical) spectral regions along with the usual contributions from the physical region $\rho_s(s,t,u)$. Analogously treating the denominators $\frac{1}{t'-t}$ and $\frac{1}{u'-u}$, one obtains such representation also for u- and t-channels.

Unfortunately, the spectral functions ρ_{st}, ρ_{su}, ρ_{ut} are in general unknown, which makes it impossible to use the Mandelstam representation for practical calculations. The great value of this representation consists, however, in combining the information about the singularities in all three channels and defining the invariant amplitude on the whole Mandelstam plane by means of analytical continuations from the physical and spectral regions.

2.4.3 Mandelstam plot

The kinematical regions for $\pi\pi$-scattering that correspond to physical processes in the three channels and to the spectral regions are illustrated by the Mandelstam plot. Since the variables s, t and u are not independent, it is possible to plot them on a two-dimensional plane.

The energy threshold in the s-channel is given by the line

$$s \;=\; 4m_\pi^2 \,, \tag{2.52}$$

and the condition of "physicality" for the scattering angle limits the values of t and u:

$$\begin{aligned} t \;&=\; -(s-4m_\pi^2) \quad \sin^2\frac{\Theta^{CM}}{2} \,, \\ u \;&=\; -(s-4m_\pi^2) \quad \cos^2\frac{\Theta^{CM}}{2} \,, \\ &\qquad\Downarrow \\ -(s-4m_\pi^2) \;&\leq \quad t,u \quad \leq\; 0 \,, \end{aligned} \tag{2.53}$$

and similarly for the t and u-channels.

If we apply the crossing transformation, which relates kinematical regions of two different channels, to such a scattering process with four identical particles, the transformation relates the reaction to itself. This property is called *crossing invariance* and is the case if at least two of the particles are identical. If all the four particles are identical, the amplitude $A(s,t,u)$ is invariant under all possible crossing transformations.

Turning to the singularity structure of the $\pi\pi$-scattering amplitude, we find that the first singularity comes from the two pion intermediate state at $4m_\pi^2$ and is a branch cut, while one particle intermediate states do not appear at all because no particle has the quantum numbers of the $\pi\pi$-system. This picture holds for all three channels due to symmetry, and thus the invariant amplitude is purely real within a triangle around the origin defined by the threshold in three channels.

The integration range of the double spectral integrals runs over that region of the plane for which the on-shell intermediate states are possible in two channels simultaneously. It is possible to determine this region by considering the so-called Cutkosky diagrams. We first study the spectral region for s and t. We write down the unitarity condition in the s-channel,

$$2\mathrm{Im}T_{fi} = \sum_X \int \frac{d^3\vec{q}_1}{(2\pi)^3 2E_1}\frac{d^3\vec{q}_2}{(2\pi)^3 2E_2}\cdots\frac{d^3\vec{q}_1}{(2\pi)^3 2E_{N_X}} T_{fX}T_{iX}^*(2\pi)^4\delta^4(q_n-q_i)\,, \quad (2.54)$$

where N_X is the number of the particles in the intermediate state X. We keep now only the first intermediate state in the s-channel, two pions, and make use of the two body kinematics in the c.m. frame. We denote the initial and the intermediate pions momenta by q_i, p_i, and $q_n = (\omega_n, \vec{q}_n)$, $p_n = (E_n, \vec{p}_n)$, respectively.

$$\begin{aligned} 2\mathrm{Im}T_{fi} &= \int \frac{d^3\vec{q}_n}{(2\pi)^3 2\omega_n}\frac{d^3\vec{p}_n}{(2\pi)^3 2E_n} T_{fn}T_{in}^*(2\pi)^4\delta^4(q_n+p_n-q_i-p_i) \\ &= \frac{1}{(4\pi)^2}\int \frac{|\vec{q}_n|^2 d|\vec{q}_n|}{\omega_n E_n} d\Omega_n\,\delta(\sqrt{s}-\omega_n-E_n)\,T_{fn}T_{in}^* \\ &= \frac{1}{(4\pi)^2}\frac{|\vec{q}_n|}{\sqrt{s}}\int d\Omega_n\, T_{fn}T_{in}^*\,, \end{aligned} \quad (2.55)$$

where $|\vec{q}_n| \equiv |\vec{q}| = \sqrt{\frac{s}{4}-m_\pi^2}$ is the modulus of the c.m. three-momentum of the pions. Since a three pion vertex is not possible due to negative G-parity of the pion, the lowest intermediate state in the t-channel corresponds to four pions.

The singularity in t is possible if the denominators of the corresponding t-channel propagators in T_{fn} and T_{in}^* vanish due to the threshold for intermediate two-pion states. We are therefore looking for the kinematical region where the integral

$$\int d\Omega_{q_n}\frac{1}{(t'-4m_\pi^2)(t''-4m_\pi^2)} \quad (2.56)$$

has singularities. We consider now the kinematics for the subprocesses I and II,

$$t = -2\vec{q}^{\,2} + 2\vec{q}_i\cdot\vec{q}_f$$

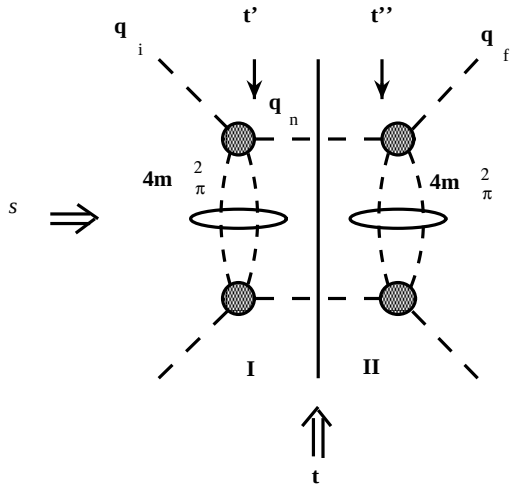

Figure 2.7: Cutkosky diagramm for the *st*-spectral region for $\pi\pi$ – *scattering*

$$\begin{aligned} t' &= -2\vec{q}^{\,2} + 2\vec{q}_i \cdot \vec{q}_n \\ t'' &= -2\vec{q}^{\,2} + 2\vec{q}_n \cdot \vec{q}_f \ . \end{aligned} \tag{2.57}$$

To perform the integration over $d\Omega_{q_n}$, we introduce the Feynman parameter y and use the identity

$$\frac{1}{ab} = \int_0^\infty dy \frac{1}{(ay+b)^2} \ . \tag{2.58}$$

With the relations of Eq.(2.57), the integral becomes

$$\begin{aligned} \int d\Omega_{q_n} \frac{1}{(t'-4m_\pi^2)(t''-4m_\pi^2)} &= \int_0^\infty dy \int d\Omega_{q_n} \frac{1}{(A+\vec{B}\cdot\vec{q}_n)^2} \\ &= 4\pi \int_0^\infty dy \frac{1}{A^2 - \vec{B}^2\vec{q}^{\,2}} \ , \end{aligned} \tag{2.59}$$

where we denoted $A = (4m_\pi^2 + 2\vec{q}^{\,2})(y+1)$ and $\vec{B} = 2(y\vec{q}_i + \vec{q}_f)$. The requirement that the integrand is singular leads to a quadratic equation which can only have solutions if its determinant is non-negative. The boundary of the region where this condition holds is given by the line

$$t = \frac{16m_\pi^2 s}{s - 4m_\pi^2} \ , \tag{2.60}$$

a hyperbola with two asymptotas, $t = 16m_\pi^2$ as $s \to \infty$, and $s = 4m_\pi^2$ as $t \to \infty$. Analogously, two pions in the *t*-channel and four pions in the *s*-channel give

$$s = \frac{16m_\pi^2 t}{t - 4m_\pi^2} \ . \tag{2.61}$$

The region to the right of the two curves is then called the *st*-spectral region. The spectral regions *su* and *ut* are obtained from this in an analogous way. The kinematical regions defined above are shown in Fig. 2.8.

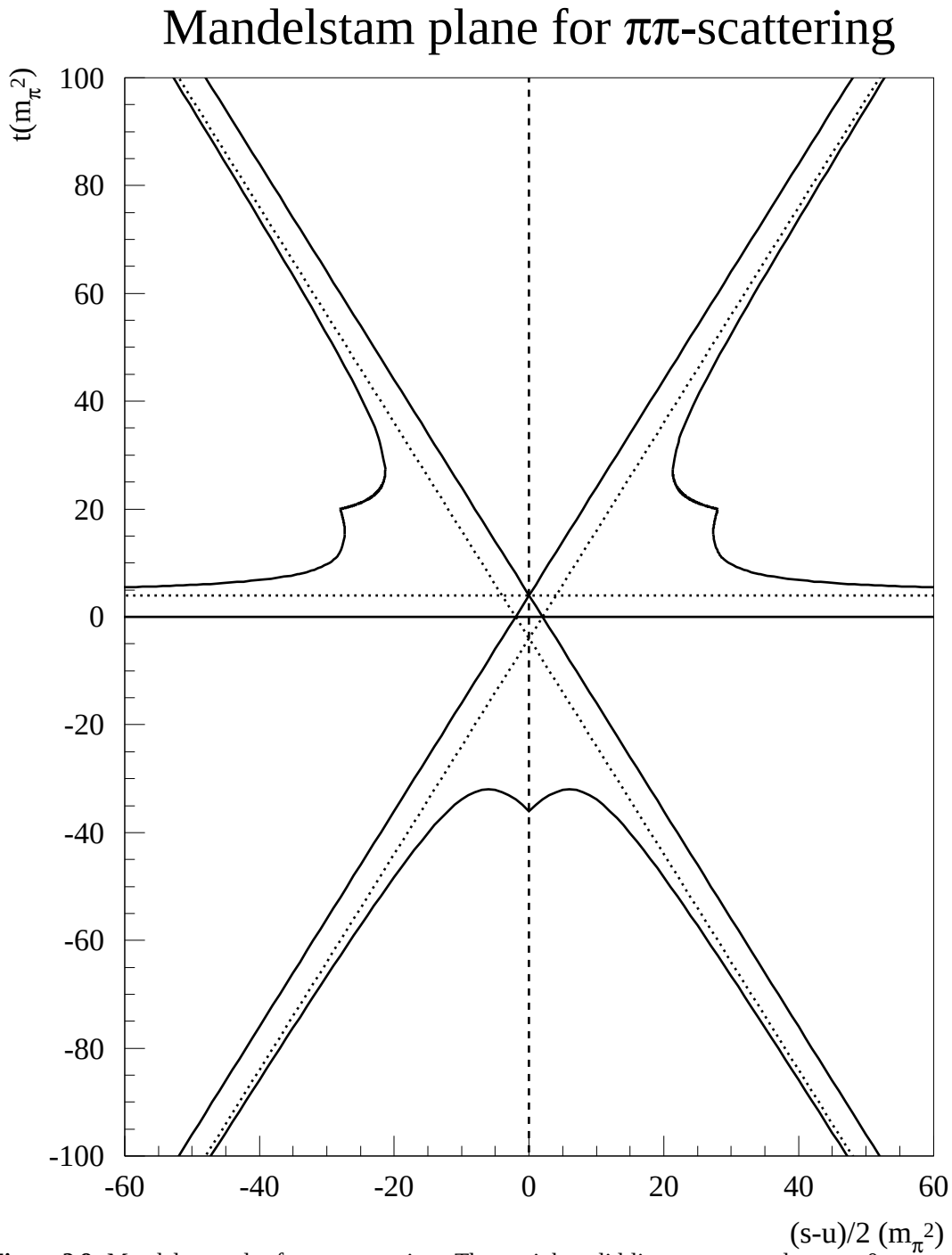

Figure 2.8: Mandelstam plot for ππ-scattering. The straight solid lines correspond to $s = 0$ ($t = 0$, $u = 0$). The dotted lines give the energetical threshold, $4m_\pi^2$, in either of the three channels. The boundaries of the spectral regions are given by the solid curves.

The considerations in this section contain the basic ideas of the S-matrix theory of strong interactions as developed in the late 1950's. This approach was believed to be an alternative to quantum field theory and originated from the work of Heisenberg who introduced the S-matrix [Hei 43]. The S-matrix theory of strong interactions pretended to operate with a minimal number of parameters, the physical masses and coupling constants (nucleon, pion and kaon masses and corresponding coupling constants), and to be able to predict all other information by use of the symmetries of the S-matrix. The main tool in this theory was analyticity of the invariant amplitude as function of all its arguments, in the sense of the double integral representation of Mandelstam. In order to determine the positions of the singularities of the invariant amplitude, which are necessary to make any use of analyticity, unitarity was used together with the assumption that only those singularities required by unitarity appear and that the positions of the singularities only depend on the masses of the particles in the initial, final and intermediate states. The unitarity relation allows for the representation of the imaginary part of the invariant amplitude as a series over all possible intermediate states, Eq.(2.54). Correspondingly, the real part of the amplitude T_{fi} is also given by the sum over the states X by means of the dispersion integral similar to the one of Kramers and Kronig (for simplicity, just one-dimensional dispersion relation in s):

$$\mathrm{Re}T_{fi}(s,t,u) \;=\; \frac{1}{\pi}\sum_X \int_{(s_{thr})_X}^{\infty} ds' \frac{\mathrm{Im}_X T_{fi}(s',t,u)}{s'-s}\;. \tag{2.62}$$

As one can see, the integrands are weighted with factors of the type $\sim \frac{1}{s'-s}$. At the given kinematical point (s,t), this supresses the contributions of those intermediate states, lie farther from this point relative to the closer one. Therefore, the behaviour of the invariant amplitude at some kinematical point is mostly dominated by the closest singularities. The distance $s-(s_{thr})_X$ depends on the masses of the particles in the intermediate state X. Since no zero-mass strongly interacting particles are observed, each further singularity is separated from the lower one by at least the pion mass, which gives one the possibility to represent the amplitude of the process as a perturbation series, though not in powers of the strong coupling constant (as in usual perturbation theory).

This idea can be illustrated for $\pi\pi$-scattering, where the first possible intermediate state is $\pi\pi$, and the next one is four pions. If looking at the kinematical point $s,t,u=0$, one obtains from Eq.(2.62):

$$\begin{aligned}
\mathrm{Re}T_{\pi\pi}(0,0,0) &= \frac{1}{\pi}\int_{4m_\pi^2}^{\infty} ds' \frac{\mathrm{Im}_{2\pi}T_{\pi\pi}(s',0,0)}{s'} + \frac{1}{\pi}\int_{16m_\pi^2}^{\infty} ds' \frac{\mathrm{Im}_{4\pi}T_{\pi\pi}(s',0,0)}{s'} + \ldots \\
&= \frac{1}{\pi}\int_{4m_\pi^2}^{\infty} ds' \frac{1}{s'}\Big[\mathrm{Im}_{2\pi}T_{\pi\pi}(s',0,0) \\
&\qquad + \frac{s'}{s'+12m_\pi^2}\mathrm{Im}_{4\pi}T_{\pi\pi}(s'+12m_\pi^2,0,0) + \ldots\Big]\;.
\end{aligned} \tag{2.63}$$

Here, $\mathrm{Im}_{\pi\pi}T_{\pi\pi}$ and $\mathrm{Im}_{4\pi}T_{\pi\pi}$ are the contributions to the imaginary part from two- and four-pions intermediate states, respectively. The four-pions contribution is now supressed by a factor of $\frac{s'}{s'+12m_\pi^2} \approx \frac{1}{4}$ at $s' \approx 4m_\pi^2$. The contribution of the further intermediate state, $K\bar{K}$, is supressed by the factor $(4m_\pi^2)/(4m_K^2) \approx \frac{1}{13}$.

Chapter 3

Dispersion relations for RCS

3.1 Kinematics for real Compton scattering

3.1.1 Kinematics

Referring to real Compton scattering, we will consider the elastic scattering of the *real* photon off the proton (four momenta q^μ and p^μ, respectively) with a real photon and proton in the final state (q'^μ and p'^μ).

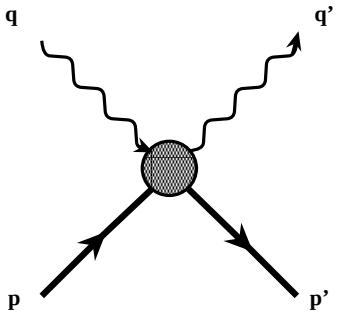

Figure 3.1: Kinematics for real Compton scattering

From the four-vectors of the particles, one can construct three Lorentz scalars, the Mandelstam variables

$$\begin{aligned} s &= (p+q)^2 \\ t &= (q-q')^2 \\ u &= (p-q')^2 \,. \end{aligned} \tag{3.1}$$

Their sum is fixed by the energy-momentum conservation law to the sum of the squared masses of the particles involved in the process,

$$s + t + u = 2M^2 \,, \tag{3.2}$$

where M is the nucleon mass, and the real photon is massless. Since the three variables are not independent, a combination of s and u is usually introduced,

$$\nu = \frac{s-u}{4M}\,. \tag{3.3}$$

Throughout this work, the center-of-mass (c.m.) frame will be used. This frame is defined by the condition $\vec{p}+\vec{q}=\vec{p}^{\,'}+\vec{q}^{\,'}=0$. The variable s is then the full c.m. energy squared, whereas t and u are related to the c.m. scattering angle.

We choose the incoming photon direction along the positive z-axis with the outgoing particles' momenta lying in the xz-plane,

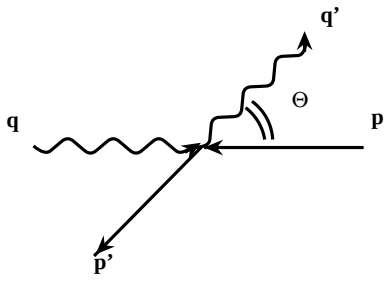

Figure 3.2: Center-of-mass kinematics for RCS

The c.m. scattering angle is defined as the angle between the incoming and outgoing photons' direction in the xz-plane.

$$\begin{aligned}
q^{\mu} &= (\omega_{cm}, 0, 0, \omega_{cm}) \\
p^{\mu} &= (E, 0, 0, -\omega_{cm}) \\
q'^{\mu} &= \left(\omega'_{cm}, \omega'_{cm}\sin\Theta_{cm}, 0, \omega'_{cm}\cos\Theta_{cm}\right) \\
p'^{\mu} &= \left(E'_{cm}, -\omega'_{cm}\sin\Theta_{cm}, 0, -\omega'_{cm}\cos\Theta_{cm}\right)\,,
\end{aligned} \tag{3.4}$$

where $E_{cm} = \sqrt{\omega_{cm}^2 + M^2}$. The c. m. photon energy and scattering angle can be related to the invariants of Eq. (3.1):

$$\begin{aligned}
\omega_{cm} &= \omega'_{cm} = \frac{s-M^2}{2\sqrt{s}} \\
E_{cm} &= E'_{cm} = \frac{s+M^2}{2\sqrt{s}} \\
\sin^2\frac{\Theta_{cm}}{2} &= -\frac{st}{(s-M^2)^2}\,.
\end{aligned} \tag{3.5}$$

3.1.2 Compton tensor

Each particle in the process can have two different polarizations, therefore $2^4 = 16$ helicity T-matrix elements can be constructed,

$$< \gamma'(q',\lambda')N'(p',\lambda'_N)\,|\,S-1\,|\,\gamma(q,\lambda)N(p,\lambda_N) > = \; i(2\pi^4)\delta^4(p+q-p'-q')\,T_{\lambda'\lambda'_N,\lambda\lambda_N}\;. \tag{3.6}$$

We consider now the *parity transformation* $\vec{p}_i \;\rightarrow\; -\vec{p}_i$, which does not change the spin, but flips the *helicity*, i.e. the projection of the spin onto the three-momentum of the particle.

$$T_{\lambda'\lambda'_N,\lambda\lambda_N} \;\rightarrow\; T_{-\lambda'-\lambda'_N,-\lambda-\lambda_N} \;=\; (-)^{\Lambda'-\Lambda}\cdot T_{\lambda'\lambda'_N,\lambda\lambda_N}\;, \tag{3.7}$$

where $\Lambda = \lambda - \lambda_N$ and $\Lambda' = \lambda' - \lambda'_N$. This can be shown by performing the partial wave expansion of the helicity amplitudes,

$$T_{\lambda'\lambda'_N,\lambda\lambda_N} \;=\; \sum_J \frac{2J+1}{2} T^J_{\lambda'\lambda'_N,\lambda\lambda_N} d^J_{\Lambda\Lambda'}(\Theta)\;, \tag{3.8}$$

where $d^J_{\Lambda\Lambda'}(\Theta)$ are the Wigner d-functions. The latter behave under space inversion $\Theta \rightarrow -\Theta$ as

$$d^J_{\Lambda\Lambda'}(-\Theta) \;=\; (-)^{\Lambda'-\Lambda} d^J_{\Lambda\Lambda'}(\Theta)\;. \tag{3.9}$$

This reduces the number of independent helicity amplitudes by a factor of 2. Considering finally *time reversal*, which interchanges the initial and the final states, one obtains two more relations between the helicity amplitudes, due to the fact that the types of the particles before and after the interaction are the same (for example, T-invariance is not valid for the virtual Compton scattering helicity amplitudes), leaving us with only six independent amplitudes:

$$T_{1\frac{1}{2},1\frac{1}{2}},\quad T_{-1\frac{1}{2},-1\frac{1}{2}},\quad T_{1\frac{1}{2},-1\frac{1}{2}},\quad T_{1-\frac{1}{2},-1\frac{1}{2}},\quad T_{-1-\frac{1}{2},1\frac{1}{2}},\quad T_{1-\frac{1}{2},1\frac{1}{2}} \tag{3.10}$$

The helicity amplitudes with no helicity flip on the nucleon side do not change sign under parity transformation.

We next introduce the covariant *Compton tensor*

$$T_{fi} \;=\; \varepsilon^{\mu}\varepsilon'^{*\nu} H_{\mu\nu}\;, \tag{3.11}$$

which contains all the information about the scattering process. The polarization vectors of the incoming and the outgoing photons, ε and ε', respectively, are defined in Appendix A.1. The main requirement for this tensor is gauge invariance $q^{\mu} H_{\mu\nu} \;=\; q'^{\nu} H_{\mu\nu} \;=\; 0$ (charge and current conservation).

Six independent tensorial structures can be built from the four-vectors $q^{\mu},\; p^{\mu},\; q'^{\mu},\; p'^{\mu},\; \gamma^{\mu}$ and tensor $\sigma^{\mu\nu}$ in the following way [Pra 58]:

$$
\begin{aligned}
P^\mu &\equiv \frac{1}{2}(p+p')^\mu\,, \\
K^\mu &\equiv \frac{1}{2}(q+q')^\mu\,, \\
Q^\mu &\equiv \frac{1}{2}(p-p')^\mu \;=\; \frac{1}{2}(q'-q)^\mu\,, \\
P'^\mu &\equiv P^\mu - \frac{(P\cdot K)}{K^2}K^\mu\,, \\
N^\mu &\equiv \varepsilon^{\mu\nu\alpha\beta}P'_\nu Q_\alpha K_\beta\,.
\end{aligned}
\tag{3.12}
$$

The Compton tensor can now be written in the form:

$$
\begin{aligned}
H^{\mu\nu} \;=\; \bar{N}'(p',s')\Big[\quad & -\frac{P'^\mu P'^\nu}{P'^2}\Big(T_1+T_2\not{K}\Big) \\
& -\frac{N^\mu N^\nu}{N^2}\Big(T_3+T_4\not{K}\Big) \\
& -i\frac{P'^\mu N^\nu - P'^\nu N^\mu}{P'^2K^2}\gamma_5\,T_5 \\
& +i\frac{P'^\mu N^\nu + P'^\nu N^\mu}{P'^2K^2}\gamma_5\not{K}T_6\Big]\; N(p,s)\,,
\end{aligned}
\tag{3.13}
$$

where the six tensors form a basis and the scalar coefficients $T_1,...,T_6$ are the invariant amplitudes of Prange. Note that all the tensors in Eq.(3.13) are orthogonal to each other. It is an easy exercise to prove that the Compton tensor in this form is gauge-invariant. By construction, however, the tensors in Eq.(3.13) have singularities at forward and backward directions:

$$
\begin{aligned}
K^2 &= -\frac{t}{4} \;=\; \frac{(s-M^2)^2}{8s}(1-\cos\Theta_{cm}) \\
P'^2K^2 &= \frac{su-M^4}{4} \;\sim\; (1+\cos\Theta_{cm}) \\
N^2 &= P'^2(K^2)^2 \;\sim\; \sin^2\Theta_{cm}\,,
\end{aligned}
\tag{3.14}
$$

which leads to linear dependences among the amplitudes T_i at these kinematical points (*kinematical constraints*). Therefore, to avoid this problem, the set of amplitudes (and, correspondingly, the basis) can be modified as [L'vo 81]:

$$
\begin{aligned}
A_1 &= \frac{1}{t}\left[T_1+T_3+\nu(T_2+T_4)\right] \;=\; -\frac{1}{2}A_1^{BT} \\
A_2 &= \frac{1}{t}\left[2T_5+\nu(T_2+T_4)\right] \;=\; \frac{M}{2}A_2^{BT} \\
A_3 &= \frac{M^2}{M^4-su}\left[T_1-T_3-\frac{t}{4\nu}(T_2-T_4)\right] \;=\; -\frac{M^2}{4}A_5^{BT} \;-\; \frac{M^2}{4\nu}A_6^{BT} \\
A_4 &= \frac{M^2}{M^4-su}\left[2M_NT_6-\frac{t}{4\nu}(T_2-T_4)\right] \;=\; -\frac{M^2}{4\nu}A_6^{BT}
\end{aligned}
$$

$$
\begin{aligned}
A_5 &= \frac{1}{4\nu}\left[T_2 + T_4\right] = \frac{M}{2\nu}A_3^{BT} \\
A_6 &= \frac{1}{4\nu}\left[T_2 - T_4\right] = -\frac{M}{2}A_4^{BT} + \frac{4M^2 - t}{16\nu}A_6^{BT} \,,
\end{aligned} \tag{3.15}
$$

These equations also provide relations to the invariant amplitudes A_i^{BT} introduced by Bardeen and Tung [Bar 68]. All amplitudes $A_i(\nu, t)$ are even functions of ν, due to the crossing invariance of the Compton tensor, have neither kinematical singularities nor kinematical constraints, and their dimension is GeV^{-3}.

3.1.3 Observables

The unpolarized differential c.m. cross section is given by

$$
\frac{d\sigma}{d\Omega_{cm}} = \frac{1}{64\pi^2 s}\,\Sigma\bar{\Sigma}|T_{fi}|^2 \,, \tag{3.16}
$$

where $\Sigma\bar{\Sigma}$ denotes the sum over final and average over initial particle polarizations. In terms of the invariant amplitudes T_i, it reads

$$
\begin{aligned}
\frac{d\sigma}{d\Omega_{cm}} = \frac{1}{64\pi^2 s} \quad & \Big\{ \frac{1}{2}(4M^2 - t)\,\left(|T_1|^2 + |T_3|^2\right) \\
& - \frac{1}{2}(s - M^2)(u - M^2)\,\left(|T_2|^2 + |T_4|^2\right) \\
& + M(s - u)\,\mathrm{Re}(T_1 T_2^* + T_3 T_4^*) \\
& - t|T_5|^2 + (M^4 - su)|T_6|^2 \Big\}
\end{aligned} \tag{3.17}
$$

3.1.4 Mandelstam plane for Compton scattering

We now apply the DR formalism to real Compton scattering off the nucleon. We start considering the analytical structure of the invariant Compton amplitudes of 3.1.1 in the Mandelstam plane. Due to the crossing symmetry of the Compton amplitude with respect to either nucleon or photon crossing, the natural choice of the independent variables is t and $\nu = \frac{s-u}{4M}$ instead of s and u. In Fig. 3.3, the variables s, t, and u are shown in the $\nu - t$ plane . The straight lines

$$t = 2M^2 \pm 4M\nu \tag{3.18}$$

correspond to the axes $s = 0$ and $u = 0$, respectively. The energy threshold for the reaction in the s-channel is given by

$$s = M^2 \tag{3.19}$$

as the lightest possible intermediate state in this channel is the single nucleon. The region where the Compton scattering angle is physical lies between the forward scattering line

$$t = 0 \tag{3.20}$$

and the hyperbolic boundary line,

$$t = -\frac{(s-M^2)^2}{s}\,, \tag{3.21}$$

which corresponds to backward scattering. The physical region for the u-channel reaction is obtained from the s-channel by crossing, $\nu \to -\nu$.
The threshold of the t-channel process $\gamma\gamma \to N\bar{N}$ is

$$t = (2M)^2\,. \tag{3.22}$$

The physical region lies above the line

$$4M^2\nu^2 = t\left(\frac{t}{4} - M^2\right)\,. \tag{3.23}$$

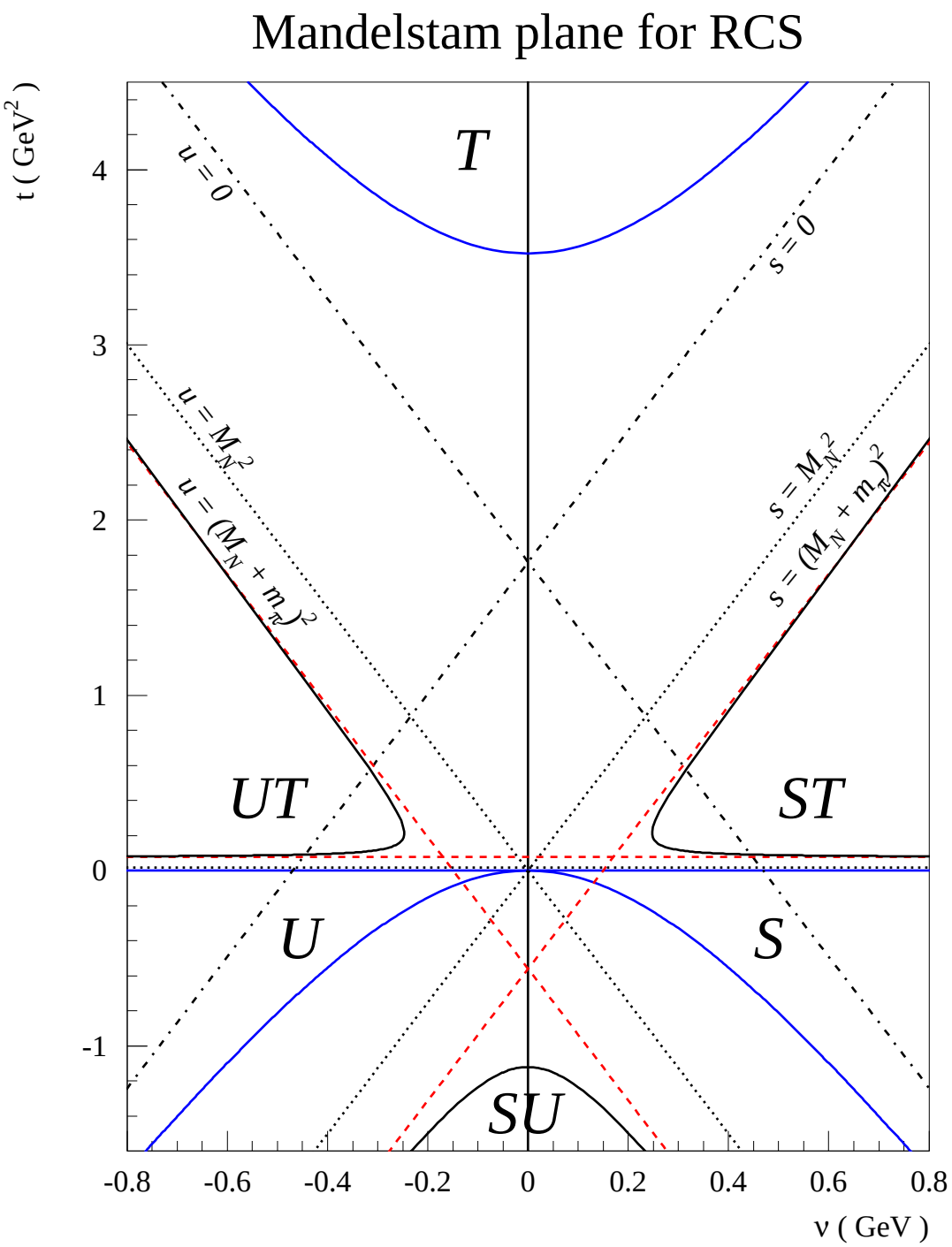

Figure 3.3: Mandelstam plot for real Compton scattering. The kinematical regions for real Compton scattering are shown on the plane of ν and t. The dashed-dotted lines show the axes $s = 0$ and $u = 0$. The dotted straight lines correspond to the poles in the three channels (see text), whereas the dashed lines show the inelastical thresholds in the s, t and u-channels. The area below the line $t = 0$ and above the solid parabolic line at negative t's, corresponds to the physical scattering region for s-channel reaction, at positive values of ν, and for u-channel reaction otherwise. The region above the parabola at positive t gives the scattering region of t-channel process.

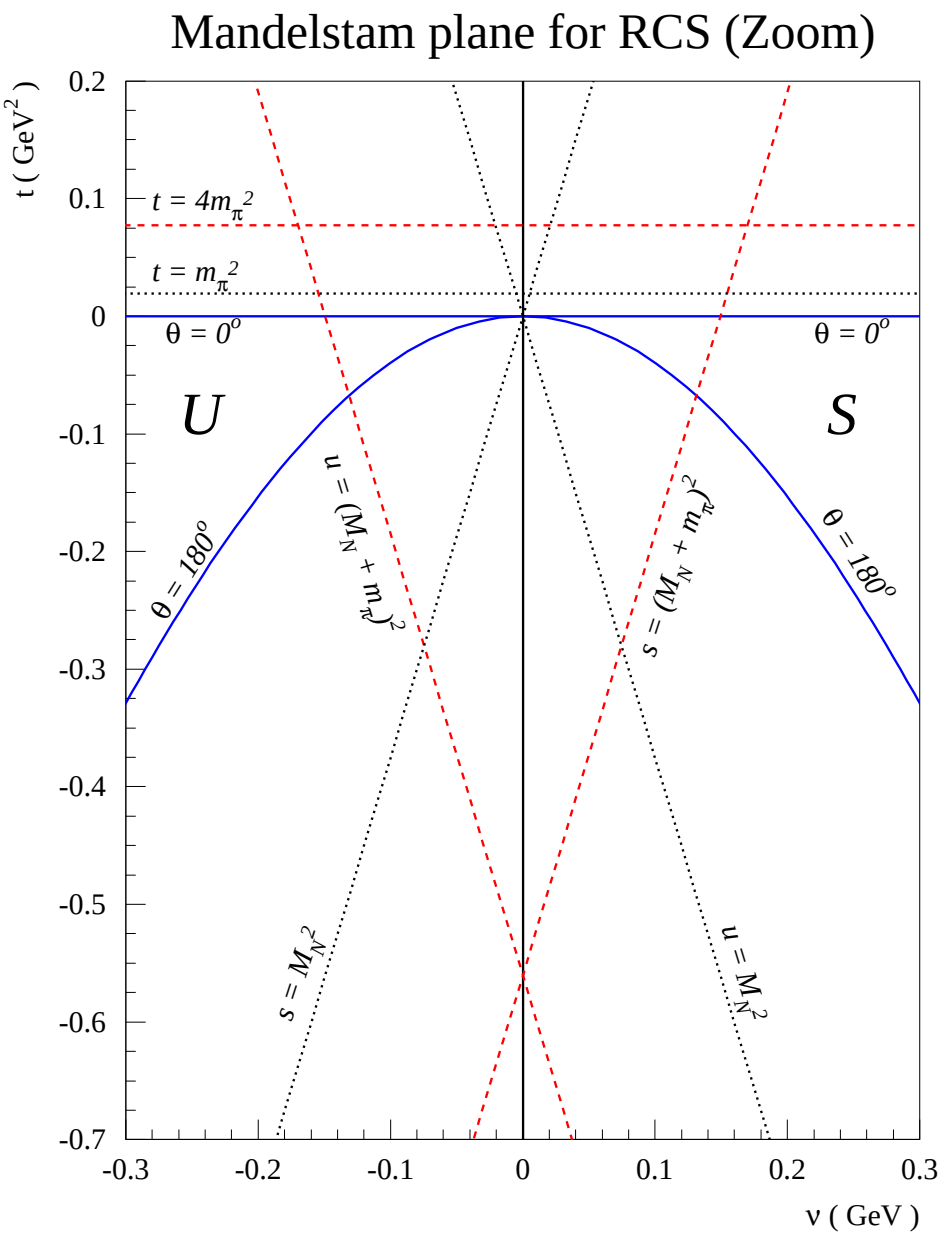

Figure 3.4: Zoomed version of Fig. 3.3. Inside the triangle formed by the three inelastic thresholds in three channels (dashed lines), the Compton amplitude is purely real.

We next turn to the singularities of the invariant amplitudes in the $\nu - t$ plane. The poles at $s = M^2$ and $u = M^2$ are due to one-nucleon intermediate states in the $s-$ and u-channels, respectively. In the t-channel, the π^0 can be exchanged, giving rise to the pole at $t = m_\pi^2$. The positions of the poles are shown by the dotted lines.
The further singularities are the branch cuts given by dashed lines, which correspond to the possibility to produce two or more on-shell particles in the intermediate state. In the s- and u-channels, this is possible if $s \geq (M+m_\pi)^2$, or $u \geq (M+m_\pi)^2$, respectively. In the t-channel, two pions can be produced for $t \geq 4m_\pi^2$. Thus, in the triangle formed by the denoted lines around the origin, the Compton amplitude is purely real, because all variables are below their inelastic thresholds. This area is shown in a larger scale in Fig. 3.4. The only common point of the kinematical s- and u-channel regions, $s = u = M^2$ and $t = 0$, corresponds to the low energy limit, $q' \to 0$, and is the point where the polarizabilities of real Compton scattering are defined.
We now define the spectral regions of the Mandelstam representation. For the $s-t$ spectral region, the corresponding Cutkosky diagram is shown in Fig. 3.5.

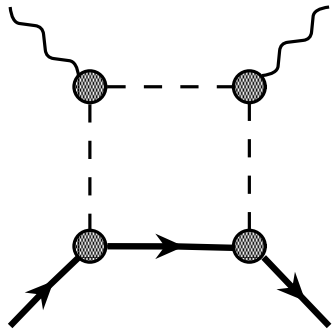

Figure 3.5: Cutkosky diagram for $s-t$ spectral region for real Compton scattering

An analogous calculation as was carried out in the previous section, requires the integral

$$\int d\Omega_{q_n} \frac{1}{(t' - m_\pi^2)(t'' - m_\pi^2)} \tag{3.24}$$

to be singular. Here,

$$\begin{aligned} t &= -2\omega_{cm}^2 + 2\vec{q}\cdot\vec{q}' \\ t' &= m_\pi^2 - 2\omega_{cm}E_\pi + 2\vec{q}\cdot\vec{q}_\pi \\ t'' &= m_\pi^2 - 2\omega_{cm}E_\pi + 2\vec{q}'\cdot\vec{q}_\pi\,, \end{aligned} \tag{3.25}$$

where ω_{cm} is the c.m. photon energy, defined in Sec. 3.1.1, $\vec{q}$ and $\vec{q}'$ are the c.m. three-momenta of the incoming and outgoing photons, respectively. Furthermore, the c.m. energy of the pion in the intermediate state is given by $E_\pi = \frac{s-M^2+m_\pi^2}{2\sqrt{s}}$, and $\vec{q}_\pi$ its three momentum with $\vec{q}_\pi{}^2 = \frac{[s-(M+m_\pi)^2][s-(M-m\pi)^2]}{4s}$. After introducing the integration over the Feynman parameter y and performing the angular integration (see 2.4), the integral becomes

$$\int d\Omega_{q_n} \frac{1}{(t'-m_\pi^2)(t''-m_\pi^2)} \;=\; \pi \int_0^\infty dy \frac{1}{m_\pi^2 \omega_{cm}^2 (1+y)^2 - y t q_\pi^2} \,. \tag{3.26}$$

The denominator has zeroes provided the discriminant is non-negative, i.e.

$$t q_\pi^2 - 4 m_\pi^2 \omega^2 \;\geq\; 0 \,, \tag{3.27}$$

or, in terms of the invariants,

$$t \left[s - (M_N + m_\pi)^2 \right] \left[s - (M_N - m_\pi)^2 \right] - 4 m_\pi^2 \left(s - M_N^2 \right)^2 \;\geq\; 0 \,. \tag{3.28}$$

This inequality defines the $s-t$ spectral region, the area with the asymptotas $s = (M+m_\pi)^2$ and $t = 4m_\pi^2$. The $u-t$ spectral region is its reflection to negative ν-values. In order to determine the kinematical region where intermediate states in the s and u-channels are simultaneously possible, Fig. 3.6 has to be considered,

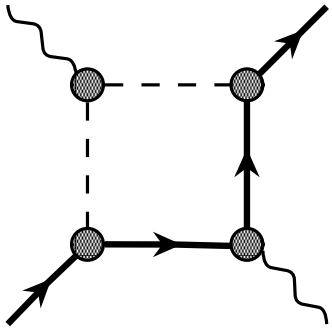

Figure 3.6: Cutkosky diagram for *su*-spectral region for real Compton scattering

The calculation leads to the expression

$$\left[s - (M_N + m_\pi)^2 \right] \left[u - (M_N + m_\pi)^2 \right] - (m_\pi^2 + 2 M_N m_\pi) \;\geq\; 0 \tag{3.29}$$

for the spectral region.

3.2 Fixed-t dispersion relations

In the framework of fixed-t dispersion relations, we use the analyticity of the invariant amplitudes $A_i(\nu, t)$ in ν. We explicitly separate out the Born (pole) part and apply Cauchy's theorem to the residual amplitude, which has no poles in energy. The symmetric Cauchy contour runs from $-\nu_{max}$ to ν_{max} along the real ν-axis, and closes by the semicircle of radius ν_{max} in the upper half of the complex ν-plane.

$$A_i^{NB}(\nu, t) \;=\; \frac{1}{2\pi i} \oint \frac{A_i^{NB}(\nu', t)}{\nu' - \nu - i\varepsilon} d\nu' \;=\; \left[\int_C + \int_{-\nu_{max}}^{\nu_{max}} \right] \frac{A_i^{NB}(\nu', t)}{\nu' - \nu - i\varepsilon} d\nu' \,, \tag{3.30}$$

The crossing behaviour of the amplitudes, $A_i(-\nu,t) = A_i(\nu,t)$, together with the Schwarz reflection rule, $A_i(\nu^*,t) = A_i^*(\nu,t)$ allows us to combine the positive and the negative region s of the integral,

$$\mathrm{Re}A_i^{NB}(\nu,t) \;=\; \frac{2}{\pi}\,\mathcal{P}\int_{\nu_{thr}}^{\nu_{max}} d\nu'\,\frac{\nu'\;\mathrm{Im}_s A_i(\nu',t)}{\nu'^2-\nu^2} \;+\; A_i^{as}(\nu,t)\,, \tag{3.31}$$

with $\mathrm{Im}_s A_i$ the discontinuities across the s-channel cut of the Compton process which start at $\nu_{thr} = m_\pi + (m_\pi^2 + t/2)/(2M)$. The term A_i^{as} represents the integral over the semi-circle in the complex plane. We let now $\nu_{max} \to \infty$ and investigate the convergence of the integrals and the behaviour of the asymptotic part.

3.2.1 Regge behaviour of the invariant amplitudes

In the Regge limit, $\nu \gg t$, the energy dependene of the helicity amplitudes is governed by meson exchange in the t-channel,

$$T_{\lambda'\lambda'_N,\lambda\lambda_N} \;\sim\; \nu^{\alpha(t)}\,, \tag{3.32}$$

where $\alpha(t)$ is the Regge trajectory, depending on the quantum numbers of the helicity amplitude. From the relations between the amplitudes A_i and the Compton helicity amplitudes, we obtain in the Regge limit the following asymptotical relations:

$$\begin{aligned}
A_1 &\sim \frac{1}{Mt}T_{1\frac12,-1\frac12} - \frac{1}{4M\sqrt{-t}\nu}\left(T_{-1-\frac12,1\frac12}+T_{1-\frac12,-1\frac12}\right)\\
A_2 &\sim \frac{2}{(-t)^{3/2}}T_{1-\frac12,-1\frac12} - \frac{1}{2M^2\nu}T_{-1-\frac12,1\frac12} - \frac{1}{2M\nu\sqrt{-t}}T_{1-\frac12,-1\frac12}\\
A_3 &\sim \frac{1}{(2\nu)^3}\left(T_{1\frac12,1\frac12}+T_{-1\frac12,-1\frac12}\right) + \frac{1}{2\nu^2\sqrt{-t}}T_{1-\frac12,1\frac12}\\
A_4 &\sim \frac{1}{(2\nu)^3}\left(T_{1\frac12,1\frac12}-T_{-1\frac12,-1\frac12}\right) + \frac{2\sqrt{-t}}{(2\nu)^4}T_{1-\frac12,1\frac12}\\
A_5 &\sim \frac{1}{4M\nu^2}T_{1\frac12,-1\frac12} - \frac{1}{4\sqrt{-t}\nu^2}\left(T_{-1-\frac12,1\frac12}+T_{1-\frac12,-1\frac12}\right)\\
A_6 &\sim -\frac{1}{8M\nu^2}\left(T_{1\frac12,1\frac12}+T_{-1\frac12,-1\frac12}\right) + \frac{1}{2\sqrt{-t}\nu^2}T_{1-\frac12,1\frac12}\,,
\end{aligned} \tag{3.33}$$

where we keep only leading coefficients of the helicity amplitudes. The asymptotical energy dependence of the invariant amplitudes is then

$$A_{1,2} \sim \nu^{\alpha(t)}\,, \qquad A_{3,5,6} \sim \nu^{\alpha(t)-2}\,, \qquad A_4 \sim \nu^{\alpha(t)-3}\,. \tag{3.34}$$

For meson trajectories, $\alpha_M \lesssim 1$, whereas for the soft pomeron, $\alpha_P = 1.08$. As a consequence the dispersion integrals converge for $A_{3,4,5,6}$, and the corresponding asymptotical parts vanish. These four amplitudes therefore obey the unsubtracted dispersion relations

$$\mathrm{Re}A_i^{NB}(\nu,t) \;=\; \frac{2}{\pi}\,\mathcal{P}\int_{\nu_{thr}}^{\infty} d\nu'\,\frac{\nu'\;\mathrm{Im}_s A_i(\nu',t)}{\nu'^2-\nu^2}\,, \quad \text{for } i=3,4,5,6\,. \tag{3.35}$$

However, for A_1 and A_2, such dispersion relations diverge, and the asymptotical contributions do not vanish. The method suggested by L'vov et al. [L'vo 97] is to cut off the integrals at some appropriate (sufficiently large but finite) value of ν_{max}. In the actual calculations, the s-channel integral is typically evaluated up to a maximum photon energy $E_\gamma = \nu_{max}(t) - t/(4M) \approx 1.5$GeV, for which the imaginary part of the amplitudes can be expressed through unitarity by the meson photoproduction amplitudes (mainly 1π and 2π photoproduction) taken from experiment. All contributions from higher energies are then absorbed in the asymptotic term, which is replaced by a finite number of energy independent poles in the t channel. In particular, the asymptotic part of A_1 is parametrized by the exchange of a scalar particle in the t channel, i.e. an effective "σ meson"[L'vo 97],

$$A_1^{as}(\nu,t) \approx A_1^{\sigma}(t) \;=\; \frac{F_{\sigma\gamma\gamma}\, g_{\sigma NN}}{t - m_\sigma^2}\;, \tag{3.36}$$

where m_σ is the σ mass, and $g_{\sigma NN}$ and $F_{\sigma\gamma\gamma}$ are the couplings of the σ to nucleons and photons respectively. In a similar way the asymptotic part of A_2 is described by the π^0 t-channel pole.

This procedure is relatively safe for A_2 because of the dominance of the π^0 pole or triangle anomaly, which is well established both experimentally and on general grounds as Wess-Zumino-Witten term. However, it introduces a considerable model-dependence in the case of A_1. Though σ mesons have been repeatedly reported in the past, their properties were never clearly established. Therefore, this particle should be interpreted as a parametrization of the $I = J = 0$ part of the two-pion spectrum, which shows up differently in different experiments and hence has been reported with varying masses and widths.

3.2.2 Fixed-t subtracted dispersion relations

It is the aim of our present contribution to avoid the convergence problem of unsubtracted DR and the phenomenology necessary to determine the asymptotic contribution. The alternative we shall pursue in the following is to consider DR at fixed t that are once subtracted at $\nu = 0$,

$$\mathrm{Re}A_i^{NB}(\nu,t) \;=\; A_i^{NB}(0,t) \;+\; \frac{2}{\pi}\,\nu^2\,\mathcal{P}\int_{\nu_{thr}}^{+\infty} d\nu'\;\frac{\mathrm{Im}_s A_i(\nu',t)}{\nu'\,(\nu'^2-\nu^2)}\;. \tag{3.37}$$

These subtracted DR should converge for all 6 invariant amplitudes due to the two additional powers of ν' in the denominator, and they are essentially saturated by the πN intermediate states as will be shown in section 3.3. In other words, the lesser known contributions of two and more pions as well as higher continua are small and may be treated reliably by simple models.

The price to pay for this alternative is the appearance of the subtraction functions $A_i(\nu = 0, t)$, which have to be determined at some small (negative) value of t. We do this by setting up once-subtracted DR, this time in the variable t,

$$\begin{aligned} A_i^{NB}(0,t) &= A_i^{NB}(0,0) + \left[A_i^{t-pole}(0,t) - A_i^{t-pole}(0,0)\right] \\ &+ \frac{t}{\pi}\int_{(2m_\pi)^2}^{+\infty} dt' \, \frac{\mathrm{Im}_t A_i(0,t')}{t'\,(t'-t)} - \frac{t}{\pi}\int_{-\infty}^{-2m_\pi^2-4Mm_\pi} dt' \, \frac{\mathrm{Im}_t A_i(0,t')}{t'\,(t'-t)} \,, \end{aligned} \tag{3.38}$$

where $A_i^{t-pole}(0,t)$ represents the contribution of poles in the t channel, in particular of the π^0 pole in the case of A_2, which is given by

$$A_2^{\pi^0}(0,t) = \frac{F_{\pi^0\gamma\gamma}\, g_{\pi NN}}{t - m_\pi^2} \,. \tag{3.39}$$

The coupling $F_{\pi^0\gamma\gamma}$ is determined through the $\pi^0 \to \gamma\gamma$ decay as

$$\Gamma\left(\pi^0 \to \gamma\gamma\right) = \frac{1}{64\pi} m_{\pi^0}^3 F_{\pi^0\gamma\gamma}^2 \,. \tag{3.40}$$

Using $\Gamma\left(\pi^0 \to \gamma\gamma\right)$ = 7.74 eV [PDG 98], one obtains $F_{\pi^0\gamma\gamma}$ = -0.0252 GeV^{-1}, the sign being in accordance with the $\pi^0\gamma\gamma$ coupling in the chiral limit, given by the Wess-Zumino-Witten effective chiral Lagrangian. The πNN coupling is taken from Ref.[Arn 98] : $g_{\pi NN}^2/4\pi$ = 13.72, which yields $F_{\pi^0\gamma\gamma} g_{\pi NN} \approx$ -0.331 GeV^{-1} for the product of the couplings in Eq. (3.39).

The imaginary part in the integral from $4m_\pi^2$ to $+\infty$ in Eq.(3.39) can be expressed by unitarity through the possible intermediate states for the t-channel process (see Fig.3.7), which lead to cuts along the positive t-axis.

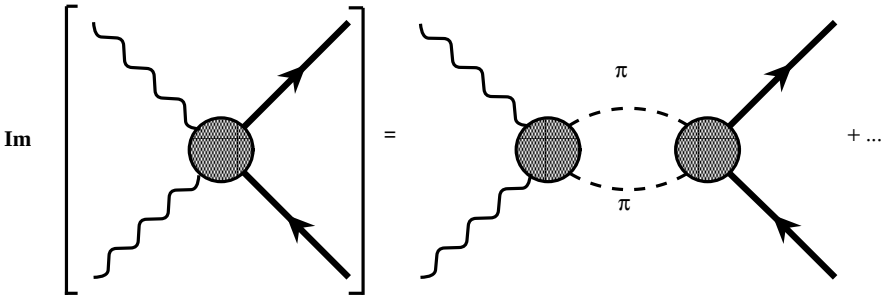

Figure 3.7: Unitarity diagram in the t-channel

For values of t below $K\bar{K}$ threshold, the t-channel discontinuity is dominated by $\pi\pi$ intermediate states.

The second integral in Eq. (3.39) extends from $-\infty$ to $a = -2(m_\pi^2 + 2Mm_\pi) \approx -0.56$ GeV^2 and is due to inelastic thresholds simultaneously open in the s and u-channels.

One should not be misled by the similarity of the definitions of this region and the double spectral $s-u$ region in the section 3.1.4. The latter one corresponds to the integration limits in the variables s and u of the double integral representation of section 2.4, whereas the former one corresponds to the one-dimensional dispersion relations.

For small (negative) values of t, the integral from $-\infty$ to a will be suppressed, as compared to the positive-t integral, by the denominator of the subtracted DR. We therefore approximate the imaginary part along the negative t-axis by the dominant contribution of the $\Delta(1232)$ resonance. The corresponding formulas are given in the Appendix C.1.

The t dependence of the subtraction functions $A_i(0,t)$ is now determined, and only the subtraction constants $A_i(0,0)$ remain to be fixed. We note that the quantities

$$a_i = A_i(0,0) \; - \; A_i^B(0,0) \tag{3.41}$$

are directly related to the polarizabilities. For the spin-independent (scalar) polarizabilities α and β, one finds the two combinations

$$\alpha+\beta \;\; = \;\; -\frac{1}{2\pi}\,(a_3 \,+\, a_6)\,, \tag{3.42}$$

$$\alpha-\beta \;\; = \;\; -\frac{1}{2\pi}\,a_1\,, \tag{3.43}$$

related to forward and backward Compton scattering, respectively. Furthermore, the forward combination $\alpha+\beta$ is related to the total absorption spectrum through Baldin's sum rule [Bal 60],

$$(\alpha+\beta)_N \;\; = \;\; \frac{1}{2\pi^2}\int_{\nu_{thr}}^{\infty} d\nu'\,\frac{\sigma(\gamma N\to X)}{\nu'^2}\,. \tag{3.44}$$

The 4 spin-dependent (vector) polarizabilities γ_1 to γ_4 of Ragusa [Rag 93] are defined by

$$\gamma_0 \;\; \equiv \;\; \gamma_1-\gamma_2-2\gamma_4 \;=\; \frac{1}{2\pi M}\,a_4\,, \tag{3.45}$$

$$\gamma_{13} \;\; \equiv \;\; \gamma_1+2\gamma_3 \;=\; -\,\frac{1}{4\pi M}\,(a_5 \,+\, a_6)\,, \tag{3.46}$$

$$\gamma_{14} \;\; \equiv \;\; \gamma_1-2\gamma_4 \;=\; \frac{1}{4\pi M}\,(2\,a_4 \,+\, a_5 \,-\, a_6)\,, \tag{3.47}$$

$$\gamma_\pi \;\; \equiv \;\; \gamma_1+\gamma_2+2\gamma_4 \;=\; -\,\frac{1}{2\pi M}\,(a_2 \,+\, a_5)\,, \tag{3.48}$$

where γ_0 and γ_π are the spin polarizabilities in the forward and backward directions, respectively. Since the π^0 pole contributes to A_2 only, the combinations γ_0, γ_{13} and γ_{14} of Eqs. (3.45)-(3.47) are independent of this pole term [Dre 98d], and only the backward spin polarizability γ_π is affected by the anomaly.

Although all 6 subtraction constants a_1 to a_6 of Eq. (3.41) could be used as fit parameters, we shall restrict the fit to the parameters a_1 and a_2, or equivalently to $\alpha-\beta$ and γ_π. The subtraction constants a_4, a_5 and a_6 will be calculated through an unsubtracted sum rule, as derived from Eq. (3.31),

$$a_{4,5,6} \;=\; \frac{2}{\pi}\int_{\nu_{thr}}^{+\infty} d\nu' \,\frac{\mathrm{Im}_s A_{4,5,6}(\nu', t=0)}{\nu'}\,. \tag{3.49}$$

The remaining subtraction constant a_3, which is related to $\alpha+\beta$ through Eq.(3.42), will be fixed through Baldin's sum rule, Eq.(3.44), using the value obtained in Ref.[Bab 98] : $\alpha+\beta = 13.69$.

3.3 s-channel dispersion integral

In this section we describe the calculation of the *s*-channel contributions, which enter the once-subtracted dispersion integral of Eq. (3.37) and the calculation of subtraction constants a_4, a_5 and a_6 through Eq. (3.49). The imaginary part of the Compton amplitude due to the *s*-channel cuts is determined from the scattering amplitudes of photoproduction on the nucleon by the unitarity relation

$$2\,\mathrm{Im}_s\, T_{fi} = \sum_X (2\pi)^4 \delta^4(P_X - P_i) T^\dagger_{Xf}\, T_{Xi}\,, \tag{3.50}$$

where the sum runs over all possible states that can be formed in the photon-nucleon reaction. Due to the energy denominator $1/\nu'(\nu'^2-\nu^2)$ in the subtracted dispersion integrals, the most important contribution is from the πN intermediate states, while mechanisms involving more pions or heavier mesons in the intermediate states are largely suppressed. In our calculation, we evaluate the πN contribution using the multipole amplitudes from the analysis of Hanstein, Drechsel and Tiator (HDT) [Han 98] at energies $E_\gamma \leq 500$ MeV, and at the higher energies we take as input the SAID multipoles (SP98K solution) [SAID]. The expansion of $\mathrm{Im}_s A_i$ into this set of multipoles is truncated at a maximum angular momentum $j_{max} = l \pm 1/2 = 7/2$, with the exception of the lower energy range ($E_\gamma \leq 400$ MeV) where we use $j_{\max} = 3/2$. The higher partial waves with $j \geq j_{max}+1$ are evaluated analytically in the one-pion exchange (OPE) approximation. The relevant formulas to implement the calculation are reported in Appendices B and C of Ref.[L'vo 97].

We note that the pion photoproduction multipoles below two-pion threshold were derived in Ref.[Han 98] by use of Watson's theorem, assuming that these multipoles carry the phases of pion-nucleon scattering. As pointed out by Ref.[Ben 92], unitarity also requires to account for the phases of photon-nucleon scattering, δ_i^{C}, which is $O(e^2)$ relative to the strong phase. Moreover, consistency requires that isospin-breaking effects be included at the level of the strong scattering amplitudes [Ben 92]. Such considerations are of big potential interest, particularly in the threshold region where the pion mass difference becomes important or in studies of the small electric quadrupole strength in the Δ region. However such effects are beyond the scope of our present work, in particular because only the imaginary part of the amplitudes is needed

as input for DR. As may be seen from Eq.(11) of Ref.[Ben 92], this imaginary part is a function of $\cos\delta_i^C$, i.e. corrections are expected to be of order $O(e^4)$.

The multipion intermediate states are approximated by the inelastic decay channels of the πN resonances. In the spirit of Ref.[L'vo 97] and the more recent work of Ref.[Dre 99b], we assume that this inelastic contribution follows the helicity structure of the one-pion photoproduction amplitudes. In this approximation, we first calculate the resonant part of the pion photoproduction multipoles using the Breit-Wigner parametrization of Ref.[Arn 90], which is then scaled by a suitable factor to include the inelastic decays of the resonances. The resulting contribution to $\mathrm{Im}_s A_i$ is

$$[\mathrm{Im}_s A_i]^{(N^*\to\pi\pi N,\eta N,\ldots)} = R\,[\mathrm{Im}_s A_i]^{(N^*\to\pi N)}, \tag{3.51}$$

with the ratio R given by

$$R = \frac{1-B_\pi}{B_\pi}\frac{\bar{\Gamma}_{\mathrm{inel}}(W)}{\Gamma_\pi(W)}. \tag{3.52}$$

In Eq.(3.52), B_π is the single-pion branching ratio of the resonance N^* and $\bar{\Gamma}_\pi(W)$ the energy-dependent pionic width [Arn 90], while the inelastic widths $\bar{\Gamma}_{\mathrm{inel}}(W)$ of the decays $N^*\to(\pi\pi N,\eta N,\pi\pi\pi N,..)$ are parametrized as in Ref.[L'vo 97] in order to provide the correct threshold behavior for the resonant two-pion contribution.

The πN channel consistently reproduces the measured photoabsorption cross section in the energy range $E_\gamma \leq 500$ MeV, while at the higher energies nonresonant mechanisms should be included to fully describe the multipion channels. In Ref.[L'vo 97], the nonresonant contribution to the two-pion photoproduction channel was approximately taken into account by calculating the OPE diagram of the $\gamma N\to\pi\Delta$ reaction. The difference between the data and the model for two-pion photoproduction consisting of resonant mechanisms plus the OPE diagram for the nonresonant mechanism, was then fitted in Ref.[L'vo 97] and attributed to a phenomenological, nonresonant $\gamma N\to\pi\Delta$ s-wave correction term.

A more detailed description of the $\pi\pi N$ channel is clearly worthwhile to be undertaken, especially in view of the new two-pion photoproduction data (both unpolarized and polarized) that will be available from MAMI and JLab (CLAS) in the near future. However, for the extraction of the polarizabilities, the strategy followed in this paper is to minimize the sensitivity and hence model dependence with regard to these higher channels.

In Fig.3.8 we show that in subtracted DR, the sensitivity to the multipion channels is indeed very small and that subtracted DR are essentially saturated at $\nu \approx 0.4$ GeV.

The importance of the multipion channels is even weaker in the case of the amplitudes A_3 to A_6. For unsubtracted DR, on the other hand, the influence of the multipion channels amounts to about 30 % for the amplitude A_2.

In Table I and II, we show our dispersion predictions for the spin polarizabilities of proton and neutron, respectively. We list the separate contribution of the πN channel, HDT(1π), and the total result, HDT, which includes the inelastic resonance channels. The last column shows the values of the dispersion calculation of Ref.[Bab 98b], which is based on the one-pion multipoles of SAID-SP97K and the model for double-pion production mentioned above. The small differences between the one-pion multipoles of SAID-SP97K and SAID-SP98K at the higher energies are practically negligible for the spin polarizabilities, while the results are very sensitive to the differences between the HDT and SAID analyses. As discussed in Ref.[Dre 98c], this fact is mainly due to wrong threshold behavior of the E_{0+} partial wave, giving rise to substantial effects in the case of the forward spin polarizability. While the one-pion contributions from SAID-SP98K are $\gamma_0^p = -1.26$ and $\gamma_0^n = -0.03$, we obtain $\gamma_0^p = -0.75$ and $\gamma_0^n = -0.06$ with the HDT multipoles for $E_\gamma \leq 500$ MeV. However, the more recent versions of SAID respect the low energy theorem.

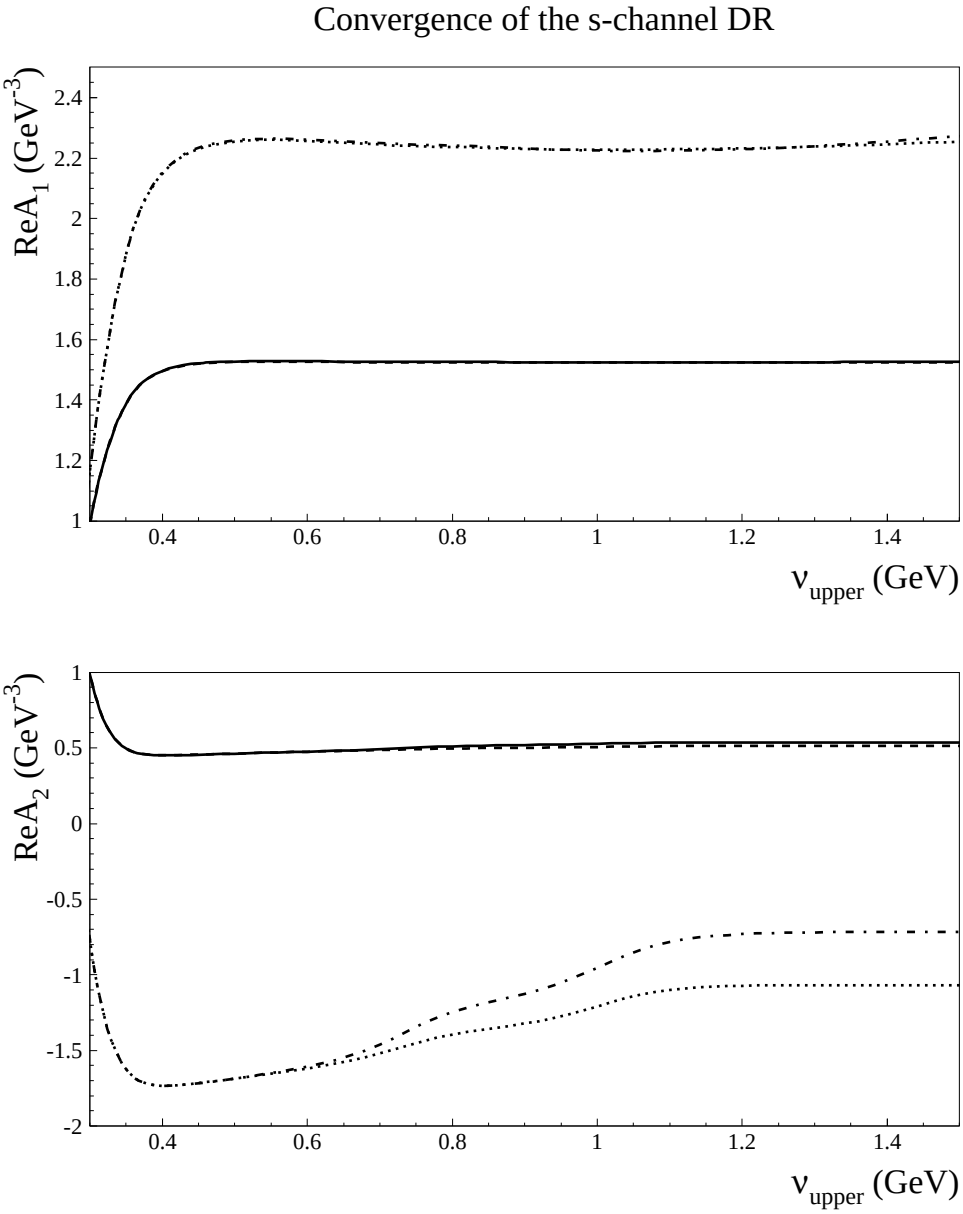

Figure 3.8: Convergence of the *s*-channel integral for the amplitudes A_1 and A_2. Results for the unsubtracted dispersion integral for the one-pion channel (dotted lines) and including the two-pion channel (dashed-dotted lines) are shown in comparison with the subtracted dispersion integral for the one-pion channel (dashed lines) and including the two-pion channel (solid lines), as a function of the upper integration limit ν_{upper}

Table 3.1: The contribution of the dispersion integrals to the spin polarizabilities of the proton. The set HDT(1π) is calculated from the one-pion photoproduction multipoles of the HDT analysis [Han 98], while the column HDT gives the total results with the additional contribution of inelastic resonance channels. The entries in the last column are the predictions of the dispersion calculation of Ref.[Bab 98b].

γ_i-excit.	HDT(1π)	HDT	Ref.[Bab 98b]
$\gamma_1^{(p)}$	+4.83	+4.33	+3.1
$\gamma_2^{(p)}$	-0.81	-0.74	-0.8
$\gamma_3^{(p)}$	-0.30	-0.02	+0.3
$\gamma_4^{(p)}$	+3.19	+2.93	+2.7
$\gamma_o^{(p)}$	-0.75	-0.80	-1.5
$\gamma_{13}^{(p)}$	+4.23	+4.29	+3.7
$\gamma_{14}^{(p)}$	-1.56	-1.53	-2.3
$\gamma_\pi^{(p)}$	+10.41	+9.46	+7.8

Table 3.2: The contribution of the dispersion integrals to the spin polarizabilities of the neutron. Notation as in Table 3.1

γ_i-excit.	HDT(1π)	HDT	Ref.[Bab 98b]
$\gamma_1^{(n)}$	+7.10	+7.00	+6.3
$\gamma_2^{(n)}$	-0.68	-0.68	-0.9
$\gamma_3^{(n)}$	-1.04	-0.99	-0.7
$\gamma_4^{(n)}$	+3.92	+3.88	+3.8
$\gamma_o^{(n)}$	-0.06	-0.09	-0.4
$\gamma_{13}^{(n)}$	+5.02	+5.02	+4.9
$\gamma_{14}^{(n)}$	-0.74	-0.77	-1.3
$\gamma_\pi^{(n)}$	+14.27	+14.09	+13.0

3.4 t-channel dispersion integral

We next evaluate the t-channel dispersion integral of Eq.(3.39) from $4m_\pi^2$ to ∞. The kinematics of the t-channel reaction $\gamma\gamma \to N\bar{N}$ is shown in Fig.3.9.

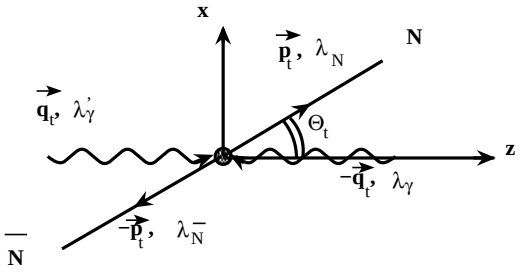

Figure 3.9: Center-of-mass kinematics for the t-channel process

The subtracted dispersion integral is essentially saturated by the imaginary part of the t-channel amplitude $\gamma\gamma \to N\bar{N}$ due to $\pi\pi$ intermediate states. To calculate this contribution, we have to construct the amplitudes $\gamma\gamma \to \pi\pi$ and $\pi\pi \to N\bar{N}$.

We start with the isospin and helicity structure of the $\gamma\gamma \to \pi\pi$ amplitude, denoted by F. Because of the Bose symmetry of the $\gamma\gamma$ state, only the even isospin values $I = 0$ and 2 are possible. We can express the charged ($\gamma\gamma \to \pi^+\pi^-$) and neutral ($\gamma\gamma \to \pi^0\pi^0$) amplitudes in terms of those with good isospin by

$$\begin{aligned} F^{(\pi^+\pi^-)} &= \sqrt{\frac{2}{3}}\,F^{I=0} + \sqrt{\frac{1}{3}}\,F^{I=2} \quad (\textit{charged pions})\,, \\ F^{(\pi^0\pi^0)} &= -\sqrt{\frac{1}{3}}\,F^{I=0} + \sqrt{\frac{2}{3}}\,F^{I=2} \quad (\textit{neutral pions})\,. \end{aligned} \tag{3.53}$$

The reaction $\gamma\gamma \to \pi\pi$ has two independent helicity amplitudes $F_{\Lambda_\gamma}(t, \theta_{\pi\pi})$, where $\Lambda_\gamma \equiv \lambda'_\gamma - \lambda_\gamma$, the difference of the final (λ'_γ) and initial (λ_γ) photon helicities, takes on the values 0 or 2, depending upon whether the photons have the same ($\Lambda_\gamma = 0$) or opposite ($\Lambda_\gamma = 2$) helicities. The $\gamma\gamma \to \pi\pi$ helicity amplitudes depend on t, the c.m. energy squared, and the pion c.m. scattering angle $\theta_{\pi\pi}$. In terms of the helicity amplitudes F_{Λ_γ}, the $\gamma\gamma \to \pi\pi$ differential c.m. cross section is given by

$$\left(\frac{d\sigma}{d\cos\theta_{\pi\pi}}\right)_{\text{c.m.}} = \frac{\beta}{64\pi t}\left\{|F_{\Lambda_\gamma=0}(t,\theta_{\pi\pi})|^2 + |F_{\Lambda_\gamma=2}(t,\theta_{\pi\pi})|^2\right\}\,, \tag{3.54}$$

with $\beta = \sqrt{1-4m_\pi^2/t}$ the pion velocity. In Appendix B.1, we give the partial wave expansion of the $\gamma\gamma \to \pi\pi$ helicity amplitudes $F^I_{\Lambda_\gamma}(t, \theta_{\pi\pi})$ for a state of isospin I, and thus define the partial wave amplitudes $F^I_{J\Lambda_\gamma}(t)$ (see Eqs. (B.6) and (B.10)), where J

can only take on even values.

To construct the helicity amplitudes F_{Λ_γ} for the process $\gamma\gamma \to \pi\pi$, we first evaluate the Born graphs as shown in Fig.3.10.

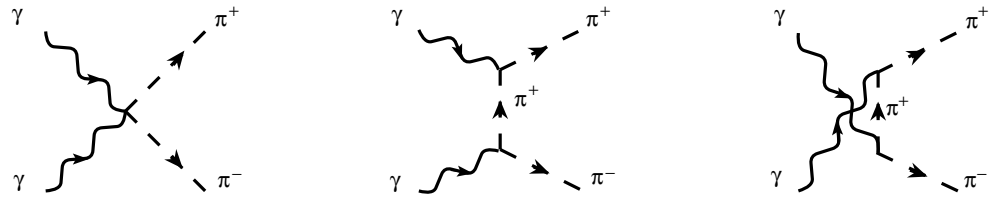

Figure 3.10: Born diagramms for the process $\gamma\gamma \to \pi^+\pi^-$

These graphs only contribute to the charged channel $\gamma\gamma \to \pi^+\pi^-$. The Born contributions to the helicity amplitudes $F_{\Lambda_\gamma}^{(\pi^+\pi^-)}$ are denoted as B_{Λ_γ} and given by

$$\begin{aligned} B_{\Lambda_\gamma=0}(t,\theta_{\pi\pi}) &= 2e^2\,\frac{1-\beta^2}{1-\beta^2\cos^2\theta_{\pi\pi}}\,, \\ B_{\Lambda_\gamma=2}(t,\theta_{\pi\pi}) &= 2e^2\,\frac{\beta^2\sin^2\theta_{\pi\pi}}{1-\beta^2\cos^2\theta_{\pi\pi}}\,. \end{aligned} \tag{3.55}$$

The partial wave expansion of the Born terms, $B_{J\Lambda_\gamma}(t)$, is discussed in Appendix B.1 (Eq. (B.11)). As the Born amplitudes are only non-zero for the charged pion channel, the two isospin amplitudes of Eq. (3.53) are related by

$$B^{I=0}_{J\Lambda_\gamma} = \sqrt{\frac{2}{3}}\,B_{J\Lambda_\gamma}\,, \qquad\qquad B^{I=2}_{J\Lambda_\gamma} = \sqrt{\frac{1}{3}}\,B_{J\Lambda_\gamma}\,. \tag{3.56}$$

We now construct the unitarized amplitudes $F^I_{J\Lambda_\gamma}(t)$, starting from the Born amplitudes $B^I_{J\Lambda_\gamma}(t)$ and following the method outlined in Refs.[Mor 88, Pen 95]. We first note that the low energy theorem requires that each partial wave obeys

$$\frac{F^I_{J\Lambda_\gamma}}{B^I_{J\Lambda_\gamma}} \to 1\,,\ \text{as}\ t \to 0\,. \tag{3.57}$$

Next, the invariant amplitude for the process $\gamma\gamma \to \pi\pi$ is assumed to have Mandelstam analyticity. Each partial wave then has a right-hand cut from $t = 4m_\pi^2$ to $+\infty$ and a left-hand cut from $t = -\infty$ to 0. Though the Born amplitude is real for all values of t, its partial waves are complex below $t = 0$. The partial waves of the full amplitude have no other sources of complexity in this region, and so we can write DR for the difference of the full and the Born amplitudes,

$$\frac{F^I_{J\Lambda_\gamma}(t) - B^I_{J\Lambda_\gamma}(t)}{t(t-4m_\pi^2)^{\frac{J}{2}}} = \frac{1}{\pi}\int_{4m_\pi^2} dt' \, \frac{\mathrm{Im}F^I_{J\Lambda_\gamma}(t')}{t'(t'-4m_\pi^2)^{\frac{J}{2}}(t'-t)}, \tag{3.58}$$

with an additional factor of $(t(t-4m_\pi^2)^{\frac{J}{2}})^{-1}$ providing the right asymptotics for the convergence of the integral. The next step is to evaluate the imaginary part of the amplitude in Eq.(3.58). To do this, we exploit the unitarity condition

$$\mathrm{Im}F^I_{J\Lambda_\gamma}(\gamma\gamma \to \pi\pi) = \sum_n \rho_n \, F^{I*}_{J\Lambda_\gamma}(\gamma\gamma \to n) \; I^I_J(n \to \pi\pi), \tag{3.59}$$

where ρ_n are the appropriate kinematical and isospin factors for the intermediate channels n, and $I(n \to \pi\pi)$ is a hadronic amplitude. Below the next inelastic threshold, it follows from unitarity that the phase $\phi_J^{I\,(\gamma\gamma\to\pi\pi)}$ of each partial wave $F^I_{J\Lambda_\gamma}$ is equal to the phase $\delta^{IJ}_{\pi\pi}$ of the corresponding $\pi\pi \to \pi\pi$ partial wave,

$$\begin{aligned} \mathrm{Im}F^I_{J\Lambda_\gamma}(\gamma\gamma \to \pi\pi) &= \rho_{\pi\pi} \, F^{I*}_{J\Lambda_\gamma}(\gamma\gamma \to \pi\pi) \; I^I_J(\pi\pi \to \pi\pi) \\ &\Downarrow \\ \phi_J^{I\,(\gamma\gamma\to\pi\pi)}(t) &= \delta^{IJ}_{\pi\pi}(t). \end{aligned} \tag{3.60}$$

This fact can be incorporated into the Omnès function, which is constructed to have the phase of the $\pi\pi$ scattering amplitude above $\pi\pi$ threshold, and to be real otherwise,

$$\Omega^I_J(t) = \exp\left[\frac{t}{\pi}\int_{4m_\pi^2} dt' \, \frac{\delta^{IJ}_{\pi\pi}(t')}{t'(t'-t-i\varepsilon)}\right]. \tag{3.61}$$

The function $F^I_{J\Lambda_\gamma}(\Omega^I_J)^{-1}(t)$ is by construction real above $\pi\pi$ threshold, but complex below threshold due to the complexity of the Born partial waves $B^I_{J\Lambda_\gamma}$. Hence we can write a dispersion relation for the function
$\left[F^I_{J\Lambda_\gamma} - B^I_{J\Lambda_\gamma}\right](\Omega^I_J)^{-1}(t)/t(t-4m_\pi^2)^{J/2}$,

$$\begin{aligned} F^I_{J\Lambda_\gamma}(t) &= \Omega^I_J(t) \left\{ B^I_{J\Lambda_\gamma}(t)\,\mathrm{Re}\left[(\Omega^I_J)^{-1}(t)\right] \right. \\ &- \left. \frac{t(t-4m_\pi^2)^{J/2}}{\pi}\int_{4m_\pi^2} dt' \, \frac{B^I_{J\Lambda_\gamma}(t')\,\mathrm{Im}\left[(\Omega^I_J)^{-1}(t')\right]}{t'(t'-4m_\pi^2)^{J/2}(t'-t)} \right\}. \end{aligned} \tag{3.62}$$

For $t > 4m_\pi^2$, this integral is understood to be a principal value integral, which we implement by subtracting the integrand at $t' = t$. In this way we obtain a regular integral, which can be performed without numerical problems,

$$\begin{aligned} F^I_{J\Lambda_\gamma}(t) &= \Omega^I_J(t)\, B^I_{J\Lambda_\gamma}(t) \\ &\cdot \left(\mathrm{Re}\left[(\Omega^I_J)^{-1}(t)\right] + \mathrm{Im}\left[(\Omega^I_J)^{-1}(t)\right] \frac{1}{\pi}\ln\left(\frac{t}{4m_\pi^2} - 1\right) \right) \end{aligned} \tag{3.63}$$

$$- \quad \Omega_J^I(t)\,\frac{t(t-4m_\pi^2)^{J/2}}{\pi}\int_{4m_\pi^2}^{\infty}\frac{dt'}{t'(t'-t)}$$
$$\cdot \quad \left(\frac{B^I_{J\Lambda_\gamma}(t')\,\mathrm{Im}\left[(\Omega_J^I)^{-1}(t')\right]}{(t'-4m_\pi^2)^{J/2}} - \frac{B^I_{J\Lambda_\gamma}(t)\,\mathrm{Im}\left[(\Omega_J^I)^{-1}(t)\right]}{(t-4m_\pi^2)^{J/2}}\right) .$$

In our formalism, the s($J=0$)- and d($J=2$)-waves are unitarized. For the s- and d-wave $\pi\pi$ phaseshifts, we use the solutions that were determined in Ref. [Fro 77]. For the higher partial waves, the corresponding $\pi\pi$ phaseshifts are rather small and not known with good precision. Therefore, we will approximate all higher partial waves ($J \geq 4$) by their Born contribution. The full amplitudes for the charged and neutral channels can then be cast into the forms

$$F_{\Lambda_\gamma}^{(\pi^+\pi^-)}(t,\theta_{\pi\pi}) = B_{\Lambda_\gamma}(t,\theta_{\pi\pi}) + \sum_{J=0,2}\sqrt{2J+1}\sqrt{\frac{(J-\Lambda_\gamma)!}{(J+\Lambda_\gamma)!}} \tag{3.64}$$
$$\cdot \quad \left[\sqrt{\frac{2}{3}}F^{I=0}_{J\Lambda_\gamma}(t) + \sqrt{\frac{1}{3}}F^{I=2}_{J\Lambda_\gamma}(t) - B_{J\Lambda_\gamma}(t)\right] P_J^{\Lambda_\gamma}(\cos\theta_{\pi\pi}) ,$$

$$F_{\Lambda_\gamma}^{(\pi^0\pi^0)}(t,\theta_{\pi\pi}) = \sum_{J=0,2}\sqrt{2J+1}\sqrt{\frac{(J-\Lambda_\gamma)!}{(J+\Lambda_\gamma)!}} \tag{3.65}$$
$$\cdot \quad \left[-\sqrt{\frac{1}{3}}F^{I=0}_{J\Lambda_\gamma}(t) + \sqrt{\frac{2}{3}}F^{I=2}_{J\Lambda_\gamma}(t)\right] P_J^{\Lambda_\gamma}(\cos\theta_{\pi\pi}) .$$

These expressions hold to good precision up to $K\bar{K}$ threshold (≈ 1 GeV^2), because the four-pion intermediate states couple only weakly and give only small inelasticities in the $\pi\pi$ phaseshifts.

In Figs. 3.11 and 3.12, we show our results for the total and differential $\gamma\gamma \to \pi^+\pi^-$ cross sections and a comparison to the existing data. In the threshold region, the charged pion cross sections are clearly dominated by the Born graphs of Fig. 3.10 because of the vicinity of the pion pole in the t channel of the $\gamma\gamma \to \pi^+\pi^-$ process.

However, the results for the unitarized calculation show that s-wave rescattering is not negligible but leads to a considerable enhancement at energies just above threshold. Besides the low-energy structure, which is driven by the Born terms, the $\gamma\gamma \to \pi\pi$ process has a prominent resonance structure at energies corresponding to excitation of the isoscalar $f_2(1270)$ resonance, with mass m_{f_2} = 1275 MeV and width Γ_{f_2} = 185.5 MeV [PDG 98]. The f_2 resonance shows up in the partial wave $F_{J=2\Lambda_\gamma=2}$ as outlined in Appendix B.2. Therefore, the most efficient way to unitarize this particular partial wave is to make a Breit-Wigner ansatz for the f_2 excitation, which is described in Appendix B.2. The Breit-Wigner ansatz for the f_2 contribution to the partial wave $F_{J=2\Lambda_\gamma=2}$ depends upon the couplings $f_2\pi\pi$ and $f_2\gamma\gamma$. The coupling $f_2\pi\pi$ is known from the decay $f_2 \to \pi\pi$ and is taken from Ref. [PDG 98]. The coupling $f_2\gamma\gamma$ is then fitted to the $\gamma\gamma \to \pi\pi$ cross section at the f_2 resonance position, and is consistent with the value quoted in Ref. [PDG 98]. The resulting amplitude, consisting of unitarized s-wave, f_2 excitation and Born terms for all other partial waves (with $J \geq 4$) is seen from Figs. 3.11 and 3.12 to give a rather good description of the $\gamma\gamma \to \pi^+\pi^-$ data up to

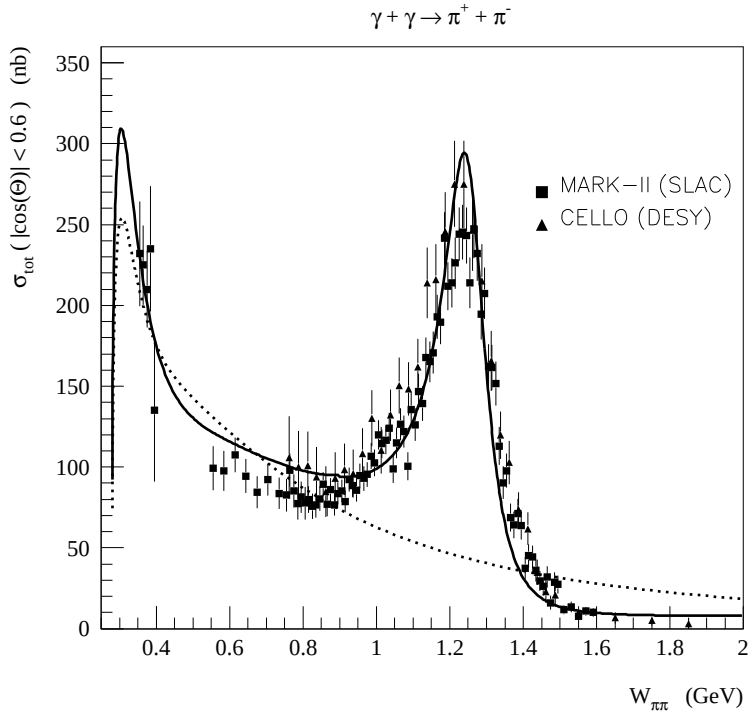

Figure 3.11: Total cross section for the $\gamma\gamma \to \pi^+\pi^-$ reaction as function of the c.m. energy. The dotted line corresponds to the Born contribution alone. The solid line show the full result with unitarized *s*- and *d*-waves and $f_2(1270)$ resonance.

$W_{\pi\pi} \simeq 1.8$ GeV. Only in the region $W_{\pi\pi} \approx 0.7$ - 0.8 GeV, does our description slightly overestimate the data.

Having constructed the $\gamma\gamma \to \pi\pi$ amplitudes, we next need the $\pi\pi \to N\bar{N}$ amplitudes in order to estimate the contribution of the $\pi\pi$ states to the *t*-channel dispersion integral for Compton scattering. As we only kept s- and d-waves for $\gamma\gamma \to \pi\pi$, we will only need the s- and d-waves (J = 0, 2) for $\pi\pi \to N\bar{N}$. For each partial wave J, there are two independent $\pi\pi \to N\bar{N}$ helicity amplitudes $f^J_\pm(t)$, depending on whether the nucleon and anti-nucleon have the same ($f^J_+(t)$) or opposite ($f^J_-(t)$) helicities. We refer the reader to Appendix B.1 (Eqs.(B.7) and (B.9)) for details. In this work, we take the s- and d-waves from the work of H¨ohler and collaborators [H¨oh 83], in which the lowest $\pi\pi \to N\bar{N}$ partial wave amplitudes were constructed from a partial wave solution of pion-nucleon scattering, by use of the $\pi\pi$ phaseshifts of Ref. [Fro 77], which we also used to construct the $\gamma\gamma \to \pi\pi$ amplitudes. In Ref. [H¨oh 83], the $\pi\pi \to N\bar{N}$ amplitudes are given for t values up to $t \approx 40 \cdot m_\pi^2 \approx 0.78$ GeV^2, which will serve well for our purpose since the subtracted *t*-channel dispersion integrals have converged much below this value as shown in the following.

Finally, we can now combine the $\gamma\gamma \to \pi\pi$ and $\pi\pi \to N\bar{N}$ amplitudes to construct the discontinuities of the Compton amplitudes across the *t*-channel cut. In Appendix B.1, we show in detail how the Compton invariant amplitudes $A_1, ..., A_6$ are expressed by the *t*-channel ($\gamma\gamma \to N\bar{N}$) helicity amplitudes. Through unitarity we then express

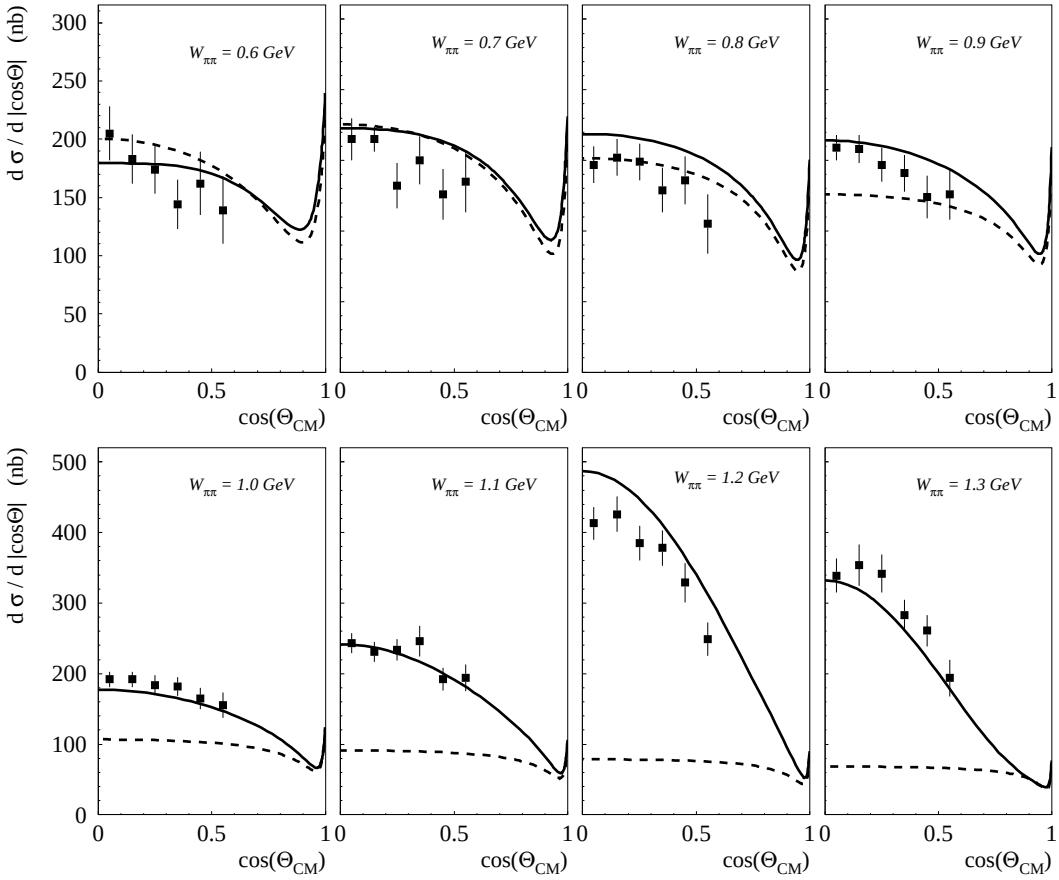

Figure 3.12: Differential cross sections at various c.m. energies for the $\gamma\gamma \to \pi^+\pi^-$ process. The Born contribution (dashed lines) and the result of the unitarization procedure plus $f_2(1270)$ resonance (solid lines) are shown.

the imaginary parts of these t-channel ($\gamma\gamma \to N\bar{N}$) helicity amplitudes in terms of the $\gamma\gamma \to \pi\pi$ and $\pi\pi \to N\bar{N}$ amplitudes. We finally express the discontinuities $\mathrm{Im}_t A_i$ of the invariant amplitudes A_i (i = 1,...,6) in terms of the corresponding $\gamma\gamma \to \pi\pi$ and $\pi\pi \to N\bar{N}$ partial wave amplitudes (see Eq.(B.13)). As we restrict ourselves to s- and d-wave intermediate states in the actual calculations, we give the expressions at $\nu = 0$, including s- and d-waves only, that are needed for the subtracted t-channel dispersion integral of Eq.(3.39),

$$
\begin{aligned}
\mathrm{Im}_t A_1(\nu=0,t)^{2\pi} &= -\sqrt{\frac{t/4-m_\pi^2}{t}}\,\frac{1}{t\,(M^2-t/4)}\,F_{0\Lambda_\gamma=0}(t)\;f_+^{0*}(t) \\
&\quad -\left(\frac{t/4-m_\pi^2}{t}\right)^{3/2}\,\frac{\sqrt{5}}{2}\,F_{2\Lambda_\gamma=0}(t)\;f_+^{2*}(t)\,, \\
\mathrm{Im}_t A_2(\nu=0,t)^{2\pi} &= 0\,, \\
\mathrm{Im}_t A_3(\nu=0,t)^{2\pi} &= -\left(\frac{t/4-m_\pi^2}{t}\right)^{3/2}\,\frac{M^2}{(M^2-t/4)}\,\frac{\sqrt{5}}{2}
\end{aligned}
$$

$$\cdot F_{2\Lambda_\gamma=2}(t)\left\{\sqrt{\frac{3}{2}}\,f_+^{2*}(t) - M\,f_-^{2*}(t)\right\},$$

$$\begin{aligned}
\mathrm{Im}_t A_4(\nu=0,t)^{2\pi} &= 0\,,\\
\mathrm{Im}_t A_5(\nu=0,t)^{2\pi} &= -\left(\frac{t/4-m_\pi^2}{t}\right)^{3/2} M\sqrt{\frac{15}{2}}\,F_{2\Lambda_\gamma=0}(t)\;f_-^{2*}(t)\,,\\
\mathrm{Im}_t A_6(\nu=0,t)^{2\pi} &= -\left(\frac{t/4-m_\pi^2}{t}\right)^{3/2} M\,\frac{\sqrt{5}}{2}\,F_{2\Lambda_\gamma=2}(t)\;f_-^{2*}(t)\,. \qquad (3.66)
\end{aligned}$$

The reader should note that the s-wave $\pi\pi$ intermediate state only contributes to the amplitude A_1. It is the t-dependence of this $I = J = 0$ $\pi\pi$ state in the t-channel that is approximated in Ref.[L'vo 97] and parametrized by a σ pole. The d-wave $\pi\pi$ intermediate state gives rise to imaginary parts for the amplitudes A_1, A_3, A_5 and A_6. The amplitude A_2 (at $\nu = 0$) corresponds to the t-channel exchange of an object with the quantum numbers of the pion (e.g., π^0 pole in Eq.(3.39)), therefore two-pion intermediate states do not contribute to A_2. The imaginary part of A_4 receives only contributions from $\pi\pi$ intermediate states with $J \geq 4$ (see Eq.(B.13)) and therefore is neglected in our description, as we keep only s- and d-waves.

In Fig.3.13 we show the convergence of the t-channel integral from $4m_\pi^2$ to ∞ in the subtracted DR of Eq. (3.39). We do so by calculating the dispersion integral as function of the upper integration limit $t_{\rm upper}$ and by showing the ratio to the integral for $t_{\rm upper}$ = 0.78 GeV^2. The latter value corresponds to the highest t value for which the $\pi\pi \to N\bar{N}$ amplitudes are given in Ref. [H¨oh 83]. One clearly sees from Fig. 3.13 that the unsubtracted t-channel DR shows only a slow convergence, whereas the subtracted t-channel DR has already reached its final value, within the percent level, at a t value as low as 0.4 GeV^2. Although the cross section $\gamma\gamma \to \pi\pi$ shows appreciable strength above $t > 0.78$ GeV^2 (see Fig. 3.11), its contribution to the Compton amplitudes is negligibly small due to the subtraction in the t-channel integral. By estimating the $\pi\pi \to N\bar{N}$ d-wave amplitudes in Born approximation, we checked that the influence of the $f_2(1270)$ resonance on the Compton observables shown in the following section, does not exceed 1% and usually is even smaller.

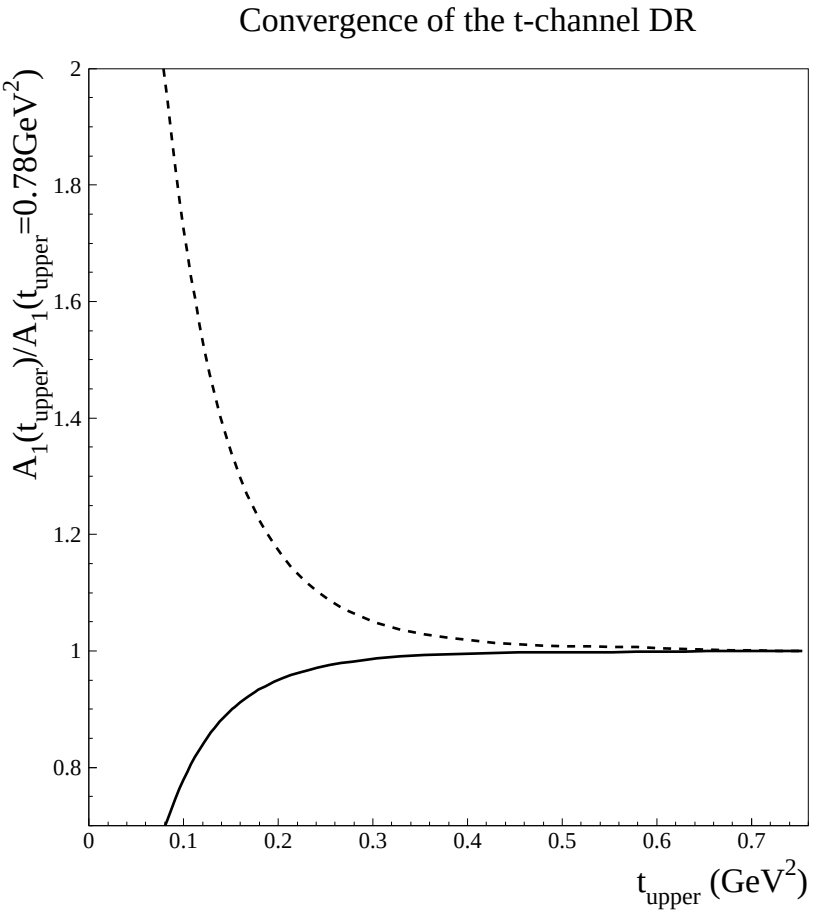

Figure 3.13: Convergence of the subtracted *t*-channel integral (solid line) in comparison with that for the unsubtracted *t*-channel integral (dashed line).

3.5 Results and discussion

In this section we shall present our results for Compton scattering off the nucleon in the dispersion formalism presented above.

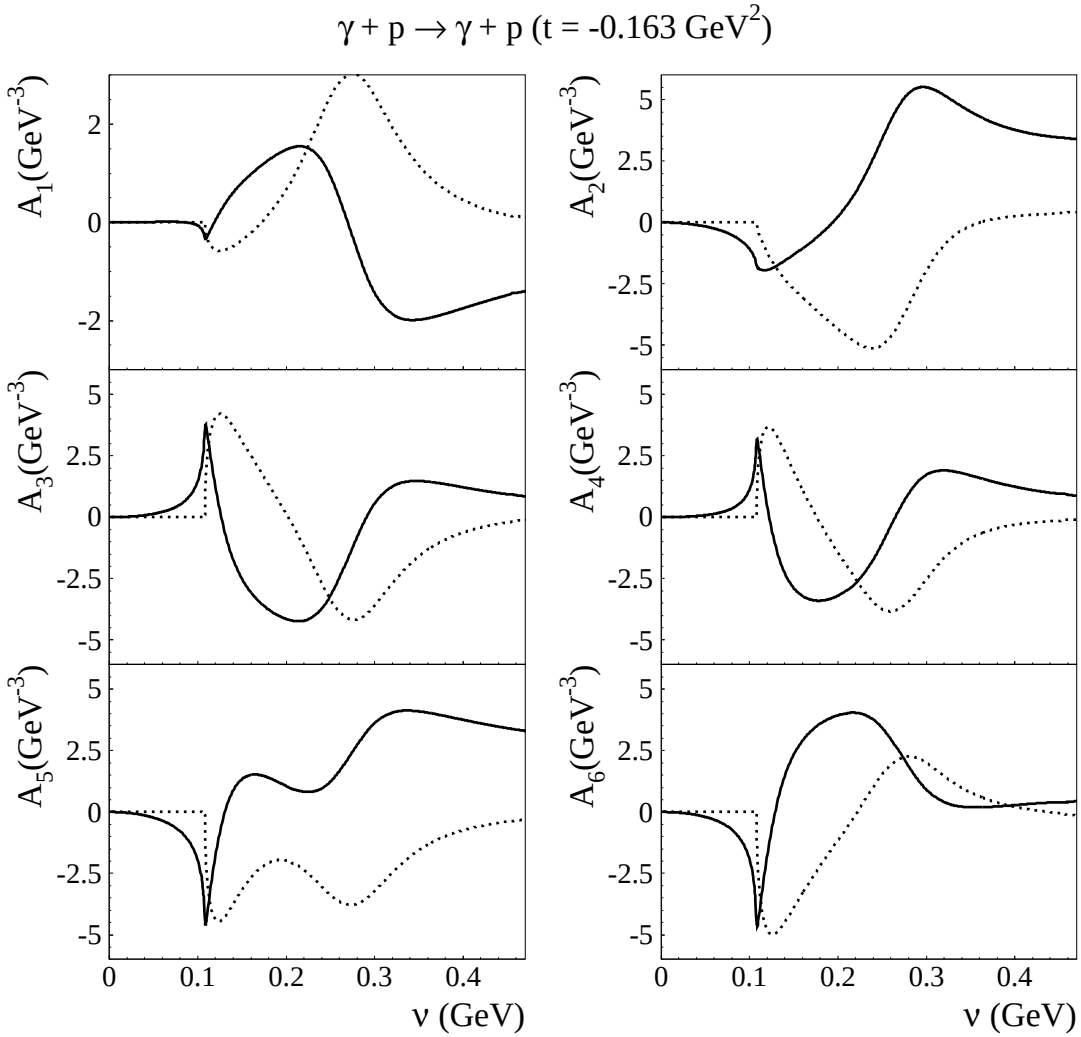

Figure 3.14: Real parts (solid lines) of the subtracted *s*-channel integrals and imaginary parts (dashed lines) of the invariant amplitudes A_i as functions of ν at fixed t.

The real and imaginary parts of the six Compton amplitudes are displayed in Fig. 3.14. Note that for the real part, we only show the subtracted *s*-channel integral of Eq.(3.37). As can be seen from Fig. 3.14, these amplitudes show strong oscillations due to interference effects between different pion photoproduction multipoles, in particular between threshold pion production (E_{0+}) and Δ excitation (M_{1+}).

3.5.1 Comparison with the data

We start with the review of the available Compton data at low energy (below π^0 threshold). The measurement of the scalar polarizabilities was performed by Ref.[Fed 91] at energies between 32 and 72 MeV and at scattering angles between 60° and 135°. The low energy expansion was used to extract the value of $\alpha - \beta$ whereas their sum was fixed by the Baldin sum rule. With the new sum rule value recently obtained by Babusci et al. [Bab 98],

$$\alpha + \beta \;=\; (13.8 \pm 0.4) \cdot 10^{-4} fm^3 \,, \tag{3.67}$$

the result of Ref.[Fed 91] for the proton polarizabilities reads ([Olm 01]):

$$\begin{aligned} \alpha &= [10.8 \pm 2.2(stat) \mp 1.3(syst)] \cdot 10^{-4} fm^3 \,, \\ \beta &= [3.0 \pm 2.2(stat) \pm 1.3(syst)] \cdot 10^{-4} fm^3 \,. \end{aligned} \tag{3.68}$$

The large statistical and systematical errors can be noticed, especially in view of the small value of the magnetic polarizability β.

Backward Compton scattering at energies of 98 and 132 MeV was exploited to determine the value of $\alpha - \beta$ in Ref.[Zie 92]. Their result, renormalized to the most recent value of the Baldin sum rule, is [Olm 01]

$$\alpha - \beta \;=\; [6.4 \pm 2.3(stat) \pm 1.9(syst)] \cdot 10^{-4} fm^3 \,. \tag{3.69}$$

However, the applicability of the low energy expansion is limited in energy up to about 100 MeV, because above this energy, the higher order terms are no longer negligible due to the closeness of pion threshold and of the $\Delta(1232)$-resonance.

In the early 90's, Compton scattering was measured at SAL in the energy range of 70-148 MeV and at laboratory angles of 90° and 135°. These data were used in Ref.[McG 95] to determine the scalar polarizabilities α and β through a global fit,

$$\begin{aligned} \alpha &= [11.9 \pm 0.5(stat) \mp 0.8(syst)] \cdot 10^{-4} fm^3 \,, \\ \beta &= [1.9 \pm 0.5(stat) \pm 0.8(syst)] \cdot 10^{-4} fm^3 \,. \end{aligned} \tag{3.70}$$

In the analysis of Ref.[McG 95], the unsubtracted dispersion relation formalism was used and the asymptotic contributions (Eq.(3.31)) to the invariant Compton amplitudes A_1 and A_2 were parametrized. In particular, A_2^{as} was described by the π^0 pole, which yields the value $\gamma_\pi \simeq -45 \cdot 10^{-4}$ fm^4. The free parameter entering in A_1^{as} was related to $\alpha - \beta$, for which the fit obtained the value $\alpha - \beta \simeq 10 \cdot 10^{-4}$ fm^3. In the remainder of this chapter, we will show our results within the subtracted DR formalism. Keeping $\alpha - \beta$ fixed close to the value $\alpha - \beta \simeq 10 \cdot 10^{-4}$ fm^3 of the fit of Eq.(3.70), we demonstrate in Fig. 3.15 that the sensitivity to γ_π is not at all negligible, especially at the backward angles and the higher energies.

We investigate this further in Fig. 3.16, where we show our results for different $\alpha - \beta$ and for a fixed value of $\gamma_\pi = -36 \cdot 10^{-4}$ fm^4, which is consistent with the heavy baryon ChPT prediction [Hem 98] and close to the value obtained in Ref. [L'vo 99]

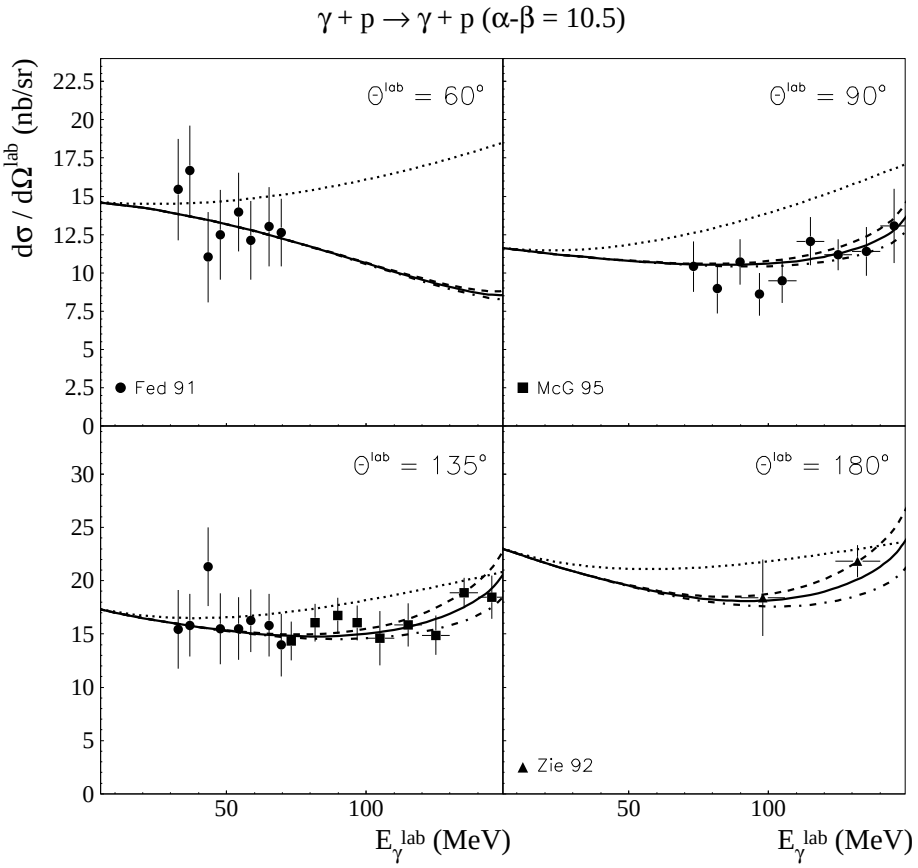

Figure 3.15: Differential cross section for Compton scattering off the proton as function of the lab photon energy E_γ and at four scattering angles Θ_γ^{lab}. The sensitivity to γ_π at fixed $\alpha - \beta = 10.5 \cdot 10^{-4} fm^3$ is shown. The dashed lines correspond to $\gamma_\pi = -31 \cdot 10^{-4} fm^4$, the solid lines to $\gamma_\pi = -36 \cdot 10^{-4} fm^4$, and the dashed-dotted lines to $\gamma_\pi = -41 \cdot 10^{-4} fm^4$. The dotted lines correspond to the Born approximation. The data points are from Refs. [Fed 91] (circles), [Zie 92] (triangles), and [McG 95] (squares).

in a backward dispersion relation formalism. For that value of γ_π, our results are compatible with those of Ref. [McG 95].

Finally, the most recent low energy Compton data were taken at MAMI in the range $59^\circ \leq \Theta_\gamma^{lab} \leq 155^\circ$ and photon energies between 55 and 165 MeV [Olm 01]. The data were analysed by means of unsubtracted dispersion relations of Ref. [L'vo 97] with $\alpha + \beta$ fixed to the sum rule value of Eq.(3.67),

$$\begin{aligned} \alpha &= [12.1 \pm 0.3(stat) \mp 0.4(syst) \pm 0.3(mod)] \cdot 10^{-4} fm^3 , \\ \beta &= [1.6 \pm 0.4(stat) \pm 0.4(syst) \pm 0.4(mod)] \cdot 10^{-4} fm^3 . \end{aligned} \tag{3.71}$$

The model dependent errors originate from the following factors:

- the uncertainty in the strength of the resonant M_{1+} multipole of $\pm 1\%$ leads to an uncertainty in $\alpha(\beta)$ of $\pm 0.10(\mp 0.10)$ in the usual units;

- the uncertainty in the E2/M1 ratio of $\pm 1\%$ leads to an uncertainty in $\alpha(\beta)$ of

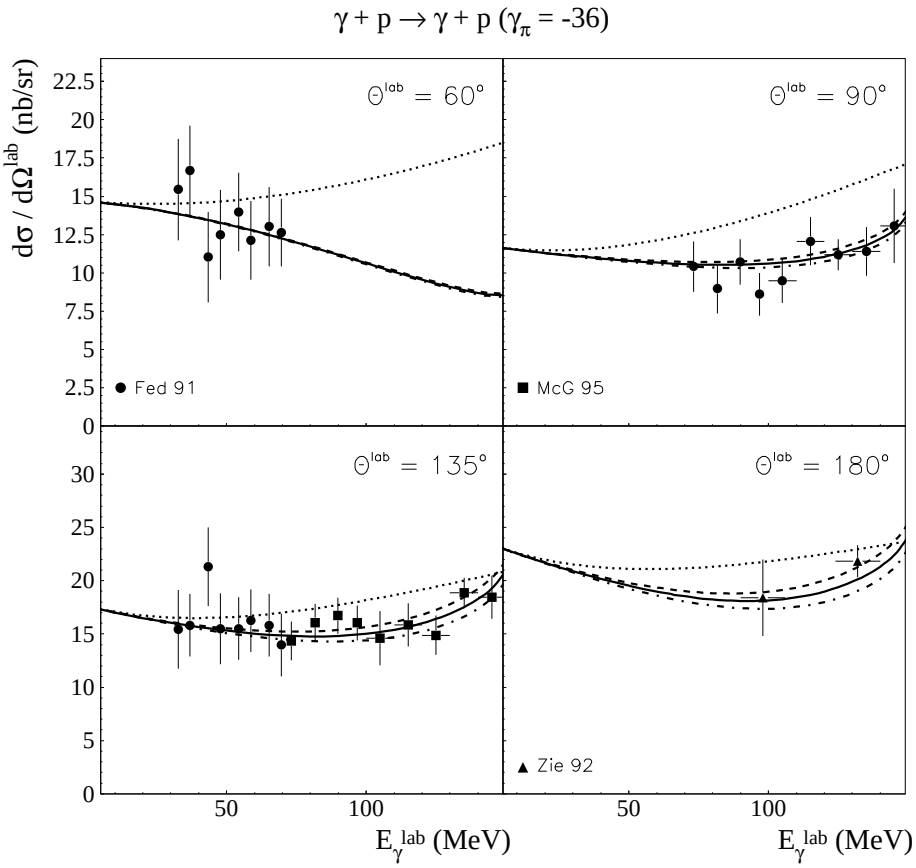

Figure 3.16: Differential cross section for Compton scattering off the proton as function of the lab photon energy E_γ and at four scattering angles Θ_γ^{lab}. The sensitivity to $\alpha - \beta$ at fixed $\gamma_\pi = -36 \cdot 10^{-4} fm^4$ is shown. The dashed-dotted lines correspond to $\alpha - \beta = 12.5 \cdot 10^{-4} fm^3$, the solid lines to $\alpha - \beta = 10.5 \cdot 10^{-4} fm^3$, and the dashed lines to $\alpha - \beta = 8.5 \cdot 10^{-4} fm^3$. The dotted lines give the result of the Born approximation. The data points are the same as in Fig. 3.15.

$\mp 0.08(\pm 0.08)$ in the usual units;

- the variation of the backward spin polarizability $\pm 1 \cdot 10^{-4} fm^4$ leads to an uncertainty in $\alpha(\beta)$ of $\mp 0.26(\pm 0.26) \cdot 10^{-4} fm^3$.

In Fig. 3.17, we illustrate this correlation between the extracted values of α, β, and γ_π. For each fixed value of γ_π, a fit to experimental data has been made, by means of which the two scalar polarizabilities α and β were determined [Ahr 02]. The sum rule constraint on $\alpha + \beta$ (shown by the narrow band in the upper panel of Fig. 3.17) was not applyed to this fit procedure. For each choice of γ_π, the minimal value of χ^2 was obtained and, finally, the dependence of χ^2 on γ_π was fitted by a parabola. Its minimum corresponds to the values of Eq.(3.71).

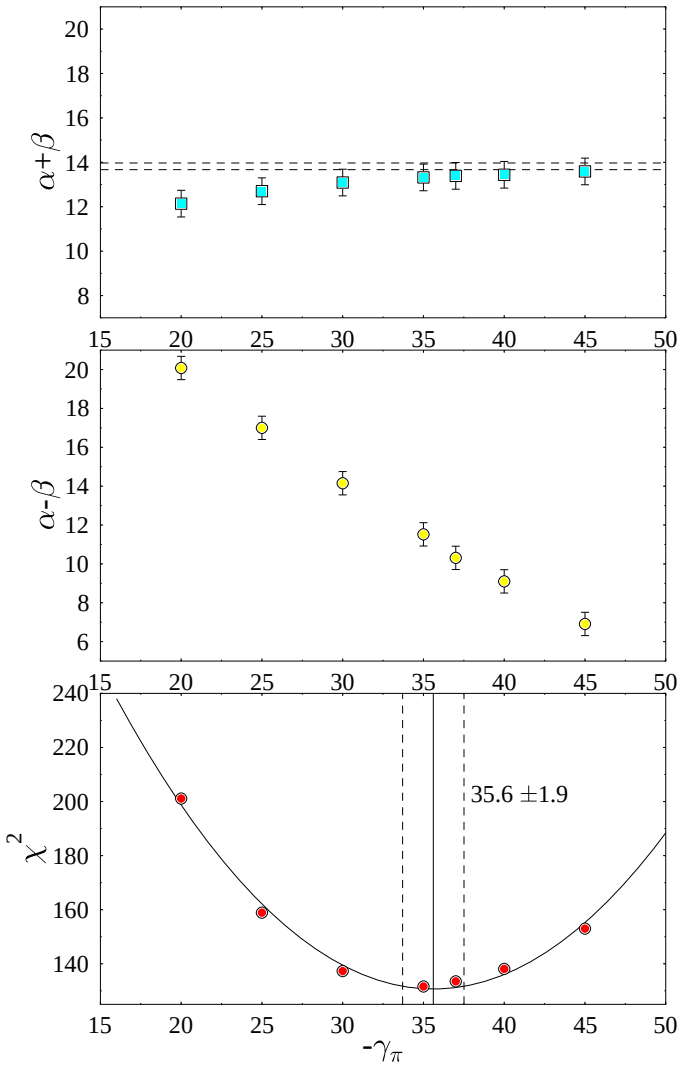

Figure 3.17: Fit of the experimental Compton data of Ref. [Olm 01] by means of unsubtracted DR of Ref. [L'vo 97]. At fixed values of γ_π, a fit to the full data set was made in order to obtain $\alpha - \beta$ and $\alpha + \beta$ by minimizing the χ^2 value. χ^2 was then minimized as function of γ_π, which was fitted by a parabola. The extracted values of the polarizabilities are those given in Eq.(3.71).

In the unsubtracted DR, the value of γ_π is fixed by the π^0 asymptotic contribution and the dispersive contributions from the *s*-channel to the amplitude A_2. The results of [Olm 01] show the correlation between $\alpha - \beta$ and γ_π in the unpolarized cross sections already at low energies. In the subtracted DR formalism, both backward polarizabilities are free parameters, which allows for the determination of the two from a simultaneous fit. In Figs. 3.19 and 3.18, we compare the subtracted DR predictions with the data of Ref. [Olm 01].

The latter data "prefer" substantially higher values of the backward polarizability

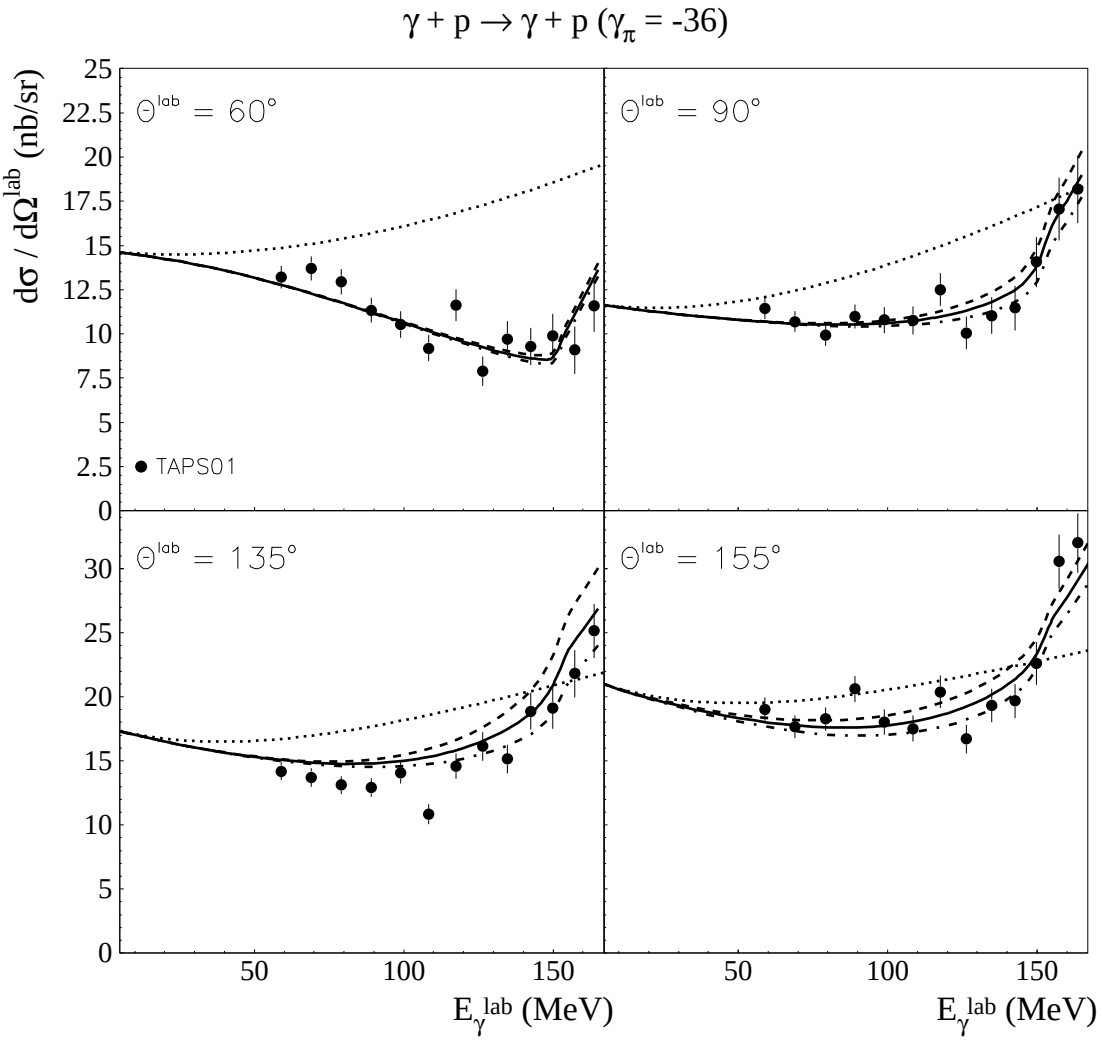

Figure 3.18: Notation as in Fig. 3.16. The data points are from Ref.[Olm 01].

$\alpha - \beta$ (see Eq.(3.71)), as compared to the old results (Eqs.(3.68) and (3.69)), and are compatible with those of McGibbon et al. (Eq.(3.70)), also obtained in the framework of unsubtracted DR of [L'vo 97].

In Fig. 3.20, we finally compare the results of our subtracted dispersion relation formalism with those obtained by unsubtracted DR, using the polarizabilities of Eq.(3.71). We find that also the subtracted dispersion relations describe the data with the polarizabilities very close to the values of Eq.(3.71). This result can be seen as a cross-check of the dispersion relation formalism with and without subtraction. It shows that at moderate energies, the singularities of the Compton invariant amplitudes A_i are well under control, and that the model dependence in the analysis is small in this energy range.

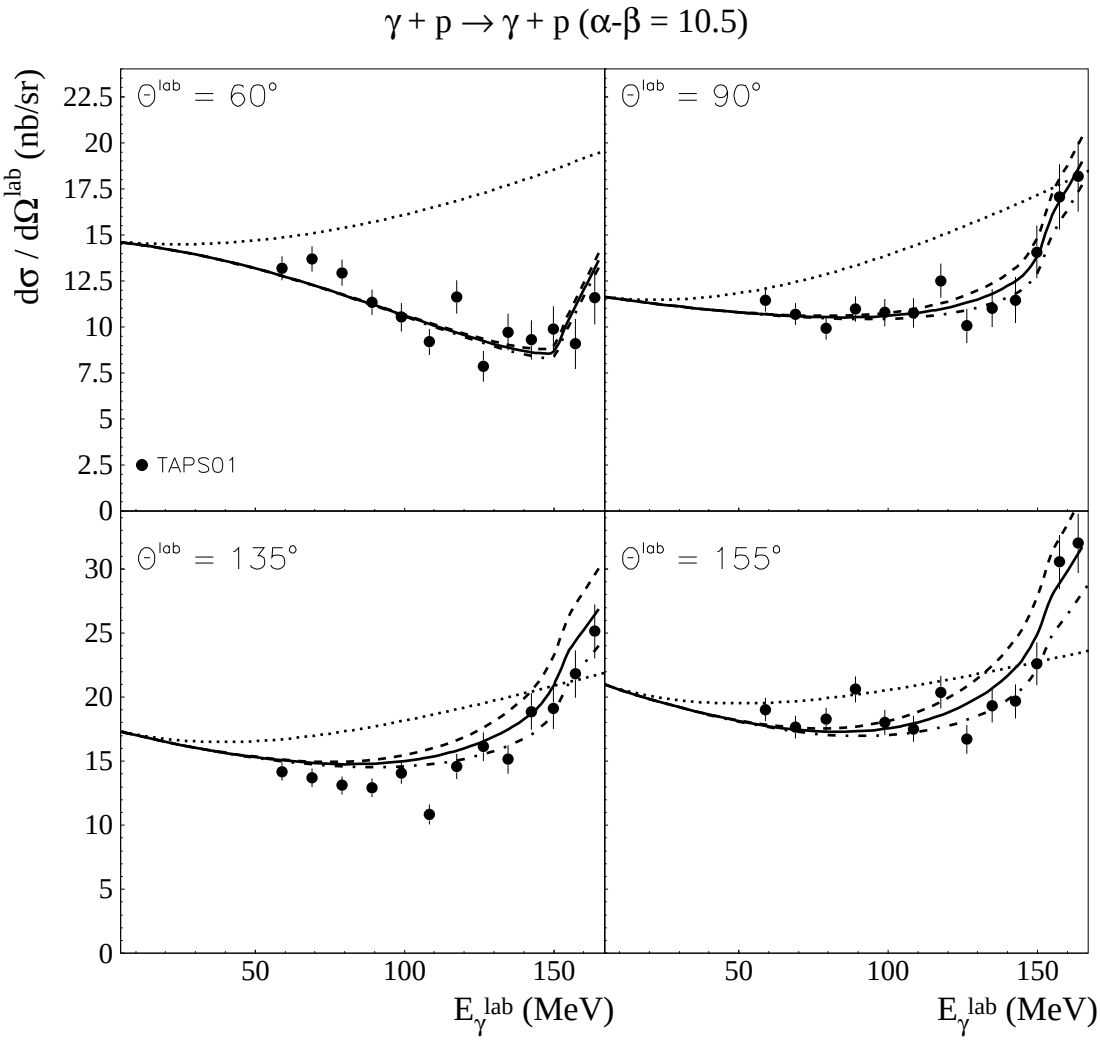

Figure 3.19: Notation as in Fig. 3.15. The data points are from Ref.[Olm 01].

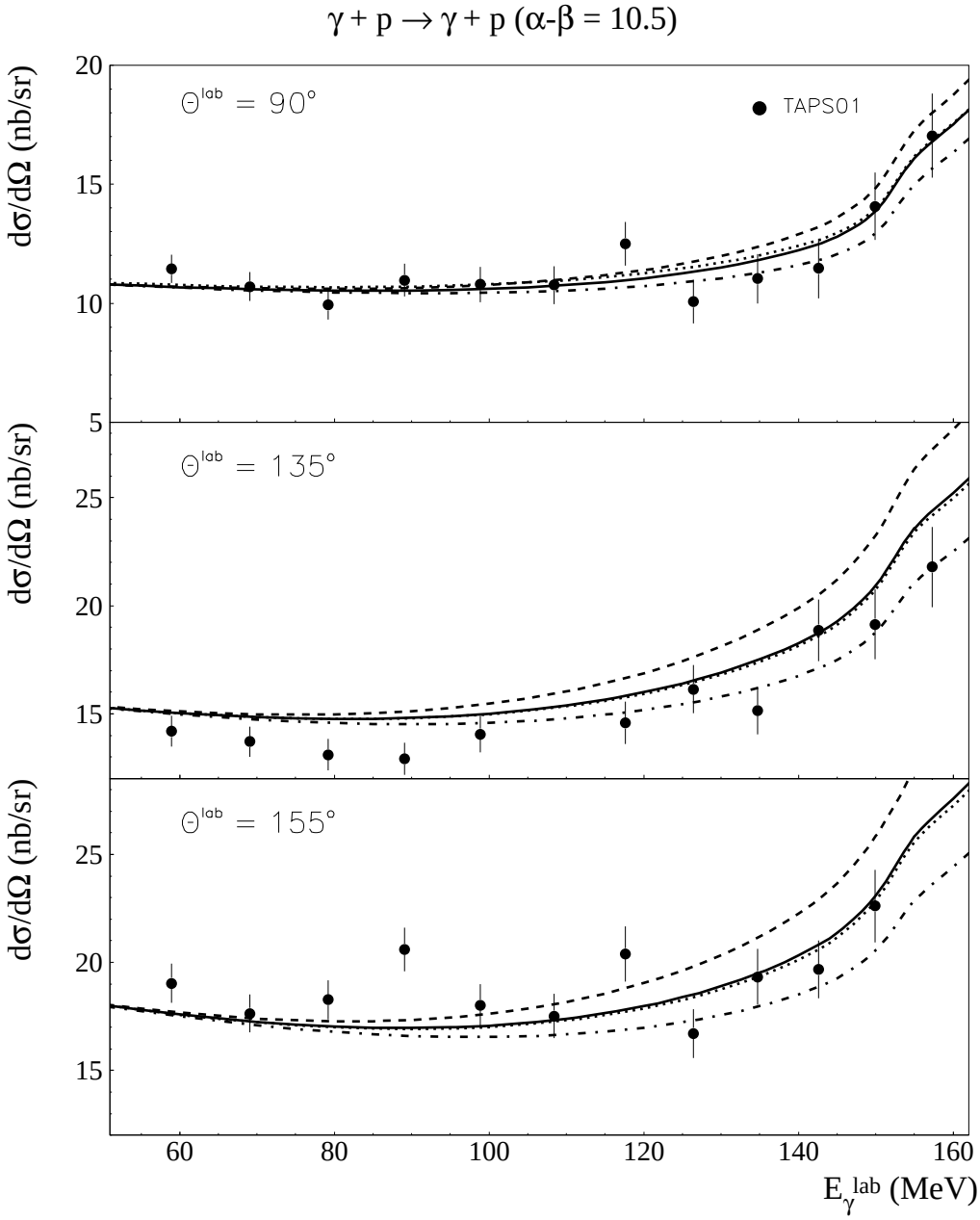

Figure 3.20: The solid, dashed and dashed-dotted lines are the same as in Fig. 3.15. The dotted lines correspond to the unsubtracted DR calculations with $\alpha - \beta = 10.5 \cdot 10^{-4}$ fm^3 and $\gamma_\pi = -36.1 \cdot 10^{-4}$ fm^4. The data points are from Ref.[Olm 01].

As one moves to energies above pion threshold, the Compton cross section rises rapidly because of the unitarity coupling to the much stronger pion photoproduction channel (the so called unitarity cusp can be seen, for example, in Figs. 3.18 and 3.19, especially at 60°). Therefore, this higher energy region is usually considered less "pure" to extract polarizabilities because the procedure would require a rather precise knowledge of pion photoproduction. With the new pion photoproduction data on the proton that have become available in recent years, the energy region above pion threshold could however serve as a valuable complement to determine the polarizabilities, provided one can minimize the model uncertainties in the dispersion formalism.

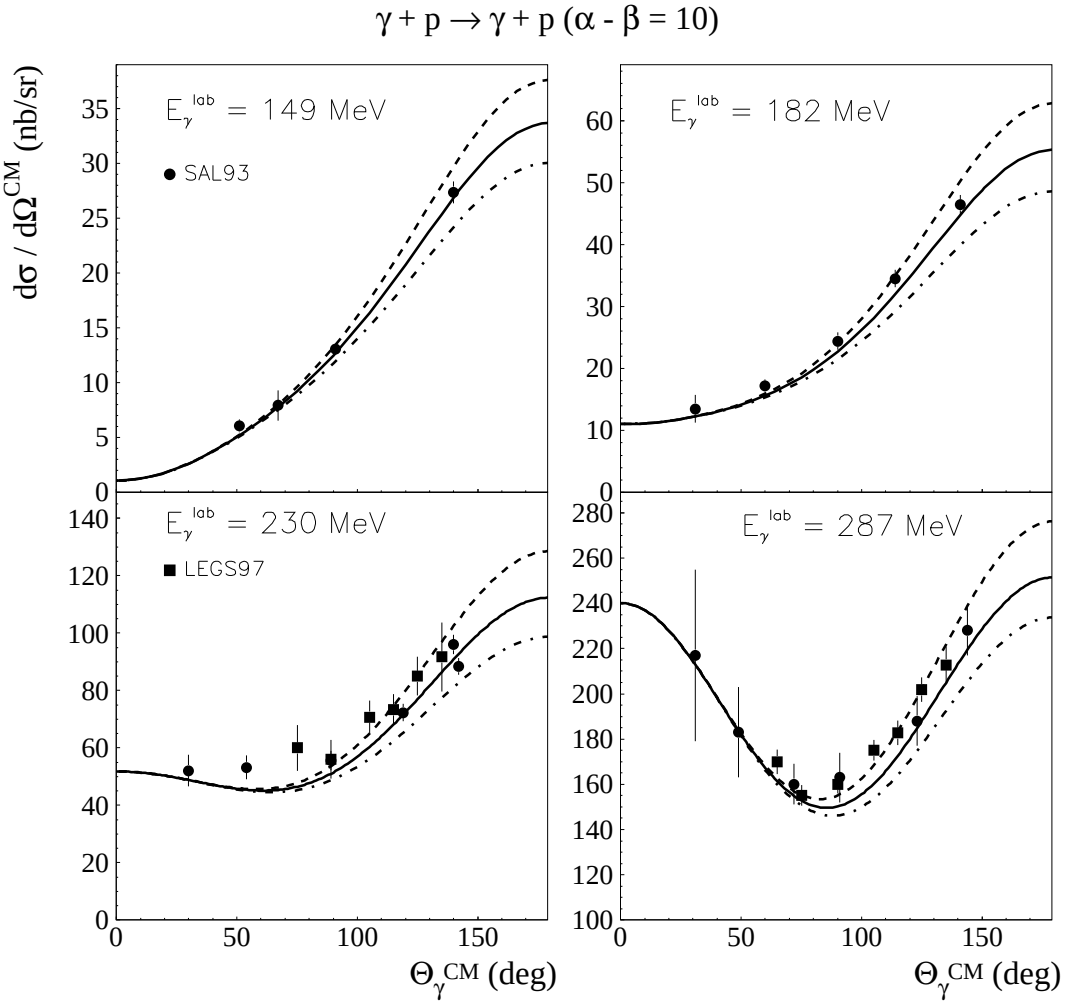

Figure 3.21: Differential cross section for Compton scattering off the proton as function of the c.m. scattering angle Θ_γ^{cm} for different lab energies.The sensitivity to γ_π at fixed $\alpha - \beta = 10 \cdot 10^{-4} fm^3$ is shown. The dashed lines correspond to $\gamma_\pi = -27 \cdot 10^{-4} fm^4$, the solid lines to $\gamma_\pi = -32 \cdot 10^{-4} fm^4$, and the dashed-dotted lines to $\gamma_\pi = -37 \cdot 10^{-4} fm^4$. The data points are from Ref. [Hal 93].

In this work, we use the most recent information on the pion photoproduction channel by taking the HDT [Han 98] multipoles at energies $E_\gamma \leq 500$ MeV and the SAID-SP99K solution [SAID] at higher energies. As previously shown in Fig. 3.8, the subtracted DR are practically saturated by the one-pion channel for photon energies through the Δ region, which minimizes the uncertainty due to the modeling of the two-pion photoproduction channels.

In Fig. 3.21 we compare the predictions of our subtracted dispersion relations with the Compton data of Ref. [Hal 93] at photon energies in the lower part of the Δ region and display the high sensitivity of the Compton cross sections to γ_π in this energy range.

This sensitivity was exploited in Ref. [Ton 98] within the context of an unsubtracted dispersion relation formalism for the analysis of the laser backscattering Compton data of Ref. [Bla 97]. In this analysis, the presence of additional asymptotic contributions to γ_π was claimed, which led to a modification of the asymptotic part A_2^{as}, and the value $\gamma_\pi \simeq -27 \cdot 10^{-4} fm^4$ was extracted from the LEGS 97 data, which are shown at the higher energies in Fig. 3.21.

In Fig. 3.22, we compare our predictions with both differential cross section and photon asymmetry data obtained at LEGS [Bla 97]. One finds that at both energies (E_γ = 265 MeV and 323 MeV) our subtracted dispersion relation formalism provides a good description of the asymmetries, which however shows little sensitivity to γ_π, but underestimates the absolute values of the cross sections. In particular close to the resonance position at E_γ = 323 MeV, our formalism does not allow us to find any reasonable combination of γ_π and $\alpha - \beta$ to describe these data. Since the uncertainties due to two-pion and heavier meson photoproduction in the *s* channel as well as *t*-channel contributions above the $f_2(1270)$ resonance are expected to be less than 1 %, the only possibility to describe the E_γ = 323 MeV LEGS data would be an increase of the HDT M_{1+} multipole by about 2%. Indeed such a fit was obtained by Tonnison et al. [Ton 98] by use of the LEGS pion photoproduction multipole set of Ref. [Bla 97] for photon energies between 200 and 350 MeV and the SAID-SM95 multipole solution [SAID] outside this interval.

In the experiment of Ref. [Bla 97], Compton scattering and pion photoproduction were investigated simultaneously, thus giving a possibility to analyse the data for the two reactions consistently within the same analysis. Since the results of Ref. [Bla 97] for the pion photoproduction in the $\Delta(1232)$-region are in contradiction with other experiments, they also lead to consistently wrong results for Compton scattering in this energy region.

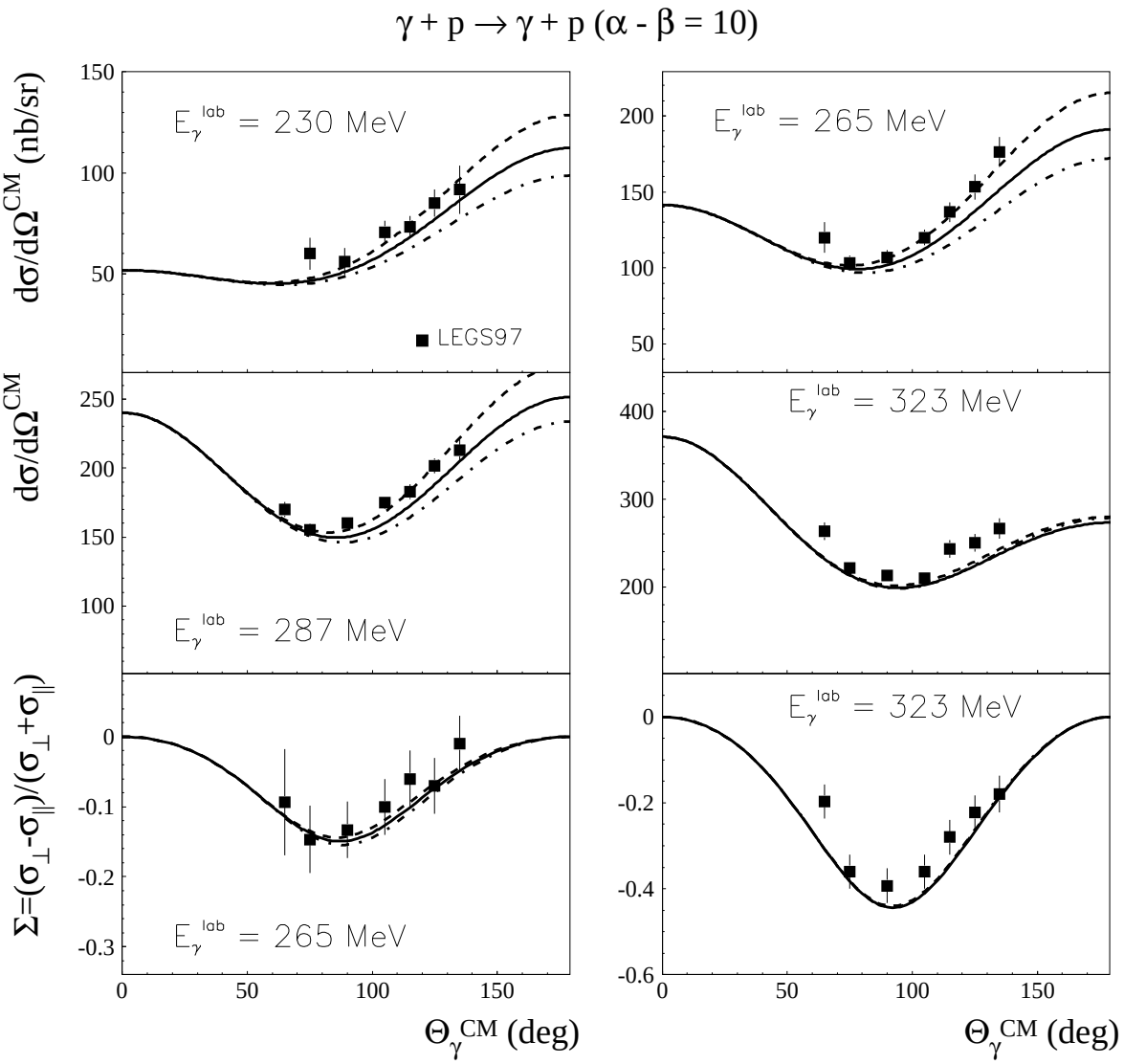

Figure 3.22: Differential cross section for Compton scattering off the proton as function of the c.m. scattering angle Θ_γ^{cm} for different lab energies.The sensitivity to the γ_π at fi xed $\alpha - \beta = 10 \cdot 10^{-4} fm^3$ is shown. The dashed line correspond to $\gamma_\pi = -27 \cdot 10^{-4} fm^4$, solid line to $\gamma_\pi = -32 \cdot 10^{-4} fm^4$, and dashed-dotted line to $\gamma_\pi = -37 \cdot 10^{-4} fm^4$.

In spite of the strong correlation of the extracted value of the backward spin polarisability and the strength of the M_{1+} multipole, a consistency check between Compton and pion photoproduction data is necessary. This became possible with the most recent data taken at Mainz with the **LAR**ge **A**cceptance arrangement (LARA) [Gal 01]. The covered energy range was between 250 MeV and 800 MeV with the scattering angles varied from 30° to 150°. The data were analysed by means of the unsubtracted DR formalism of Ref. [L'vo 97], using for comparison three sets of pion photoproduction multipoles, SAID-SM99K, SAID-SM00K and MAID. The value of the scalar polarizability difference was fixed to $10 \cdot 10^{-4}$ fm^3. The fit to the lower energy ($\leq$ 455 MeV) data led to a range of the three parameters (here, we use $EMR \equiv \frac{E2}{M1}$), from

$$\begin{aligned} \mid M_{1+}^{3/2}(320\,MeV) \mid &= (39.7 \pm 0.3_{stat+syst} \pm 0.03_{model}) \times 10^{-3}/m_{\pi^+} \\ \mathrm{EMR}(340\,MeV) &= (-1.6 \pm 0.4_{stat+syst} \pm 0.2_{model})\% \\ \gamma_\pi &= (-37.9 \pm 0.6_{stat+syst} \pm 3.5_{model}) \times 10^{-4}\,fm^4 \end{aligned} \quad (3.72)$$

for the SAID-SM99K solution, to

$$\begin{aligned} \mid M_{1+}^{3/2}(320\,MeV) \mid &= (39.8 \pm 0.3_{stat+syst} \pm 0.03_{model}) \times 10^{-3}/m_{\pi^+} \\ \mathrm{EMR}(340\,MeV) &= (-1.9 \pm 0.4_{stat+syst} \pm 0.2_{model})\% \\ \gamma_\pi &= (-41.4 \pm 0.4_{stat+syst} \pm 2.5_{model}) \times 10^{-4}\,fm^4 \end{aligned} \quad (3.73)$$

with the MAID multipoles. It can be noticed that the value of the $E2/M1$ ratio of Eqs.(3.72) and (3.73) lie somewhat below the "standard" value, an average [Arn 01] obtained by means of a number of theoretical models for pion photoproduction [MAID], [Han 98], [Kam 99], [Azn 99], [Dav 91], [Ome 83]:

$$EMR \equiv \frac{E2}{M1} = -(2.38 \pm 0.27)\% \,. \quad (3.74)$$

Also the strength $\mid M_{1+}^{3/2}(320\,MeV) \mid$ differs only slightly from the value obtained within the corresponding analyses from the pion photoproduction data directly.

The above mentioned results for the backward polarizability γ_π and the parameters of the resonant multipoles for pion photoproduction, Eqs.(3.72) and (3.73) show that in the $\Delta(1232)$-region, even minor variations of these parameters (first of all, of the value $\mid M_{1+}^{3/2}(320\,MeV) \mid$) within their error bars lead to a noticeable change in the extracted result for γ_π. The results of Eqs. (3.72) and (3.73) for both $\mid M_{1+}^{3/2}(320\,MeV) \mid$ and EMR by themselves, however, should not be considered as too informative, since Compton scattering is not the best way to extract the pion photoproduction multipoles.

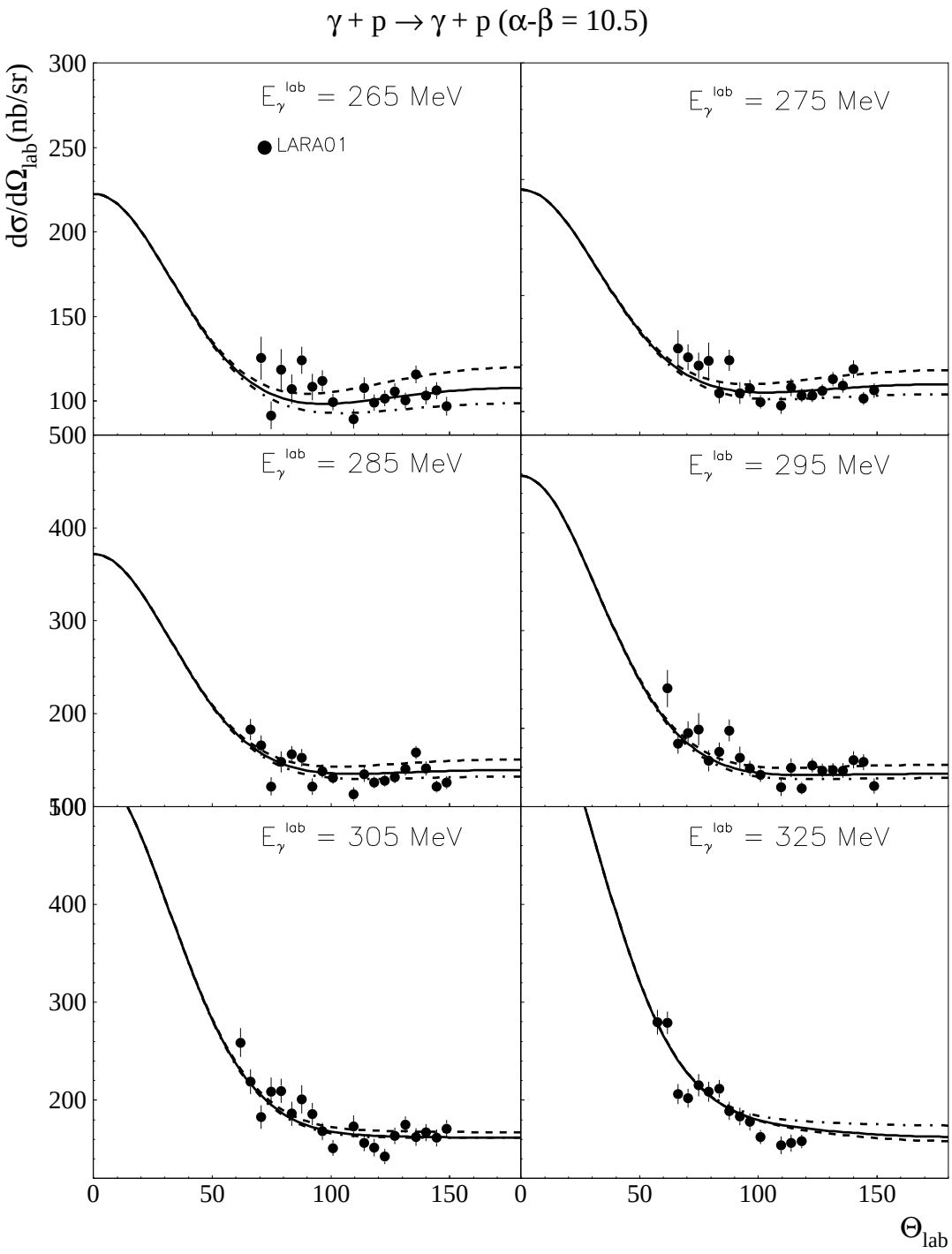

Figure 3.23: Differential cross section for Compton scattering off the proton as function of the *lab* scattering angle Θ_γ^{lab} for different lab energies.The sensitivity to γ_π at fixed $\alpha - \beta = 10 \cdot 10^{-4} fm^3$ is shown. The dashed lines correspond to $\gamma_\pi = -32 \cdot 10^{-4} fm^4$, the solid lines to $\gamma_\pi = -37 \cdot 10^{-4} fm^4$, and the dashed-dotted lines to $\gamma_\pi = -42 \cdot 10^{-4} fm^4$.

In Fig. 3.23, we show the data points of Ref. [Gal 01] in comparison with our predictions for the angular distributions of the differential cross sections with $\alpha - \beta$ fixed to $10 \cdot 10^{-4} fm^3$, and γ_π varying from $-27 \cdot 10^{-4} fm^4$ to $-37 \cdot 10^{-4} fm^4$.

Also in our formalism, it is impossible to describe these data at any of the displayed energies with the value of $\gamma_\pi = -27 \cdot 10^{-4} fm^4$ of Ref. [Ton 98], which reflects the fact that the two data sets are not compatible. This agreement between subtracted and unsubtracted DRs states that there is no additional asymptotic contribution beyond the π^0 pole in the case of the backward spin polarizability γ_π.

Finally, in Fig. 3.24 we show that double polarization observables will be ultimately necessary to extract the spin polarizabilities in a unique way. In particular, an experiment with a circularly polarized photon and a polarized proton target displays quite some sensitivity on the backward spin polarizability γ_π, especially at energies between threshold and the Δ resonance. Such measurement would be more selective to γ_π due to a much lesser sensitivity to $\alpha - \beta$. Comparing the difference between the full lines and the dotted lines with the difference between the full lines and the dashed lines in Fig. 3.24, one sees that the sensitivity to $\alpha - \beta$ at the lab photon energy of 230 MeV is about twice smaller than to γ_π.

Furthermore, in spite of the quite sizeable dependence of the Compton cross section on the strength of the resonance magnetic multipole $| M_{1+}^{3/2}(320 MeV) |$, a measurement of the asymmetries seems to be very promising. Since these observables contain only ratios of the cross sections, it should be possible to diminish the correlation of the extracted value of the backward spin polarizability and the pion photoproduction multipole parameters by measuring the appropriate asymmetry.

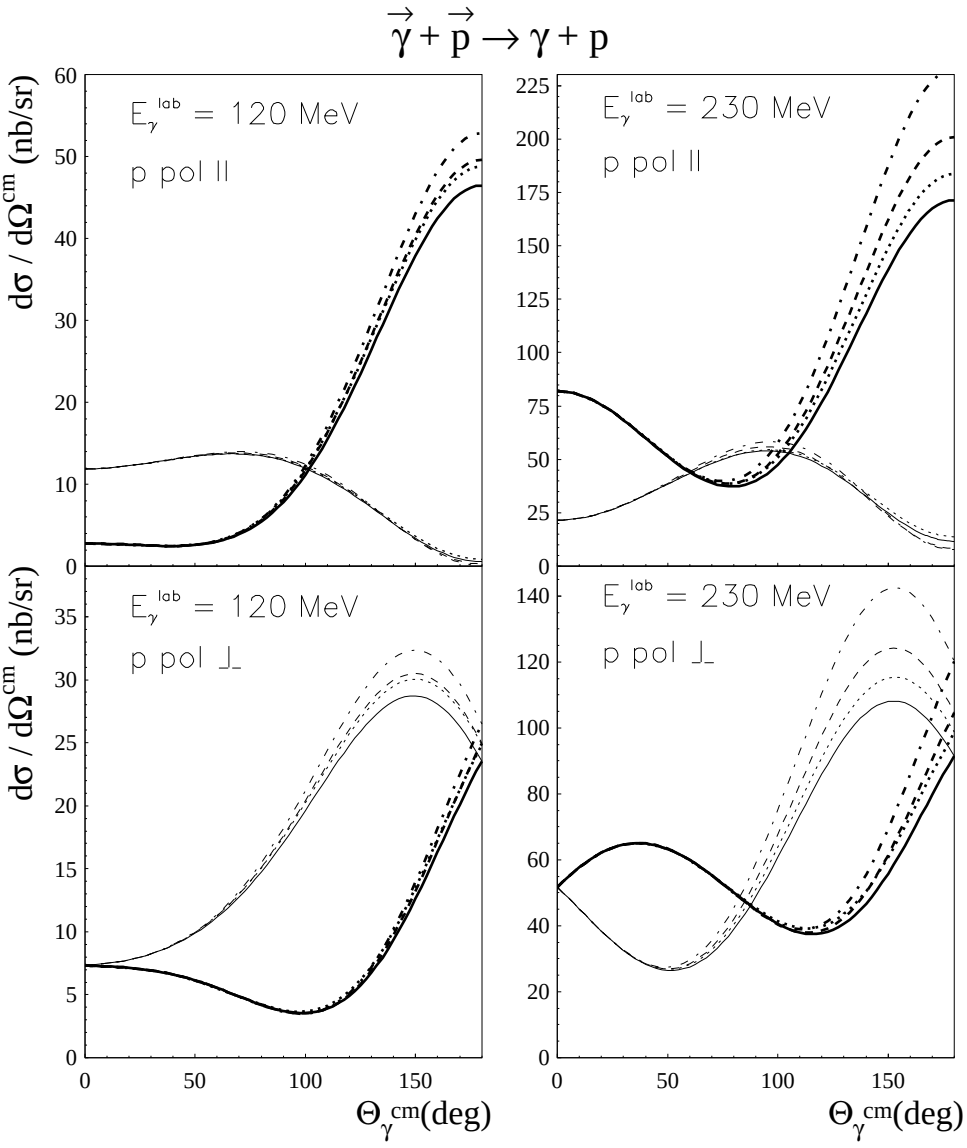

Figure 3.24: Double polarization cross section with circularly polarized photons and proton polarization along the photon direction (upper panels), and perpendicularly and in the reaction plane (lower panels). The thick (thin) lines correspond to positive (negative) spin projection, respectively. The scalar backward polarizability $\alpha - \beta$ is fixed to $10 \cdot 10^{-4} fm^3$, and γ_π takes the values $-27 \cdot 10^{-4} fm^4$ (dashed-dotted lines), $-32 \cdot 10^{-4} fm^4$ (dashed lines), and $-37 \cdot 10^{-4} fm^4$ (full lines). For comparison, the sensitivity to the variation of $\alpha - \beta$ is shown by the dotted lines, which correspond to $\alpha - \beta = 8 \cdot 10^{-4} fm^3$ and $\gamma_\pi = -37 \cdot 10^{-4} fm^4$.

3.6 Conclusions

We have presented a formalism of fixed-t subtracted dispersion relations for Compton scattering off the nucleon at energies $E_\gamma \leq 500$ MeV. Due to the subtraction, the s-channel dispersion integrals converge very fast and are practically saturated by the πN intermediate states, which are described by the recent pion photoproduction multipoles of HDT. In this way we minimize the uncertainties from multi-pion and heavier meson intermediate states.

To calculate the dependence of the subtraction functions on the momentum transfer t, we include the experimental information on the t-channel process through $\pi\pi$ intermediate states as $\gamma\gamma \to \pi\pi \to N\bar{N}$. We construct a unitarized amplitude for the $\gamma\gamma \to \pi\pi$ subprocess and find a good description of the available data. This information is then combined with the $\pi\pi \to N\bar{N}$ amplitudes determined from dispersion theory by analytical continuation of πN scattering. In this way, we also avoid the uncertainties in Compton scattering associated with the two-pion continuum in the t channel, which is usually modeled through the exchange of a somewhat fictitious σ meson. Altogether we estimate that the uncertainties in the s- and t- channel integrals, due to unknown high energy contributions, should be less than 1%. As a consequence our formalism provides a direct cross check between Compton scattering and one-pion photoproduction. In particular it has become possible to study the consistency between the Compton scattering and pion photoproduction data sets at LEGS and MAMI. We repeat that in Compton scattering near the Δ resonance, the leading M_{1+} multipole of pion photoproduction enters to the fourth power, and thus has to be known very precisely in order to describe the absolute value of the cross section over the full angular range.

Since two of the polarizabilities enter as subtraction constants, the subtracted dispersion relation formalism can be used to extract the nucleon polarizabilities from the data with a minimum of model dependence. However the existing data are not sufficient to determine $\alpha - \beta$ and γ_π independently. A full study of the spin (or vector) polarizabilities will therefore require double polarization experiments. As we have shown, the scattering of polarized photons on polarized protons is very sensitive to γ_π, in particular in the backward hemisphere and at energies between threshold and the Δ-resonance region. In addition, possible normalization problems can be avoided by measuring appropriate asymmetries. Therefore such polarization experiments hold the promise to disentangle scalar and vector polarizabilities of the nucleon and to quantify the nucleon spin response in an external electromagnetic field.

The uncertainties of the method are concerned with the dispersion contributions from the unphysical region of the Mandelstam plane. The integral along the negative t-axis samples the information on the possible intermediate states in the s- and u-channels. This integral can be evaluated by means of partial wave decomposition of the amplitudes A_i, continued into unphysical region. However, the factors $1/\nu$ in

the corresponding expressions do not allow one to use these expressions numerically, because the crossing symmetry is violated due to truncation of the partial wave expansion of the amplitudes A_i. In principle, such factors would be no problem for the full expansion, or a closed form of the amplitude which possesses the crossing symmetry explicitly. For the latter, only an estimation is possible, and we use the dominant $\Delta(1232)$-resonance to approximate the contribution of the πN intermediate states to the negative t-integral. Being a fairly small correction at small t-values (quite in the spirit of the S-matrix theory of strong interaction, see Sec. 2.4!), it becomes more important at higher (i.e. more negative) values of t, giving rise to a certain model dependence.

If the discussed above uncertainty is only the case for the subtracted DR, the second one is unavoidable in the framework of fixed-t dispersion relations in general (either subtracted or not) and arises from the s-channel dispersion integral. The integration path in the s-channel is a constant-t line at $s \geq (M+m_\pi)^2$, which necessarily goes out of the physical region for Compton scattering, unless one is looking at the very low values of t. The farther one moves into negative-t region, the larger becomes the unphysical part of the integration path, with a cosine of the "scattering angle", $\cos\Theta \ll -1$. For example, for $t = -0.4 GeV^2$ and the lowest possible value of $s = (M+m_\pi)^2$,

$$\cos\Theta \;=\; 1 + \frac{t}{2\omega_{cm}^2} \;\approx\; -10\,. \tag{3.75}$$

At some point, the partial wave expansion does not converge any longer, since the (physically small) higher partial wave are boosted by the corresponding power of $\cos\Theta$. This effect can be seen in the energy distributions of the differential cross section at higher energies, especially in the backward hemisphere, see Fig. 3.25. At low t, the two additional powers of ν in the denominator of the subtracted DR, in comparison to the unsubtracted one (cf. Eq.(3.37)), diminish the dependence on the higher energy contributions. At increasingly more negative values of t, however, this denominator emphasizes the unphysical region more and more. In fact, the threshold ν_0 for a finite imaginary part moves accordingly to the relation

$$2M\nu \;=\; 2Mm_\pi + m_\pi^2\,\frac{t}{2}\,, \tag{3.76}$$

which makes the divergence even more dangerous in the case of the subtracted DR.

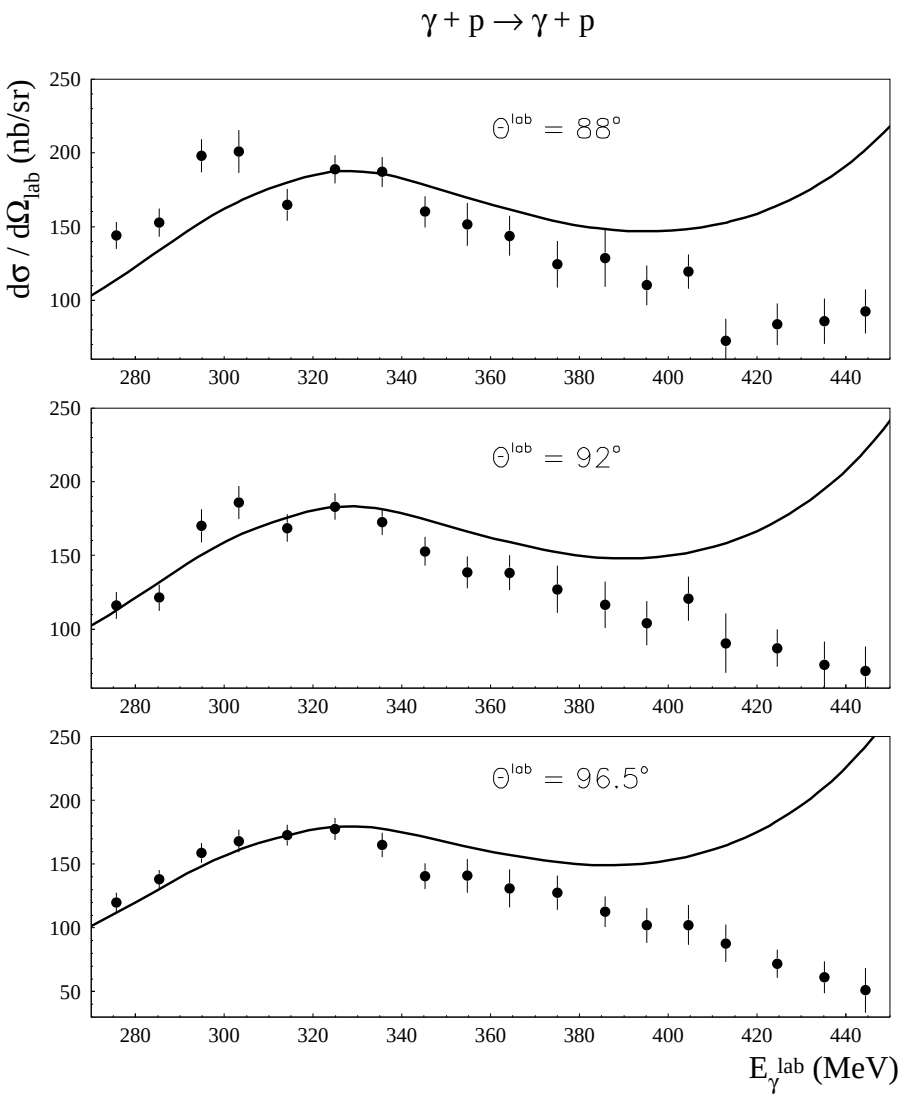

Figure 3.25: Differential cross section for Compton scattering off the proton as function of the lab photon energy E_γ and at three scattering angles Θ_γ^{lab}. The full lines correspond to the subtracted DR calculation with $\alpha - \beta = 10 \cdot 10^{-4} fm^3$ and $\gamma_\pi = -37 \cdot 10^{-4} fm^4$. The data points are from Ref. [Olm 01].

A possible cure could be to use hyperbolic DRs, for which the integral path is a hyperbola of the form

$$t(\frac{t}{4} - M^2 + a) \; = \; 4M^2\nu^2 \, , \tag{3.77}$$

where the parameter a takes values between 0 (backward scattering) and $-\infty$ (forward scattering). At negative values of t, these trajectories always stay inside the physical region for Compton scattering.

For positive t, however, ν^2 becomes negative, i.e., the energy becomes complex. The troubles are now shifted to the t-channel, where the $\gamma\gamma \to \pi\pi$ and the $\pi\pi \to NN$ partial waves (and corresponding Legendre polynomials!) have to be evaluated at

$$\cos^2\Theta_t \; = \; \frac{4M^2\nu^2}{t(t/4 - M^2)} \; = \; 1 + \frac{a}{t/4 - M^2} \; > \; 1 \, . \tag{3.78}$$

The amplitudes for the $\pi\pi \to NN$ subprocess were obtained by extrapolating the πN scattering amplitudes to the unphysical region by means of the hyperbolic dispersion relations [H¨oh 83] and are analytic functions of ν and t, as well as the partial waves for the process $\gamma\gamma \to \pi\pi$. Therefore, both can be continued analytically into the complex plane. Nevertheless, the singularity structure of such DR should be studied properly for the specific case of Compton scattering. Furthermore, one should not depart too far from the physical sheet to keep the possible uncertainties under control. As one can easily see, the "more imaginary" values of ν at positive t correspond to higher values of a, i.e. to more forward angles at negative t in the s-channel region. Therefore, a modification has been suggested, which uses fixed-t DR at forward angles (where both subtracted and unsubtracted DR are in good agreement), and hyperbolic DR at backward angles.

Chapter 4

VCS

4.1 $e + p \to e + p + \gamma$ process

The natural generalization of the real Compton scattering, in which a real (massless) photon is elastically scattered off the nucleon, is the case when one or both of the two photons are virtual. The term virtual Compton scattering (VCS) usually refers to an incident spacelike photon and an outgoing real photon. Such process is experimentally accessible through radiative lepton scattering. In this work, we will consider electron scattering as the source of the virtual photon.

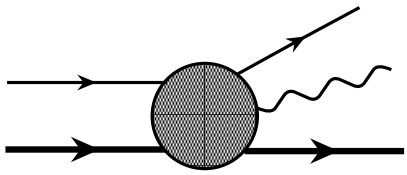

Figure 4.1: The $e + p \to e + p + \gamma$ process.

In the Born approximation, the interaction of the electron with the proton is given by the exchange of one virtual photon. The real photon in the final state can originate from two different processes.

The Bethe-Heitler process corresponds to the real photon being emitted either by the initial or the outgoing electron. The corresponding amplitude can be calculated in QED, provided the elastic form factors of the nucleon are (phenomenologically) known:

$$T^{BH} \;=\; -\frac{e^3}{t}\varepsilon'^{*}_{\mu} L^{\mu\nu}\, \bar{u}(p')\,\Gamma_{\nu}(p',p)\,u(p)\;, \tag{4.1}$$

where the leptonic tensor is given by

$$L^{\mu\nu} \;=\; \bar{u}(k')\left\{\gamma^{\mu}\frac{1}{\not{k}+\not{q}-m_e}\gamma^{\nu} \;+\; \gamma^{\nu}\frac{1}{\not{k}-\not{q}'-m_e}\gamma^{\mu}\right\}u(k)\;, \tag{4.2}$$

where $k(k')$ are the momenta of the initial (final) lepton, respectively, and m_e the electron mass. The proton electromagnetic vertex is

$$\Gamma_\nu(p',p) \;=\; F_1(\Delta^2)\gamma_\nu \;+\; iF_2(\Delta^2)\sigma_{\nu\alpha}\frac{\Delta^\alpha}{2M}\;, \tag{4.3}$$

where $\Delta \equiv p' - p$ and the Dirac and Pauli form factors of the proton are normalized to $F_1(0) = 1$, $F_2(0) = 1.79$, respectively.

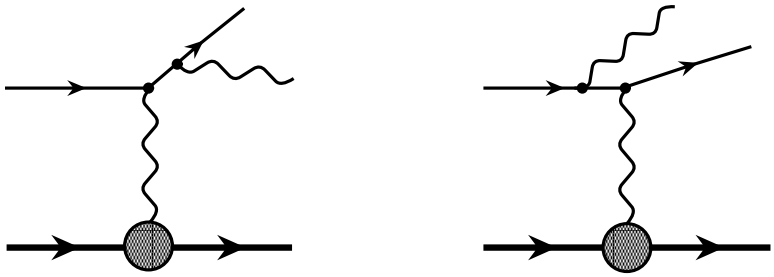

Figure 4.2: The Bethe-Heitler process.

The new information on the hadronic structure is provided from the process in which the real photon is emitted by the proton,

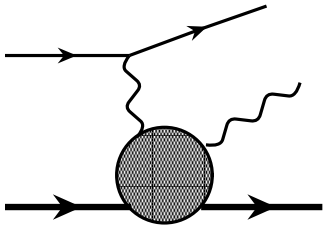

Figure 4.3: The FVCS process.

leading to the T-matrix element

$$T^{FVCS} \;=\; \frac{e^3}{q^2}\,\varepsilon'^*_\nu H^{\mu\nu}\,\bar{u}(k')\gamma_\mu u(k)\;. \tag{4.4}$$

The hadronic tensor $H^{\mu\nu}$ contains the information about the interaction represented by the blob in Fig.(4.3). The superscript "FVCS" at the T-matrix element denotes that also the leptonic vertex is included.

4.2 VCS kinematics

We choose the kinematics so that the VCS reaction $\gamma^* + p \to \gamma + p$ takes place in the xz plane, which is shifted against the leptonic plane by an angle ϕ.

$$\begin{aligned}
k^\mu &= (E_e, |\vec{k}|\sin\alpha\cos\phi, |\vec{k}|\sin\alpha\sin\phi, |\vec{k}|\cos\alpha)\;,\\
k'^\mu &= (E'_e, |\vec{k}'|\sin\alpha'\cos\phi, |\vec{k}'|\sin\alpha'\sin\phi, |\vec{k}'|\cos\alpha')\;,\\
q^\mu &= k^\mu - k'^\mu \;=\; (q_0, 0, 0, |\vec{q}|)
\end{aligned} \tag{4.5}$$

with the electron scattering angle $\Theta_e = \alpha' - \alpha$. Normally, the electron mass ($m_e = 0.511$ MeV) can be neglected compared to the energy of the electron (for instance, $E_e = 855$ MeV at MAMI), thus $|\vec{k}| = \sqrt{E_e^2 - m_e^2} \approx E_e$, and similarly for $|\vec{k}'|$. The virtual photon resulting from electron scattering is spacelike,

$$q^2 \;=\; (k-k')^2 \;=\; 2m_e^2 - 2k\cdot k' \;\approx\; -4E_eE_e'\sin^2\frac{\Theta_e}{2} \;\equiv\; -Q^2 \;\leq\; 0\,, \tag{4.6}$$

with Q^2 the negative value of the virtual photon mass squared.

To decouple the hadronic information from the FVCS amplitude of Eq.(4.4), we note that

$$\bar{u}(k',h)\,\gamma_\mu\,u(k,h) \;=\; \sum_{\lambda=0,\pm1} \Omega(h,\lambda)\,\varepsilon_\mu(q,\lambda)\;, \tag{4.7}$$

where h is the (conserved) electron helicity, ε_μ is the polarization vector of the virtual photon with the four-momentum q and polarization λ. The function $\Omega(h,\lambda)$ is defined by

$$\begin{aligned}
\Omega(h,\lambda) &= \left(-\lambda e^{i\lambda\phi}\alpha(\lambda h) + \delta_{\lambda 0}\sqrt{2\varepsilon}\right)\frac{Q}{\sqrt{1-\varepsilon}}\,,\\
\alpha(z) &= \frac{\sqrt{1+\varepsilon}+2z\sqrt{1-\varepsilon}}{\sqrt{2}}\,,\\
\varepsilon &\equiv \frac{(k+k')^2-\vec{q}^{\,2}}{(k+k')^2+\vec{q}^{\,2}} \;=\; \left[1+2\frac{\vec{q}^{\,2}}{Q^2}\tan^2\frac{\Theta_e}{2}\right]^{-1}\,,
\end{aligned} \tag{4.8}$$

where $Q = \sqrt{Q^2}$, and ε is the virtual photon linear polarization. We next define the VCS helicity amplitude by

$$T^{VCS}(\lambda',\lambda) \;=\; \varepsilon'^{*}_{\nu}(\lambda')\,H^{\mu\nu}\varepsilon_\mu(\lambda)\,, \tag{4.9}$$

where λ' is the helicity of the outgoing real photon. Finally, we can write the FVCS amplitude as

$$T^{FVCS}(\lambda') \;=\; \frac{e^3}{q^2}\sum_\lambda \Omega(h,\lambda)\,T^{VCS}(\lambda',\lambda)\,. \tag{4.10}$$

This decoupling is necessary to take the limit $Q^2 \to 0$ in the amplitude T^{VCS}, which leads to the real Compton amplitude.

We turn now to the kinematics of the hadronic reaction.

The Mandelstam variables for the process $\gamma^* + p \to \gamma + p$ are defined in the standard way,

$$\begin{aligned}
s &= (p+q)^2\,,\\
u &= (p-q')^2\,,\\
t &= (q-q')^2 \;=\; (p'-p)^2\,,
\end{aligned} \tag{4.11}$$

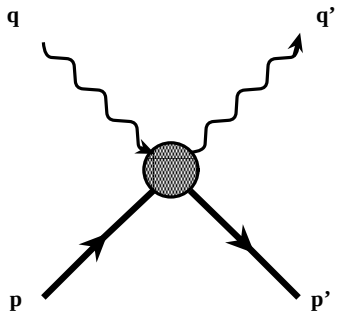

Figure 4.4: VCS kinematics.

with their sum fixed to

$$s + u + t \;=\; 2M^2 - Q^2 \tag{4.12}$$

4.2.1 C.m. kinematics for VCS

In the center-of-mass of the target proton and the virtual photon,

$$\vec{q} + \vec{p} \;=\; \vec{q}\,' + \vec{p}\,' \;=\; 0\,. \tag{4.13}$$

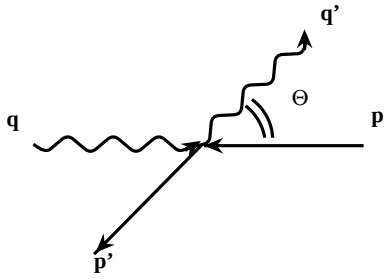

Figure 4.5: Center-of-mass kinematics for VCS.

The c. m. scattering angle is defined as the angle between the incoming and outgoing photon directions in the *xz*-plane.

$$\begin{aligned} q^\mu &= (q_0, 0, 0, |\vec{q}|) \\ p^\mu &= (E, 0, 0, -|\vec{q}|) \\ q'^\mu &= \left(|\vec{q}\,'|, |\vec{q}\,'|\sin\Theta, 0, |\vec{q}\,'|\cos\Theta\right) \\ p'^\mu &= \left(E', -|\vec{q}\,'|\sin\Theta, 0, -|\vec{q}\,'|\cos\Theta\right)\,, \end{aligned} \tag{4.14}$$

where the c.m. quantities can be expressed through the invariants,

$$q_0 \;=\; \frac{s - M^2 - Q^2}{2\sqrt{s}}\,,$$

$$
\begin{aligned}
E &= \frac{s+M^2+Q^2}{2\sqrt{s}}\,, \\
|\vec{q}\,'| &= \frac{s-M^2}{2\sqrt{s}}\,, \\
E' &= \frac{s+M^2}{2\sqrt{s}}\,, \\
|\vec{q}| &= \sqrt{E^2-M^2} \;=\; \sqrt{q_0^2+Q^2}\,, \\
\cos\Theta &= \frac{q_0}{|\vec{q}|} + \frac{t+Q^2}{2|\vec{q}\,'||\vec{q}|}\,.
\end{aligned}
\tag{4.15}
$$

4.3 Generalized polarizabilities

4.3.1 Low energy theorem for VCS

As we have seen for the scattering of the very low energy real photons, a general prescription can be found, which allows one to disentangle the effects of the internal structure of the nucleon from the interaction of the electromagnetic field with the nucleon as a whole. This prescription is given by the low energy theorem (LET), based on the gauge invariance and crossing. For real Compton scattering the pole (Born) contribution is defined by the static properties of the nucleon, i.e. the charge e, the mass M and the anomalous magnetic moment κ. For the VCS the separation of the Born part involves the phenomenological knowledge of the nucleon formfactors. The pole contribution has the form

$$H_B^{\mu\nu} = \bar{u}(p') \left\{ \Gamma^\nu(p', p'+q') \frac{1}{\not{p}+\not{q}-M} \Gamma^\mu(p+q, p) + \Gamma^\mu(p', p'-q) \frac{1}{\not{p}-\not{q}'-M} \Gamma^\nu(p-q', p) \right\} u(p) \qquad (4.16)$$

where the proton electromagnetic vertex is given by Eq.(4.3). It should be stressed that the Born amplitude in this form automatically obeys the gauge invariance with respect to both real and virtual photons,

$$q_\mu H_B^{\mu\nu} = q'_\nu H_B^{\mu\nu} = 0 \,. \qquad (4.17)$$

This means that also the the residual amplitude, $H_{NB} \equiv H - H_B$, is gauge invariant.

It has been shown in Ref. [Gui 95] that H_{NB} is a regular function of q'_ν and q_μ and therefore permits a symbolic expansion with respect to q'_ν:

$$H_{NB} = a^{\mu\nu} + b_\alpha^{\mu\nu} q'^\alpha + c_{\alpha\beta}^{\mu\nu} q'^\alpha q'^\beta + \dots \,, \qquad (4.18)$$

with the coefficients $a^{\mu\nu}$, $b_\alpha^{\mu\nu}$ independent of q'. Contracting now this expansion with q'_ν and averaging over the direction of the three-momentum $\vec{q}\,'$, one obtains

$$a^{\mu\nu} = 0 \,. \qquad (4.19)$$

The same statement holds for the expansion of the VCS tensor in the series in powers of q.

The low energy limit for virtual Compton scattering is defined by

$$|\vec{q}\,'| \to 0 \quad \text{at fixed} \quad |\vec{q}\,| \,, \qquad (4.20)$$

or, in terms of the invariants,

$$s \to M^2 \quad \text{and} \quad t \to -Q^2 \,. \qquad (4.21)$$

For finite Q^2, the Born part starts at the order of $1/|\vec{q}\,'|$. The LET of Eq.(4.19) therefore states that the first two terms of the low energy expansion of the full VCS amplitude are completely fixed by the form factors of the nucleon and its mass, whereas

the effects of the nucleon excitations start with the first power of $|\vec{q}\,'|$.

In the low energy limit, two kinematical quantities appear, which will be useful in the following:

$$\begin{aligned} \tilde{q}_0 &= \lim_{\substack{|\vec{q}\,'|\to 0 \\ \text{at fixed } |\vec{q}\,|}} q_0 = M - \sqrt{M^2+|\vec{q}\,|^2} \\ \tilde{Q} &= \sqrt{|\vec{q}\,|^2 - \tilde{q}_0^2} \end{aligned} \tag{4.22}$$

4.3.2 Multipole expansion of the VCS tensor

The unknown non-Born part of the VCS amplitude should now be parametrized, as in the case of real Compton scattering. In Ref. [Gui 95], it was suggested to perform a multipole expansion of the VCS tensor. This allows one to factorize the angular and spin dependence out of $H_{NB}^{\mu\nu}$ and to obtain a set of multipoles,

$$\begin{aligned} 4\pi\mathcal{N} H_{NB}^{(\rho' L',\rho L)S}(q',q) &= \frac{1}{2S+1} \sum_{\sigma,\sigma',M,M'} (-1)^{\frac{1}{2}+\sigma'+L+M} C^{Ss}_{\frac{1}{2}-\sigma',\frac{1}{2}\sigma} C^{Ss}_{L'M',L-M} \\ &\cdot \int d\hat{q}'\, d\hat{q}\, V_\nu^*(\rho' L' M',\hat{q}')\, H_{NB}^{\mu\nu}(\vec{q}'\sigma',\vec{q}\sigma)\, V_\mu(\rho L M,\hat{q}) \,, \end{aligned} \tag{4.23}$$

where $L(L')$ is the relative angular momentum and $\sigma(\sigma')$ is the nucleon spin in the initial (final) state. The basis vectors $V_\mu(\rho LM,\hat{q})$ can be found in Appendix B of Ref. [Gui 98]. For the Clebsch-Gordan coefficients $C^{JM}_{j_1 m_1, j_2 m_2}$, the conventions of Ref. [Edm 57] are used. The index $\rho(\rho')$ denotes the transition type in the initial (final) state and can take four values, $\rho = 0$ (charge), $\rho = 1$ (magnetic), $\rho = 2$ (electric), and $\rho = 3$ (longitudinal). Finally, the index S corresponds to spin-flip ($S = 1$) or no-spin-flip ($S = 0$) of the nucleon. The longitudinal multipoles are related to the charged ones by gauge invariance,

$$\begin{aligned} |\vec{q}\,'| H_{NB}^{(3L',\rho L)S}(|\vec{q}\,'|,|\vec{q}\,|) + |\vec{q}\,'| H_{NB}^{(0L',\rho L)S}(|\vec{q}\,'|,|\vec{q}\,|) &= 0 \,, \\ q H_{NB}^{(\rho' L',3L)S}(|\vec{q}\,'|,|\vec{q}\,|) + q_0 H_{NB}^{(\rho' L',0L)S}(|\vec{q}\,'|,|\vec{q}\,|) &= 0 \,. \end{aligned} \tag{4.24}$$

Furthermore, Siegert theorem [Sie 37] relates charge and electric multipoles at low momenta,

$$\begin{aligned} H_{NB}^{(2L',\rho L)S}(|\vec{q}\,'|,|\vec{q}\,|) &= -\sqrt{\frac{L'+1}{L'}} H_{NB}^{(0L',\rho L)S}(|\vec{q}\,'|,|\vec{q}\,|) + O(|\vec{q}\,'|^{L'+1}) \\ &\text{for} \quad |\vec{q}\,'| \to 0 \,, \\ H_{NB}^{(\rho' L',2L)S}(|\vec{q}\,'|,|\vec{q}\,|) &= -\sqrt{\frac{L+1}{L}} \frac{\tilde{q}_0}{|\vec{q}\,|} H_{NB}^{(\rho' L',0L)S}(|\vec{q}\,'|,|\vec{q}\,|) + O(|\vec{q}\,|^{L+1}) \\ &\text{for} \quad |\vec{q}\,| \to 0 \,, \end{aligned} \tag{4.25}$$

Therefore, in the low energy limit for VCS, $|\vec{q}\,'| \to 0$ at fixed $|\vec{q}\,|$, the index ρ takes the values (0,1,2), and ρ′ (1,2).

Parity and angular momentum conservation leads to following selection rules:

$$|L'-S| \leq L \leq L'+S\,, \qquad (-1)^{\rho'+L'} = (-1)^{\rho+L}\,. \tag{4.26}$$

4.3.3 Generalized polarizabilities

The low energy behaviour of the multipoles is well established,

$$H_{NB}^{(\rho' L',\rho L)S}(|\vec{q}\,'|,|\vec{q}\,|) \;\sim\; |\vec{q}\,'|^{L'}|\vec{q}\,|^{L} \quad \text{as } |\vec{q}\,|,|\vec{q}\,'| \to 0\,. \tag{4.27}$$

As we are looking for the parametrization of the leading term in the momentum which is linear in q' due to the LET of Eq.(4.19), we consider dipole transitions in the final state only, i.e. $L' = 1$. Together with the selection rules of Eq.(4.26), the restriction $L' = 1$ limits the number of the multipoles to 10:

$$H_{NB}^{(11,00)1},\, H_{NB}^{(11,02)1},\quad H_{NB}^{(11,22)1},\quad H_{NB}^{(11,11)0},\, H_{NB}^{(11,11)1},$$

$$H_{NB}^{(21,01)0},\, H_{NB}^{(21,01)1},\quad H_{NB}^{(21,21)0},\quad H_{NB}^{(21,21)1},\, H_{NB}^{(21,12)1}. \tag{4.28}$$

According to the low energy behaviour of Eq.(4.27), one can define ten functions of $|\vec{q}\,|$ that parametrize the low energy behaviour of the VCS amplitude, the "generalized polarizabilities" of the nucleon (GP's):

$$P^{(\rho' L',\rho L)S}(|\vec{q}\,|) \;\equiv\; \lim_{|\vec{q}\,'|\to 0}\left[\frac{1}{|\vec{q}\,'|}\frac{1}{|\vec{q}\,|^{L}}H_{NB}^{(\rho' L',\rho L)S}(|\vec{q}\,'|,|\vec{q}\,|)\right]\,. \tag{4.29}$$

However, not all these GPs are adequatly defined. This can be seen by considering two different paths to reach the point $q' = 0$, $|\vec{q}\,| = 0$, where the VCS tensor should coincide with its counterpart of real Compton scattering. The problem arises in the Siegert relation of Eq.(4.25). If one takes the RCS limit, i.e. $|\vec{q}\,'| = \tilde{q}_0 = |\vec{q}\,| \to 0$, in Eq.(4.25) the factor $\tilde{q}_0/|\vec{q}\,|$ approaches 1.

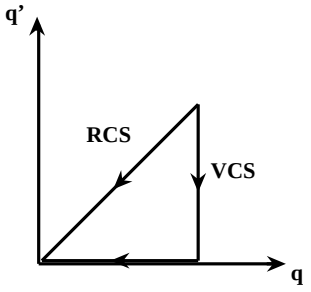

Figure 4.6: Low energy limit for RCS and VCS as a path on the plane of q and q', the three momenta of the initial and final photons, respectively

In the VCS limit, $|\vec{q}\,'| \to 0$ at fixed $|\vec{q}\,|$, and then $|\vec{q}\,| \to 0$. For small values of $|\vec{q}\,|$,

$$\tilde{q}_0 \;=\; M - \sqrt{M^2 + |\vec{q}\,|^2} \;\approx\; -\frac{|\vec{q}\,|^2}{2M}\,, \tag{4.30}$$

thus in the VCS limit, $\tilde{q}_0/|\vec{q}\,|$ approaches 0.

By now, the only property of the VCS tensor that has been used, is the gauge invariance. However, the VCS amplitude should also be symmetric with respect to nucleon crossing (the only two identical particles in the process). In Ref. [Dre 98], it was shown that invariance under nucleon crossing combined with charge conjugation, leads to four relations between GPs allowing one to eliminate those GPs for which the Siegert relation states different RCS and VCS limits (in other words, to keep either electric or charge GP's, with respect to the virtual photon):

$$\begin{aligned}
P^{(11,00)1}(|\vec{q}\,|) &= \sqrt{3}\frac{|\vec{q}\,|^2}{\tilde{q}_0}P^{(01,01)1}(|\vec{q}\,|) - \frac{1}{\sqrt{2}}|\vec{q}\,|^2 P^{(11,02)1}(|\vec{q}\,|)\,,\\
P^{(21,21)0}(|\vec{q}\,|) &= -\frac{\tilde{q}_0}{|\vec{q}\,|}\,P^{(11,11)0}(|\vec{q}\,|)\,,\\
P^{(21,21)1}(|\vec{q}\,|) &= \sqrt{2}|\vec{q}\,|P^{(01,12)1}(|\vec{q}\,|) - 2\frac{|\vec{q}\,|}{\tilde{q}_0}\,P^{(11,11)1}(|\vec{q}\,|)\\
P^{(11,22)1}(|\vec{q}\,|) &= \frac{1}{|\vec{q}\,|}\,P^{(11,11)1}(|\vec{q}\,|)\,.
\end{aligned} \tag{4.31}$$

Finally, one chooses the following six independent GP's:

$$\begin{aligned}
&P^{(01,01)0}(|\vec{q}\,|)\,,\quad P^{(01,01)1}(|\vec{q}\,|)\,,\; P^{(11,11)0}(|\vec{q}\,|)\,,\quad P^{(11,11)1}(|\vec{q}\,|)\,,\\
&\qquad\qquad P^{(01,12)1}(|\vec{q}\,|)\,,\; P^{(11,02)1}(|\vec{q}\,|)\,.
\end{aligned} \tag{4.32}$$

Recently, another nomenclature is getting more popular, where one uses index M (magnetic) instead of $\rho,\rho' = 1$, and E (electric) for $\rho,\rho' = 0$. In this nomenclature, the six GP's are:

$$\begin{aligned}
&P^{(E1,E1)0}(|\vec{q}\,|)\,,\quad P^{(E1,E1)1}(|\vec{q}\,|)\,,\; P^{(M1,M1)0}(|\vec{q}\,|)\,,\quad P^{(M1,M1)1}(|\vec{q}\,|)\,,\\
&\qquad\qquad P^{(E1,M2)1}(|\vec{q}\,|)\,,\; P^{(M1,E2)1}(|\vec{q}\,|)\,.
\end{aligned} \tag{4.33}$$

The ten leading order multipoles are now parametrized through GP's as follows:

$$\begin{aligned}
H_{NB}^{(11,00)1}(|\vec{q}\,'|,|\vec{q}\,|) &= |\vec{q}\,'|\left[\sqrt{3}\frac{|\vec{q}\,|^2}{\tilde{q}_0}P^{(E1,E1)1}(|\vec{q}\,|) - \frac{1}{\sqrt{2}}|\vec{q}\,|^2 P^{(M1,E2)1}(|\vec{q}\,|)\right] + O(|\vec{q}\,'|^2)\,,\\
H_{NB}^{(11,02)1}(|\vec{q}\,'|,|\vec{q}\,|) &= |\vec{q}\,'||\vec{q}\,|^2 P^{(M1,E2)1}(|\vec{q}\,|) + O(|\vec{q}\,'|^2)\,,\\
H_{NB}^{(11,11)S}(|\vec{q}\,'|,|\vec{q}\,|) &= |\vec{q}\,'||\vec{q}\,|P^{(M1,M1)S}(|\vec{q}\,|) + O(|\vec{q}\,'|^2)\,,\; S=0,1\,,\\
H_{NB}^{(21,01)S}(|\vec{q}\,'|,|\vec{q}\,|) &= -\sqrt{2}|\vec{q}\,'||\vec{q}\,|P^{(E1,E1)S}(|\vec{q}\,|) + O(|\vec{q}\,'|^2)\,,\; S=0,1\,,
\end{aligned}$$

$$
\begin{aligned}
H_{NB}^{(21,12)1}(|\vec{q}\,'|,|\vec{q}\,|) &= -\sqrt{2}|\vec{q}\,'||\vec{q}\,|^2 P^{(E1,M2)1}(|\vec{q}\,|) + O(|\vec{q}\,'|^2)\,, \\
H_{NB}^{(11,22)1}(|\vec{q}\,'|,|\vec{q}\,|) &= |\vec{q}\,'||\vec{q}\,|P^{(M1,M1)1}(|\vec{q}\,|) + O(|\vec{q}\,'|^2)\,, \\
H_{NB}^{(21,21)0}(|\vec{q}\,'|,|\vec{q}\,|) &= -|\vec{q}\,'|\tilde{q}_0 P^{(M1,M1)0}(|\vec{q}\,|) + O(|\vec{q}\,'|^2)\,, \\
H_{NB}^{(21,21)1}(|\vec{q}\,'|,|\vec{q}\,|) &= -|\vec{q}\,'|\left[2\frac{|\vec{q}\,|^2}{\tilde{q}_0}P^{(M1,M1)1}(|\vec{q}\,|) - \sqrt{2}|\vec{q}\,|^2 P^{(E1,M2)1}(|\vec{q}\,|)\right] + O(|\vec{q}\,'|^2)\,.
\end{aligned}
\tag{4.34}
$$

At the real photon point $Q^2 = 0$, one finds the following relations between the GP's and the real Compton scattering polarizabilities:

$$
\begin{aligned}
-\frac{e^2}{4\pi}P^{(E1,E1)0}(0) &= \sqrt{\frac{2}{3}}\alpha\,, \\
P^{(E1,E1)1}(0) &= 0\,, \\
-\frac{e^2}{4\pi}P^{(M1,M1)0}(0) &= 2\sqrt{\frac{2}{3}}\beta\,, \\
P^{(M1,M1)1}(0) &= 0\,, \\
-\frac{e^2}{4\pi}P^{(M1,E2)1}(0) &= \frac{2}{3}\sqrt{\frac{2}{3}}(\gamma_2+\gamma_4)\,, \\
-\frac{e^2}{4\pi}P^{(E1,M2)1}(0) &= \frac{\sqrt{2}}{3}\gamma_3\,.
\end{aligned}
\tag{4.35}
$$

4.3.4 A physical interpretation of the GP's

We start with a physical interpretation of the polarizabilities of real Compton scattering. Putting a system of charges (e.g., the nucleon) into a weak electromagnetic field of very low frequency, one first observes the global properties of the system, i.e. its mass, electric charge and magnetic moment. Increasing the frequency of the field (but still keeping it weak enough), one observes that the "elementary" charges inside the system start moving, which leads to the induction of an electric dipole moment $\vec{P}$ which in first approximation grows linearly with the field $\vec{E}$. The coefficient of proportionality is (up to a conventional factor of 4π) the electric polarizability α. In this way, the electric polarizability can be interpreted as the measure of the rigidity of the system of charges in presence of a weak electric field. For a hydrogen atom, the electric polarizability is of the order of its volume, $\alpha_H \approx 1$ Å^3. For the proton, its value is about 10^3 times smaller than its volume (~ 1 fm^3), $\alpha_p \approx 10^{-3}$ fm^3, which characterizes the proton as a very rigid object.

A similar interpretation is also possible for the magnetic polarizability β, though in this case attention should be paid to two different mechanisms that provide the response of the proton to the external magnetic field $\vec{B}$. Paramagnetism is characterized by a positive value of β and comes about due to alignment of the "elementary" magnetic moments inside the proton along the direction of the field, thus increasing its

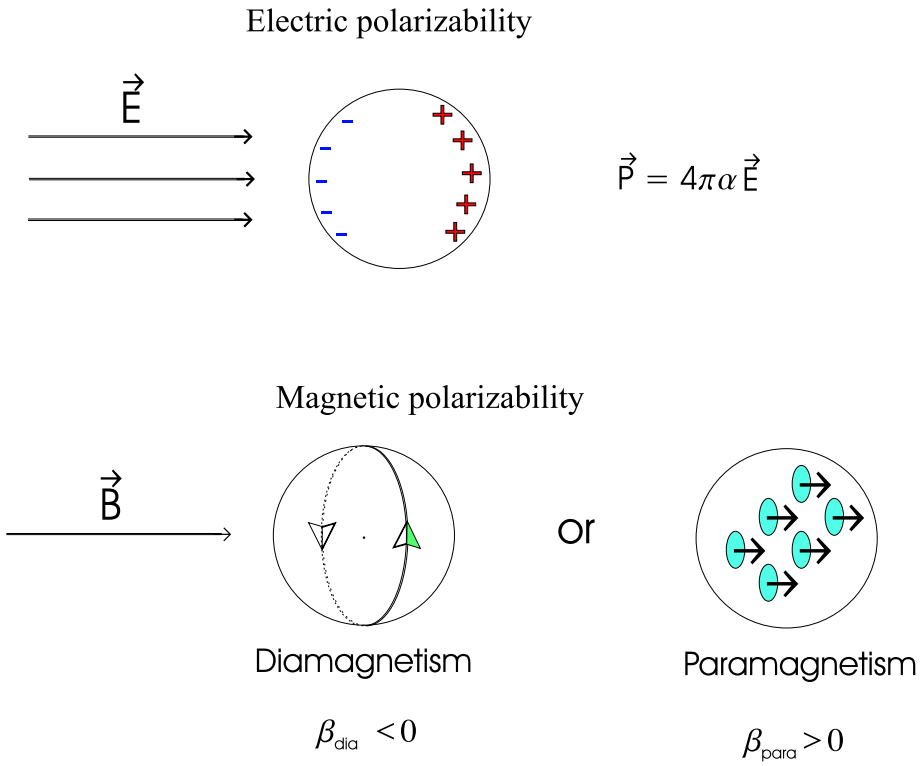

Figure 4.7: A simple interpretation of the electric and magnetic polarizabilities.

strength. On the other hand, the free charges on the surface of the proton (e.g., "pions") get involved into induced surface currents which give rise to an induced magnetic dipole moment $\vec{M}$. Its direction is fixed by Lentz's rule to point opposite to the field $\vec{B}$, and the corresponding diamagnetic polarizability is negative (cf. Fig. 4.7).

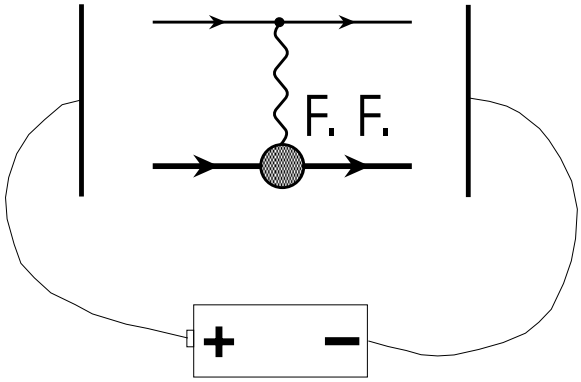

Figure 4.8: Illustration of low energy VCS by replacing the outgoing photon by an external electromagnetic field (for simplicity, a constant electric field of a condensator). The shorthand F.F. stands for the electromagnetic form factors of the proton, accessible in the elastic electron scattering.

In Ref. [Gui 95], it was pointed out that the outgoing photon of very low energy

can be considered as a source of a weak external electromagnetic field constant in time. This allows for a simple picture, illustrating low energy VCS as elastic electron scattering off a proton between the plates of a condensator (Fig. 4.8).

In the Breit frame, the electric form factor of the nucleon is related to the charge distribution inside the nucleon through a Fourier transformation . The dipole electric GP $P^{(E1,E1)0}(|\vec{q}\,|)$ can be then understood as the "local" polarizability, i.e. the measure of the rigidity of the charge distribution of the proton at the distance $r \sim \hbar/|\vec{q}\,|$.

Similarly, the magnetic GP $P^{(M1,M1)0}(|\vec{q}\,|)$ describes the spatial distribution of dia- and paramagnetism inside the nucleon. For a more detailed and strict spatial interpretation of the GP's, performed for the case of a spinless hadron, we refer the reader to the work of Ref. [L'vo 01].

4.3.5 VCS observables

The unpolarized lab cross section for the process $(e,e'\gamma)$ is given in terms of the invariant $\mathcal{M}$ by

$$\frac{d\sigma}{dk'd\Omega_{k'}d\Omega_{p'}} = \frac{1}{(2\pi)^5}\frac{1}{32M}\frac{k'}{k}\frac{|\vec{q}\,'|}{\sqrt{s}}\mathcal{M}\,, \tag{4.36}$$

with

$$\mathcal{M} = \frac{1}{4}\sum_{\sigma,\sigma',h,h',\lambda'} |\,T^{ee'\gamma}\,|^2\,, \tag{4.37}$$

the Lorentz invariant function of the kinematical variables.

A characteristical feature of virtual Compton scattering is the presence of the Bethe-Heitler contribution. This part contains, however, no additional information about the nucleon structure other than the form factors known from elastic scattering. The same is true for the Born contribution. Both processes can be calculated exactly in QED.

The differential $(e,e'\gamma)$ cross section due to these two contributions is shown in Fig. 4.9. The two strong peaks in the upper panel of Fig. 4.9 correspond to the emission of the photon in the direction of the incoming or the outgoing electrons, so that in this angular region the Born contribution is dominated by the BH contribution by several orders of magnitude. If going out of plane, however, the BH contribution can be decreased significantly (cf. lower panel of Fig. 4.9).

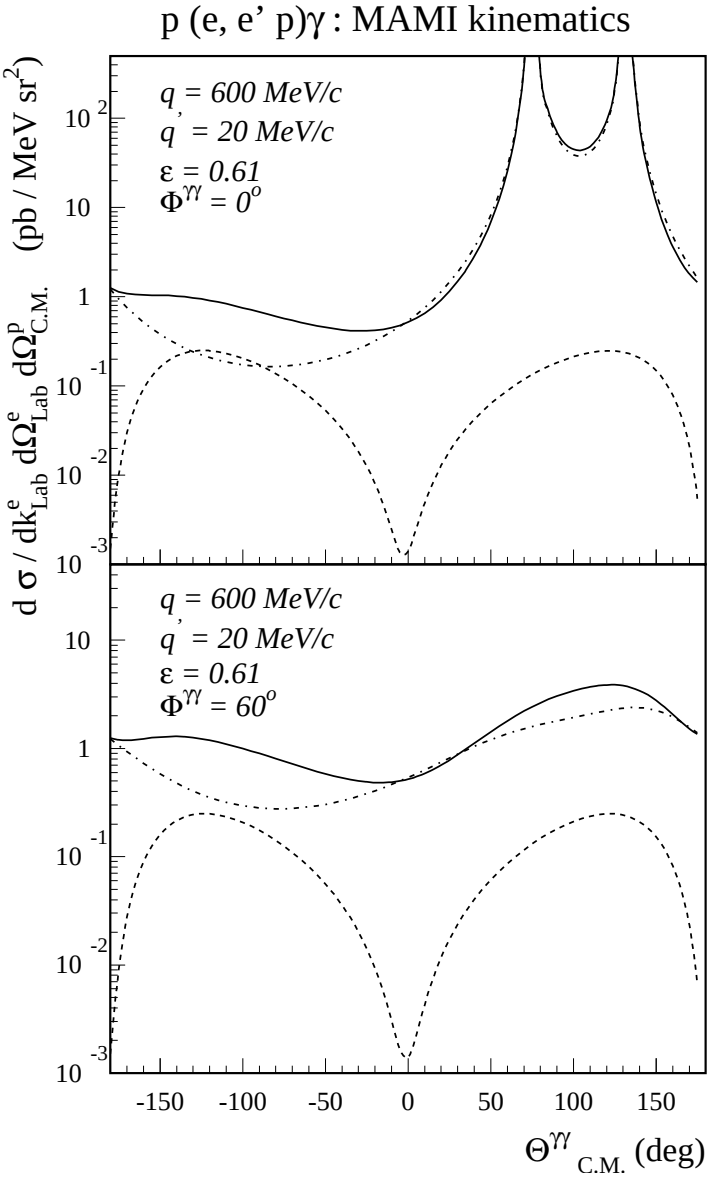

Figure 4.9: The $p(e,e'p)\gamma$ differential cross section in MAMI kinematics. The dashed line corresponds to the Born contribution, the dashed-dotted to the Bethe-Heitler contribution, and the solid line shows their coherent sum. The upper panel shows the results for $\phi = 0°$ (in plane), and the lower panel shows the results for $\phi = 60°$ (out-of-plane).

We now use the low energy theorem to write down the symbolical decomposition of the T-matrix element,

$$T^{ee'\gamma} = T^{BH} + T_B^{FVCS} + T_{NB}^{FVCS} . \tag{4.38}$$

Grouping the first two terms together, we obtain by squaring,

$$\mathcal{M} = \frac{1}{4} \sum_{\sigma,\sigma',h,h',\lambda'} \Big[\mid T^{BH} + T_B^{FVCS} \mid^2 + 2\mathrm{Re}\left([T^{BH} + T_B^{FVCS}]^* T_{NB}^{FVCS} \right) + \mid T_{NB}^{FVCS} \mid^2 \Big] . \tag{4.39}$$

The low energy theorem states that at zero final photon energy, the VCS process is described by BH and Born parts alone. The effects of the internal structure of the nucleon appear with the first power of the energy, compared to the $\sim 1/|\vec{q}\,'|$ behaviour of BH and Born, and therefore can be neglected at very low energies. The further one goes away from the point $|\vec{q}\,'| = 0$, the more important becomes the effect of the polarizabilities. The dominance of the BH and Born signals in the low energy region makes it difficult to measure the relatively small effects of the nucleon structure. On the other hand, however, these large contributions 'amplify' the small non-Born part in the cross term. Expanding Eq.(4.39) in energy and keeping the terms up to order $|\vec{q}\,'|^0$, we obtain

$$\mathcal{M} = \frac{\mathcal{M}_{-2}^{BH+Born}}{|\vec{q}\,'|^2} + \frac{\mathcal{M}_{-1}^{BH+Born}}{|\vec{q}\,'|} + \mathcal{M}_0^{BH+Born} + \mathcal{M}_0^{NB} + O(|\vec{q}\,'|) , \tag{4.40}$$

The measurement of the $(e,e'\gamma)$ cross section at very low outgoing photon energy can be used as a test of the low energy expansion. At higher energies, the effects of the GP's cause deviations of the measured cross section from the Bethe-Heitler and Born terms. The low energy expansion of the difference

$$\mathcal{M}^{exp} - \mathcal{M}^{BH+Born} = \mathcal{M}_0^{NB} + O(|\vec{q}\,'|) \tag{4.41}$$

starts with the zeroth power of energy and contains the signal of the GP's which govern the low energy expansion of T_{NB}^{FVCS}. The leading term, $\mathcal{M}_0^{NB}$, can be expressed in terms of three structure functions, [Gui 95], [Vdh 97],

$$\mathcal{M}_0^{exp} - \mathcal{M}_0^{BH+Born} = 2K_2 \quad \{ v_1 [\varepsilon P_{LL}(|\vec{q}|) - P_{TT}(|\vec{q}|)] + (v_2 - \frac{\tilde{q}_0}{|\vec{q}|} v_3) \sqrt{2\varepsilon(1+\varepsilon)} P_{LT}(|\vec{q}|) \Big\} , \tag{4.42}$$

with

$$P_{LL}(|\vec{q}|) = -2\sqrt{6} M G_E(\tilde{Q}^2) P^{(E1,E1)0}(|\vec{q}|) , \tag{4.43}$$

$$P_{TT}(|\vec{q}|) = -3 G_M(\tilde{Q}^2) \frac{|\vec{q}|^2}{\tilde{q}_0} \left(P^{(M1,M1)1}(|\vec{q}|) - \sqrt{2}\tilde{q}_0 P^{(E1,M2)1}(|\vec{q}|) \right) , \tag{4.44}$$

$$P_{LT}(|\vec{q}|) = \sqrt{\frac{3}{2}}\frac{M|\vec{q}|}{\tilde{Q}} G_E(\tilde{Q}^2) P^{(M1,M1)0}(|\vec{q}|) + \frac{3}{2}\frac{\tilde{Q}|\vec{q}|}{\tilde{q}_0} G_M(\tilde{Q}^2) P^{(E1,E1)1}(|\vec{q}|) . \tag{4.45}$$

These equations contain a phase space factor K_2

$$K_2 = e^6 \frac{|\vec{q}|}{\tilde{Q}^2}\frac{2M}{1-\varepsilon}\sqrt{\frac{2E_q}{E_q+M}}, \quad E_q = \sqrt{|\vec{q}|^2+M^2}, \tag{4.46}$$

and the kinematical factors

$$\begin{aligned} v_1 &= \sin\Theta\,(\omega'' \sin\Theta - k_T\omega' \cos\Theta\cos\phi) , \\ v_2 &= -(\omega'' \sin\Theta\cos\phi - k_T\omega' \cos\Theta) , \\ v_3 &= -(\omega'' \sin\Theta\cos\Theta\cos\phi - k_T\omega'(1-\sin^2\Theta\cos^2\phi) , \end{aligned} \tag{4.47}$$

where

$$\begin{aligned} \omega &= \lim_{|\vec{q}'|\to 0}\left[-|\vec{q}'|(\frac{1}{p\cdot q'}+\frac{1}{k\cdot q'})\right] , \\ \omega' &= \lim_{|\vec{q}'|\to 0}\left[|\vec{q}'|(\frac{1}{k'\cdot q'}-\frac{1}{k\cdot q'})\right] , \\ \omega'' &= \omega|\vec{q}| - \omega'\sqrt{\tilde{k}'^2 - k_T^2} , \\ k_T &= \tilde{Q}\sqrt{\frac{\varepsilon}{2(1-\varepsilon)}} . \end{aligned} \tag{4.48}$$

By measuring at fixed ε and $|\vec{q}|$, and different scattering angles, it is then possible to extract $\varepsilon P_{LL} - P_{TT}$ and P_{LT} due to the different angular dependence of the corresponding kinematical factors. Performing such a measurement at two values of ε, it is possible to extract all three structure functions P_{LL}, P_{TT} and P_{LT}.

For the first time, this formalism was exploited for the analysis of the VCS experiment at Mainz [Roc 00] at $|\vec{q}| = 600$ Mev/c, $\varepsilon = 0.62$, $\tilde{Q}^2 = 0.33$ (GeV/c)^2 and in the photon energy range $33.6 - 111.5$ MeV/c to extract the generalized polarizabilities of the nucleon.

In Fig. 4.10, the comparison of the measured VCS cross section with the Bethe-Heitler and Born contributions is shown. Comparison with the data at low $|\vec{q}'|$ confirms the low energy theorem of Ref.[Gui 95], and at higher energies, the deviation of the data from the theoretical cross section shows the effect of the GP's.

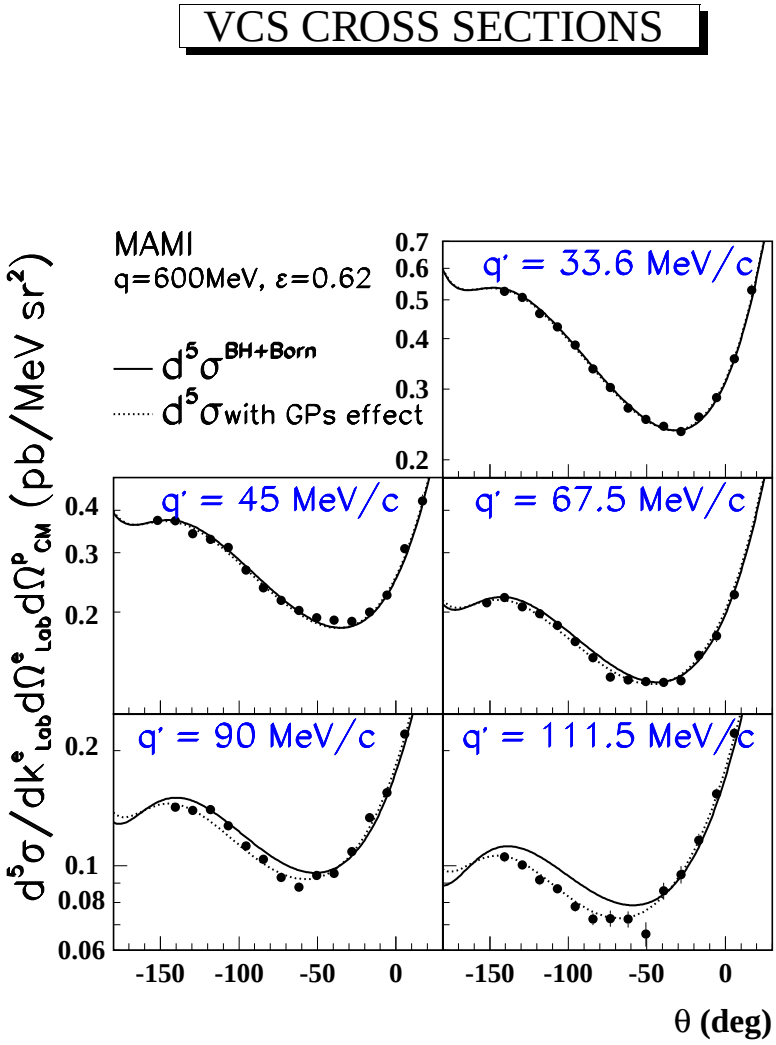

Figure 4.10: The 5-fold differential cross section for the reaction $e + p \rightarrow e' + p' + \gamma$ as a function of the c.m. photon scattering angle at different photon energies. The full line corresponds to the Bethe-Heitler + Born contributions. The dotted line is the fi t to the MAMI data [Roc 00].

The difference between the measured cross section and the BH + Born cross section, divided by $|\vec{q}\,'|$ and a phase space factor Φ, is shown in Fig.4.11. As a function of photon energy, the leading term is roughly constant in $|\vec{q}\,'|$. At each photon scattering angle, the fit with a constant was performed.

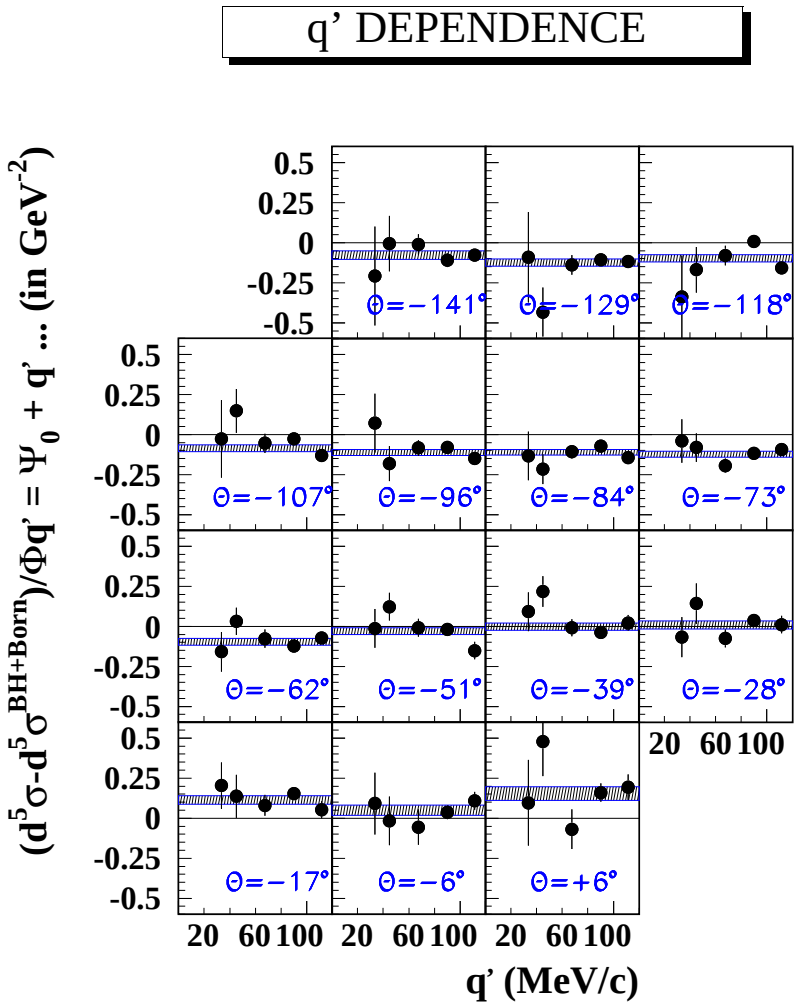

Figure 4.11: The 5-fold differential cross section difference for the reaction $e + p \to e' + p' + \gamma$ as a function of the photon energy at different c.m. photon scattering angles. The bands correspond to the fi t of the data by a constant term in the energy [Roc 00].

Finally, the constants Ψ_0 obtained from the fit, are shown in Fig.4.12 in a plot Ψ_0/ν_2 versus ν_1/ν_2. The structure functions parametrizing Ψ_0 were then extracted from the fit with a straight line. The value at the point $\nu_1/\nu_2 = 0$ gives the structure function P_{LT}, and the slope gives the value of $P_{LL} - P_{TT}/\varepsilon$. The results of this pioneering experiment are:

$$P_{LT} = (-5.0 \pm 0.8)\, GeV^{-2} \qquad P_{LL} - \frac{P_{TT}}{\varepsilon} = (23.7 \pm 2.2)\, GeV^{-2}\,. \tag{4.49}$$

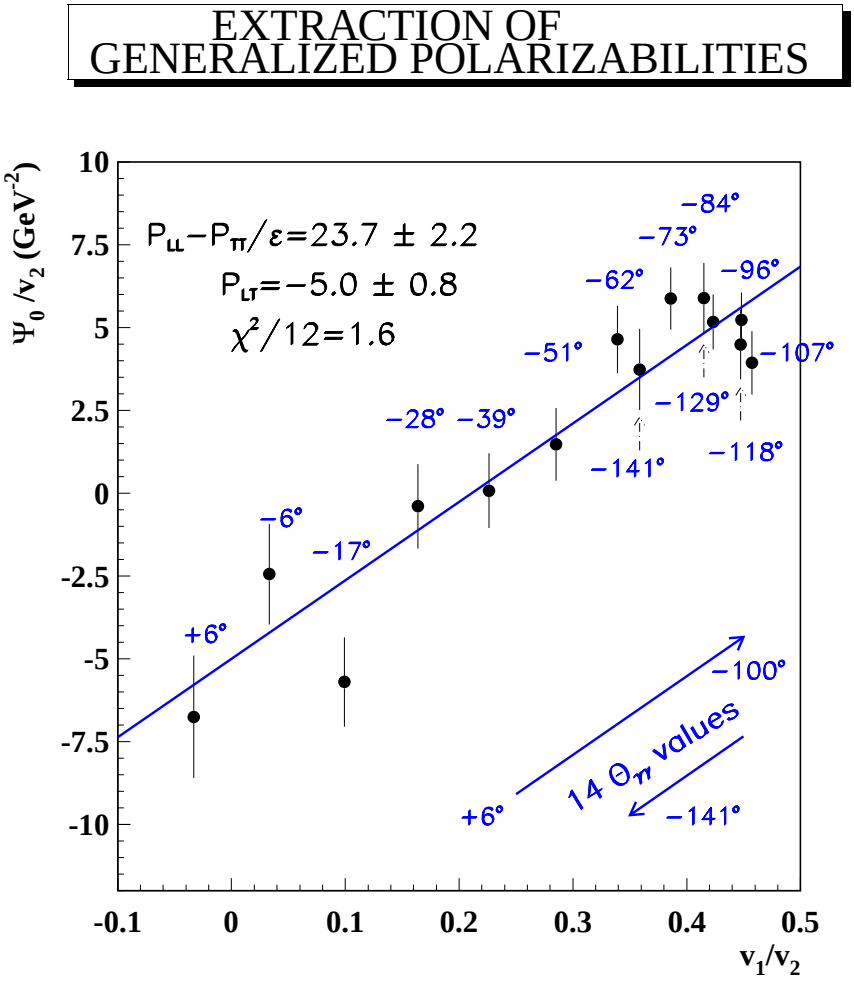

Figure 4.12: The data points represent the constants Ψ_0 obtained in the fit of Fig. 4.11 at different scattering angles. The straight line corresponds to the linear fit with the structure function P_{LT} determined from the value of Ψ_0/ν_2 at $\nu_1 = 0$, and the combination $P_{LL} - P_{LL}/\varepsilon$ is obtained from the slope.

By measuring the unpolarized VCS cross section at low energies (below pion threshold), it is in principle possible to extract three of the six GP's. To get access to the other three, one has to consider polarizations of the particles. Since the single spin asymmetry, being sensitive to the imaginary part of the VCS amplitude, is almost zero below pion threshold, it was suggested to use a polarized electron beam and measure the recoil proton polarization [Vdh 97], [Gui 98]. We denote

$$\Delta\mathcal{M}(h,i) \;=\; \mathcal{M}(h,\sigma_i') - \mathcal{M}(h,-\sigma_i')\;, \tag{4.50}$$

with

$$\mathcal{M}(h,\sigma_i') \;=\; \frac{1}{2}\sum_{\sigma,h',\lambda'} \mid T^{ee'\gamma} \mid^2 , \tag{4.51}$$

where, σ_i' is the projection of the outgoing nucleon spin onto the basis vector i.

Decomposing this observable into Bethe-Heitler plus Born and non-Born parts, and performing the low energy expansions, one obtains [Vdh 97],[Gui 98]:

$$\begin{aligned}\Delta\mathcal{M}_0^{exp}(h,z) \;-\; \Delta\mathcal{M}_0^{BH+Born}(h,z) \;=\; 4(2h)K_2 \Big\{ & -v_1\sqrt{1-\varepsilon^2}P_{TT}(|\vec{q}\,|) \\ & + \sqrt{2\varepsilon(1-\varepsilon)}\,\left(v_2 P_{LT}^{z}(|\vec{q}\,|) + v_3 P_{LT}^{\prime z}(|\vec{q}\,|)\right)\Big\}\;,\end{aligned} \tag{4.52}$$

for the recoil proton polarization along the z-axis;

$$\begin{aligned}\Delta\mathcal{M}_0^{exp}(h,x) \;-\; & \Delta\mathcal{M}_0^{BH+Born}(h,x) \\ =\; 4(2h)K_2 \;\; & \Big\{ v_1^x\sqrt{2\varepsilon(1-\varepsilon)}P_{LT}^{\perp}(|\vec{q}\,|) + v_2^x\sqrt{1-\varepsilon^2}P_{TT}^{\perp}(|\vec{q}\,|) \\ & + v_3^x\sqrt{1-\varepsilon^2}P_{TT}^{\prime\perp}(|\vec{q}\,|) + v_4^x\sqrt{2\varepsilon(1-\varepsilon)}P_{LT}^{\prime\perp}(|\vec{q}\,|)\Big\}\;,\end{aligned} \tag{4.53}$$

for the recoil proton polarization along the x-axis and finally,

$$\begin{aligned}\Delta\mathcal{M}_0^{exp}(h,y) \;-\; & \Delta\mathcal{M}_0^{BH+Born}(h,y) \\ =\; 4(2h)K_2 \;\; & \Big\{ v_1^y\sqrt{2\varepsilon(1-\varepsilon)}P_{LT}^{\perp}(|\vec{q}\,|) + v_2^y\sqrt{1-\varepsilon^2}P_{TT}^{\perp}(|\vec{q}\,|) \\ & + v_3^y\sqrt{1-\varepsilon^2}P_{TT}^{\prime\perp}(|\vec{q}\,|) + v_4^y\sqrt{2\varepsilon(1-\varepsilon)}P_{LT}^{\prime\perp}(|\vec{q}\,|)\Big\}\;,\end{aligned} \tag{4.54}$$

for the recoil proton polarization along the y-axis.

In the above formulas, the three more structure functions appear,

$$\begin{aligned} P_{LT}^{z}(|\vec{q}\,|) &= \frac{3}{2}\frac{\tilde{Q}|\vec{q}\,|}{\tilde{q}_0}G_M(\tilde{Q}^2)P^{(E1,E1)1}(|\vec{q}\,|) - \frac{3M|\vec{q}\,|}{\tilde{Q}}G_E(\tilde{Q}^2)P^{(M1,M1)1}(|\vec{q}\,|)\;, \\ P_{LT}^{\prime z}(|\vec{q}\,|) &= -\frac{3}{2}\tilde{Q}\,G_M(\tilde{Q}^2)P^{(E1,E1)1}(|\vec{q}\,|) + \frac{3M|\vec{q}\,|^2}{\tilde{Q}\tilde{q}_0}G_E(\tilde{Q}^2)P^{(M1,M1)1}(|\vec{q}\,|)\;, \end{aligned}$$

$$P'^{\perp}_{LT}(|\vec{q}|) = G_M(\tilde{Q}^2)\frac{3|\vec{q}|\tilde{Q}}{2\tilde{q}_0}\left(P^{(E1,E1)1}(|\vec{q}|) - \sqrt{\frac{3}{2}}\tilde{q}_0 P^{(M1,E2)1}(|\vec{q}|)\right) , \tag{4.55}$$

and three combinations of already defined structure functions were introduced for convenience,

$$\begin{aligned} P^{\perp}_{LT} &= \frac{MG_E}{\tilde{Q}G_M}P_{TT} - \frac{\tilde{Q}G_M}{4MG_E}P_{LL} , \\ P^{\perp}_{TT} &= \frac{\tilde{Q}G_M}{2MG_E}(P^z_{LT} - P_{LT}) , \\ P'^{\perp}_{TT} &= \frac{\tilde{Q}G_M}{2MG_E}\left(P'^z_{LT} + \frac{\tilde{q}_0}{|\vec{q}|}P_{LT}\right) . \end{aligned} \tag{4.56}$$

The kinematical factors in the above formulas are:

$$\begin{aligned} v^x_1 &= \sin\Theta\cos\phi\,(\omega''\sin\Theta - k_T\omega'\cos\Theta\cos\phi) , \\ v^x_2 &= -(\omega''\sin\Theta - k_T\omega'\cos\Theta\cos\phi) , \\ v^x_3 &= -\cos\Theta\,(\omega''\sin\Theta - k_T\omega'\cos\Theta\cos\phi) , \\ v^x_4 &= k_T\omega'\sin\Theta\sin^2\phi , \end{aligned}$$

$$\begin{aligned} v^y_1 &= \sin\Theta\sin\phi\,(\omega''\sin\Theta - k_T\omega'\cos\Theta\cos\phi) , \\ v^y_2 &= k_T\omega'\cos\Theta\sin\phi , \\ v^y_3 &= k_T\omega'\sin\phi , \\ v^x_4 &= -k_T\omega'\sin\Theta\sin\phi\cos\phi . \end{aligned} \tag{4.57}$$

In conclusion there appear six independent structure functions,

$$P_{LL} ,\ P_{LT} ,\ P_{TT} ,\ P^z_{LT} ,\ P'^z_{LT} ,\ P^{\perp}_{LT} , \tag{4.58}$$

whose leading terms are given by the six independent GP's. In this way, the low energy formalism for VCS allows one to measure all six GP's by carrying out unpolarized and doubly polarized VCS experiments.

However, VCS experiments below pion electroproduction threshold are complicated due to the dominance of the Bethe-Heitler and Born contributions, and the effect of the GP's in the cross section is of the order 10-15% in the kinematics of the MAMI experiment. To increase the sensitivity to the GP's, one has to go to energies close to or above pion threshold, in which range the low energy expansion is no longer valid.

Our aim is therefore to extend the theoretical analysis of the VCS observables to energies above pion threshold. For this, the dispersion relation formalism presented in the RCS part of this work has to be generalized to the case of finite Q^2.

For this purpose, a complete set of invariant VCS amplitudes has to be constructed,

which should be linearly independent and non-singular. The possible polarizations of the particles yield

$$2_{(p_{in})} \times 3_{(\gamma^*)} \times 2_{(p_{out})} \times 2_{(\gamma)} \,/\, 2_{(Parity)} \;=\; 12 \tag{4.59}$$

independent helicity amplitudes. Accordingly, twelve linearly independent and non-singular basis tensors can be found. In Section 4.4, the appropriate tensor basis will be chosen, and the properties of the invariant amplitudes will be investigated.

In order to provide the input into the dispersion integrals and to investigate the high energy behaviour of the invariant amplitudes, the analytical relations between the invariant amplitudes and the s-channel helicity amplitudes have to be found. These relations should not contain any kinematical singularities. Though very technical, this calculation is very important for the following. It was therefore decided to present this calculation in detail in Appendix G.1.

4.4 VCS tensor basis

The total amplitude for the VCS process has the form

$$T^{VCS} \;=\; -ie^2\varepsilon_\mu(q,\lambda)\;\varepsilon_\nu^{'*}(q',\lambda')\;\bar{u}(p',\sigma')H^{\mu\nu}u(p,\sigma)\;, \tag{4.60}$$

and the VCS tensor $H^{\mu\nu}$ can be parametrized in terms of 12 independent amplitudes. In Ref. [Dre 98], which used the basis of Tarrach [Tar 75] as the starting point, a tensor basis was found so that the resulting invariant amplitudes are free from kinematical singularities and constraints, which is an important property when setting up a dispersion relation formalism. In detail, we denote the tensor $H^{\mu\nu}$ as

$$H^{\mu\nu} \;=\; \sum_{i=1}^{12} f_i(Q^2,\nu,t)\,\rho_i^{\mu\nu}\;. \tag{4.61}$$

The 12 independent invariant amplitudes f_i are expressed in terms of the invariants Q^2, ν and t, but are otherwise identical with the amplitudes used in Ref. [Dre 98]. Introducing the four-vectors $P=\frac{1}{2}(p+p')$ and $K=\frac{1}{2}(q+q')$, the 12 independent tensors $\rho_i^{\mu\nu}$ of Ref. [Dre 98] are given by:

$$\begin{aligned}
\varepsilon_\mu\varepsilon_\nu^{'*}\,\rho_1^{\mu\nu} &= -q\cdot q'\,\varepsilon\cdot\varepsilon^{'*} + \varepsilon\cdot q'\,\varepsilon^{'*}\cdot q\;, \\
\varepsilon_\mu\varepsilon_\nu^{'*}\,\rho_2^{\mu\nu} &= -(2M\nu)^2\,\varepsilon\cdot\varepsilon^{'*} - 4q\cdot q'\,\varepsilon\cdot P\,\varepsilon^{'*}\cdot P \\
&+ 4M\nu\left(\varepsilon\cdot P\,\varepsilon^{'*}\cdot q + \varepsilon^{'*}\cdot P\,\varepsilon\cdot q'\right)\;, \\
\varepsilon_\mu\varepsilon_\nu^{'*}\,\rho_3^{\mu\nu} &= -2M\nu\,Q^2\,\varepsilon\cdot\varepsilon^{'*} - 2M\nu\,\varepsilon\cdot q\,\varepsilon^{'*}\cdot q \\
&+ 2Q^2\varepsilon^{'*}\cdot P\,\varepsilon\cdot q' + 2q\cdot q'\varepsilon^{'*}\cdot P\,\varepsilon\cdot q\;, \\
\varepsilon_\mu\varepsilon_\nu^{'*}\,\rho_4^{\mu\nu} &= 8\,\varepsilon\cdot P\,\varepsilon^{'*}\cdot P\not{K} - 4M\nu\left(\varepsilon\cdot P\not{\varepsilon}^{'*} + \varepsilon^{'*}\cdot P\not{\varepsilon}\right) \\
&+ i4M\nu\,\gamma_5\,\varepsilon_{\mu\nu\alpha\beta}\,\varepsilon^\mu\varepsilon^{'*\nu}K^\alpha\gamma^\beta\;, \\
\varepsilon_\mu\varepsilon_\nu^{'*}\,\rho_5^{\mu\nu} &= \varepsilon^{'*}\cdot P\,\varepsilon\cdot q\not{K} - \frac{Q^2}{2}\left(\varepsilon\cdot P\not{\varepsilon}^{'*} - \varepsilon^{'*}\cdot P\not{\varepsilon}\right) - M\nu\,\varepsilon\cdot q\not{\varepsilon}^{'*} \\
&- \frac{i}{2}Q^2\gamma_5\,\varepsilon_{\mu\nu\alpha\beta}\,\varepsilon^\mu\varepsilon^{'*\nu}K^\alpha\gamma^\beta\;, \\
\varepsilon_\mu\varepsilon_\nu^{'*}\,\rho_6^{\mu\nu} &= -8\,q\cdot q'\,\varepsilon\cdot P\,\varepsilon^{'*}\cdot P + 4M\nu\left(\varepsilon\cdot P\,\varepsilon^{'*}\cdot q + \varepsilon^{'*}\cdot P\,\varepsilon\cdot q'\right) \\
&+ 4M\,q\cdot q'\left(\varepsilon\cdot P\not{\varepsilon}^{'*} + \varepsilon^{'*}\cdot P\not{\varepsilon}\right) \\
&- (2M)^2\nu\left(\varepsilon\cdot q'\not{\varepsilon}^{'*} + \varepsilon^{'*}\cdot q\not{\varepsilon}\right) \\
&+ i4M\nu\left(\varepsilon\cdot q'\,\sigma^{\nu\alpha}\varepsilon_\nu^{'*}K_\alpha - \varepsilon^{'*}\cdot q\,\sigma^{\mu\alpha}\varepsilon_\mu K_\alpha + q\cdot q'\,\sigma^{\mu\nu}\varepsilon_\mu\varepsilon_\nu^{'*}\right) \\
&+ i4M\,q\cdot q'\,\gamma_5\,\varepsilon_{\mu\nu\alpha\beta}\,\varepsilon^\mu\varepsilon^{'*\nu}K^\alpha\gamma^\beta\;, \\
\varepsilon_\mu\varepsilon_\nu^{'*}\,\rho_7^{\mu\nu} &= \left(\varepsilon\cdot P\,\varepsilon^{'*}\cdot q - \varepsilon^{'*}\cdot P\,\varepsilon\cdot q'\right)\not{K} \\
&- q\cdot q'\left(\varepsilon\cdot P\not{\varepsilon}^{'*} - \varepsilon^{'*}\cdot P\not{\varepsilon}\right) + M\nu\left(\varepsilon\cdot q'\not{\varepsilon}^{'*} - \varepsilon^{'*}\cdot q\not{\varepsilon}\right)\;, \\
\varepsilon_\mu\varepsilon_\nu^{'*}\,\rho_8^{\mu\nu} &= M\nu\,\varepsilon\cdot q\,\varepsilon^{'*}\cdot q + \frac{Q^2}{2}\left(\varepsilon\cdot P\,\varepsilon^{'*}\cdot q - \varepsilon^{'*}\cdot P\,\varepsilon\cdot q'\right)
\end{aligned} \tag{4.62}$$

$$
\begin{aligned}
&- \quad q\cdot q'\,\varepsilon'^{*}\cdot P\,\varepsilon\cdot q - M\,\varepsilon\cdot q\,\varepsilon'^{*}\cdot q\not{K} \\
&+ \quad M\,q\cdot q'\,\varepsilon\cdot q\not{\varepsilon}'^{*} + \frac{M}{2}Q^2\left(\varepsilon\cdot q'\not{\varepsilon}'^{*} - \varepsilon'^{*}\cdot q\not{\varepsilon}'\right) \\
&- \quad \frac{i}{2}Q^2\left(\varepsilon\cdot q'\,\sigma^{\nu\alpha}\varepsilon'^{*}_{\nu}K_{\alpha} - \varepsilon'^{*}\cdot q\,\sigma^{\mu\alpha}\varepsilon_{\mu}K_{\alpha} + q\cdot q'\,\sigma^{\mu\nu}\varepsilon_{\mu}\varepsilon'^{*}_{\nu}\right) , \\
\varepsilon_{\mu}\varepsilon'^{*}_{\nu}\rho_{9}^{\mu\nu} &= 2M\nu\left(\varepsilon\cdot P\,\varepsilon'^{*}\cdot q - \varepsilon'^{*}\cdot P\,\varepsilon\cdot q'\right) \\
&- \quad 2M\,q\cdot q'\left(\varepsilon\cdot P\not{\varepsilon}'^{*} - \varepsilon'^{*}\cdot P\not{\varepsilon}\right) \\
&+ \quad 2M^2\nu\left(\varepsilon\cdot q'\not{\varepsilon}'^{*} - \varepsilon'^{*}\cdot q\not{\varepsilon}\right) \\
&+ \quad i2q\cdot q'\left(\varepsilon\cdot P\,\sigma^{\nu\alpha}\varepsilon'^{*}_{\nu}K_{\alpha} + \varepsilon'^{*}\cdot P\,\sigma^{\mu\alpha}\varepsilon_{\mu}K_{\alpha}\right) \\
&- \quad i2M\nu\left(\varepsilon\cdot q'\,\sigma^{\nu\alpha}\varepsilon'^{*}_{\nu}K_{\alpha} + \varepsilon'^{*}\cdot q\,\sigma^{\mu\alpha}\varepsilon_{\mu}K_{\alpha}\right) , \\
\varepsilon_{\mu}\varepsilon'^{*}_{\nu}\rho_{10}^{\mu\nu} &= 2\left(\varepsilon\cdot P\,\varepsilon'^{*}\cdot q + \varepsilon'^{*}\cdot P\,\varepsilon\cdot q'\right) + 4M\,\varepsilon\cdot\varepsilon'^{*}\not{K} \\
&- \quad 2M\left(\varepsilon\cdot q'\not{\varepsilon}'^{*} + \varepsilon'^{*}\cdot q\not{\varepsilon}\right) - 4M\nu\,\varepsilon\cdot\varepsilon'^{*} \\
&- \quad 2i\left(\varepsilon\cdot q'\,\sigma^{\nu\alpha}\varepsilon'^{*}_{\nu}K_{\alpha} - \varepsilon'^{*}\cdot q\,\sigma^{\mu\alpha}\varepsilon_{\mu}K_{\alpha} + q\cdot q'\,\sigma^{\mu\nu}\varepsilon_{\mu}\varepsilon'^{*}_{\nu}\right) , \\
\varepsilon_{\mu}\varepsilon'^{*}_{\nu}\rho_{11}^{\mu\nu} &= 4\left(\varepsilon\cdot P\,\varepsilon'^{*}\cdot q + \varepsilon'^{*}\cdot P\,\varepsilon\cdot q'\right)\not{K} - 4M\nu\left(\varepsilon\cdot q'\not{\varepsilon}'^{*} + \varepsilon'^{*}\cdot q\not{\varepsilon}\right) \\
&+ \quad i4q\cdot q'\,\gamma_5\,\varepsilon_{\mu\nu\alpha\beta}\,\varepsilon^{\mu}\varepsilon'^{*\nu}K^{\alpha}\gamma^{\beta} , \\
\varepsilon_{\mu}\varepsilon'^{*}_{\nu}\rho_{12}^{\mu\nu} &= 2Q^2\,\varepsilon\cdot P\,\varepsilon'^{*}\cdot P + 2M\nu\,\varepsilon'^{*}\cdot P\,\varepsilon\cdot q \\
&- \quad 2MQ^2\,\varepsilon\cdot P\not{\varepsilon}'^{*} - 2M^2\nu\,\varepsilon\cdot q\not{\varepsilon}'^{*} \\
&+ \quad iQ^2\left(\varepsilon\cdot P\,\sigma^{\nu\alpha}\varepsilon'^{*}_{\nu}K_{\alpha} + \varepsilon'^{*}\cdot P\,\sigma^{\mu\alpha}\varepsilon_{\mu}K_{\alpha} - M\nu\,\sigma^{\mu\nu}\varepsilon_{\mu}\varepsilon'^{*}_{\nu}\right) \\
&+ \quad i2M\nu\,\varepsilon\cdot q\,\sigma^{\nu\alpha}\varepsilon'^{*}_{\nu}K_{\alpha} - iMQ^2\,\gamma_5\,\varepsilon_{\mu\nu\alpha\beta}\,\varepsilon^{\mu}\varepsilon'^{*\nu}K^{\alpha}\gamma^{\beta} ,
\end{aligned}
$$

The tensor basis of Eq.(4.63) was chosen in Ref. [Dre 98] such that the resulting invariant amplitudes f_i are either even or odd under crossing. Photon crossing leads to the following symmetry relations among the f_i at the real photon point :

$$
\begin{aligned}
f_i\left(Q^2=0,\nu,t\right) &= +\,f_i\left(Q^2=0,-\nu,t\right) , \quad (i=1,2,6,11) , \\
f_i\left(Q^2=0,\nu,t\right) &= -\,f_i\left(Q^2=0,-\nu,t\right) , \quad (i=4,7,9,10) .
\end{aligned} \tag{4.63}
$$

The amplitudes f_3, f_5, f_8, f_{12} do not contribute in this limit, because the corresponding tensors in Eq.(4.63) vanish for $Q^2 \to 0$.

Nucleon crossing combined with charge conjugation provides the following constraints on the f_i at arbitrary virtuality Q^2 :

$$
\begin{aligned}
f_i\left(Q^2,\nu,t\right) &= +\,f_i\left(Q^2,-\nu,t\right) , \quad (i=1,2,5,6,7,9,11,12) , \\
f_i\left(Q^2,\nu,t\right) &= -\,f_i\left(Q^2,-\nu,t\right) , \quad (i=3,4,8,10) ,
\end{aligned} \tag{4.64}
$$

It will be convenient to set up dispersion relations with amplitudes which are all even in ν. Therefore, we define new amplitudes F_i (i = 1,...,12) as follows:

$$
\begin{aligned}
F_i\left(Q^2,\nu,t\right) &= f_i\left(Q^2,\nu,t\right) , \quad (i=1,2,5,6,7,9,11,12) , \\
F_i\left(Q^2,\nu,t\right) &= \frac{1}{\nu} f_i\left(Q^2,\nu,t\right) , \quad (i=3,4,8,10) .
\end{aligned} \tag{4.65}
$$

These amplitudes satisfy $F_i\left(Q^2,-\nu,t\right) = F_i\left(Q^2,\nu,t\right)$ for i = 1,...,12. As the non-Born invariant amplitudes $f_{3,4,8,10} \sim \nu$ for $\nu \to 0$, the definition of Eq.(4.65) ensures that all the non-Born F_i (i = 1,...,12) are also free from kinematical singularities.

From Eqs.(4.63) and (4.64), one furthermore sees that F_7 and F_9 vanish at the real photon point. Taking into account that 4 tensors vanish in the limit $Q^2 \to 0$, only the six amplitudes F_1, F_2, F_4, F_6, F_{10} and F_{11} enter in real Compton scattering (RCS). It is useful to relate the amplitudes $F_{1,2,4,6,10,11}(0,\nu,t)$ with the RCS amplitudes $A_i(\nu,t)$ $(i=1,...,6)$. We find after some algebra the following relations at $Q^2=0$:

$$
\begin{aligned}
(-e^2)F_1 &= -A_1 - \left(\frac{t-4M^2}{4M^2}\right) A_3 + \frac{\nu^2}{M^2} A_4 + A_6 , \\
(-e^2)F_2 &= -\frac{1}{2M^2}\left[A_3 + A_6 - \frac{t}{4M^2} A_4\right] , \\
(-e^2)F_4 &= \frac{1}{2M^2} A_4 , \\
(-e^2)F_6 &= \frac{1}{4M^2}\left[-\left(\frac{t-4M^2}{4M^2}\right) A_4 + A_6\right] , \\
(-e^2)F_{10} &= -\frac{1}{2M}\left[A_5 - A_6\right] , \\
(-e^2)F_{11} &= -\frac{1}{4M}\left[A_2 - \frac{t-4M^2+4\nu^2}{4M^2} A_4 + A_6\right] ,
\end{aligned} \tag{4.66}
$$

where the charge factor $\left(-e^2\right)$ appears explicitely on the *lhs* of Eq.(4.66), because this factor is already included in the usual definition of the A_i.

In Ref. [Dre 98], the low energy limit of the tensors of Eq.(4.63) was found, thus providing the relations between the invariant amplitudes F_i and the GP's. In terms of invariants, the limit $|\vec{q}\,'| \to 0$ at finite three-momentum of the virtual photon $|\vec{q}\,|$ corresponds to $\nu \to 0$ and $t \to -Q^2$ at finite Q^2. One can therefore express the GP's in terms of the VCS invariant amplitudes F_i at the point $\nu = 0, t = -Q^2$ for finite Q^2, for which we introduce the shorthand:

$$
\bar{F_i}(Q^2) \equiv F_i^{NB}\left(Q^2,\nu=0,t=-Q^2\right) . \tag{4.67}
$$

The relations between the GP's and the $\bar{F_i}(Q^2)$ are [Dre 98]:

$$
\begin{aligned}
P^{(E1,E1)0}(|\vec{q}\,|) &= \sqrt{\frac{1}{3}}\sqrt{\frac{E+M}{E}}\left[\bar{F_1}(Q^2) - \frac{2M\vec{q}^{\,2}}{\tilde{q}_0}\bar{F_2}(Q^2)\right. \\
&\qquad \left. - 2M\tilde{q}_0(2\bar{F_6}(Q^2) + \bar{F_9}(Q^2) - \bar{F_{12}}(Q^2))\right] , \\
P^{(E1,E1)1}(|\vec{q}\,|) &= \frac{1}{3\sqrt{2}}\sqrt{\frac{E+M}{E}}\,\tilde{q}_0\left[\bar{F_5}(Q^2) + \bar{F_7}(Q^2)\right.
\end{aligned}
$$

$$
\begin{aligned}
& + 4\bar{F}_{11}(Q^2) + 4M\bar{F}_{12}(Q^2)\big] \,, \\
P^{(M1,M1)0}(|\vec{q}|) &= -\frac{2}{\sqrt{3}}\sqrt{\frac{E+M}{E}}\bar{F}_1(Q^2) \,, \\
P^{(M1,M1)1}(|\vec{q}|) &= -\frac{\sqrt{2}}{3}\sqrt{\frac{E+M}{E}}M\frac{\tilde{q}_0^2}{\vec{q}^{\,2}}\left[\bar{F}_5(Q^2) + \tilde{q}_0\bar{F}_{12}(Q^2)\right] \\
P^{(M1,E2)1}(|\vec{q}|) &= \frac{1}{3\sqrt{3}}\sqrt{\frac{E+M}{E}}\frac{\tilde{q}_0}{\vec{q}^{\,2}}\Bigg[\left(\bar{F}_7 + 4\bar{F}_{11}\right)(\tilde{q}_0 - 2M) \\
& \qquad + \tilde{q}_0\left(\bar{F}_5(Q^2) + 2M\bar{F}_{12}(Q^2)\right)\Bigg] \\
P^{(E1,M2)1}(|\vec{q}|) &= \frac{1}{3}\sqrt{\frac{E+M}{E}}\frac{M\tilde{q}_0}{\vec{q}^{\,2}}\Bigg[\bar{F}_7(Q^2) + 4\bar{F}_{11}(Q^2) \\
& \qquad - \tilde{q}_0\bar{F}_{12}(Q^2) + 4M\left(2\bar{F}_6(Q^2) + \bar{F}_9(Q^2)\right)\Bigg]
\end{aligned}
\tag{4.68}
$$

4.4.1 VCS invariant amplitudes B_i of Berg and Lindner

For further reference, it will be useful to work with an alternative tensor basis for VCS, as introduced by Berg and Lindner [Ber 61].

One starts by defining, besides the four-vectors P and K , the combination

$$
L^\mu = \frac{1}{2}(q'^\mu - q^\mu) \,, \tag{4.69}
$$

and constructs from $K, P,$ and $L,$ the following four-vectors which are orthogonal to each other :

$$
\begin{aligned}
L'^\mu &\equiv L^\mu - \frac{(L\cdot K)}{K^2}K^\mu \,, \\
P'^\mu &\equiv P^\mu - \frac{(P\cdot K)}{K^2}K^\mu - \frac{(P\cdot L')}{L'^2}L'^\mu \,, \\
N^\mu &\equiv \varepsilon^{\mu\nu\alpha\beta}P'_\nu L'_\alpha K_\beta \,.
\end{aligned}
\tag{4.70}
$$

Next one constructs the combination of the four-vectors K and L' that is gauge-invariant with respect to the virtual photon q :

$$
K'^\mu \equiv K^\mu - \frac{q\cdot K}{q\cdot L'}L'^\mu \,, \tag{4.71}
$$

which satisfies $q\cdot K' = 0$. In terms of these four-vectors, the Lorentz- and gauge-invariant VCS tensor $H^{\mu\nu}$ can now be constructed as :

$$
\begin{aligned}
H^{\mu\nu} &= \frac{P'^\mu P'^\nu}{P'^{\,2}}\left(B_1 + B_2\not{K}\right) + \frac{N^\mu N^\nu}{N^2}\left(B_3 + B_4\not{K}\right) \\
&\quad + \frac{P'^\mu N^\nu + P'^\nu N^\mu}{P'^{\,2}N^2}\left(B_5\, i\gamma_5 + B_6\not{N}\right) + \frac{P'^\mu N^\nu - P'^\nu N^\mu}{P'^{\,2}N^2}\left(B_7\, i\gamma_5 + B_8\not{N}\right) \\
&\quad + \frac{K'^\mu P'^\nu}{K^2P'^{\,2}}\left(B_9 + B_{10}\not{K}\right) + \frac{K'^\mu N^\nu}{K^2N^2}\left(B_{11}\, i\gamma_5 + B_{12}\not{N}\right) \,,
\end{aligned}
\tag{4.72}
$$

where $B_i (i = 1, ..., 12)$ are the VCS invariant amplitudes of Berg and Lindner [Ber 61].

Berg and Lindner constructed their basis in a very similar manner as Prange did for real Compton scattering [Pra 58]. At the real photon point, we find the following relations between these two sets of amplitudes:

$$\begin{aligned} B_{1,2,3,4} &= -T_{1,2,3,4} \\ B_6 &= P'^2 T_6 \\ B_7 &= \frac{t}{4} P'^2 T_5 \\ B_{5,8,9,10,11,12} &= 0 \,. \end{aligned} \tag{4.73}$$

The convenience of the basis of Berg and Lindner is due to the orthogonality of all six tensor structures to each other, therefore projection of the full VCS tensor $H^{\mu\nu}$ onto one of these tensors leaves only the corresponding two amplitudes B_i. Projecting tensor basis $\rho_i^{\mu\nu}$ onto the same tensor, one obtains relations between the amplitudes B_i and F_i. These relations are listed in Appendix D.1. The decomposition of the Born contribution into invariant amplitudes B_i and F_i can be found in Appendix E.1.

However, this set of invariant amplitudes can not be used directly for the dispersion calculations due to kinematical singularities at forward and backward scattering angles, similarly as for the amplitudes of Prange.

4.5 Relations between the invariant amplitudes and the VCS helicity amplitudes.

By inserting the single tensors of Eq.(4.63) into the T-matrix elements

$$T_{\lambda'\lambda'_N;\lambda\lambda_N} \equiv -e^2 \varepsilon_\mu(\vec{q},\lambda)\, \varepsilon'^{*}_\nu(\vec{q}\,',\lambda')\, \bar{u}(\vec{p}\,',\lambda'_N) H^{\mu\nu} u(\vec{p},\lambda_N)$$

with polarization vectors and helicity spinors defined in Appendix A.1, it is straightforward to express the VCS helicity amplitudes as functions of the amplitudes F_i. These expressions are given in the Appendix F.1.

In the following, we will need the expressions of the invariant amplitudes F_i as functions of the *reduced* helicity amplitudes, defined in Appendix A.3. In order to be applicable for numerical calculations, these expressions should not contain any kinematical singularities.

The direct analytical inversion of Appendix F.1 is cumbersome. We therefore proceed in the following way:

First, the formulas of Appendix F.1 are inverted numerically. Second, the analytical inversion is performed in two steps. As a first step, we obtain the amplitudes of Berg and Lindner B_i as functions of the helicity amplitudes, which are then combined into F_i's, using the relations between the two sets of amplitudes. The details of this calculation and final formulas are given in Appendix G.1. A numerical comparison of both analytic and numerical inversion procedures serves as a cross check for this complicated calculation.

4.6 Dispersion relations at fixed t and Q^2 for VCS

4.6.1 Mandelstam plane for VCS

Before starting to set up the dispersion relations for the amplitudes F_i, we study the singularity structure of these amplitudes. For this purpose we consider the Mandelstam plane for VCS shown in Fig.4.13 in the kinematics of the MAMI experiment.

The thresholds for the reactions in the s- and u-channels are given by the straight lines $s = M^2$ and $u = M^2$, respectively, or, in terms of ν and t,

$$2M\nu = \pm\frac{t+Q^2}{2} . \tag{4.74}$$

Comparing to the real Compton scattering case, we note that these two lines do not cross at $\nu, t = 0$ but at $\nu = 0$, $t = -Q^2$.

The scattering process in the t-channel is possible for

$$t \geq 4M^2 , \tag{4.75}$$

and the corresponding allowed kinematical region lies above the line

$$\nu = \pm\frac{t+Q^2}{4M}\sqrt{1-\frac{4M^2}{t}} \tag{4.76}$$

at large positive values of t. The same equation for negative values of t gives the boundaries of the physical regions in the s- and u-channels shown in Fig.4.13 by the solid lines. The branch of Eq.(4.76) corresponding to the minus sign, describes the forward scattering in the u-channel at negative ν values and backward scattering in the s-channel at positive ν's, and analogously, if taking the plus sign. Unlike in the RCS case, where the forward scattering was taking place along the line $t = 0$, for VCS $t = 0$ is reached only asymptotically.

The singularity structure of the VCS amplitude consists of nucleon poles in the s and u channels at $s = M^2$ and $u = M^2$, respectively, and the π^0-pole in the t-channel. Further singularities are branch cuts due to πN- and higher intermediate states in the s and u channels, and $\pi\pi$- and higher intermediate states in the t-channel.

Besides the absorptive singularities due to physical intermediate states, one might wonder whether other singularities give rise to branch cuts. Such additional singularities could come from so-called anomalous thresholds [Bjo 65], [Pil 79], which arise when a hadron is a loosely bound system of other hadronic constituents which can go on-shell (such as is the case of a nucleus in terms of its nucleon constituents). However, it was shown that in the case of strong confinement within QCD, the quark-gluon structure of the hadrons does not give rise to additional anomalous thresholds [Jaf 92, Oeh 95], and the quark singularities turn into hadron singularities described through an effective field theory. Therefore, the only anomalous thresholds arise for those hadrons which are loosely bound composite systems of other hadrons, such as, e.g., the Σ particle in terms of Λ and π. For the nucleon case, such anomalous thresholds are absent and the imaginary parts entering the dispersion integrals as in Eq.(3.31) are calculated from absorptive singularities due to πN, πNN, *etc.*

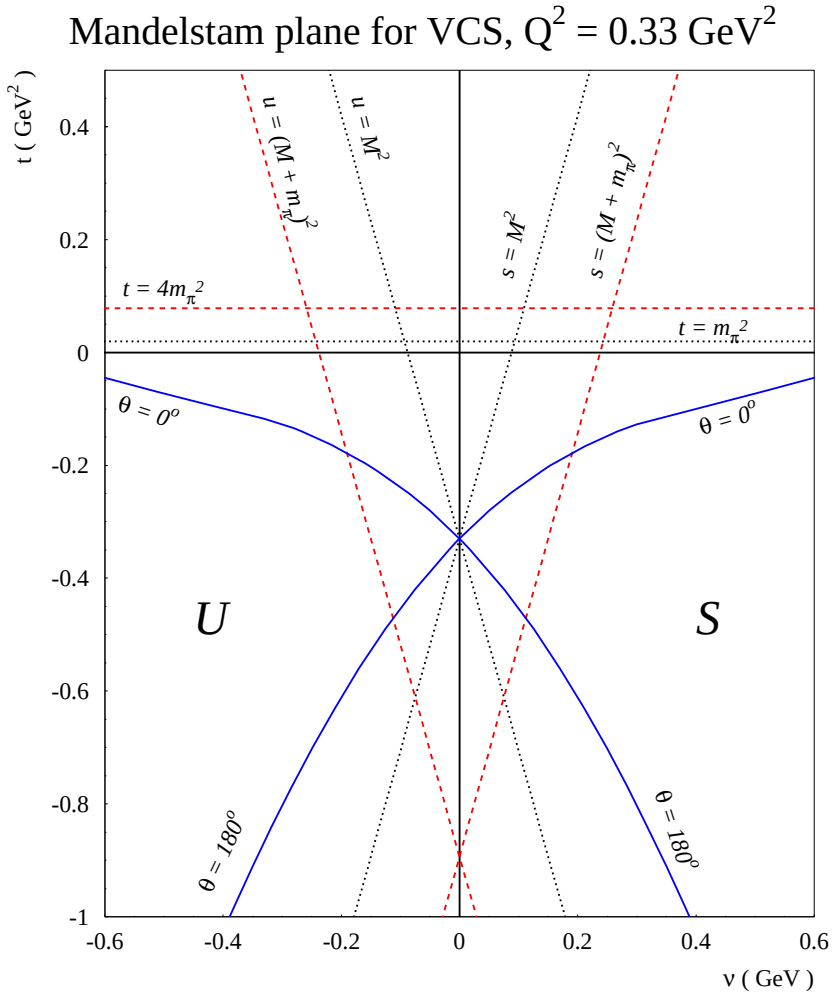

Figure 4.13: The Mandelstam plane for virtual Compton scattering for the MAMI kinematics, $Q^2 = 0.33\,(\mathrm{GeV/c})^2$. The dotted lines correspond to nucleon poles in the s and u channels, and to the pion pole in the t-channel. The inelastic thresholds are shown by dashed lines. The solid lines correspond to the boundaries of the physical regions in the s (positive values of ν) and u channels. The scattering region in the t-channel lies above $t = 4M^2$ and is not shown in this figure.

4.6.2 Dispersion relations

Following the same scheme as in the case of real Compton scattering, we fix t and the virtuality Q^2, and write unsubtracted DR in ν for the amplitudes F_i:

$$\mathrm{Re}F_i^{NB}(Q^2,\nu,t) \;=\; \frac{2}{\pi}\,\mathcal{P}\int_{\nu_{thr}}^{+\infty} d\nu'\;\frac{\nu'\;\mathrm{Im}_s F_i(Q^2,\nu',t)}{\nu'^2-\nu^2}\;. \tag{4.77}$$

The discontinuities $\mathrm{Im}_s F_i$ across the s-channel cuts of the VCS process start at the pion production threshold, at $\nu_{thr} = m_\pi + (m_\pi^2 + t/2 + Q^2/2)/(2M)$, with m_π the pion mass.

The assumption that unsubtracted dispersion relations as in Eq.(4.77) hold, requires that at high energies ($\nu \to \infty$ at fixed t and fixed Q^2) the amplitudes $\mathrm{Im}_s F_i(Q^2,\nu,t)$ (i = 1,...,12) drop fast enough so that the integrals of Eq.(4.77) are convergent and the contribution from the semi-circle at infinity can be neglected.

4.6.3 High energy behaviour of the invariant amplitudes

We next consider the VCS amplitudes $F_1,...,F_{12}$, in the Regge limit ($\nu \to \infty$ at fixed t and fixed Q^2) to determine for which of the amplitudes unsubtracted dispersion relations as in Eq.(4.77) exist. The high-energy behavior of the amplitudes F_i are deduced from the high-energy behavior of the VCS helicity amplitudes,

$$T_{1\frac{1}{2},1\frac{1}{2}} + T_{-1\frac{1}{2},-1\frac{1}{2}} \;\sim\; \nu^{\alpha_P(t)}\;, \tag{4.78}$$

and

$$T_{\lambda_N'\lambda',\lambda_N\lambda} \;\sim\; \nu^{\alpha_M(t)}\;, \tag{4.79}$$

otherwise.

Here, $\alpha_P(t)$ denotes the Pomeron trajectory with an intercept $\alpha_P(0) \approx 1.08$, and $\alpha_M(t), \leq 0.5$ (for $t \leq 0$) the meson Regge trajectory. This leads, after some algebra, to the following behavior for $\nu \to \infty$, at fixed t and fixed Q^2

$$\begin{aligned}
F_1,\,F_5 \;&\sim\; \nu^{\alpha_P(t)-2}\,, \quad \nu^{\alpha_M(t)}\,, && (4.80)\\
(F_5+4F_{11}) \;&\sim\; \nu^{\alpha_P(t)-2}\,, \quad \nu^{\alpha_M(t)-1}\,, && (4.81)\\
F_2,\,F_6,\,F_{10} \;&\sim\; \nu^{\alpha_P(t)-2}\,, \quad \nu^{\alpha_M(t)-2}\,, && (4.82)\\
F_7 \;&\sim\; \nu^{\alpha_P(t)-3}\,, \quad \nu^{\alpha_M(t)-1}\,, && (4.83)\\
F_3,\,F_8 \;&\sim\; \nu^{\alpha_P(t)-3}\,, \quad \nu^{\alpha_M(t)-2}\,, && (4.84)\\
F_9,\,F_{12} \;&\sim\; \nu^{\alpha_P(t)-4}\,, \quad \nu^{\alpha_M(t)-2}\,, && (4.85)\\
F_4 \;&\sim\; \nu^{\alpha_P(t)-4}\,, \quad \nu^{\alpha_M(t)-3}\,. && (4.86)
\end{aligned}$$

In Eqs.(4.80 - 4.86), we have separately indicated the high energy behavior of the pomeron (α_P) and the meson (α_M) contributions. It then follows that for two amplitudes F_1 and F_5, an unsubtracted dispersion integral as in Eq.(4.77) does not exist, whereas the other ten amplitudes on the *lhs* of Eqs.(4.81 - 4.86) can be evaluated through unsubtracted dispersion integrals as in Eq.(4.77).

In the following sections, we will elaborate on the DR formalism. Firstly, we will show that 4 of the 6 GPs of the nucleon can be evaluated using unsubtracted DR. Subsequently, we will discuss how the s-channel dispersion integrals of Eq.(3.31) are evaluated. Through unitarity the imaginary parts of the VCS amplitudes correspond to the excitation of πN, $\pi\pi N$,... intermediate states. Finally, we will show how to parametrize the remaining 2 VCS invariant amplitudes for which one cannot write down an unsubtracted DR, and express them in terms of two GPs, which enter as free parameters in the present DR formalism.

4.7 Dispersion relations for the generalized polarizabilities

The present work aims at evaluating the GP's through unsubtracted dispersion relations of the type of Eq.(4.77). We have seen from the high-energy behavior that the unsubtracted dispersion relations do not exist for the amplitudes F_1 and F_5, but can be written down for the other amplitudes. Therefore, unsubtracted dispersion relations for the GP's will hold for those GP's which do not depend on the two amplitudes F_1 and F_5. Note that the amplitude F_5 can appear in the combination $F_5 + 4F_{11}$, because its a high-energy behavior (Eq.(4.82)) leads to a convergent unsubtracted dispersion integral. Among the six GP's we find four combinations which do not depend on F_1 and F_5:

$$P^{(M1,M1)0} + \frac{1}{2}P^{(11,11)0} = \frac{-2}{\sqrt{3}}\left(\frac{E+M}{E}\right)^{1/2} M\tilde{q}_0 \times \left\{\frac{|\vec{q}|^2}{\tilde{q}_0^2}\bar{F}_2 + (2\bar{F}_6 + \bar{F}_9) - \bar{F}_{12}\right\}, \tag{4.87}$$

$$P^{(E1,E1)1} = \frac{1}{3\sqrt{2}}\left(\frac{E+M}{E}\right)^{1/2} \tilde{q}_0 \left\{(\bar{F}_5 + \bar{F}_7 + 4\bar{F}_{11}) + 4M\bar{F}_{12}\right\}, \tag{4.88}$$

$$P^{(E1,M2)1} - \frac{1}{\sqrt{2}\tilde{q}_0}P^{(M1,M1)1} = \frac{1}{3}\left(\frac{E+M}{E}\right)^{1/2} \frac{M\tilde{q}_0}{|\vec{q}|^2} \times \left\{(\bar{F}_5 + \bar{F}_7 + 4\bar{F}_{11}) + 4M(2\bar{F}_6 + \bar{F}_9)\right\}, \tag{4.89}$$

$$P^{(E1,M2)1} + \frac{\sqrt{3}}{2}P^{(M1,E2)1} = \frac{1}{6}\left(\frac{E+M}{E}\right)^{1/2} \frac{\tilde{q}_0}{|\vec{q}|^2} \times \left\{\tilde{q}_0(\bar{F}_5 + \bar{F}_7 + 4\bar{F}_{11}) + 8M^2(2\bar{F}_6 + \bar{F}_9)\right\}. \tag{4.90}$$

We note that in the limit $|\vec{q}\,'| = 0$, the value of Q^2 is always understood as $\tilde{Q}^2 \equiv |\vec{q}|^2 - \tilde{q}_0^2$, which we further denote as Q^2 for simplicity of the notation.

The four combinations of GP's on the *lhs* of Eqs.(4.87 - 4.90) can then be evaluated in an unsubtracted dispersion framework, through the following dispersion integrals for the corresponding $\bar{F}_i(Q^2)$:

$$\bar{F}_i(Q^2) = \frac{2}{\pi}\int_{\nu_{thr}}^{+\infty} d\nu' \, \frac{\mathrm{Im}_s F_i(Q^2, \nu', t = -Q^2)}{\nu'}. \tag{4.91}$$

4.8 s-channel dispersion integrals

The imaginary parts of the amplitudes F_i in Eq. (3.31) are obtained by the imaginary part of the VCS helicity amplitudes defined in Eq.(4.60), where the latter are determined by unitarity. With the shorthand T_{fi} for the VCS helicity amplitudes, the unitarity relation takes the generic form

$$2\,\mathrm{Im}_s\, T_{fi} = \sum_X (2\pi)^4 \delta^4(P_X - P_i) T^\dagger_{Xf} T_{Xi}\,, \tag{4.92}$$

where the sum runs over all possible intermediate states X. In this work, we are mainly interested in VCS up to the Δ-resonance region. Therefore, we restrict ourselves to the dominant contribution by only taking into account the πN intermediate states. The influence of additional channels, like the $\pi\pi N$ intermediate state which are indispensable when extending the dispersion formalism to higher energies, will be investigated in a future work.

The s-channel helicity amplitudes are calculated through unitarity taking into account the contributions of πN intermediate states. They are expressed in terms of pion photo- and electroproduction multipoles as specified in Appendix H.1. For the calculation of the pion photo- and electroproduction multipoles, we use the phenomenological MAID analysis [MAID], which contains both resonant and non-resonant pion production mechanisms.

4.9 Asymptotic parts and dispersive contributions beyond πN

To evaluate the VCS amplitudes F_1 and F_5 in an unsubtracted dispersion framework, we proceed as in the case of RCS [L'vo 97]. This amounts to perform the unsubtracted dispersion integrals Eq.(3.31) for F_1 and F_5 along the real ν-axis only in the range $-\nu_{max} \leq \nu \leq +\nu_{max}$, and to close the contour by a semi-circle with radius ν_{max} in the upper half of the complex ν-plane, with the result

$$\mathrm{Re}F_i^{NB}(Q^2,\nu,t) \;=\; F_i^{int}(Q^2,\nu,t) \;+\; F_i^{as}(Q^2,\nu,t)\;, \qquad (\text{for } i=1,5)\;, \tag{4.93}$$

where the integral contributions F_i^{int} (for $i=1,5$) are given by:

$$F_i^{int}(Q^2,\nu,t) \;=\; \frac{2}{\pi}\,\mathcal{P}\int_{\nu_{thr}}^{\nu_{max}} d\nu'\;\frac{\nu'\;\mathrm{Im}_s F_i(Q^2,\nu',t)}{\nu'^2-\nu^2}\;, \qquad (\text{for } i=1,5)\;, \tag{4.94}$$

and where the contributions of the semi-circle of radius ν_{max} are then identified with the asymptotic contributions (F_1^{as}, F_5^{as}).

Evidently, the separation between asymptotic and integral contributions in Eq.(4.93) is a matter of choice, which is specified by the value of ν_{max}. The total result for F_i^{NB}, is formally independent of the specific value of ν_{max}. In practice however, ν_{max} is chosen small enough so that one can evaluate the dispersive integrals of Eq.(4.94) from threshold up to ν_{max} sufficiently accurate. On the other hand, ν_{max} should also be large

enough so that one can approximate the asymptotic contribution F_i^{as} by some energy (i.e. ν) independent function. In the calculations, one therefore chooses some intermediate value $\nu_{max} \approx 1.5$ GeV, and parametrizes the asymptotic contributions F_i^{as} by t-channel poles, which will be discussed next for F_5^{as} and F_1^{as}.

4.9.1 The asymptotic contribution F_5^{as}

The asymptotic contribution to the amplitudes F_5 is mostly due to t-channel π^0-exchange,

$$F_5^{as}(Q^2,\nu,t) \approx F_5^{\pi^0}(Q^2,t) = -4F_{11}^{\pi^0}(Q^2,t) = \frac{1}{M}\frac{g_{\pi NN}\, F_{\pi^0\gamma\gamma}\left(Q^2\right)}{t-m_\pi^2}\,. \qquad (4.95)$$

Note that the π^0-pole only contributes to the amplitudes F_5 and F_{11}, but drops out in the combination $(F_5 + 4F_{11})$, which has therefore a different high-energy behavior as is expressed in Eq.(4.82). In Eq.(4.95), $F_{\pi^0\gamma\gamma}\left(Q^2\right)$ represents the $\pi^0\gamma^*\gamma$ form factor. Its value at $Q^2 = 0$ is fixed by the axial anomaly: $F_{\pi^0\gamma\gamma}(0) = 1/(4\pi^2 f_\pi) = 0.274$ GeV^{-1}, where $f_\pi = 0.0924$ GeV is the pion decay constant. In Eq.(4.95), the πNN coupling is taken from Ref. [Pav 99]: $g_{\pi NN}^2/(4\pi) = 13.73$. For the Q^2-dependence of $F_{\pi^0\gamma\gamma}\left(Q^2\right)$, we use the interpolation formula given by Brodsky-Lepage [Bro 81]:

$$F_{\pi^0\gamma\gamma}\left(Q^2\right) = \frac{1/(4\pi^2 f_\pi)}{1+Q^2/(8\pi^2 f_\pi^2)}\,, \qquad (4.96)$$

which provides a rather good parametrization of the $\pi^0\gamma^*\gamma$ form factor data over the whole Q^2 range, and which leads to the asymptotic prediction at large Q^2 : $F_{\pi^0\gamma\gamma}\left(Q^2 \gg\right) \to 2\, f_\pi/Q^2$.

When fixing the asymptotic contribution F_5^{as} through its π^0-pole contribution, one can determine one more GP of the nucleon, besides the four combinations of Eqs. (4.87 - 4.90). In particular, this allows us to calculate the GP $P^{(11,11)1}$ through:

$$P^{(M1,M1)1}\left(Q^2\right) = -\frac{\sqrt{2}}{3}\left(\frac{E+M}{E}\right)^{1/2}\frac{M\,\tilde{q}_0^2}{|\vec{q}\,|^2}\left\{\bar{F}_5(Q^2) + \tilde{q}_0\,\bar{F}_{12}(Q^2)\right\}. \qquad (4.97)$$

In Fig.4.14, we show the dispersive contribution to the four spin GPs and compare them to the results of the $O(p^3)$ HBChPT [Hem 97], the linear σ-model [Met 96], and the nonrelativistic constituent quark model [Pas 01]. It is obvious that the DR calculations show more structure in Q^2 than the different model calculations.

The $O(p^3)$ HBChPT results predict for the GPs $P^{(E1,E1)1}$ and $P^{(M1,M1)1}$, a rather strong increase in Q^2, which would have to be checked by a $O(p^4)$ calculation.

The constituent quark model calculation gives negligibly small contributions for the GPs $P^{(E1,E1)1}$ and $P^{(M1,E2)1}$, whereas the GPs $P^{(M1,M1)1}$ and $P^{(E1,M2)1}$ receive their dominant contribution from the excitation of the $\Delta(1232)$ ($M1 \to M1$ transition) and N^* resonances ($E1 \to M2$ transition) respectively.

The linear σ-model, which takes account of part of the higher-order terms of a consistent chiral expansion, in general results in smaller values for the GPs than the corresponding calculations to leading order in HBChPT.

The comparison in Fig.4.14 clearly indicates that a satisfying theoretical description of the GPs over a larger range in Q^2 is still a challenge.

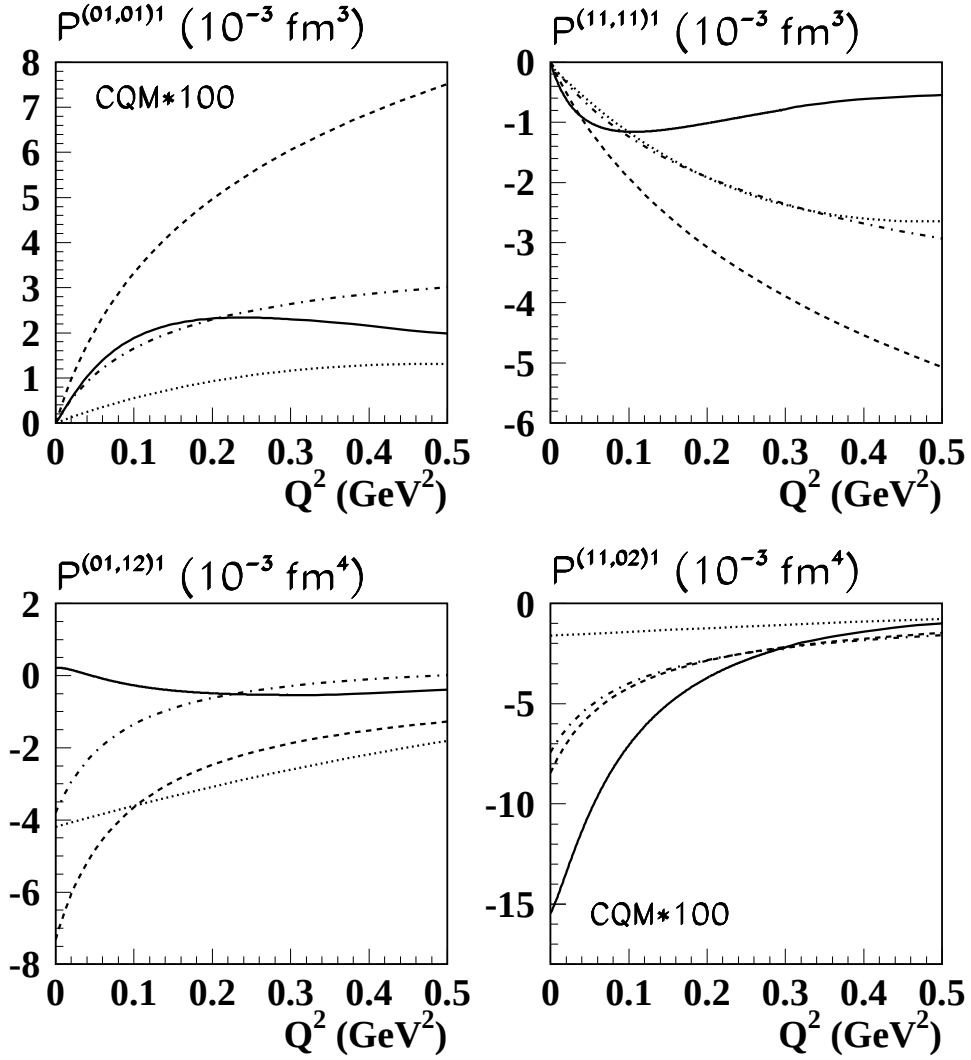

Figure 4.14: Results for the spin-flip GPs excluding the π^0-pole contribution in different model calculations, as functions of Q^2. The full curves correspond to the dispersive πN contribution. The dashed curves show the results of $O(p^3)$ HBChPT [Hem 97], the dashed-dotted curves correspond to the predictions of the linear σ-model [Met 96], and the dotted curves are the results of the non-relativistic constituent quark model (CQM) [Pas 01]. Note that the CQM results for $P^{(E1,E1)1}$ and $P^{(M1,E2)1}$ are multiplied (for visibility) by a factor 100.

In Fig.4.15, the dispersive and π^0-pole contributions to the 4 spin GPs are compared. The π^0-pole does not contribute to the GP $P^{(01,01)1}$, but dominates the other three spin GPs. It is however possible to find, besides the GP $P^{(01,01)1}$, two combinations of the remaining three spin GPs (Eqs. (4.89,4.90)) where the π^0-pole contribution drops out, as has been shown in Ref. [Pas 00].

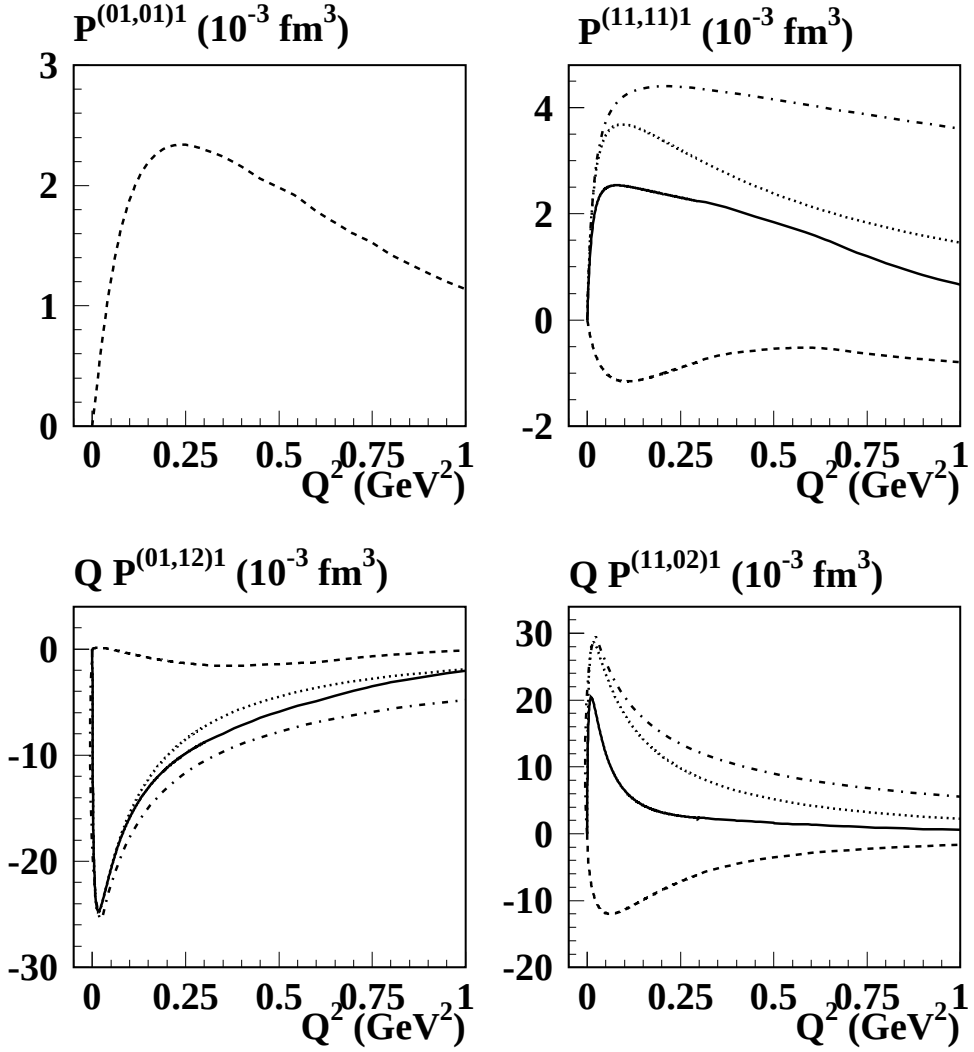

Figure 4.15: Results for the spin-flip GPs , as functions of Q^2. The dashed curves correspond to the dispersive πN contribution, the dotted curves show the π^0-pole contribution, and the full curves are the sum of the dispersive and π^0-pole contributions. For comparison, we also show the π^0-pole contribution for a $\pi^0\gamma^*\gamma$ form factor equal to 1 (dashed-dotted curves).Note that $P^{(E1,E1)1}$ has no π^0-pole contribution.

4.9.2 The asymptotic part and dispersive contributions beyond πN to F_1

We next turn to the high-energy contribution to F_1. As we are mainly interested in a description of VCS up to $\Delta(1232)$-resonance energies, we saturate the dispersion integrals by their πN contribution. Furthermore, we will estimate the remainder by an energy-independent function, which models the asymptotic contribution (i.e. the contour with radius ν_{max} in the complex ν-plane), and all dispersive contributions beyond πN up to the value $\nu_{max} = 1.5$ GeV (e.g. $\pi\pi N$, ...).

At $Q^2 = 0$, the VCS invariant amplitude F_1 reduces to the combination of the RCS invariant amplitudes, in particular A_1 (cf. Eq.(4.66)). The asymptotic contribution to the amplitude A_1 originates predominantly from the t-channel $\pi\pi$ intermediate states. In the phenomenological analysis, this continuum was parametrized through the exchange of a scalar particle in the t-channel, i.e. an effective "σ"-meson, as suggested in Ref. [L'vo 97]. For RCS, this led to the parametrization of the difference of $F_1^{NB}(Q^2 = 0)$ (i.e., A_1^{NB}) and its πN contribution, as an energy-independent function:

$$F_1^{NB}(Q^2 = 0, \nu, t) - F_1^{\pi N}(Q^2 = 0, \nu, t) \;\approx\; \left[F_1^{NB}(0,0,0) - F_1^{\pi N}(0,0,0)\right] \frac{1}{1 - t/m_\sigma^2} \,, \tag{4.98}$$

where $F_1^{\pi N}$ on the *lhs* and *rhs* are evaluated through a dispersive integral as discussed in Section 4.8. In Eq.(4.98), the effective "σ"-meson mass parameter m_σ is a free parameter in the RCS dispersion analysis, which is obtained from a fit to the t-dependence of RCS data, and turns out to be around $m_\sigma \approx 0.6$ GeV [L'vo 97]. The value $F_1^{NB}(0,0,0)$ is then considered as a remaining gobal fit parameter to be extracted from experiment. It can be expressed physically in terms of the magnetic polarizability β, which is obtained as:

$$F_1^{NB}(0,0,0) \;=\; \frac{4\pi}{e^2}\,\beta \,. \tag{4.99}$$

In RCS, one usually takes $\alpha - \beta$ as fit parameter instead of β because the sum $(\alpha + \beta)$ at the real photon point can be independently determined rather accurately through Baldin's sum rule, which yields for the proton the phenomenological value [Bab 98]:

$$(\alpha + \beta) \;=\; (13.69 \pm 0.14) \times 10^{-4}\,\mathrm{fm}^3. \tag{4.100}$$

Using a dispersive formalism as outlined above, the most recent fit to RCS data yields for $(\alpha - \beta)$ of the proton as value [Olm 01], already mentioned in Eq.(3.71):

$$\begin{aligned} \alpha &= [12.1 \pm 0.3(stat) \mp 0.4(syst) \pm 0.3(mod)] \,, \\ \beta &= [1.6 \pm 0.4(stat) \pm 0.4(syst) \pm 0.4(mod)] \,. \end{aligned} \tag{4.101}$$

where α and β are expressed here and in the following in units $10^{-4}\,fm^3$

From Eq.(3.71), one obtains for the difference the following global average [Olm 01]:

$$\alpha - \beta \;=\; 10.5 \pm 0.9(stat. + sys.) \pm 0.7(mod.) \,. \tag{4.102}$$

The term $F_1^{\pi N}(0,0,0)$ in Eq.(4.98), when calculated through a dispersion integral, has the value:

$$F_1^{\pi N}(0,0,0) = \frac{4\pi}{e^2}\,\beta^{\pi N} = \frac{4\pi}{e^2}\,\left(9.1\times 10^{-4}\,\mathrm{fm}^3\right)\,. \tag{4.103}$$

From this πN contribution $\beta^{\pi N}$ of Eq.(4.103), and the phenomenological value β of Eq.(3.71), one obtains the difference:

$$(\beta - \beta^{\pi N}) = -7.5\times 10^{-4}\,\mathrm{fm}^3\,, \tag{4.104}$$

which enters in the *rhs* of Eq.(4.98). By comparing the value of Eq. (4.104) with the total value for β (Eq.(3.71)), one sees that the small value of the magnetic polarizability comes about by a near cancellation between a large (positive) paramagnetic contribution (in $\beta^{\pi N}$) and a large (negative) diamagnetic contribution ($\beta - \beta^{\pi N}$), i.e. the asymptotic part of F_1 parametrizes the diamagnetism.

Turning next to VCS, we proceed analogously by parametrizing the non-Born part of $F_1^{NB}(Q^2,\nu,t)$ beyond the πN dispersive contribution, by an energy-independent t-channel pole contribution of the form:

$$F_1^{NB}(Q^2,\nu,t) - F_1^{\pi N}(Q^2,\nu,t) \approx \frac{f(Q^2)}{1-t/m_\sigma^2}\,, \tag{4.105}$$

where the parameter m_σ is taken as for RCS : $m_\sigma \approx 0.6$ GeV. The function $f(Q^2)$ in Eq.(4.105) can be obtained by evaluating the *lhs* of Eq.(4.105) at the point where the GP's are defined, i.e. $\nu = 0$ and $t = -Q^2$, at finite Q^2. This leads to:

$$f(Q^2) = \left[\bar{F_1}(Q^2) - \bar{F_1}^{\pi N}(Q^2)\right]\,\left(1+Q^2/m_\sigma^2\right)\,, \tag{4.106}$$

where we introduced the shorthand $\bar{F_1}(Q^2)$ as defined in Eq.(4.67). $\bar{F_1}(Q^2)$ can be expressed in terms of the generalized magnetic polarizability $P^{(M1,M1)0}(Q^2)$:

$$\begin{aligned}\bar{F_1}(Q^2) &= -\sqrt{\frac{3}{8}}\left(\frac{2E}{E+M}\right)^{1/2} P^{(11,11)0}(Q^2) &(4.107)\\ &\equiv \frac{4\pi}{e^2}\left(\frac{2E}{E+M}\right)^{1/2}\beta(Q^2)\,, &(4.108)\end{aligned}$$

where $\beta(Q^2)$ is the generalized magnetic polarizability, which reduces at $Q^2 = 0$ to the polarizability β of RCS.

Eqs.(4.105, 4.106) lead to the following expression for the VCS amplitude F_1^{NB}:

$$F_1^{NB}(Q^2,\nu,t) \approx F_1^{\pi N}(Q^2,\nu,t) + \left[\bar{F_1}(Q^2) - \bar{F_1}^{\pi N}(Q^2)\right]\,\frac{1+Q^2/m_\sigma^2}{1-t/m_\sigma^2}\,, \tag{4.109}$$

where the πN contributions $F_1^{\pi N}(Q^2,\nu,t)$ and $\bar{F_1}^{\pi N}(Q^2)$ (or equivalently $\beta^{\pi N}(Q^2)$) are calculated through a dispersion integral, as outlined above. Consequently, the only unknown quantity on the *rhs* of Eq.(4.109) is $\bar{F_1}(Q^2)$, which can be directly used as a fit parameter at finite Q^2. This amounts to determine the generalized magnetic polarizability $\beta(Q^2)$ from VCS observables.

We stress that one can apply the phenomenological formula of Eq. (4.109) to VCS data at some fixed Q^2 to extract $\beta(Q^2)$ without assuming any functional form for $\beta(Q^2)$. In the following, we consider a convenient parametrization of the Q^2 dependence of $\beta(Q^2)$ in order to provide predictions for VCS observables. For this purpose, we propose a dipole form for the difference of $\beta(Q^2) - \beta^{\pi N}(Q^2)$ which enters in the *rhs* of Eq. (4.109) (through the definition of Eq. (4.108)) as:

$$\beta(Q^2) - \beta^{\pi N}(Q^2) = \frac{\left(\beta - \beta^{\pi N}\right)}{\left(1 + Q^2/\Lambda_\beta^2\right)^2}, \tag{4.110}$$

where the RCS value $(\beta - \beta^{\pi N})$ on the *rhs* is given by Eq. (4.104). The mass scale Λ_β in Eq. (4.110) determines the Q^2 dependence, and hence gives us the information of how the diamagnetism is spatially distributed in the nucleon. Using the dipole parametrization of Eq. (4.110), one can extract Λ_β from a fit to VCS data at different Q^2 values.

To have some educated guess on the physical value of Λ_β, we next discuss two microscopic calculations of the diamagnetic contribution to the GP $\beta(Q^2)$. The diamagnetism of the nucleon originates predominantly from the pion cloud surrounding the nucleon. Therefore, we calculate the diamagnetic contribution through a dispersion relation estimate of the t-channel $\pi\pi$ intermediate state contribution to F_1. Such a dispersive estimate has been previously performed for RCS ([Hol 94], [Dre 99], and Chapter 3 of this thesis), where it was shown that the asymptotic part of F_1 can be related to the $\gamma\gamma \to \pi\pi \to N\bar{N}$ process. The dominant contribution comes from the $\pi\pi$ intermediate state with spin and isospin zero ($I = J = 0$). The generalization to VCS leads to the identification of F_1^{as} with the following unsubtracted DR in t at fixed energy $\nu = 0$:

$$\bar{F}_1^{as}(Q^2) = \frac{1}{\pi} \int_{4m_\pi^2}^{\infty} dt' \frac{\mathrm{Im}_t F_1(Q^2, 0, t')}{t' + Q^2}. \tag{4.111}$$

The evaluation of the imaginary part on the *rhs* of Eq. (4.111) which is mainly due to $\pi\pi$ intermediate states, requires the information of the subprocesses $\gamma^*\gamma \to \pi\pi$ and $\pi\pi \to N\bar{N}$, as already discussed in the RCS case. The relations between the t-channel VCS helicity amplitudes and the amplitudes F_i, as well as partial waves for the subprocess $\gamma^*\gamma \to \pi\pi$ are given in Appendix I.1.

At the pion electromagnetic vertex, the pion electromagnetic form factor is included. For RCS, it was found [Dre 98] that the unitarization procedure enhances the $\gamma\gamma \to \pi\pi$ cross section in the threshold region, compared to the Born result, and is needed to obtain agreement with the data. One sees that in the DR of Eq. (4.111), the imaginary part of F_1 is weighted by $1/t$, so that the threshold region gives the largest contribution to the dispersion integral. The dispersive evaluation of Eq. (4.111) contains no free parameters as it uses as input the $\gamma\gamma \to \pi\pi$ and $\pi\pi \to N\bar{N}$ processes, and therefore provides a more microscopic model for the phenomenological "σ"-exchange. For RCS, the dispersion integral Eq. (4.111) yields the value $\beta^{as} \approx -7.3 \times 10^{-4}\,\mathrm{fm}^3$. However, the unsubtracted dispersion integral can only be evaluated up to $-t = 0.778$ GeV^2, because the $\pi\pi \to N\bar{N}$ amplitudes of Ref.[H¨oh 83] could only be determined

up to this value, and the dispersion integral of Eq. (4.111) may not have fully converged at this point. Therefore, one should consider the nearly perfect agreement between the value of β^{as} from this calculation with the phenomenological value of Eq. (4.104), as a coincidence. However, our calculation indicates that the dispersive estimate through $\pi\pi$ t-channel intermediate states provides the dominant physical contribution to the diamagnetism, and can be considered as a first guess of the distribution of diamagnetism in the nucleon. With this model, we show the Q^2-dependence of $\bar{F}_1^{as}$ in Fig. 4.16.

To have a second microscopic calculation for comparison, we also show in Fig. 4.16 an evaluation of $\bar{F}_1^{as}(Q^2)$ in the linear σ-model (LSM) of Ref. [Met 96]. The LSM calculation overestimates the value of $\bar{F}_1^{as}(0)$ (or equivalently β_{as}) by about 30% at any realistic value of m_σ (which is a free parameter in this calculation). However, as for the dispersive calculation, it also shows a steep Q^2 dependence.

Furthermore, we compare in Fig. 4.16 the two model calculations discussed above with the dipole parametrization for $\beta(Q^2)$ of Eq. (4.110), for two values of Λ_β, i.e. Λ_β = 0.4 GeV and Λ_β = 0.6 GeV. It is seen that these values are compatible with the microscopic estimates discussed before. In particular, the result for Λ_β = 0.4 GeV is nearly equivalent with the dispersive estimate of $\pi\pi$ exchange in the t-channel. This value of the mass-scale Λ_β is small compared to the typical scale $\Lambda_D \approx 0.84$ GeV which appears in the nucleon magnetic (dipole) form factor. This reflects the fact that the diamagnetism has its physical origin in the pionic degrees of freedom, i.e. is situated in the surface and intermediate region of the nucleon.

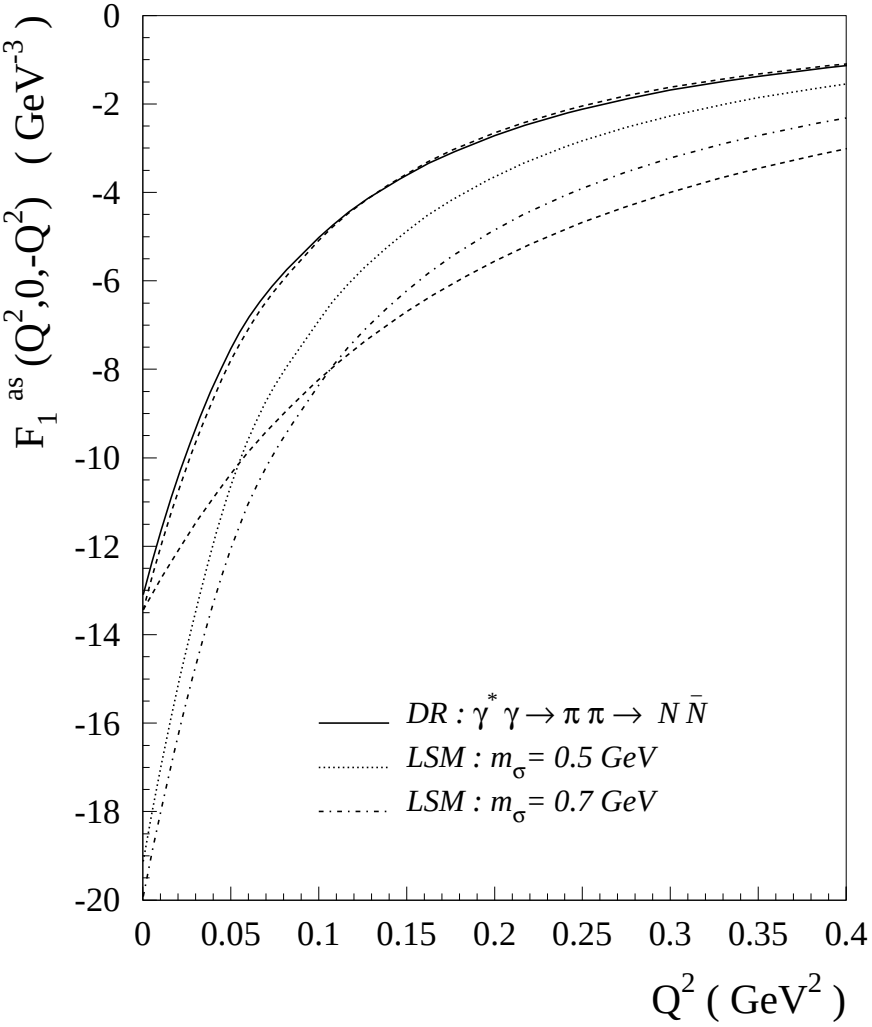

Figure 4.16: Theoretical estimates of the asymptotic contribution $\bar{F}_1^{as}$: DR calculation of the $\gamma^*\gamma \to \pi\pi \to N\bar{N}$ process as described in the text (full line); linear σ-model calculation of Ref. [Met 96] with $m_\sigma = 0.5$ GeV (dotted curve) and $m_\sigma = 0.7$ GeV (dashed-dotted curve). The dashed curves are dipole parametrizations according to Eq.(4.110), which are fixed to the experimental value at $Q^2 = 0$ and are shown for two values of the mass scale, $\Lambda_\beta = 0.4$ GeV (upper dashed curve) and $\Lambda_\beta = 0.6$ GeV (lower dashed curve).

4.9.3 Dispersive contributions beyond πN to F_2

We next investigate the size of dispersive contributions beyond πN, in particular for the amplitude F_2, and start again with the case of RCS. For the amplitude F_2, one can quantify the higher dispersive corrections, because the value of F_2^{NB} at the real photon point can be expressed exactly (using Eqs.(4.87)) in terms of the sum of the scalar polarizabilities $(\alpha+\beta)$ as:

$$F_2^{NB}(0,0,0) \,=\, -\frac{4\pi}{e^2}\,\frac{1}{(2M)^2}\,(\alpha+\beta)\,. \tag{4.112}$$

The πN dispersive contribution to $(\alpha+\beta)$ provides the value:

$$(\alpha+\beta)^{\pi N} = 11.6\times 10^{-4}\,\mathrm{fm}^3\,, \tag{4.113}$$

which falls short by about 15 % compared to the sum rule value of Eq.(4.100). The remaining dispersive contributions to the amplitude F_2, such as $\pi\pi N$ *etc.* are modelled by an energy-independent constant, which is fixed to the phenomenological value at $\nu = t = 0$. This yields:

$$F_2^{NB}(Q^2=0,\nu,t) \approx F_2^{\pi N}(Q^2=0,\nu,t) \,-\, \frac{4\pi}{e^2}\,\frac{1}{(2M)^2}\,\Big[\,(\alpha+\beta) \,-\, (\alpha+\beta)^{\pi N}\,\Big]\,, \tag{4.114}$$

which is an exact formula at $\nu = t = 0$, the point where the polarizabilities are defined.

In order for such an approximation as in Eq.(4.114) to be valid, one has to stay below the thresholds for those higher contributions. Since the next threshold beyond πN is $\pi\pi N$, the approximation of Eq.(4.114) restricts us in practise to energies up to $\Delta(1232)$-resonance energies. In order to extend the DR formalism to energies above two-pion production threshold, we proceed in an analogous way by replacing Eq.(4.114) as follows:

$$\begin{aligned} F_2^{NB}(Q^2=0,\nu,t) \;&\approx\; F_2^{\pi N}(Q^2=0,\nu,t) \,+\, F_2^{\pi\pi N}(Q^2=0,\nu,t) \\ &-\; \frac{4\pi}{e^2}\,\frac{1}{(2M)^2}\,\Big[\,(\alpha+\beta) \,-\, (\alpha+\beta)^{\pi N} \,-\, (\alpha+\beta)^{\pi\pi N}\,\Big]\,, \end{aligned} \tag{4.115}$$

i.e. we explicitely calculate the energy-dependence associated with πN and $\pi\pi N$ dispersive contributions and parametrize the remainder by an energy-independent constant which is fixed to the phenomenological value of $(\alpha+\beta)$. Eq.(4.115), and Eq.(4.98) for F_1^{NB} modified in an analogous way to include the $\pi\pi N$ dispersive contributions, would then allow an extension of the DR formalism to energies into the second resonance region. Such an extension remains to be investigated in a future work, while we restrict ourselves in the present work to energies in the $\Delta(1232)$-resonance region.

We next consider the extension to VCS, and focus our efforts to a description of VCS into the $\Delta(1232)$-resonance region. Analogously to Eq.(4.114) for RCS, the dispersive contributions beyond πN to the VCS amplitude F_2^{NB} can be approximated by an energy-independent constant. This constant is fixed at arbitrary Q^2, at $\nu = 0$, and $t = -Q^2$, which is the point where the GP's are defined. One thus obtains for F_2^{NB} :

$$F_2^{NB}(Q^2,\nu,t) \approx F_2^{\pi N}(Q^2,\nu,t) \,+\, \left[\bar{F}_2(Q^2) - \bar{F}_2^{\pi N}(Q^2)\right]\,, \tag{4.116}$$

where $\bar{F}_2(Q^2)$ is defined as in Eq. (4.67), and can be expressed in terms of GP's. In this paper, we saturate the three combinations of spin GP's of Eqs.(4.88 - 4.90) by their πN contribution, and calculate the fourth spin GP's of Eq.(4.97) through its πN contributions and by adding a π^0-pole contribution as shown in Fig. 4.15. Therefore, we only consider contributions beyond the πN intermediate states for the two scalar GP's, which are then considered as the two fit quantities that enter our DR formalism for VCS. In this way, and by using Eq.(4.87), one can express the difference $\bar{F}_2(Q^2) - \bar{F}_2^{\pi N}(Q^2)$ entering in the *rhs* of Eq.(4.116) as:

$$\begin{aligned} \bar{F}_2(Q^2) - \bar{F}_2^{\pi N}(Q^2) \;\; &\approx \;\; \frac{4\pi}{e^2}\left(\frac{2E}{E+M}\right)^{1/2} \frac{\tilde{q}_0}{|\vec{q}\,|^2}\,\frac{1}{2M} \\ &\times \Big\{ \left[\alpha(Q^2) - \alpha^{\pi N}(Q^2)\right] + \left[\beta(Q^2) - \beta^{\pi N}(Q^2)\right] \Big\}\,, \end{aligned} \tag{4.117}$$

where $\beta(Q^2)$ is the generalized magnetic polarizability of Eq.(4.108). Furthermore, $\alpha(Q^2)$ is the generalized electric polarizability which reduces at $Q^2 = 0$ to the electric polarizability α of RCS, and which is related to the GP $P^{(E1,E1)0}(Q^2)$ through:

$$P^{(E1,E1)0}(Q^2) \equiv -\frac{4\pi}{e^2}\sqrt{\frac{2}{3}}\,\alpha(Q^2)\,. \tag{4.118}$$

We stress that one can apply the phenomenological formulas of Eqs.(4.109, 4.116) to VCS data at some fixed Q^2 to extract the two GP's $\alpha(Q^2)$ and $\beta(Q^2)$ without assuming any functional form for their Q^2 dependence. As for $\beta(Q^2)$ before, we next consider a convenient parametrization of the Q^2 dependence of $\alpha(Q^2)$ in order to provide predictions for VCS observables. We also propose a dipole form for the difference of $\alpha(Q^2) - \alpha^{\pi N}(Q^2)$ which enters in the *rhs* of Eq.(4.117) as:

$$\alpha(Q^2) - \alpha^{\pi N}(Q^2) \,=\, \frac{\left(\alpha - \alpha^{\pi N}\right)}{\left(1 + Q^2/\Lambda_\alpha^2\right)^2}\,, \tag{4.119}$$

where the Q^2 dependence is governed by the mass-scale Λ_α, which is a free parameter. In Eq.(4.119), the RCS value

$$\left(\alpha - \alpha^{\pi N}\right) \,=\, 9.6 \times 10^{-4}\,\mathrm{fm}^3\,, \tag{4.120}$$

is obtained from the phenomenological value of α (Eq.(3.71)), and from the calculated πN contribution: $\alpha^{\pi N} = 2.6 \times 10^{-4}\,\mathrm{fm}^3$. Using the dipole parametrization of Eq.(4.119), one can then extract the free parameter Λ_α from a fit to VCS data at different Q^2 values.

4.10 Results for $ep \to ep\gamma$ observables

Having set up the dispersion relation formalism for VCS, we now show predictions for the different $ep \to ep\gamma$ observables for energies up to the $\Delta(1232)$-resonance region. The aim of the experiments is to extract the six GPs from both unpolarized and polarized observables. We will compare the DR results, which take account of the full dependence of the $ep \to ep\gamma$ observables on the energy q' of the emitted photon, with the low energy expansion where only the first three terms in the expansion of the difference $\mathcal{M}^{exp} - \mathcal{M}^{BH+Born}$ are taken into account.

In Fig. 4.17, we show the calculations of $P_{LL} - P_{TT}/\varepsilon$ and P_{LT}, which have been measured at MAMI at $Q^2 = 0.33$ GeV^2 [Roc 00]. The virtual photon polarization ε is fixed to the experimental value $\varepsilon = 0.62$, and for the electromagnetic form factors in Eq.(4.45), we use the H¨ohler parametrization [H¨oh 76] as in the analysis of the MAMI experiment [Roc 00].

In the lower panel of Fig. 4.17, the Q^2-dependence of the VCS response function P_{LT} is displayed, which reduces (up to a factor) to the magnetic polarizability β at the real photon point. At finite Q^2, it contains both the scalar GP $\beta(Q^2)$ and the spin-flip GP $P^{(E1,E1)1}$ (see Eq.(4.45)). It is obvious from Fig.4.17 that the structure function P_{LT} results from a large dispersive πN contribution and a large asymptotic contribution with opposite sign, leading to a relatively small total result. At the real photon point, the small value of β is indeed known to result from the near cancellation of a large paramagnetic contribution from the $\Delta(1232)$-resonance, and a large diamagnetic contribution (asymptotic part). The latter is shown in Fig. 4.17 with the parametrization of Eq.(4.110) for the values of $\Lambda_\beta = 0.4$ and $\Lambda_\beta = 0.6$ GeV of Fig.4.16. Due to the large cancellation in P_{LT}, its Q^2-dependence is a very sensitive observable to study the interplay of the two mechanisms. In particular, one expects a faster fall off of the asymptotic contribution with Q^2 in comparison to the dispersive πN contribution, as discussed before. This is already highlighted by the measured value of P_{LT} at $Q^2 = 0.33$ GeV^2 [Roc 00], which is comparable with the value of P_{LT} at $Q^2 = 0$ [Olm 01]. As seen from Fig.4.16, this points to an interesting structure in the Q^2 region around 0.1 GeV^2, where forthcoming data are expected from an experiment at MIT-Bates [Sha 97].

In the upper panel of Fig. 4.17, we show the Q^2-dependence of the VCS response function $P_{LL} - P_{TT}/\varepsilon$, which reduces at $Q^2 = 0$ to the electric polarizability α. At finite Q^2, P_{LL} is directly proportional to the scalar GP $\alpha(Q^2)$ as seen from Eq.(4.110), and the response function P_{TT} contains only spin GPs. As is shown in Fig.4.17, the dispersive contributions to α and to the spin GPs are smaller than the asymptotic contribution to α, which is evaluated for $\Lambda_\alpha = 1$ GeV. At $Q^2 = 0$, the dispersive πN contribution and the asymptotic contributions to α have the same sign, in contrast to β where both contributions have opposite sign and nearly cancel each other in their sum.

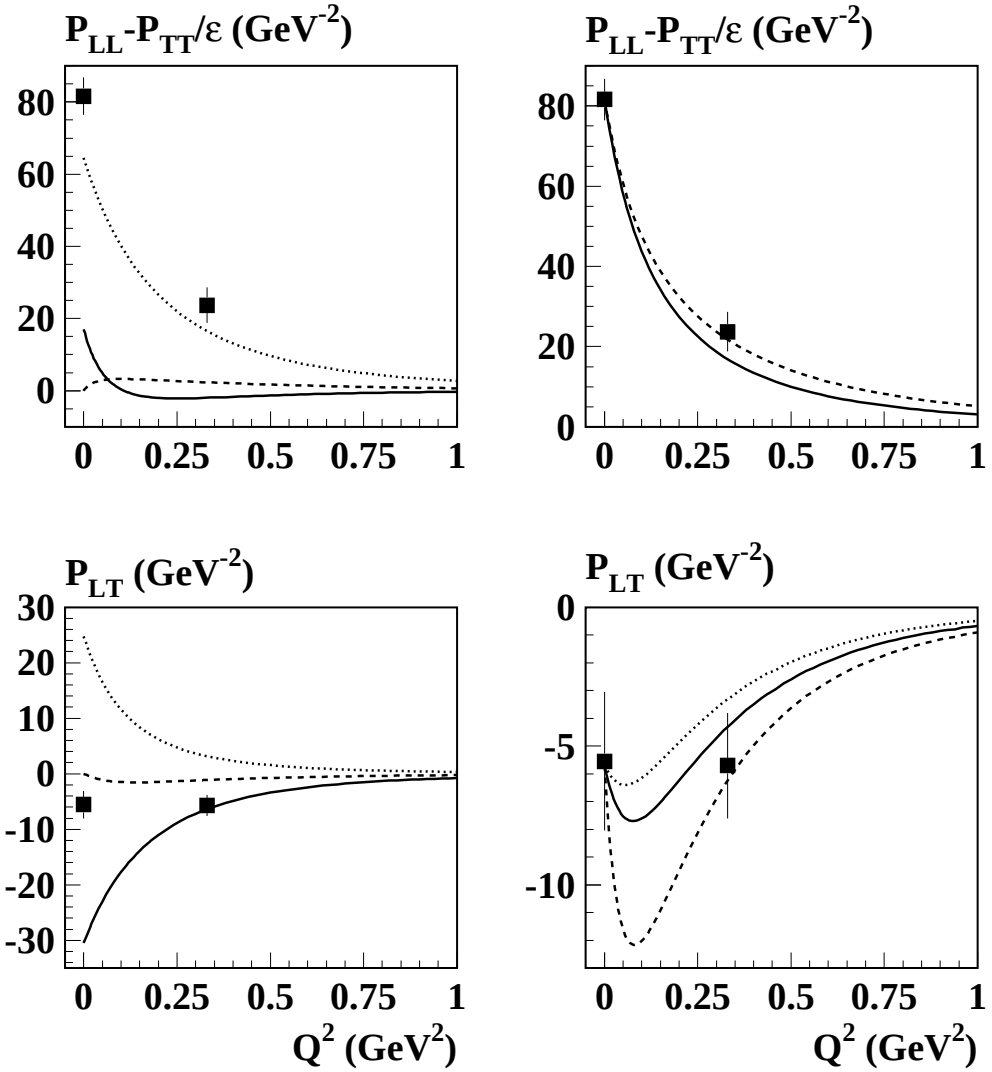

Figure 4.17: Results for the unpolarized structure functions $P_{LL} - P_{TT}/\varepsilon$ (upper panels) and P_{LT} (lower panels), for $\varepsilon = 0.62$. Upper left panel: dispersive πN contribution to the GP $\alpha(Q^2)$ (full curve), dispersive πN contribution to the spin-flip GPs (dashed curve), and the asymptotic contribution to α, according to Eq.(4.119) with $\Lambda_\alpha = 1$ GeV (dotted curve). Upper right panel: total result for $P_{LL} - P_{TT}/\varepsilon$ (sum of the three contributions on the upper left panel) for $\Lambda_\alpha = 1$ GeV (solid curve) and $\Lambda_\alpha = 1.4$ GeV (dashed curve). Lower left panel: dispersive πN contribution to $\beta(Q^2)$ (full curve), dispersive πN contribution to the spin-flip GPs (dashed curve), and the asymptotic contribution to β, according to Eq.(4.110) with $\Lambda_\beta = 0.6$ GeV (dotted curve). Lower right panel: total result for P_{LT} for $\Lambda_\beta = 0.7$ GeV (dotted curve), $\Lambda_\beta = 0.6$ GeV (full curve), and $\Lambda_\beta = 0.4$ GeV (dashed curve). The data points at $Q^2 = 0$ are from Ref. [Olm 01], and the VCS data at $Q^2 = 0.33$ from Ref. [Roc 00].

The response functions $P_{LL} - P_{TT}/\varepsilon$ and P_{LT} were extracted in Ref. [Roc 00] by applying a LEX to VCS data (cf. Fig. 4.12), according to Eq.(4.43). To test the validity of such LEX, we show in Fig. 4.18 the DR predictions for the full energy dependence of the non-Born part of the $ep \to ep\gamma$ cross section in the kinematics of the MAMI experiment [Roc 00]. This energy dependence is compared with the LEX, which predicts a linear dependence in q' for the difference between the measured experimental cross section and its BH + Born contribution. The result of the best fit to the data is indicated by the horizontal bands in Fig. 4.18 for the quantity $(d^5\sigma - d^5\sigma^{BH+Born})/\Phi q'$. It is seen from Fig. 4.18 that the DR results predict only a modest additional energy dependence up to $q' \simeq 0.1$ GeV/c for most of the proton angles involved, and therefore seem to support the LEX analysis of Ref. [Roc 00]. Only for forward angles, $\Theta_{\gamma\gamma}^{cm} \approx 0$, which is the angular range from which the value of P_{LT} is extracted, the DR calculation predicts a stronger energy dependence in the range up to $q' \simeq 0.1$ GeV/c, as compared to the LEX.

Increasing the energy, we show in Fig. 4.19 the DR predictions for photon energies in the $\Delta(1232)$-resonance region. It is seen that the $ep \to ep\gamma$ cross section rises strongly when crossing the pion threshold due to a strong coupling of the VCS process to the pion photo- and electroproduction reactions by means of unitarity. It is furthermore seen from Fig. 4.19 that the region between pion threshold and the Δ-resonance peak displays an enhanced sensitivity to the GPs through the interference with the rising Compton amplitude due to Δ-resonance excitation. For example, at $q' \simeq 0.2$ GeV/c, the predictions for P_{LT} in the lower right panel of Fig. 4.17 for $\Lambda_\beta = 0.4$ GeV and $\Lambda_\beta = 0.6$ GeV give a difference of about 20 % in the non-Born squared amplitude. In contrast, the LEX prescription results in a relative effect for the same two values of P_{LT} of about 10 % or less. This is similar to the situation in RCS, where the region between pion threshold and the Δ-resonance position also provides an enhanced sensitivity to the polarizabilities. Therefore, this energy region seems promising to measure the VCS observables with an increased sensitivity to the GPs. The present DR formalism can be used as a tool for such extraction.

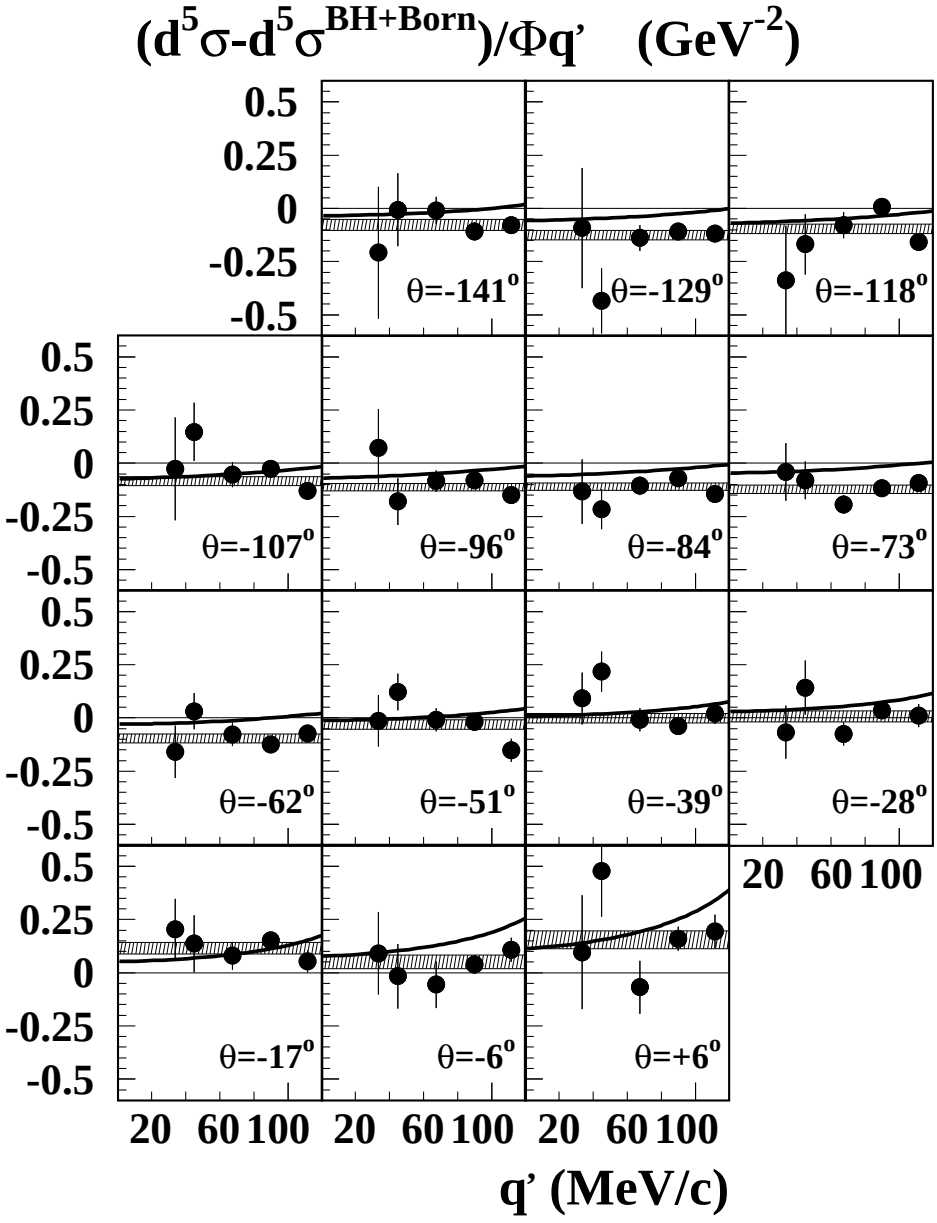

Figure 4.18: $(d^5\sigma - d^5\sigma^{BH+Born})/\Phi q'$ for the $ep \to ep\gamma$ reaction as a function of the outgoing photon energy q' in MAMI kinematics: $\varepsilon = 0.62$, $q = 0.6$ GeV, and for different photon c.m. angles Θ. The data points and the shaded bands, representing the best fit to the data within the LEX formalism, are from Ref. [Roc 00]. The solid curves are the DR results taking into account the full q' dependence of the non-Born contribution to the cross section. The asymptotic contributions are calculated according to Eqs.(4.119) and (4.110), with $\Lambda_\beta = 0.6$ GeV and $\Lambda_\alpha = 1$ GeV, respectively.

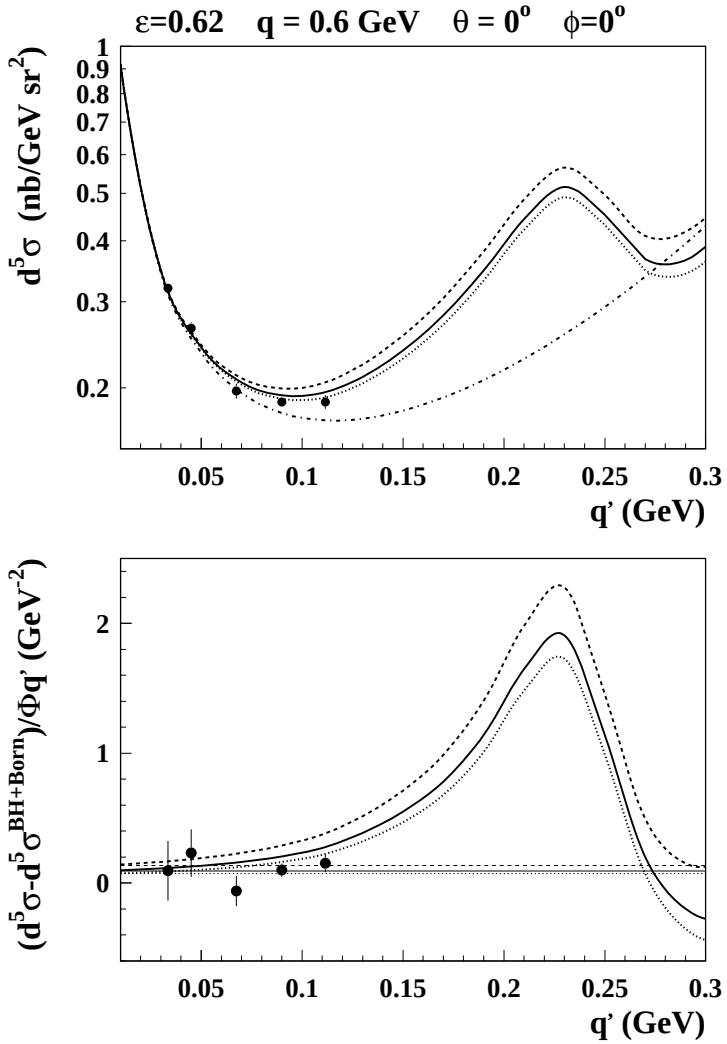

Figure 4.19: Upper panel: The differential cross section for the $ep \to ep\gamma$ reaction as a function of the outgoing photon energy q' in MAMI kinematics: $\varepsilon = 0.62$, $q = 0.6$ GeV, and for $\Theta = 0^\circ$, in plane ($\phi = 0^\circ$). The BH + Born contribution is given by the dashed-dotted curve. The total DR results are obtained with the asymptotic parts of Eqs. 4.110, 4.119, using a fixed value of $\Lambda_\alpha = 1$ GeV and for the three values of Λ_β as displayed in the lower right plot of Fig. 4.17, *i.e.* $\Lambda_\beta = 0.7$ GeV (dotted curve), $\Lambda_\beta = 0.6$ GeV (full curve), and $\Lambda_\beta = 0.4$ GeV (dashed curve). Lower panel: Results for $(d^5\sigma - d15\sigma^{BH+Born})/\Phi q'$ as a function of q'. The DR calculations taking into account the full energy dependence of the non-Born contribution (thick curves) are compared to the corresponding results within the LEX formalism (thin curves). The curves in the lower pannel correspond to the same values of Λ_α and Λ_β as in the upper panel. The data points are from Ref. [Roc 00].

When increasing the value of ε, the Born and non-Born parts of the $ep \to ep\gamma$ cross section increase relative to the BH contribution, due to the increasing photon flux factor [Gui 98]. This is seen by comparing the non-Born cross section in Fig. 4.19 (corresponding to $\varepsilon = 0.62$) with the result for $\varepsilon = 0.8$ at the same value of q and photon scattering angle, as is shown in Fig. 4.20.

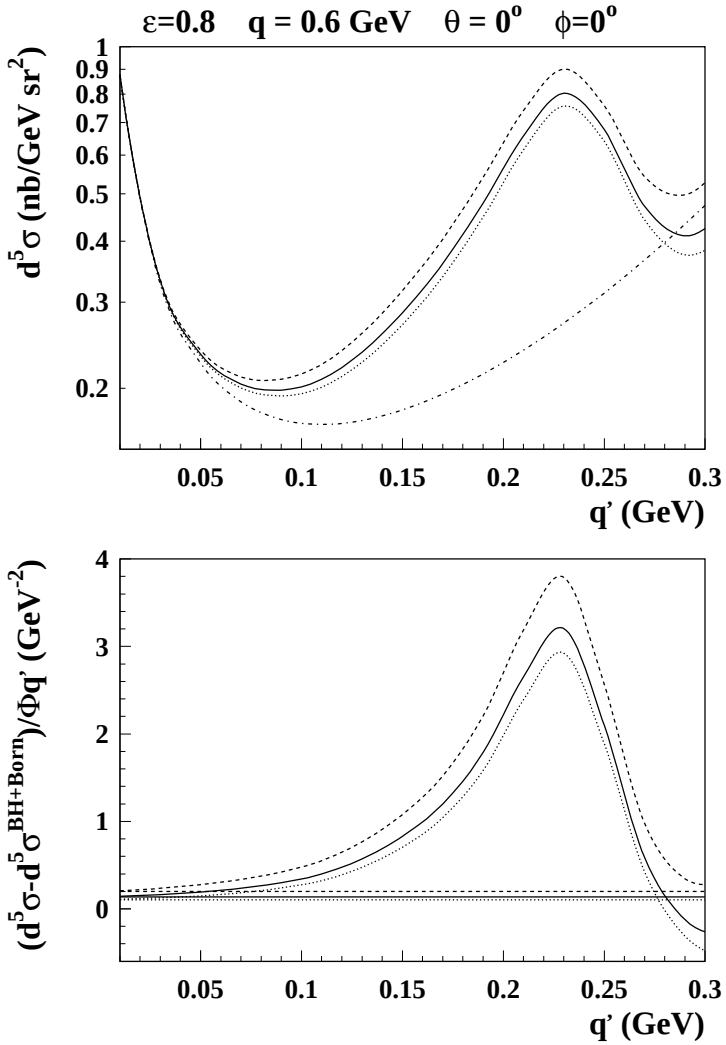

Figure 4.20: Notation as in Fig. 4.19, but for $\varepsilon = 0.8$.

Besides giving rise to higher non-Born cross sections, an experiment at a higher value of ε (keeping q fixed) also allows one to disentangle the unpolarized structure functions P_{LL} and P_{TT} in Eq.(4.43). This will provide a nice opportunity for the MAMI-C facility where such a higher ε value (as compared to the value $\varepsilon = 0.62$ of the first VCS experiment of Ref. [Roc 00]) can be reached for the same value of q.

Recently, the VCS data were also taken at JLab [Ber 93a] below pion threshold at $Q^2 = 1$ GeV^2 [Deg 01, Jam 01] and at $Q^2 = 1.9$ GeV^2 [Jam 00, Jam 01] as well as in the resonance region around $Q^2 = 1$ GeV^2 [Lav 01].

The extraction of GPs from VCS data at these higher values of Q^2 requires an accurate knowledge of the nucleon electromagnetic form factors in this region. For the proton magnetic form factor $G_M^p(Q^2)$, we use the Bosted parametrization [Bos 95], which has an accuracy of around 3% in the Q^2 region of 1-2 GeV^2. The ratio of the proton electric form factor $G_E^p(Q^2)$ to the magnetic form factor $G_M^p(Q^2)$ was recently measured with high accuracy in a polarization experiment at JLab in the Q^2 range between 0.4 and 3.5 GeV^2 [Jon 00]. It was found in [Jon 00] that G_E^p drops considerably faster with Q^2 than G_M^p. In the region of interest here, i.e. $Q^2 \simeq 1-2$ GeV^2, the JLab data [Jon 00] are well described by the fit [Deg 01],

$$\frac{\mu_p G_E^p(Q^2)}{G_M^p(Q^2)} \approx 1 - 0.13(Q^2)^2 + 0.028(Q^2)^3 , \tag{4.121}$$

where μ_p is the proton magnetic moment. In the following VCS calculations at $Q^2 = 1$ GeV^2, we use the parametrization of Eq.(4.121) to specify G_E^p (with the Bosted parametrization for G_M^p). In Fig. 4.21, we show the differential cross sections for the $ep \to ep\gamma$ reaction, as well as the DR predictions for the non-Born effect relative to the BH + Born cross section, at $Q^2 = 1$ GeV^2, for three values of the outgoing photon energy below pion threshold, corresponding to the kinematics of the JLab experiment [Deg 01]. It is seen from Fig. 4.21 that the sensitivity to the GPs is largest where BH + Born becomes small, in particular in the angular region between 0° and 50°. In Fig. 4.21, we show the non-Born effect for different values of the polarizabilities. For P_{LL}, the dispersive πN calculation at $Q^2 = 1$ GeV^2 gives

$$P_{LL}^{\pi N}(1\text{GeV}^2) = -0.3\,\text{GeV}^{-2} , \tag{4.122}$$

leading to the total results for P_{LL} within the DR formalism,

$$P_{LL}(1\text{GeV}^2) = +2.3\,\text{GeV}^{-2} , \quad \text{for } (\Lambda_\alpha = 1\,\text{GeV}) , \tag{4.123}$$

$$P_{LL}(1\text{GeV}^2) = +4.2\,\text{GeV}^{-2} , \quad \text{for } (\Lambda_\alpha = 1.4\,\text{GeV}) . \tag{4.124}$$

For P_{LT}, the calculation of the πN dispersive contribution at $Q^2 = 1$ GeV^2 gives

$$P_{LT}^{\pi N}(1\text{GeV}^2) = -0.9\,\text{GeV}^{-}2 , \tag{4.125}$$

which leads to the total result

$$P_{LT}(1\mathrm{GeV}^2) = -0.6\,\mathrm{GeV}^{-2}\,, \quad \text{for } \Lambda_\beta = 0.6\,\mathrm{GeV}\,, \tag{4.126}$$

$$P_{LT}(1\mathrm{GeV}^2) = -0.9\,\mathrm{GeV}^{-2}\,, \quad \text{for } \Lambda_\beta = 0.4\,\mathrm{GeV}\,. \tag{4.127}$$

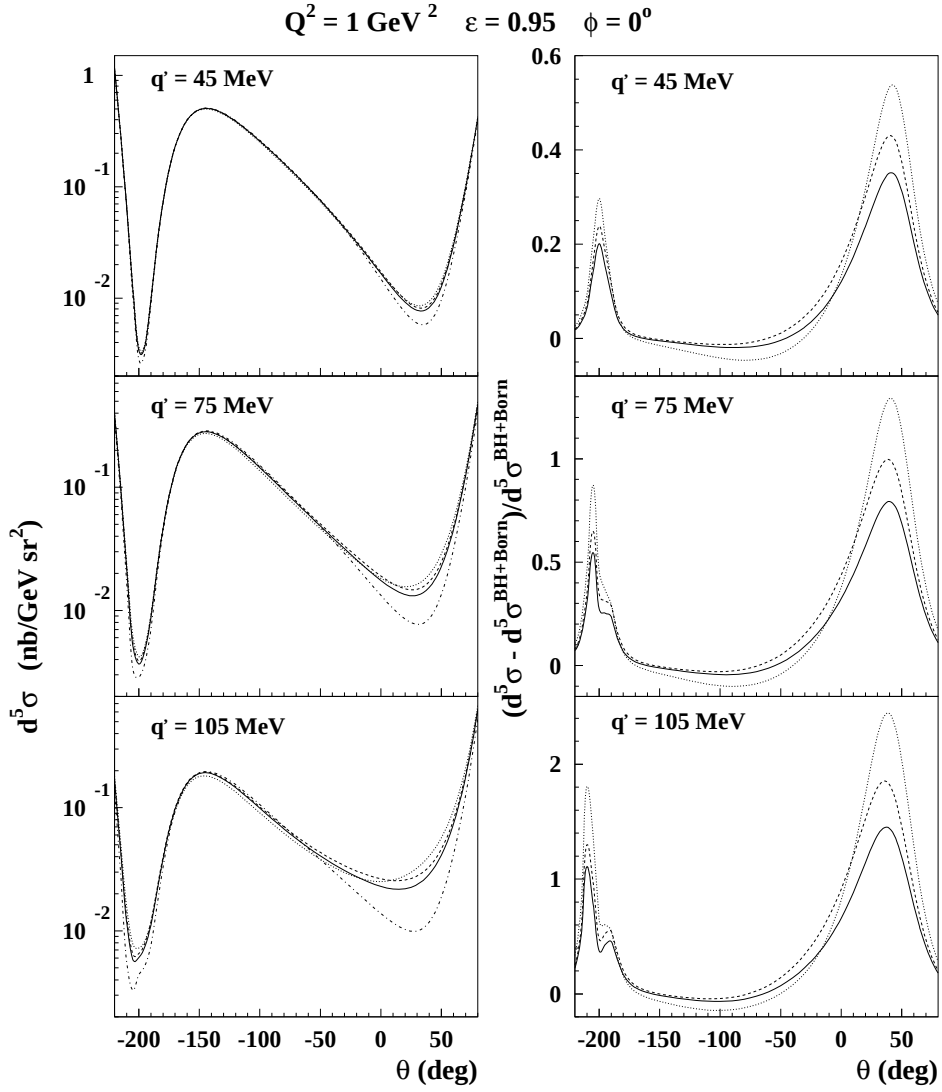

Figure 4.21: Left panels: The differential cross section for the $ep \to ep\gamma$ reaction as a function of the photon scattering angle and at different values of the outgoing photon energy q' in JLab kinematics. Right panels: Ratio of cross sections $(d\sigma - d\sigma^{BH+Born})/d\sigma^{BH+Born}$. The BH + Born contribution is given by the dashed-dotted curve. The DR results are displayed (on both left and right panels) with the asymptotic parts parametrized as in Eqs.(4.110), (4.119), using the values: $\Lambda_\alpha = 1$ GeV and $\Lambda_\beta = 0.6$ GeV (full curves), $\Lambda_\alpha = 1$ GeV and $\Lambda_\beta = 0.4$ GeV (dashed curves), $\Lambda_\alpha = 1.4$ GeV and $\Lambda_\beta = 0.6$ GeV (dotted curves).

The deviation of the experimental values from the dispersive πN values of Eq.(4.122) for P_{LL} and Eq.(4.125) for P_{LT} will provide us with interesting information, and enable us to test our understanding of the electric and magnetic polarizabilities at this large value of $Q^2 = 1$ GeV^2.

For the same kinematics as in Fig. 4.21, we compare in Fig. 4.22 the DR calculation for the non-Born cross section with the corresponding result using the LEX. It is seen that the deviation of the DR results from the LEX becomes already noticeable for $q' = 75$ MeV, over most of the photon angular range. Therefore, the DR analysis seems already to be needed at those lower values of q', in order to extract GPs from the JLab data.

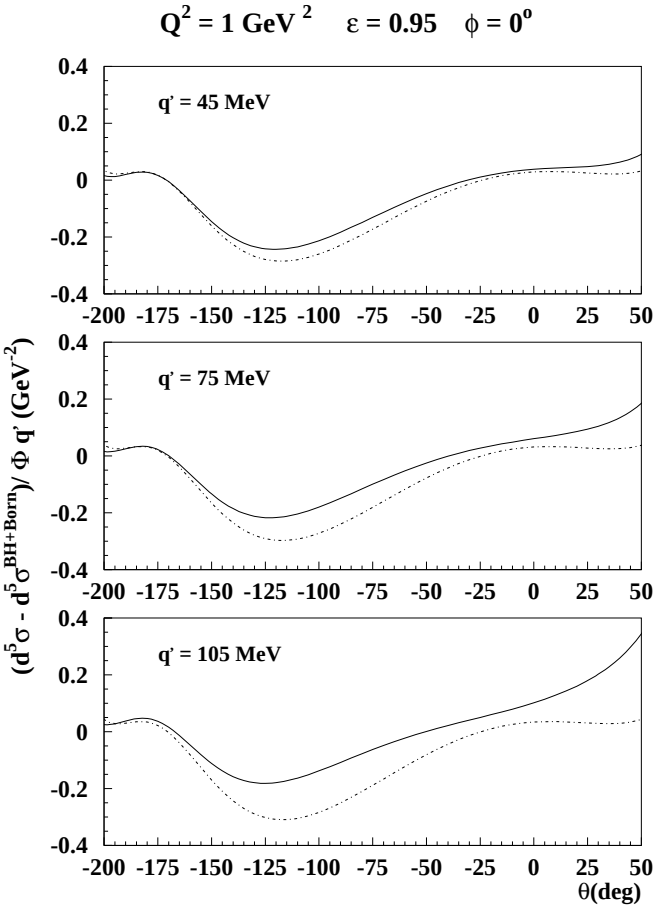

Figure 4.22: $(d\sigma - d\sigma^{BH+Born})/\Phi q'$ for the $ep \to ep\gamma$ reaction as a function of the photon scattering angle and at different values of the outgoing photon energy q' in JLab kinematics. The solid lines correspond to the DR calculation with the full energy dependence of the non-Born contribution to the cross section. The asymptotic parts have been calculated with the parametrizations of Eqs.(4.110), (4.119), using $\Lambda_\alpha = 1$ GeV and $\Lambda_\beta = 0.6$ GeV. The dashed-dotted curves are the results obtained within the LEX formalism with corresponding values of the GPs.

In Fig. 4.23, we increase the energy through the $\Delta(1232)$-resonance region, and show the results for the $ep \to ep\gamma$ reaction at $Q^2 = 1$ GeV^2 and at a backward angle. We display the sensitivity of the cross section and of the non-Born effect for the values in Eqs.(4.123) and (4.124) for P_{LL}, and for the value of Eq.(4.126) for P_{LT}. One finds a sizable sensitivity to P_{LL} in this backward cross section, and it therefore seems very promising to extract information on the electric polarizability from such future data.

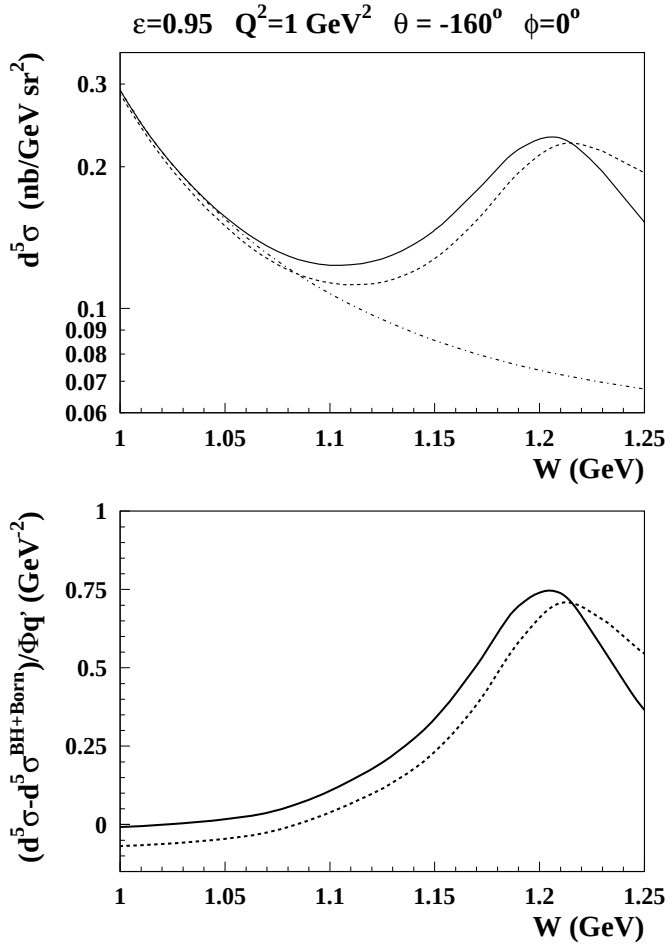

Figure 4.23: Upper panel: The differential cross section for the $ep \to ep\gamma$ reaction as a function of the c.m. energy W in JLab kinematics: $\varepsilon = 0.95$, $Q^2 = 1$ GeV^2, and for fixed scattering angles $\Theta = -160^\circ$, in plane ($\phi = 0^\circ$). The BH + Born contribution is given by the dashed-dotted curve. The total result including the full energy dependence of the non-Born contribution is shown for $\Lambda_\beta = 0.6$ GeV and for the two values of Λ_α: $\Lambda_\alpha = 1$ GeV (full curve), and $\Lambda_\alpha = 1.4$ GeV (dashed curve).Lower panel: Results for $(d^5\sigma - d15\sigma^{BH+Born})/\Phi q'$ as a function of W. The curves in the lower pannel correspond to the same values of Λ_α and Λ_β as in the upper panel.

Until now, we discussed only unpolarized observables. An unpolarized VCS experiment gives access to only 3 combinations of the 6 GPs, as shown in Eq.(4.43). Within the LEX formalism, it has been demonstrated (cf. Eqs.(4.52), (4.54), (4.55)) that double-polarization VCS observables with polarized lepton and polarized recoil (or target) nucleon, will allow us to measure three more combinations of GPs. Therefore, a measurement of unpolarized VCS observables (at different values of ε) and of 3 double-polarization observables will give the possibility to disentangle all 6 GPs. In Fig. 4.24, we show the dispersion results for these double polarization observables, with polarized electron beam and by measuring the recoil proton polarization either along the virtual photon direction (*z*-direction), or in the reaction plane and perpendicular to the virtual photon (*x*-direction).

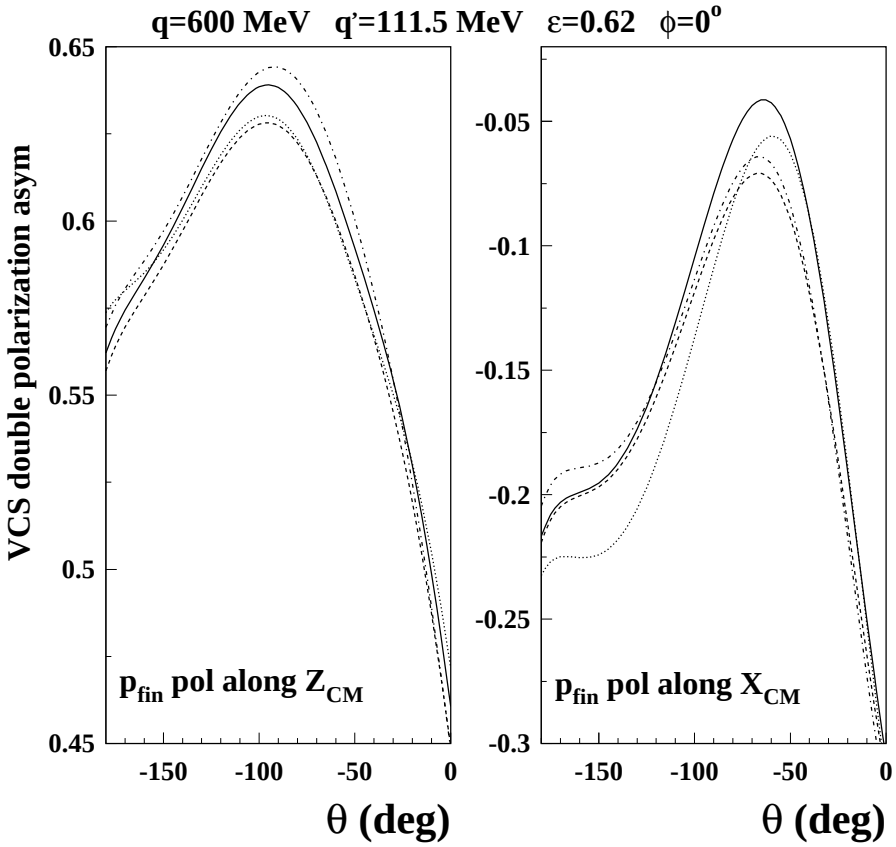

Figure 4.24: VCS double-polarization asymmetry (polarized electron, recoil proton polarization along either *z*- or $x-$ directions in the c.m. frame) in MAMI kinematics as a function of the photon scattering angle. The dotted curve corresponds to the BH + Born contribution. The dispersion results are shown for the values of the mass scales $\Lambda_\alpha = 1$ GeV, $\Lambda_\beta = 0.6$ GeV (full curves) and $\Lambda_\alpha = 1$ GeV, $\Lambda_\beta = 0.4$ GeV (dashed curves). To see the effect of the π^0-pole contribution, we also show the results for the values $\Lambda_\alpha = 1$ GeV, $\Lambda_\beta = 0.6$ GeV, when turning off the π^0-pole contribution (dashed-dotted curves).

The double polarization asymmetries are quite large (due to a finite asymmetry for the BH + Born mechanism , but our DR calculations show only small relative effects due to the spin GPs below pion threshold. Although these observables are tough to measure, a first test experiment is already planned at MAMI [d'Ho 01].

When measuring double-polarization observables above pion threshold, one can enhance the sensitivity to the GPs, as in the previously shown case of the unpolarized observables. In Fig. 4.25, we show as an example the double polarization asymmetry in MAMI kinematics for polarized beam and recoil polarization along the virtual photon direction as a function of the outgoing photon energy through the $\Delta(1232)$ region. The $\Delta(1232)$-resonance excitation clearly shows up as a deviation from the LEX result above about $q' = 100$ MeV.

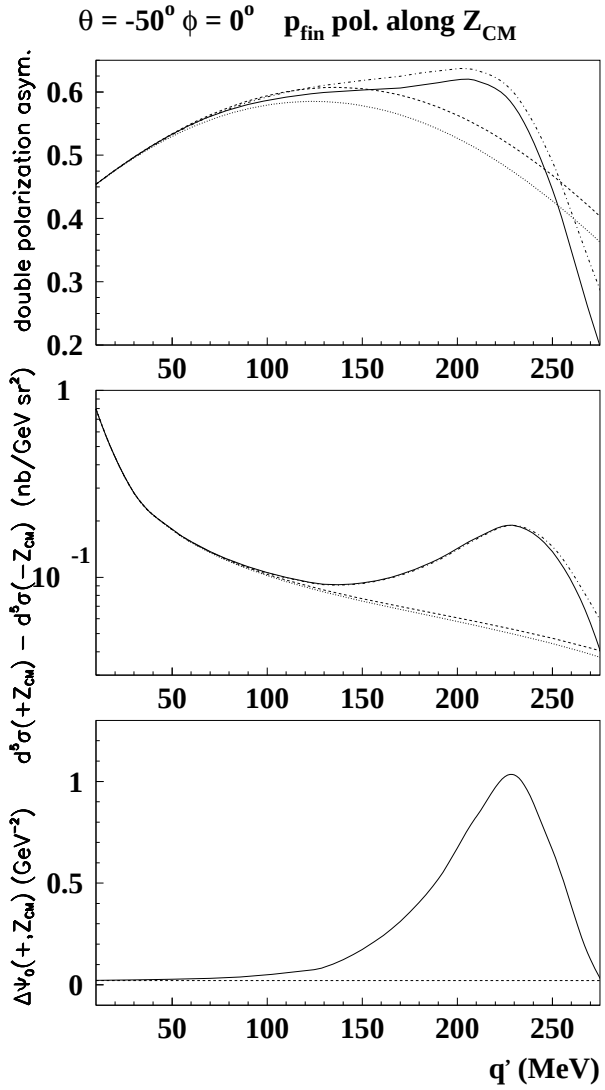

Figure 4.25: Upper panel: VCS double-polarization asymmetry (polarized electron, recoil proton polarization along the *z*-direction in the c.m. frame) in MAMI kinematics as a function of the outgoing photon energy at a fixed photon scattering angle $\Theta = -50^\circ$, in-plane ($\phi = 0^\circ$). The central panel is the corresponding difference of polarized cross sections, and the lower panel is the non-Born contribution to the corresponding polarized squared matrix element (according to Eq.(4.52)).The dotted curves correspond to the BH + Born contribution. The dispersion results for the total BH + Born + non-Born cross section (full curves) are calculated using the values $\Lambda_\alpha = 1$ GeV, $\Lambda_\beta = 0.6$ GeV. The dashed curves are the corresponding results obtained from LEX. To see the effect of the π^0-pole contribution, we also show the results of the dispersion calculations, when turning off the π^0-pole contribution (dashed-dotted curves).

A VCS single spin asymmetry below pion threshold is very small, since this observable is sensitive only to the imaginary part of the VCS amplitude. In this energy range, the latter is only due to higher order effects of QED, and is thus supressed by at least a factor of $\alpha_{em} \approx 1/137$. However, when crossing the pion threshold, the VCS amplitude acquires an imaginary part due to the coupling to the πN channel. Therefore, single-polarization observables become non-zero above pion threshold. A particularly relevant observable is the electron single spin asymmetry (SSA), which is obtained by flipping the electron beam helicity [Gui 98]. For VCS, this observable is mainly due to the interference of the real BH + Born amplitude with the imaginary part of the VCS amplitude. In Fig. 4.26, the SSA is shown for two kinematics in the $\Delta(1232)$ region.

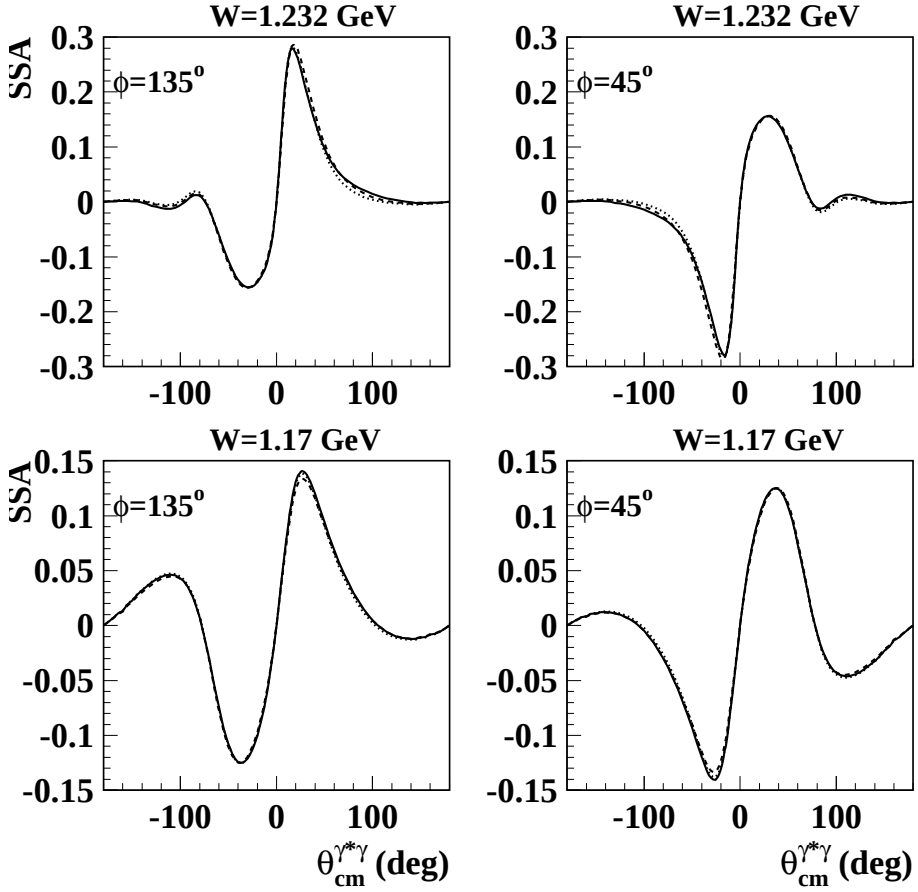

Figure 4.26: Electron single spin asymmetry (SSA) for VCS at $Q^2 = 0.12$ GeV^2, for two kinematics in the $\Delta(1232)$ region: $W = 1.232$ GeV, $\varepsilon = 0.75$ (upper plots) and $W = 1.17$ GeV, $\varepsilon = 0.81$ (lower plots). In both cases the SSA is shown as a function of the photon scattering angle for an out-of-plane angle $\phi = 45^\circ$, as accessible at MIT-Bates [Sha 97]. The full dispersion results are shown for the values: $\Lambda_\alpha = 1$ GeV, $\Lambda_\beta = 0.6$ GeV (full curves), $\Lambda_\alpha = 1$ GeV, $\Lambda_\beta = 0.4$ GeV (dashed curves), and $\Lambda_\alpha = 1.4$ GeV, $\Lambda_\beta = 0.6$ GeV (dotted curves).

As the SSA vanishes in plane, its measurement requires an out-of-plane experiment, such as at MIT-Bates [Sha 97]. Our calculation shows that the SSA is quite sizeable in the $\Delta(1232)$ region. Moreover, it displays only a rather weak dependence on the GPs, because the SSA is mainly sensitive to the imaginary part of the VCS amplitude. Therefore, it provides an excellent cross check of the dispersion formalism for VCS, in particular by comparing, at the same time, the pion and photon electroproduction channels through the $\Delta(1232)$ region.

4.11 Conclusions

In this chapter, we have presented a dispersion relation (DR) formalism for VCS off a proton target. Such a formalism can serve as a tool to extract generalized polarizabilities (GPs) from VCS observables over a larger energy range. The way we evaluated our dispersion integrals using πN intermediate states, allows us to apply the present formalism for VCS observables through the $\Delta(1232)$-resonance region.

The presented DR framework, when applied at a fixed value of Q^2, involves two free parameters which can be expressed in terms of the scalar electric and magnetic GPs, and which are to be extracted from a fit to VCS data. We proposed a parametrization of these two parameters (asymptotic parts to α and β) in terms of a dipole Q^2-dependence, and investigated the sensitivity of VCS observables to the corresponding mass scales.

We confronted our dispersive calculations with existing VCS data taken at MAMI below pion threshold. Compared to the low-eneergy expansion (LEX) analysis which was previously applied to those data, we found only a modest additional energy dependence up to photon energies of around 100 MeV, which supports such a LEX analysis. When increasing the photon energy, our dispersive calculations show that the region between pion threshold and the Δ-resonance peak displays an enhanced sensitivity to the GPs. It therefore seems very promising to measure VCS observables in this energy region in order to measure GPs with an enhanced precision.

Furthermore, we showed our DR predictions for VCS data at higher values of Q^2, in the range $Q^2 = 1 - 2$ GeV^2, where VCS data have been taken at JLab which are presently under analysis. It was found for the JLab kinematics that the DR results show a noticeable deviation from the LEX results already for outgoing photon energies as low as 75 MeV. Therefore, the DR analysis seems already to be needed below pion threshold in order to extract GPs from the JLab data. We also showed predictions at $Q^2 = 1$ GeV^2 at higher outgoing photon energies, through the Δ-resonance region, where data have also been taken at JLab. At backward scattering angles, we found a very sizeable sensitivity to the generalized electric polarizability. The two different JLab data sets, both below pion threshold and in the Δ region, at the same value of Q^2 (in the range $Q^2 = 1 - 2$ GeV^2) will provide a very interesting check for the present DR formalism. The overall aim of this formalism will be to demonstrate that consistent values of GPs can be extracted by a fit in the full energy range.

Besides unpolarized VCS experiments, which give access to a combination of 3 (out of 6) GPs, we investigated the potential of double polarization VCS observables. Although such double polarization experiments with polarized beam and recoil proton polarization are quite challenging, they are needed to access and quantify the remain-

ing three GPs. Using the DR formalism one can also analyze these observables above pion threshold.

Finally, above pion threshold also single-polarization observables are finite. In particular, the electron single spin asymmetry, to be measured with a polarized electron beam, is sizeable in the Δ-region and can provide a very valuable cross-check of the VCS dispersion calculations, as it is mainly sensitive to the imaginary part of the VCS amplitude linked through unitarity to the πN channel.

Chapter 5

Summary

Scattering of real and virtual photons off the nucleon serves as a tool for probing and understanding the structure of the nucleon. At low photon energies, real Compton scattering is governed by the global properties of the nucleon, such as its mass, electric charge, and anomalous magnetic moment. However, the resulting Powell cross section fails to describe the Compton data already at low energies. This discrepancy points to the presence of an internal structure of the nucleon. In order to separate the static properties of the nucleon from the effects of its internal structure, a general prescription has been given in Refs. [Gel 54], [Low 54], in terms of the low energy theorem (LET). This theorem is based on the general properties of the Compton tensor, such as gauge, crossing and Lorentz invariance and thus independent of the specific model used for practical calculations.

Using the LET, the Taylor expansion of the residual (non-Born) amplitude in the energy can be parametrized by means of six (unknown) structure dependent constants, which are called polarizabilities for analogy with classical electrodynamics. The two scalar polarizabilities, α (electric) and β (magnetic), parametrize the non-Born Compton amplitude in the leading order of ω^2, with ω the photon energy, while the four spin polarizabilities $\gamma_{1,2,3,4}$ appear at the order of ω^3. However, the applicability of such a low energy expansion (LEX) is limited in energy (up to about 100 MeV), and the Compton cross section at such low energies is rather small ($\sim$ 20 nb/sr), which does not allow for a determination of the nucleon polarizabilities with good precision. With increasing photon energy, the cross section rises rapidly due to the strong coupling of the Compton process to the pion photoproduction channel. To describe the data at these higher energies in a consistent way, one has to treat the strong interaction mechanism properly.

In this thesis, the fixed-t subtracted dispersion relation (DR) formalism for real Compton scattering has been presented, as a tool to extract the nucleon polarizabilities with the minimum model dependence from the experimental data over a wide energy and angular range. Based on the analyticity of the Compton amplitude, which is a reflection of causality, DRs allow one to combine the information about the singularities of the invariant amplitudes in the three reaction channels s, t, and u. The unitarity relation expresses the imaginary part of the Compton amplitude in terms of a sum over all possible hadronic contributions in the intermediate state. Thanks to considerable theoretical and experimental effort in understanding and describing the pion photo-

production reaction, the imaginary part of the Compton amplitude is known with good accuracy at energies below the next inelastic threshold ($\pi\pi N$), and the πN contributions to the nucleon structure (the polarizabilities) are given by the corresponding dispersion integrals. In our calculations we used the dispersion analysis of pion photoproduction of Ref. [Han 98]. While for the forward polarizability $\alpha+\beta$ these dispersive πN effects result in about 80% of its experimental (sum rule) value, the corresponding dispersion integral for the difference of the scalar polarizabilities appearing in the backward direction $\alpha-\beta$, has a wrong sign, $\approx -6.5\cdot 10^{-4}$ fm^3, as compared to the experimental value of $10.5\cdot 10^{-4}$ fm^3. The reason for this is the presence of t-channel singularities in the vicinity of the s-channel scattering region ("asymptotical" contributions). Furthermore, the Regge theory predicts two of the six unsubtracted dispersion integrals to diverge due to these t-channel contributions, the "σ"-pole in the case of the amplitude A_1, and the π^0-pole in the case of A_2. In the framework of the unsubtracted DR of Ref. [L'vo 81], the dispersion integrals were cut off at $\nu_{max}\approx 1.5$ GeV, and the asymptotical contributions were modelled by the poles in the t-channel, independent of ν_{max}, which introduced a certain model dependence.

To obtain convergent dispersion integrals and simultaneously diminish the dependence on the higher energy contributions in the s-channel, as well as to test the model dependence of the unsubtracted DR formalism, we have suggested to subtract the s-channel dispersion integrals at the point $\nu=0$, keeping t fixed. The subtraction functions $A_i^{NB}(0,t)$ are calculated by means of the dispersion relations in t at fixed $\nu=0$, subtracted at $t=0$.

To calculate the contributions from the t-channel $\gamma\gamma\to N\bar{N}$ process (mainly due to the $\pi\pi$ intermediate states) to the real parts of the invariant amplitudes, we constructed the unitarized Born amplitude for the $\gamma\gamma\to\pi\pi$ reaction, and used the extrapolation of the πN helicity amplitudes [H$\ddot{}$oh 83] into the t-channel kinematical region. At negative t, the πN contributions from the unphysical region to the dispersion integrals were estimated by the resonant $\Delta(1232)$ contribution.

The subtraction constants $A_i^{NB}(0,0)$ are directly related to the polarizabilities. Four of these constants can be calculated using the unsubtracted DR in the s-channel, and the other two, $\alpha-\beta$ and γ_π, are free parameters in our formalism and can be obtained from a fit to the Compton data.

We further investigated the sensitivity of different observables on the values of these two parameters. We presented the results for the unpolarized and polarized RCS observables in the kinematics of the most recent experiments, compared the results within the subtracted and unsubtracted dispersion formalisms, and found a close agreement between the two formalisms, which can be seen as a good cross check for the DRs for RCS.

The successfull description of RCS served as the motivation for a generalization of the fixed-t DRs to the case of a virtual initial photon, which situation is accessible experimentally within a VCS experiment (radiative electron scattering). The low energy theorem was formulated for VCS by Refs. [Gui 95], [Dre 97] and resulted in the introduction of six independent generalized dipole polarizabilities (GPs). The LEX formalism of Ref. [Gui 95] provided a link of the GPs to the unpolarised VCS observables. A first measurement of the GPs was performed at MAMI [Roc 00] in 1996 at a virtuality of the initial photon of $Q^2=0.33$ (GeV/c)^2 and in an energy range between 45 and 115 MeV. Presently, three further VCS data sets are under analysis at

JLab [Ber 93a] ($Q^2 = 1.$ (GeV/c)^2 and $Q^2 = 2.$ (GeV/c)^2) and MIT-Bates ($Q^2 = 0.05$ (GeV/c)^2) [Sha 97]. To provide the experimentalist with the formalism to extract the GPs from VCS data also above pion production threshold and thus to increase the sensitivity of the VCS observables to the GPs, the DR formalism for VCS was elaborated in Refs. [Pas 00], [Pas 01a] (for details, see Chapter 3 of this thesis).

As an input for the unsubtracted s-channel dispersion integrals for VCS we use the most recent version of the pion photo- and electroporoduction multipoles of Ref. [MAID] which provides the description of the experimental data over a wide Q^2 range. On the basis of the results for RCS, we model the asymptotical contributions to the amplitudes F_1 and F_5 by the energy independent σ- and π^0-poles in the t-channel, respectively. For F_5, this asymptotic part is completely fixed by the π^0-pole and is known with good precision. This allowed us to obtain DR predictions for the four spin GPs [Pas 01a].

For F_1 only the t-dependence of its asymptotic part is fixed by the σ-pole, whereas its value at $t = 0$ is the fit parameter in our formalism. Furthermore, due to the fact that the Baldin sum rule does not constrain the electric and magnetic polarizabilities at $Q^2 \neq 0$, also the asymptotic part of F_2 has to be modeled: though the dispersion integral for this amplitude is convergent, the higher energy contributions from the s-channel, not included in this work, are not negligible. Our formalism thus provides predictions for the four spin GPs, while the scalar GPs $\alpha(Q^2)$ and $\beta(Q^2)$ have to be fitted to the experimental data at each value of Q^2.

We suggested a parametrization of the asymptotic contributions to $\alpha(Q^2)$ and $\beta(Q^2)$ in terms of a dipole Q^2-dependence, and investigated the sensitivity of VCS observables to the corresponding mass scales Λ_α and Λ_β.

Having compared our predictions for the VCS observables with the MAMI VCS data [Roc 00] at $Q^2 = 0.33$ GeV/c, we found a close agreement with the LEX formalism for energies below 100 MeV. At higher energies, the deviations from the LEX become however significant because of the vicinity of pion production near threshold and in the $\Delta(1232)$ resonance. We showed that at energies between pion threshold and the resonance position, the sensitivity to the GPs can be increased significantly, as compared to low energies, where the LEX is applicable.

In the kinematics of the VCS experiment at JLab, the discrepancies between DRs and LEX become sizeable at even lower energies, which means that at $Q^2 = 1$ GeV/c, the DRs are mandatory even for the analysis below pion threshold.

Real Compton scattering provides an electromagnetic probe of the nucleon as a whole, giving access to six polarizabilities which describe the strong force acting between the constituents within the nucleon in an effective way. A more detailed information about the nucleon structure is encrypted in the GPs, since they describe the local properties of the charge, magnetic, and spin distributions inside the nucleon by probing these with the weak electromagnetic field of the outgoing photon at a distance related to virtuality of the incoming virtual photon.

The polarizabilities of RCS, as well as the GPs, have been introduced in a model independent way, that is based on the general symmetry principles, neither making assumptions about the internal structure of the nucleon, nor about the interactions between its constituents. Together with such global properties of the nucleon as its mass,

charge, magnetic moment, and electroweak form factors, the polarizabilities and GPs are fundamental properties of the nucleon in the non-perturbative regime of QCD. Therefore, a precise knowledge of the polarizabilities and the GPs helps to advance our quantitative understanding of the strong interaction at low and intermediate energies.

The DR formalism developed in this work is a new tool to analyze VCS experiments over a wide energy and Q^2 range, thus allowing one to extract the values of GPs from VCS data in different kinematics with minimum model dependence.

Appendix A

A.1 Conventions and definitions

Throughout this work, we set

$$\hbar = c = 1\,. \tag{A.1}$$

Furthermore, we choose the metric tensor

$$\gamma^{\mu\nu} = \begin{pmatrix} 1 & 0 & 0 & 0 \\ 0 & -1 & 0 & 0 \\ 0 & 0 & -1 & 0 \\ 0 & 0 & 0 & -1 \end{pmatrix}, \tag{A.2}$$

that is, the scalar product is defined by

$$a^\mu b_\mu = a^0 b^0 - \vec{a}\cdot\vec{b}\,. \tag{A.3}$$

The phase of the totally antisymmetrical tensor $\varepsilon^{\mu\nu\alpha\beta}$ is fixed by

$$\varepsilon_{0123} = +1\,. \tag{A.4}$$

Finally, we use $\gamma_5 = i\gamma^0\gamma^1\gamma^2\gamma^3 = \begin{pmatrix} 0 & 1 \\ 1 & 0 \end{pmatrix}$.

A.2 Polarization vectors and helicity spinors

We use the Lorentz gauge for the photon polarization vectors. For the initial photon (real or virtual), the polarization vector in the case of the transversal polarization is given by

$$\varepsilon^\mu(q,\lambda=\pm1) = \left(0, \mp\frac{1}{\sqrt{2}}, -\frac{i}{\sqrt{2}}, 0\right)\,. \tag{A.5}$$

For the longitudinal polarization of the initial virtual photon, we have

$$\varepsilon^\mu(q,\lambda=0) = \frac{1}{Q}\left(|\vec{q}|, 0, 0, q_0\right)\,, \tag{A.6}$$

where $Q^2 \equiv -q^2 = \vec{q}^2 - q_0^2 > 0$ is the virtuality of the initial photon. For the final photon, the photon polarization vectors reads

$$\varepsilon^{'\mu}\left(q', \lambda^{'} = \pm 1\right) = \left(0, \mp\frac{1}{\sqrt{2}}\cos\theta, -\frac{i}{\sqrt{2}}, \pm\frac{1}{\sqrt{2}}\sin\theta\right). \tag{A.7}$$

The initial nucleon is travelling in the negative z-direction, and the final nucleon is emitted at an angle $180^o - \theta$ with respect to the incoming photon, and has azimuthal angle $180^o + \phi_{\gamma^*\gamma}$. This leads to the following spinor conventions for the incoming $(\vec{p}, \lambda_N)$ and outgoing $(\vec{p}^{\,'}, \lambda'_N)$ nucleons:

$$\begin{aligned} u(\vec{p}, \lambda_N) &= \sqrt{E+M}\begin{bmatrix} \chi_{\lambda_N} \\ 2\lambda_N \frac{|\vec{p}|}{E+M}\chi(\lambda_N) \end{bmatrix}, \\ u(\vec{p}^{\,'}, \lambda'_N) &= \sqrt{E'+M}\begin{bmatrix} \chi'_{\lambda'_N} \\ 2\lambda'_N \frac{|\vec{p}^{\,'}|}{E'+M}\chi'(\lambda'_N) \end{bmatrix}, \end{aligned} \tag{A.8}$$

where

$$\begin{aligned} \chi(\tfrac{1}{2}) &= \begin{bmatrix} 0 \\ 1 \end{bmatrix}, \qquad \chi(-\tfrac{1}{2}) = \begin{bmatrix} -1 \\ 0 \end{bmatrix}, \\ \chi'(\tfrac{1}{2}) &= \begin{bmatrix} \sin\frac{\theta}{2} \\ -\cos\frac{\theta}{2} \end{bmatrix}, \qquad \chi'(-\tfrac{1}{2}) = \begin{bmatrix} \cos\frac{\theta}{2} \\ \sin\frac{\theta}{2} \end{bmatrix}. \end{aligned} \tag{A.9}$$

A.3 Reduced helicity amplitudes

The reduced helicity amplitudes τ_i are defined by factorizing the kinematical factors in $\left(\cos\frac{\theta}{2}\right)^{|\Lambda+\Lambda'|}$ and $\left(\sin\frac{\theta}{2}\right)^{|\Lambda-\Lambda'|}$, out of the helicity amplitudes $T^s_{\lambda'\lambda'_N;\lambda\lambda_N}$, with $\Lambda = \lambda - \lambda_N$ and $\Lambda' = \lambda' - \lambda'_N$. The relations between the 6 independent helicity amplitudes and the reduced helicity amplitudes τ_i $(i = 1, .., 6)$ read

$$\begin{aligned} T^s_{1\frac{1}{2};1\frac{1}{2}} &= \cos\frac{\theta}{2}\tau_1, & T^s_{-1\frac{1}{2};-1\frac{1}{2}} &= \cos^3\frac{\theta}{2}\tau_2, \\ T^s_{1-\frac{1}{2};1\frac{1}{2}} &= \cos^2\frac{\theta}{2}\sin\frac{\theta}{2}\tau_3, & T^s_{1\frac{1}{2};-1\frac{1}{2}} &= \cos\frac{\theta}{2}\sin^2\frac{\theta}{2}\tau_4, \\ T^s_{-1-\frac{1}{2};1\frac{1}{2}} &= \sin\frac{\theta}{2}\tau_5, & T^s_{1-\frac{1}{2};-1\frac{1}{2}} &= \sin^3\frac{\theta}{2}\tau_6, \\ T^s_{-1\frac{1}{2};1\frac{1}{2}} &= \cos\frac{\theta}{2}\sin^2\frac{\theta}{2}\tau_7, & T^s_{-1-\frac{1}{2};-1\frac{1}{2}} &= \cos^2\frac{\theta}{2}\sin\frac{\theta}{2}\tau_8, \\ T^s_{1\frac{1}{2};0\frac{1}{2}} &= \sin\frac{\theta}{2}\tau_9, & T^s_{-1-\frac{1}{2};0\frac{1}{2}} &= \cos\frac{\theta}{2}\tau_{10}, \\ T^s_{-1\frac{1}{2};0\frac{1}{2}} &= \sin\frac{\theta}{2}\cos^2\frac{\theta}{2}\tau_{11}, & T^s_{1-\frac{1}{2};0\frac{1}{2}} &= \cos\frac{\theta}{2}\sin^2\frac{\theta}{2}\tau_{12}. \end{aligned} \tag{A.10}$$

Appendix B

B.1 t-channel helicity amplitudes for Compton scattering

The t-channel helicity amplitudes for Compton scattering can be expressed in the orthogonal basis of Prange [Pra 58] in terms of the invariants $T_1, \ldots T_6$. In the c.m. system of the t-channel process $\gamma\gamma \to N\bar{N}$ (see Fig. 3.9 for the kinematics), we choose the photon momentum $\vec{q}_t$ (helicity λ'_γ) to point in the z-direction and the nucleon momentum $\vec{p}\,' = \vec{p}_t$ in the $x-z$ plane at an angle θ_t with respect to the z-axis (the anti-nucleon momentum is then given by $-\vec{p} = -\vec{p}_t$). In this frame, the t-channel helicity amplitudes can be cast into the form

$$
\begin{aligned}
T^t_{\lambda_N \lambda_{\bar{N}}, \lambda'_\gamma \lambda_\gamma}(\nu, t) \;=\; (-1)^{\frac{1}{2}-\lambda_{\bar{N}}}\, \bar{u}(\vec{p}_t, \lambda_N) \quad & \Big\{ -\frac{1}{2}\lambda'_\gamma \lambda_\gamma \left(T_1 + |\vec{q}_t|\,\gamma^3\, T_2\right) \\
& -\frac{1}{2}\left(T_3 + |\vec{q}_t|\,\gamma^3\, T_4\right) \\
& -\frac{1}{2}\left(\lambda'_\gamma + \lambda_\gamma\right)\gamma_5\, T_5 \\
& -\frac{1}{2}\left(\lambda'_\gamma - \lambda_\gamma\right)\gamma_5\, |\vec{q}_t|\,\gamma^3\, T_6 \Big\}\; v(-\vec{p}_t, \lambda_{\bar{N}})\,,
\end{aligned}
\tag{B.1}
$$

which behave under parity transformation as

$$
T^t_{\lambda_N \lambda_{\bar{N}}, \lambda'_\gamma \lambda_\gamma}(\nu, t) \;=\; (-1)^{\Lambda_N - \Lambda_\gamma}\, T^t_{-\lambda_N - \lambda_{\bar{N}}, -\lambda'_\gamma - \lambda_\gamma}(\nu, t)\,, \tag{B.2}
$$

with the helicity differences Λ_γ and Λ_N given by $\Lambda_\gamma = \lambda'_\gamma - \lambda_\gamma$ (with Λ_γ = 0 or 2) and $\Lambda_N = \lambda_N - \lambda_{\bar{N}}$ (with Λ_N = 0 or 1), respectively.

We next express the invariant amplitudes $A_i(\nu, t)$ (i = 1,...,6) in terms of the t-channel helicity amplitudes $T^t_{\lambda_N \lambda_{\bar{N}}, \lambda'_\gamma \lambda_\gamma}(\nu, t)$ of Eq.(B.1). We find the following expressions:

$$
\begin{aligned}
A_1 &= \frac{1}{t\sqrt{t-4M^2}} \left\{ \left[T^t_{\frac{1}{2}\frac{1}{2},11} + T^t_{\frac{1}{2}\frac{1}{2},-1-1} \right] - \frac{2\nu\sqrt{t}}{\sqrt{su-M^4}}\, T^t_{\frac{1}{2}-\frac{1}{2},11} \right\}, \\
A_2 &= \frac{1}{t\sqrt{t}} \left\{ -\left[T^t_{\frac{1}{2}\frac{1}{2},11} - T^t_{\frac{1}{2}\frac{1}{2},-1-1} \right] - \frac{2\nu\sqrt{t-4M^2}}{\sqrt{su-M^4}}\, T^t_{\frac{1}{2}-\frac{1}{2},11} \right\},
\end{aligned}
$$

$$
\begin{aligned}
A_3 &= \frac{M^2}{su-M^4}\,\frac{1}{\sqrt{t-4M^2}}\left\{ 2\,T^t_{\frac{1}{2}\frac{1}{2},1-1} + \frac{\sqrt{su-M^4}}{\nu\sqrt{t}}\,\left[T^t_{\frac{1}{2}-\frac{1}{2},1-1} + T^t_{\frac{1}{2}-\frac{1}{2},-11}\right]\right\}, \\
A_4 &= \frac{M^2}{su-M^4}\,\frac{1}{\sqrt{su-M^4}}\left\{ M\left[-T^t_{\frac{1}{2}-\frac{1}{2},1-1} + T^t_{\frac{1}{2}-\frac{1}{2},-11}\right]\right. \\
&\qquad \left. + \frac{\sqrt{t}\sqrt{t-4M^2}}{4\nu}\,\left[T^t_{\frac{1}{2}-\frac{1}{2},1-1} + T^t_{\frac{1}{2}-\frac{1}{2},-11}\right]\right\}, \\
A_5 &= \frac{\sqrt{t-4M^2}}{4\nu\sqrt{t}\sqrt{su-M^4}}\left\{ -2\,T^t_{\frac{1}{2}-\frac{1}{2},11}\right\}, \\
A_6 &= \frac{\sqrt{t-4M^2}}{4\nu\sqrt{t}\sqrt{su-M^4}}\left\{ \left[T^t_{\frac{1}{2}-\frac{1}{2},1-1} + T^t_{\frac{1}{2}-\frac{1}{2},-11}\right]\right\}. \qquad \text{(B.3)}
\end{aligned}
$$

In the subtracted DR of Eq.(3.39), the t-channel integral runs along the line $\nu = 0$. Therefore, we have to determine the imaginary parts $\mathrm{Im}_t A_i(\nu = 0, t)$ of the invariant amplitudes of Eq.(B.3). We start by decomposing the t-channel helicity amplitudes for $\gamma\gamma \to N\bar{N}$ into a partial wave series,

$$
T^t_{\lambda_N\lambda_{\bar{N}},\lambda'_\gamma\lambda_\gamma}(\nu,t) = \sum_J \frac{2J+1}{2}\,T^J_{\lambda_N\lambda_{\bar{N}},\lambda'_\gamma\lambda_\gamma}(t)\,d^J_{\Lambda_N\Lambda_\gamma}(\theta_t)\,, \qquad \text{(B.4)}
$$

where $d^J_{\Lambda_N\Lambda_\gamma}$ are Wigner d-functions and θ_t is the scattering angle in the t-channel, which is related to the invariants ν and t by $\cos\theta_t = 4M\nu/\sqrt{t}\sqrt{t-4M^2}$. It is obvious from this equation that $\nu = 0$ corresponds to 90^o scattering for the t-channel process. As explained in Section 3.4, we calculate the imaginary parts of the t-channel helicity amplitudes $T^t_{\lambda_N\lambda_{\bar{N}},\lambda'_\gamma\lambda_\gamma}(\nu,t)$ through the unitarity equation by inserting $\pi\pi$ intermediate states, which should give the dominant contribution below $K\bar{K}$ threshold,

$$
2\,\mathrm{Im}T_{\gamma\gamma\to N\bar{N}} = \frac{1}{(4\pi)^2}\,\frac{|\vec{p}_\pi|}{\sqrt{t}}\int d\Omega_\pi\,\left[T_{\gamma\gamma\to\pi\pi}\right]\cdot\left[T_{\pi\pi\to N\bar{N}}\right]^*. \qquad \text{(B.5)}
$$

Combining the partial wave expansion for $\gamma\gamma \to \pi\pi$,

$$
T^{\gamma\gamma\to\pi\pi}_{\Lambda_\gamma}(t,\theta_{\pi\pi}) = \sum_{J even}\frac{2J+1}{2}\,T^{J\,(\gamma\gamma\to\pi\pi)}_{\Lambda_\gamma}(t)\cdot\sqrt{\frac{(J-\Lambda_\gamma)!}{(J+\Lambda_\gamma)!}}\cdot P_J^{\Lambda_\gamma}(\cos\theta_{\pi\pi}), \qquad \text{(B.6)}
$$

and the partial wave expansion for $\pi\pi \to N\bar{N}$,

$$
T^{\pi\pi\to N\bar{N}}_{\Lambda_N}(t,\Theta) = \sum_J\frac{2J+1}{2}\,T^{J\,(\pi\pi\to N\bar{N})}_{\Lambda_N}(t)\cdot\sqrt{\frac{(J-\Lambda_N)!}{(J+\Lambda_N)!}}\cdot P_J^{\Lambda_N}(\cos\Theta)\,. \qquad \text{(B.7)}
$$

We can now construct the imaginary parts of the Compton t-channel partial waves,

$$
2\,\mathrm{Im}T^{J\,(\gamma\gamma\to N\bar{N})}_{\lambda_N\lambda_{\bar{N}},\lambda'_\gamma\lambda_\gamma}(t) = \frac{1}{(8\pi)}\,\frac{p_\pi}{\sqrt{t}}\left[T^{J\,(\gamma\gamma\to\pi\pi)}_{\Lambda_\gamma}(t)\right]\left[T^{J\,(\pi\pi\to N\bar{N})}_{\Lambda_N}(t)\right]^*. \qquad \text{(B.8)}
$$

The partial wave amplitudes $T^{J\,(\pi\pi\to N\bar{N})}_{\Lambda_N}$ of Eq.(B.7) are related to the amplitudes $f^J_\pm(t)$ of Frazer and Fulco [Fra 60] by the relations

$$\begin{aligned} T^{J\,(\pi\pi\to N\bar{N})}_{\Lambda_N=0}(t) &= \frac{16\pi}{p_N}\,(p_N\,p_\pi)^J\cdot f^J_+(t)\;, \\ T^{J\,(\pi\pi\to N\bar{N})}_{\Lambda_N=1}(t) &= 8\pi\,\frac{\sqrt{t}}{p_N}\,(p_N\,p_\pi)^J\cdot f^J_-(t)\;, \end{aligned} \tag{B.9}$$

with p_N and p_π the c.m. momenta of nucleon and pion, respectively ($p_N=\sqrt{t/4-M^2}$ and $p_\pi=\sqrt{t/4-m_\pi^2}$).

For the reaction $\gamma\gamma\to\pi\pi$, we will use the partial wave amplitudes $F_{J\Lambda_\gamma}(t)$, which are related to those of Eq.(B.6) by

$$T^{J\,(\gamma\gamma\to\pi\pi)}_{\Lambda_\gamma}(t) \;=\; \frac{2}{\sqrt{2J+1}}\cdot F_{J\Lambda_\gamma}(t)\;. \tag{B.10}$$

Denoting the Born partial wave amplitudes for $\gamma\gamma\to\pi^+\pi^-$ by $B_{J\Lambda_\gamma}(t)$, the lowest Born partial waves (s and d waves) are

$$\begin{aligned} B_{00}(t) &= 2e^2\,\frac{1-\beta^2}{2\beta}\,\ln\left(\frac{1+\beta}{1-\beta}\right), \\ B_{20}(t) &= 2e^2\,\frac{\sqrt{5}}{4}\,\frac{1-\beta^2}{\beta^2}\,\left\{\frac{3-\beta^2}{\beta}\ln\left(\frac{1+\beta}{1-\beta}\right)\,-\,6\right\}, \\ B_{22}(t) &= 2e^2\,\frac{\sqrt{15}}{4\sqrt{2}}\,\left\{\frac{(1-\beta^2)^2}{\beta^3}\ln\left(\frac{1+\beta}{1-\beta}\right)\,+\,\frac{10}{3}\,-\,\frac{2}{\beta^2}\right\}, \end{aligned} \tag{B.11}$$

with $\beta = p_\pi/\left(\sqrt{t}/2\right)$ the pion velocity.

Inserting the partial-wave expansion of Eq.(B.4) into Eq.(B.3), we can finally express the 2π t-channel contributions $\mathrm{Im}_t A_i(\nu=0,t)^{2\pi}$ by the partial wave amplitudes for the reactions $\gamma\gamma\to\pi\pi$ and $\pi\pi\to N\bar{N}$,

$$\begin{aligned} \mathrm{Im}_t A_1(\nu=0,t)^{2\pi} &= \frac{p_\pi}{\sqrt{t}}\,\frac{1}{t\,p_N^2}\sum_{J=0,2,4,\ldots}(p_\pi\,p_N)^J\,\sqrt{2J+1}F_{J\Lambda_\gamma=0}(t)\,f^{J*}_+(t) \\ &\qquad\cdot\left[(-1)^{J/2}\,\frac{(J-1)!!}{J!!}\right], \\ \mathrm{Im}_t A_2(\nu=0,t)^{2\pi} &= 0\,, \\ \mathrm{Im}_t A_3(\nu=0,t)^{2\pi} &= \frac{p_\pi}{\sqrt{t}}\,\frac{M^2}{t\,p_N^4}\sum_{J=2,4,\ldots}(p_\pi\,p_N)^J\,\sqrt{2J+1}\;F_{J\Lambda_\gamma=2}(t) \\ &\qquad\cdot\left[(-1)^{(J-2)/2}\sqrt{\frac{(J+1)J}{(J-1)(J+2)}}\,\frac{(J-1)!!}{J!!}\right] \\ &\quad\cdot\left\{f^{J*}_+(t)\,-\,f^{J*}_-(t)\,M\left[\frac{(J+2)(J-1)-2}{\sqrt{J(J+1)}}\right]\right\}, \end{aligned}$$

$$
\begin{aligned}
\mathrm{Im}_t A_4(\nu=0,t)^{2\pi} &= -\frac{p_\pi}{\sqrt{t}}\,\frac{M^3}{t\,p_N^4}\sum_{J=4,\ldots}(p_\pi\,p_N)^J\,\sqrt{2J+1}F_{J\Lambda_\gamma=2}(t)\,f_-^{J*}(t) \\
&\qquad\cdot\frac{(-1)^{(J-2)/2}\,2\,(J-2)(J+3)}{\sqrt{(J+2)(J-1)}}\,\frac{(J-1)!!}{J!!}\,, \\
\mathrm{Im}_t A_5(\nu=0,t)^{2\pi} &= -\frac{p_\pi}{\sqrt{t}}\,\frac{M}{t\,p_N^2}\sum_{J=2,4,\ldots}(p_\pi\,p_N)^J\,\sqrt{2J+1}\;F_{J\Lambda_\gamma=0}(t)\;f_-^{J*}(t) \\
&\qquad\cdot\left[\frac{(-1)^{(J-2)/2}}{\sqrt{J(J+1)}}\,\frac{(J+1)!!}{(J-2)!!}\right]\,, \\
\mathrm{Im}_t A_6(\nu=0,t)^{2\pi} &= -\frac{p_\pi}{\sqrt{t}}\,\frac{M}{t\,p_N^2} \qquad\qquad (B.12)\\
&\quad\cdot\sum_{J=2,4,\ldots}(p_\pi\,p_N)^J\,\sqrt{2J+1}\;F_{J\Lambda_\gamma=2}(t)\;f_-^{J*}(t) \\
&\qquad\cdot\left[\frac{(-1)^{(J-2)/2}\;[(J+2)(J-1)-2]}{\sqrt{(J+2)(J-1)}}\,\frac{(J-1)!!}{J!!}\right]\,.
\end{aligned}
$$

We note that the s-wave $(J=0)$ component of the 2π intermediate states contributes only to A_1. The amplitude A_2, corresponding to the exchange of pseudoscalar mesons (dominantly π^0) in the t channel, obtains no contribution from 2π states, because the 2π system cannot couple to the nucleon through a pseudoscalar operator. Furthermore, it is found that only waves with $J \geq 4$ contribute to the amplitude A_4. In our calculations we saturate the t-channel dispersion integral with s(J = 0)- and d($J=2$)-waves, for which the expressions of Eq.(B.13) reduce to those given in Eq.(3.66).

B.2 F_2-meson contribution to the $\gamma\gamma \to \pi\pi$ process

A spin-2 particle is described in terms of a symmetric and traceless field tensor, with five independent components, satisfying the Klein-Gordon equation. Therefore, a state of spin-2 is characterized by a symmetric and traceless polarization tensor $\varepsilon^{\mu\nu}(p,\Lambda)$ ($\Lambda = -2,-1,0,1,2$). For details, we refer to Ref. [Spe 91]. We will apply here this spin-2 formalism to describe the s-channel exchange of the f_2 meson in the process $\gamma\gamma \to \pi\pi$.

The coupling of the (isoscalar) $f_2(1270)$ meson (with momentum p and mass m_{f_2}) to a pion pair (with momenta p_π^μ, $p_\pi^{'\mu}$ and cartesian isospin indices a,b) is described by the amplitude

$$
\mathcal{M}(f_2 \to \pi\pi) = \frac{g_{f_2\pi\pi}}{m_{f_2}}\,\delta_{ab}\,p_\pi^{'\mu}\,p_\pi^\nu\,\varepsilon_{\mu\nu}(p,\Lambda)\,, \qquad (B.13)
$$

where the coupling constant $g_{f_2\pi\pi}$ is determined from the $f_2 \to \pi\pi$ decay width :

$$
\Gamma(f_2 \to \pi\pi) = \frac{1}{40\pi}\,g_{f_2\pi\pi}^2\,\frac{(p_\pi)^5}{m_{f_2}^4}\,, \qquad (B.14)
$$

with $p_\pi = \sqrt{m_{f_2}^2/4 - m_\pi^2}$ the pion three-momentum in the f_2 rest frame. Using the partial width $\Gamma(f_2 \to \pi\pi) = 0.846\,\Gamma_0$ and the total f_2-width $\Gamma_0 = 185$ MeV [PDG 98], Eq.(B.14) yields for the coupling : $g_{f_2\pi\pi} \simeq 23.64$.

The Lorentz structure of the vertex $f_2 \to \gamma\gamma$ is given by

$$\mathcal{M}(f_2 \to \gamma\gamma) = -i\,2e^2\,\frac{g_{f_2\gamma\gamma}}{m_{f_2}}\,\mathcal{F}^{\mu\delta}(q,\lambda_\gamma)\,\mathcal{F}_\delta{}^{\nu}(q',\lambda'_\gamma)\,\varepsilon_{\mu\nu}(p,\Lambda)\,, \tag{B.15}$$

where $\mathcal{F}^{\alpha\beta}$ is the electromagnetic field tensor. Using the vertex of Eq. (B.15), the $f_2 \to \gamma\gamma$ decay width is calculated as

$$\Gamma(f_2 \to \gamma\gamma) = \frac{e^4}{80\pi} g_{f_2\gamma\gamma}^2 m_{f_2}\,, \tag{B.16}$$

and the partial width $\Gamma(f_2 \to \gamma\gamma) = 1.32 \cdot 10^{-5}\,\Gamma_0$ [PDG 98], Eq.(B.16) determines the value of the coupling constant : $g_{f_2\gamma\gamma} \simeq 0.239$.

With these couplings and vertices, we can now calculate the invariant amplitude for the process $\gamma\gamma \to f_2 \to \pi\pi$:

$$\mathcal{M}(\gamma\gamma \xrightarrow{f_2} \pi\pi) = -i\,2e^2\,\frac{g_{f_2\gamma\gamma}}{m_{f_2}}\,\mathcal{F}^{\mu\delta}(q,\lambda_\gamma)\mathcal{F}_\delta{}^{\nu}(q',\lambda'_\gamma)\,\Delta_{\mu\nu\alpha\beta}(p,\Lambda)\,\frac{g_{f_2\pi\pi}}{m_{f_2}}\,p_\pi^\alpha\,p_\pi'^{\,\beta}\,, \tag{B.17}$$

where $\Delta_{\mu\nu\alpha\beta}(p,\Lambda)$ represents the spin-2 propagator (see Ref. [Spe 91]). To determine the $\gamma\gamma \to \pi\pi$ helicity amplitudes F_{Λ_γ} defined in Eq. (3.54), we shall evaluate Eq. (B.17) in the c.m. system. For the case of equal photon helicities ($\Lambda_\gamma = 0$), f_2 does not contribute, i.e. $F^{(f_2)}_{\Lambda_\gamma=0} = 0$. For the opposite photon helicities ($\Lambda_\gamma = 2$) we find after some algebra

$$F^{(f_2)}_{\Lambda_\gamma=2} = -\frac{e^2}{8}\,\frac{g_{f_2\gamma\gamma}\,g_{f_2\pi\pi}}{m_{f_2}^2}\,\frac{t^2\beta^2}{t - m_{f_2}^2 + i m_{f_2}\Gamma_0}\,\sin^2\theta_{\pi\pi}\,, \tag{B.18}$$

where $\theta_{\pi\pi}$ is the pion c.m. angle and β the pion velocity as in Eq. (3.54). It is immediately seen from Eq. (B.18) that the f_2 meson contribution to the d-wave is given by

$$F^{(f_2)}_{J=2\,\Lambda_\gamma=2}(t) = -\sqrt{\frac{2}{15}}\,\frac{e^2}{4}\,\frac{g_{f_2\gamma\gamma}\,g_{f_2\pi\pi}}{m_{f_2}^2}\,\frac{t^2\beta^2}{t - m_{f_2}^2 + i m_{f_2}\Gamma_0}\,. \tag{B.19}$$

Appendix C

C.1 $\Delta(1232)$ contribution to the negative-t dispersion integral

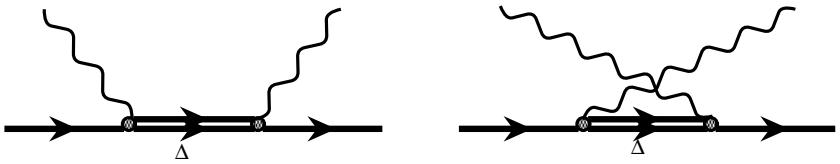

Figure C.1: The contribution of the $\Delta(1232)$ resonance to Compton scattering

For the $\gamma N\Delta$ vertex we will only take the magnetic coupling in the form,

$$\mathcal{M}^{M1}_{\gamma N\to\Delta} \;=\; -ie\,\varepsilon^{\mu}\,\bar{\Delta}^{\beta}(p_{\Delta})\,\Gamma^{M}_{\beta\mu}\,N(p)\,, \tag{C.1}$$

$$\begin{aligned}
A_1 \;=\;& -\frac{1}{4}\frac{e^2}{M^2}\frac{G_M^2}{(M+M_\Delta)^2}\left\{\frac{1}{s-M_\Delta^2+iM_\Delta\Gamma(s)}\right.\\
&\cdot\;\left[2s(M+M_\Delta)+\frac{1}{2}M_\Delta(s-M^2)+3s\nu\right]\\
&\left.+\frac{1}{u-M_\Delta^2+iM_\Delta\Gamma(s)}\left[2u(M+M_\Delta)+\frac{1}{2}M_\Delta(u-M^2)-3u\nu\right]\right\}\,,\\
A_2 \;=\;& \frac{1}{4}\frac{e^2}{M^2}\frac{G_M^2}{(M+M_\Delta)^2}\left\{\frac{1}{s-M_\Delta^2+iM_\Delta\Gamma(s)}\left[s(M-3\nu)+\frac{1}{2}M_\Delta(s+M^2)\right]\right.\\
&\left.+\frac{1}{u-M_\Delta^2+iM_\Delta\Gamma(u)}\left[u(M+3\nu)+\frac{1}{2}M_\Delta(u+M^2)\right]\right\}\,,\\
A_3 \;=\;& \frac{e^2}{M^2}\frac{G_M^2}{(M+M_\Delta)^2}\left\{M^3\left(1+\frac{3M_\Delta}{4M}\right)\right.\\
&\left.\left[\frac{1}{s-M_\Delta^2+iM_\Delta\Gamma(s)}+\frac{1}{u-M_\Delta^2+iM_\Delta\Gamma(u)}\right]\right.
\end{aligned}$$

$$+\frac{M^2[t-M(M+M_\Delta)]\left(M+iM_\Delta\frac{\Gamma(s)-\Gamma(u)}{4\nu}\right)}{\left[s-M_\Delta^2+iM_\Delta\Gamma(s)\right]\left[u-M_\Delta^2+iM_\Delta\Gamma(u)\right]}\Bigg\}\,,$$

$$A_4 = \frac{e^2}{M^2}\frac{G_M^2}{(M+M_\Delta)^2}\Bigg\{\frac{M^3}{4}\left[\frac{1}{s-M_\Delta^2+iM_\Delta\Gamma(s)}+\frac{1}{u-M_\Delta^2+iM_\Delta\Gamma(u)}\right] + \frac{M^2[t-M(M+M_\Delta)]\left(M+iM_\Delta\frac{\Gamma(s)-\Gamma(u)}{4\nu}\right)}{\left[s-M_\Delta^2+iM_\Delta\Gamma(s)\right]\left[u-M_\Delta^2+iM_\Delta\Gamma(u)\right]}\Bigg\}\,,$$

$$A_5 = \frac{e^2}{M^2}\frac{G_M^2}{(M+M_\Delta)^2}\Bigg\{\frac{1}{4}\left(M^2M_\Delta+2M[M^2-\frac{3t}{4}]\right)\cdot\left[\frac{1}{s-M_\Delta^2+iM_\Delta\Gamma(s)}+\frac{1}{u-M_\Delta^2+iM_\Delta\Gamma(u)}\right] + \frac{\left[\left(M^2-\frac{3t}{4}\right)\left(\frac{t}{2}-M^2\right)-MM_\Delta\left(M^2-\frac{t}{4}\right)\right]\left(M+iM_\Delta\frac{\Gamma(s)-\Gamma(u)}{4\nu}\right)}{\left[s-M_\Delta^2+iM_\Delta\Gamma(s)\right]\left[u-M_\Delta^2+iM_\Delta\Gamma(u)\right]}\Bigg\}\,,$$

$$A_6 = -\frac{e^2}{M^2}\frac{G_M^2}{(M+M_\Delta)^2}\Bigg\{\frac{1}{4}\left(M^2M_\Delta+2M[M^2-\frac{t}{4}]\right)\cdot\left[\frac{1}{s-M_\Delta^2+iM_\Delta\Gamma(s)}+\frac{1}{u-M_\Delta^2+iM_\Delta\Gamma(u)}\right] - \frac{\left[\left(M^2-\frac{t}{4}\right)(M^2-t)+MM_\Delta\left(M^2-\frac{t}{4}\right)-2M^2\nu^2\right]\left(M+iM_\Delta\frac{\Gamma(s)-\Gamma(u)}{4\nu}\right)}{\left[s-M_\Delta^2+iM_\Delta\Gamma(s)\right]\left[u-M_\Delta^2+iM_\Delta\Gamma(u)\right]}\Bigg\}\,, \tag{C.2}$$

where the energy dependence of the width of the $\Delta(1232)$ is given by

$$\Gamma(s) = \Gamma(M_\Delta^2)\frac{M_\Delta}{\sqrt{s}}\frac{p_\pi^3(s)}{p_\pi^3(M_\Delta^2)}\left[\frac{1+p_\pi^2(M_\Delta^2)R^2}{1+p_\pi^2(s)R^2}\right]\,, \tag{C.3}$$

with the width at the resonance position $\Gamma_{\Delta\to\gamma N}(M_\Delta^2)\approx(0.55\%)\cdot\Gamma_0 = 0.55\cdot10^{-3}\cdot 120 = 0.66$ MeV. The parameter R has the dimension of length and is taken equal to $R = 1$ fm. The pion three-momentum is given by

$$p_\pi^2(s) = \frac{[s-(M+m_\pi)^2][s-(M-m_\pi)^2]}{4s}\,. \tag{C.4}$$

Appendix D

D.1 Relations between the sets of invariant amplitudes

$$
\begin{aligned}
B_1 &= \frac{t+Q^2}{2}F_1 + \left[2(t+Q^2)P'^2 - 4M^2\nu^2\right]F_2 \\
&- 2M\nu^2\left[Q^2F_3 + 4MF_4 + 2F_{10}\right] \\
&+ 2(t+Q^2)\left[P'^2 - M^2\right]\left\{2F_6 - \frac{Q^2}{t}(F_9 - F_{12})\right\}, \\
B_2 &= 8(M^2 - t/4)\nu F_4 + 4M\nu F_{10} - \frac{8M^2\nu t}{t+Q^2}\left[2F_6 - \frac{Q^2}{t}(F_9 - F_{12})\right], \\
B_3 &= \frac{t+Q^2}{2}F_1 - 4M^2\nu^2F_2 - 2M\nu^2\left[Q^2F_3 + 2F_{10}\right], \\
B_4 &= 4M\nu F_{10}, \\
B_5 &= \frac{(t+Q^2)^2}{4t}(P'^2)^2\left[(t+Q^2)F_9 - Q^2F_{12}\right] \\
B_6 &= -4M\nu^2F_4 - M(t+Q^2)P'^2\left[2F_6 - \frac{Q^2}{t}(F_9 - F_{12})\right] \\
B_7 &= M\nu^2(t+Q^2)P'^2\left\{M\frac{t+Q^2}{t}F_4 + \frac{Q^2}{4}F_8 + F_{10}\right\} \\
&- M\frac{(t+Q^2)^2}{8t}P'^2\left\{Q^2F_5 + 4(t+Q^2)F_{11}\right\} \\
&- M^2P'^2\left[\nu^2 + \frac{(t+Q^2)^2}{4t}\right]\left\{2(t+Q^2)F_6 + Q^2F_{12}\right\}, \\
B_8 &= 4M\nu^2\frac{Q^2}{t}P'^2F_4 - \frac{t+Q^2}{2}P'^2\left[\frac{Q^2}{t}(F_5 + 4F_{11}) - F_7\right] \\
&- MQ^2\frac{t+Q^2}{t}P'^2\left[2F_6 - \frac{Q^2}{t}F_9 + F_{12}\right], \\
B_9 &= M\nu(t+Q^2)P'^2F_2 + \nu\frac{(t+Q^2)^2}{4}P'^2F_3 \\
&- 4M^3\nu^3F_4 + M^2\nu\frac{t+Q^2}{4}[F_5 + F_7 + 4F_{11}] + M\nu P'^2[2F_6 + F_9] \\
&- \nu\frac{(t+Q^2)^2}{8t}(P'^2 - M^2)\left[(t+Q^2)F_8 + 4F_{10}\right]
\end{aligned}
$$

$$
\begin{aligned}
&+ \quad M\nu\frac{(t+Q^2)^2}{2t}[P'^2-M^2]\left\{2F_6 - F_9 - \frac{t-Q^2}{t+Q^2}F_{12}\right\},\\
B_{10} &= 4M\nu^2(M^2-t/4)F_4 - (M^2-t/4)\frac{t+Q^2}{4}[F_5 + F_7 + 4F_{11}]\\
&- \quad M(t+Q^2)P'^2\,[2F_6 + F_9] + \frac{M^2\nu^2}{2}\left[(t+Q^2)F_8 + 4F_{10}\right]\\
&- \quad 2M^3\nu^2\left\{2F_6 - F_9 - \frac{t-Q^2}{t+Q^2}F_{12}\right\},\\
B_{11} &= M\nu\frac{(t+Q^2)^3}{8t}P'^2\left\{2F_6 - F_9 - \frac{t-Q^2}{t+Q^2}F_{12}\right\}\\
&+ \quad \frac{(t+Q^2)^3}{32t}P'^2\left[Q^2F_8 + 4F_{10}\right],\\
B_{12} &= -4M^2\nu^3F_4 + M\nu\frac{t+Q^2}{4}[F_5 + F_7 + 4F_{11}]\\
&+ \quad M\frac{(t+Q^2)^2}{8t}\left[(t+Q^2)F_8 + 4F_{10}\right]\\
&- \quad M^2\nu\frac{(t+Q^2)^2}{2t}\left\{2F_6 - F_9 - \frac{t-Q^2}{t+Q^2}F_{12}\right\}. \qquad \text{(D.1)}
\end{aligned}
$$

For the inverted relations, we found following expressions:

$$
\begin{aligned}
F_1 &= \frac{2}{(t+Q^2)^3P'^2}\Big\{2M^2\nu^2(t-Q^2)\Big[B_1-B_3+\nu(B_2-B_4)\Big]\\
&\qquad + (t+Q^2)^2P'^2\Big[B_3+\nu B_4\Big] - \frac{M}{P'^2}\nu^2t(t-Q^2)B_6\\
&\qquad + 8M\nu Q^2\left[B_9+\nu B_{10}-\frac{t}{4M}B_{12}\right]\Big\},\\
F_2 &= \frac{1}{2(t+Q^2)P'^2}\left\{\Big[B_1-B_3+\nu(B_2-B_4)\Big]-\frac{t}{2MP'^2}B_6\right\},\\
F_3 &= \frac{1}{(t+Q^2)^2P'^2}\Big\{-2M\Big[B_1-B_3+\nu(B_2-B_4)\Big] + \frac{t}{P'^2}B_6\\
&\qquad + \frac{4}{\nu}\left[B_9+\nu B_{10}-\frac{t}{4M}B_{12}\right]\Big\},\\
F_4 &= \frac{1}{8\nu P'^2}\Big[B_2-B_4\Big]-\frac{Mt}{(t+Q^2)^2P'^4}B_6,\\
F_5 &= \frac{2}{(t+Q^2)P'^2}\Big\{M\nu\left[1-\frac{2\nu^2(t-Q^2)}{(t+Q^2)^2}\right]\Big[B_2-B_4\Big]-\frac{\nu}{M}P'^2B_4\\
&\qquad - \frac{4M}{(t+Q^2)P'^2}\left[1+\frac{4\nu^2Q^2}{(t+Q^2)^2}\right]B_5\\
&\qquad - \left[1-\frac{4M^2-t}{2P'^2}\left(1-\frac{2\nu^2(t-Q^2)}{(t+Q^2)^2}\right)\right]B_6\\
&\qquad + \frac{4}{M(t+Q^2)}B_7-B_8-2\left[1+\frac{4\nu^2Q^2}{(t+Q^2)^2}\right]B_{10}
\end{aligned}
$$

$$
\begin{aligned}
& + \frac{32\nu Q^2}{(t+Q^2)^3}B_{11} + \frac{8\nu(t-Q^2)}{M(t+Q^2)^2}\left[M^2 + \frac{tQ^2}{4(t-Q^2)}\right]B_{12}\Bigg\}\,,\\
F_6 &= \frac{1}{(t+Q^2)^3P'^2}\Bigg\{-\frac{\nu}{4}(t^2+tQ^2+2Q^4)\Big[B_2-B_4\Big] + \frac{Q^2(t+Q^2)^2P'^2}{8M^2\nu}B_4\\
& + \frac{4Q^2}{P'^2}B_5 - \Big(M^2-\frac{t}{4}\Big)\frac{t^2+tQ^2+2Q^4}{2MP'^2}B_6\\
& + \frac{Q^4}{M}B_{10} - \frac{4Q^2}{M\nu}B_{11} + \frac{Q^4}{M^2\nu}\Big(M^2-\frac{t}{4}\Big)B_{12}\Bigg\}\,,\\
F_7 &= \frac{1}{(t+Q^2)^2P'^2}\Bigg\{2M\nu Q^2\Big[B_2-B_4\Big] - \frac{8M}{P'^2}B_5 + \frac{Q^2}{P'^2}\Big((4M^2-t)-2P'^2\Big)B_6\\
& + 2tB_8 - 4Q^2B_{10} + \frac{16M\nu tQ^2}{(t+Q^2)^2}B_{12}\Bigg\}\,,\\
F_8 &= \frac{2}{(t+Q^2)^2P'^2}\Bigg\{-2M\nu\Big[B_2-B_4\Big] + \frac{16M}{(t+Q^2)P'^2}B_5 - \frac{1}{P'^2}(4M^2-t)B_6\\
& + 4B_{10} - \frac{16}{\nu(t+Q^2)}B_{11} + \frac{4M^2-t}{M\nu}B_{12}\Bigg\}\,,\\
F_9 &= \frac{1}{(t+Q^2)^3P'^2}\Bigg\{-\frac{\nu}{2}Q^2(t-Q^2)\Big[B_2-B_4\Big] - \frac{Q^2}{4M^2\nu}(t+Q^2)^2P'^2B_4\\
& + \frac{4}{P'^2}(t-Q^2)B_5 - \frac{Q^2}{MP'^2}\Big(M^2-\frac{t}{4}\Big)(t-Q^2)B_6\\
& - \frac{2Q^4}{M}B_{10} + \frac{8Q^2}{M\nu}B_{11} - \frac{2Q^4}{M^2\nu}\Big(M^2-\frac{t}{4}\Big)B_{12}\Bigg\}\,,\\
F_{10} &= \frac{1}{4M\nu}B_4\,,\\
F_{11} &= \frac{1}{(t+Q^2)^2P'^2}\Bigg\{\frac{M\nu}{2}\left[t+\frac{2\nu^2(t-Q^2)}{t+Q^2}\right]\Big[B_2-B_4\Big] + \frac{\nu}{2M}(t+Q^2)P'^2B_4\\
& + \frac{1}{P'^2}\left[\Big(M^2-\frac{t}{4}\Big)\left(t+\frac{2\nu^2(t-Q^2)}{t+Q^2}\right) - \frac{tP'^2}{2}\right]B_6\\
& + \frac{8M\nu^2Q^2}{(t+Q^2)^2P'^2}B_5 - \frac{2}{M}B_7 + \frac{Q^2}{2}B_8 + Q^2\left[1+\frac{4\nu^2}{t+Q^2}\right]B_{10}\\
& - \frac{16\nu Q^2}{(t+Q^2)^2}B_{11} + \frac{4M\nu Q^2}{t+Q^2}\left[\frac{Q^2}{t+Q^2}-\frac{t}{4M^2}\right]B_{12}\Bigg\}\,,\\
F_{12} &= \frac{1}{(t+Q^2)^2P'^2}\Bigg\{-\frac{\nu}{2}(t-Q^2)\Big[B_2-B_4\Big] - \frac{1}{4M^2\nu}(t+Q^2)^2P'^2B_4\\
& - \frac{4}{P'^2}B_5 - \frac{1}{MP'^2}\Big(M^2-\frac{t}{4}\Big)(t-Q^2)B_6\\
& - \frac{2Q^2}{M}B_{10} + \frac{8}{M\nu}B_{11} - \frac{2Q^2}{M^2\nu}\Big(M^2-\frac{t}{4}\Big)B_{12}\Bigg\}\,. \qquad \text{(D.2)}
\end{aligned}
$$

Appendix E

E.1 Born contribution

The Born amplitude is given by:

$$\begin{aligned} H^{\mu\nu}_{Born} &= \bar{u}'(p')\left\{\left(\gamma^\nu - i\kappa_p\sigma^{\nu\alpha}\frac{q'_\alpha}{2M}\right)\frac{1}{\not p' + \not q' - M}\left(F_1(Q^2)\gamma^\mu + iF_2(Q^2)\sigma^{\mu\beta}\frac{q_\beta}{2M}\right)\right. \\ &+ \left.\left(F_1(Q^2)\gamma^\mu + iF_2(Q^2)\sigma^{\mu\beta}\frac{q_\beta}{2M}\right)\frac{1}{\not p - \not q' - M}\left(\gamma^\nu - i\kappa_p\sigma^{\nu\alpha}\frac{q'_\alpha}{2M}\right)\right\} \end{aligned} \tag{E.1}$$

Following our strategy, we first project the Born tensor onto the basis of Berg and Lindner:

$$\begin{aligned} B_1^{Born} &= \frac{2Q^2}{t+Q^2}\frac{F_2(Q^2)}{M} - \frac{2M(t+Q^2)}{(s-M^2)(u-M^2)}F_1(Q^2) \\ B_2^{Born} &= -\frac{4M\nu}{(s-M^2)(u-M^2)}\left[F_1(Q^2) - \frac{2Q^2}{t+Q^2}\left(F_1(Q^2)+F_2(Q^2)\right)\right] \\ B_3^{Born} &= \frac{1}{M}\left[\kappa_p F_1(Q^2) + (1+\kappa_p)F_2(Q^2)\right] \\ B_4^{Born} &= (1+\kappa_p)(F_1(Q^2)+F_2(Q^2))\frac{4M\nu}{(s-M^2)(u-M^2)} \\ B_5^{Born} &= -\frac{\kappa_p F_1(Q^2) - F_2(Q^2)}{2M}\frac{(t+Q^2)^3(P'^2)^2}{4t(s-M^2)(u-M^2)} \\ B_6^{Born} &= \frac{(t+Q^2)P'^2}{(s-M^2)(u-M^2)}\left[\frac{t+Q^2}{2t}\left(\kappa_p F_1(Q^2) - F_2(Q^2)\right) - F_1(Q^2) - F_2(Q^2)\right] \\ &- P'^2\frac{\kappa_p F_2(Q^2)}{2M^2} \\ B_7^{Born} &= -P'^2\frac{t+Q^2}{8M}\left\{\frac{M^2(t+Q^2)^2}{t(s-M^2)(u-M^2)}\left[(2+\kappa_p)F_1(Q^2)+F_2(Q^2)\right]\right. \\ &\left. + \kappa_p F_1(Q^2) + F_2(Q^2) + \kappa_p F_2(Q^2)\left(1-\frac{Q^2}{t}\right)\right\} \\ B_8^{Born} &= P'^2\left\{\frac{Q^2}{2t}\left[\frac{\kappa_p F_2(Q^2)}{M^2} + \frac{t+Q^2}{(s-M^2)(u-M^2)}\left((2+\kappa_p)F_1(Q^2)+F_2(Q^2)\right)\right]\right. \end{aligned}$$

$$- \frac{1}{2}\frac{t+Q^2}{(s-M^2)(u-M^2)}\left[\kappa_p F_1(Q^2) - F_2(Q^2)\right]\Bigg\}$$

$$B_9^{Born} = \nu F_2(Q^2)\left[\frac{1}{2} + \frac{(t+Q^2)P'^2}{(s-M^2)(u-M^2)}\right]$$

$$B_{10}^{Born} = \frac{t+Q^2}{(s-M^2)(u-M^2)}\left[\frac{2M^2\nu^2}{t+Q^2}F_2(Q^2) - P'^2\left(F_1(Q^2)+F_2(Q^2)\right)\right]$$

$$B_{11}^{Born} = \nu(1+\kappa_p)F_2(Q^2)\frac{(t+Q^2)^3P'^2}{8t(s-M^2)(u-M^2)}$$

$$B_{12}^{Born} = \frac{\nu}{2M}\left[(1+\kappa_p)F_2(Q^2)\frac{M^2(t+Q^2)^2}{t(s-M^2)(u-M^2)} - \kappa_p F_2(Q^2)\right]$$

Combining now these expressions into amplitudes F_i, we obtain:

$$F_1^B = \frac{1}{M_N(s-M_N^2)(u-M_N^2)}\left\{\frac{t+Q^2}{2}\left[\kappa F_1(Q^2)+(1+\kappa)F_2(Q^2)\right] - \nu^2\kappa F_2(Q^2)\right\}$$

$$F_2^B = -\frac{1}{M_N(s-M_N^2)(u-M_N^2)}\left[F_1(Q^2) + \frac{t+Q^2}{8M_N^2}\kappa F_2(Q^2)\right]$$

$$F_3^B = 0$$

$$F_4^B = \frac{1}{2M_N(s-M_N^2)(u-M_N^2)}\kappa F_2(Q^2)$$

$$F_5^B = \frac{1}{M_N^2(s-M_N^2)(u-M_N^2)}\left\{-\frac{t+Q^2}{4}\left[\kappa F_1(Q^2)+(1+2\kappa)F_2(Q^2)\right] + \nu^2\kappa F_2(Q^2)\right\}$$

$$F_6^B = \frac{1}{4M_N(s-M_N^2)(u-M_N^2)}\left[(2+\kappa)F_1(Q^2) + \kappa F_2(Q^2) + \frac{t}{4M_N^2}\kappa F_2(Q^2)\right]$$

$$F_7^B = 0$$

$$F_8^B = 0$$

$$F_9^B = \frac{1}{2M_N(s-M_N^2)(u-M_N^2)}\left[-\kappa F_1(Q^2) + \kappa F_2(Q^2) + \frac{Q^2}{4M_N^2}\kappa F_2(Q^2)\right]$$

$$F_{10}^B = \frac{1}{(s-M_N^2)(u-M_N^2)}(1+\kappa)\left[F_1(Q^2) + F_2(Q^2)\right]$$

$$F_{11}^B = \frac{1}{4M_N^2(s-M_N^2)(u-M_N^2)}\left\{\frac{t+Q^2}{4}\left[\kappa F_1(Q^2)+F_2(Q^2)\right] - \nu^2\kappa F_2(Q^2)\right\}$$

$$F_{12}^B = \frac{t+Q^2}{8M_N^3(s-M_N^2)(u-M_N^2)}\kappa F_2(Q^2) \qquad \text{(E.2)}$$

As a cross check, we compared these formulas with the results obtained by Tarrach [Tar 75] and found a complete agreement.

Appendix F

F.1 s-channel helicity amplitudes

We group the 12 independent helicity amplitudes according to whether the initial photon has longitudinal or transverse polarization, and according to whether both nucleons have the same or opposite helicities.

F.1.1 $T^s_{\lambda'=\pm1\,\lambda'_N=\frac{1}{2}\,,\,\lambda=\pm1\,\lambda_N=\frac{1}{2}}$

The s-channel helicity amplitudes for the case of transverse polarization of the initial photon and when both nucleons have the same helicities, are given by :

$$
\begin{aligned}
&T^s_{\lambda'=\pm1\,\lambda'_N=\frac{1}{2}\,,\,\lambda=\pm1\,\lambda_N=\frac{1}{2}} = \sqrt{E+M}\,\sqrt{E'+M}\,\frac{1}{2}\cos(\theta/2)\\
&\times\Big\{ F_1\left[p^t_1 + p^t_{1,\lambda\lambda'}\,\lambda\lambda'\right] + F_2\left[p^t_2 + p^t_{2,\lambda\lambda'}\,\lambda\lambda'\right] + F_3\,\nu Q^2\left[p^t_3 + p^t_{3,\lambda\lambda'}\,\lambda\lambda'\right]\\
&+F_4\,\nu\left[p^t_{4,\lambda}\,(\lambda+\lambda') + p^t_{4,\lambda\lambda'}\,\lambda\lambda'\right] + F_5\,Q^2\left[p^t_{5,\lambda}\,\lambda + p^t_{5,\lambda'}\,\lambda' + p^t_{5,\lambda\lambda'}\,\lambda\lambda'\right]\\
&+F_6\left[p^t_{6,\lambda}\,\lambda + p^t_{6,\lambda'}\,\lambda' + p^t_{6,\lambda\lambda'}\,\lambda\lambda'\right] + F_7\left[p^t_{7,\lambda}\,\lambda + p^t_{7,\lambda'}\,\lambda' + p^t_{7,\lambda\lambda'}\,\lambda\lambda'\right]\\
&+F_8\,\nu Q^2\left[p^t_{8,\lambda}\,\lambda + p^t_{8,\lambda'}\,\lambda' + p^t_{8,\lambda\lambda'}\,\lambda\lambda'\right] + F_9\left[p^t_{9,\lambda}\,\lambda + p^t_{9,\lambda'}\,\lambda' + p^t_{9,\lambda\lambda'}\,\lambda\lambda'\right]\\
&+F_{10}\,\nu\left[p^t_{10} + p^t_{10,\lambda}\,\lambda + p^t_{10,\lambda'}\,\lambda' + p^t_{10,\lambda\lambda'}\,\lambda\lambda'\right]\\
&+F_{11}\left[p^t_{11,\lambda}\,\lambda + p^t_{11,\lambda'}\,\lambda' + p^t_{11,\lambda\lambda'}\,\lambda\lambda'\right]\\
&+F_{12}\,Q^2\left[p^t_{12,\lambda}\,\lambda + p^t_{12,\lambda'}\,\lambda' + p^t_{12,\lambda\lambda'}\,\lambda\lambda'\right]\Big\}\,, \qquad \text{(F.1)}
\end{aligned}
$$

where the kinematical factors which appear for the different combinations of photon polarizations in Eq. (F.1) are given by :

$$
\begin{aligned}
p^t_1 &= -C_1\,|\vec{q}\,'|\,(q_0 - |\vec{q}|\cos\theta)\,,\\
p^t_{1,\lambda\lambda'} &= -C_1\,|\vec{q}\,'|\,(q_0\cos\theta - |\vec{q}|)\,,\\
p^t_2 &= -C_1\,(2M\nu)^2\,,\\
p^t_{2,\lambda\lambda'} &= -C_1\left\{(2M\nu)^2\cos\theta + |\vec{q}\,||\vec{q}\,'|\sin^2\theta\left[(4M\nu) + |\vec{q}\,'|(q_0 - |\vec{q}|\cos\theta)\right]\right\}\,,\\
p^t_3 &= -C_1\,(2M\nu)\,,\\
p^t_{3,\lambda\lambda'} &= -C_1\left\{2M\nu\cos\theta + |\vec{q}\,||\vec{q}\,'|\sin^2\theta\right\}\,,
\end{aligned}
$$

$$
\begin{aligned}
p^t_{4,\lambda} &= -\left\{C_2\left(q_0+|\vec{q}\,'|\right) + C_3\left(|\vec{q}|+|\vec{q}\,'|\right)\right\}(2M\nu)\,,\\
p^t_{4,\lambda\lambda'} &= \left\{C_2\left(q_0+|\vec{q}\,'|\right)+C_3\left(|\vec{q}|+|\vec{q}\,'|\right)\right\}\left\{|\vec{q}||\vec{q}\,'|\sin^2\theta-(2M\nu)\,(1-\cos\theta)\right\}\,,\\
p^t_{5,\lambda} &= 1/4\left\{C_2\left(q_0+|\vec{q}\,'|\right)+C_3\left(|\vec{q}|-|\vec{q}\,'|+2|\vec{q}\,'|\cos\theta\right)\right\}\,,\\
p^t_{5,\lambda'} &= 1/4\left\{C_2\left(q_0+|\vec{q}\,'|\right)+C_3\left(|\vec{q}|+|\vec{q}\,'|\right)\right\}\,,\\
p^t_{5,\lambda\lambda'} &= 1/4\left\{C_2\left(q_0+|\vec{q}\,'|\right)-C_3\left(|\vec{q}\,'|-|\vec{q}|\right)\right\}(1-\cos\theta)\,,\\
p^t_{6,\lambda} &= |\vec{q}\,'|(2M)\left\{C_1\nu\left[(-|\vec{q}|+|\vec{q}\,'|)(1-\cos\theta)+2(q_0-|\vec{q}|\cos\theta)\right]\right.\\
&\qquad +C_3\left[(2M\nu)(1-\cos\theta)\right.\\
&\qquad\quad -(q_0-|\vec{q}|\cos\theta)(|\vec{q}|-|\vec{q}\,'|+2|\vec{q}\,'|\cos\theta)\big]\\
&\qquad \left.-C_2\,(q_0-|\vec{q}|\cos\theta)(q_0+|\vec{q}\,'|)-C_4\nu\,(q_0+|\vec{q}\,'|)(1-\cos\theta)\right\}\,,\\
p^t_{6,\lambda'} &= (2M)\left\{C_1\nu\left[|\vec{q}|(|\vec{q}|-|\vec{q}\,'|)(1-\cos\theta)+2|\vec{q}\,'|(q_0-|\vec{q}|\cos\theta)\right]\right.\\
&\qquad +C_3\left[|\vec{q}|(2M\nu)(1-\cos\theta)\right.\\
&\qquad\quad \left.+|\vec{q}\,'|(q_0-|\vec{q}|\cos\theta)(|\vec{q}|-|\vec{q}\,'|-2|\vec{q}|\cos\theta)\right]\\
&\qquad -C_2\,|\vec{q}\,'|(q_0-|\vec{q}|\cos\theta)(q_0+|\vec{q}\,'|)\\
&\qquad \left.+C_4\nu|\vec{q}|(q_0+|\vec{q}\,'|)(1-\cos\theta)\right\}\,,\\
p^t_{6,\lambda\lambda'} &= C_1\left\{2M\nu\left[\left(|\vec{q}|-|\vec{q}\,'|\right)^2+2|\vec{q}\,'|(q_0+|\vec{q}|)\right](1-\cos\theta)\right.\\
&\qquad \left.-2|\vec{q}||\vec{q}\,'|\sin^2\theta\,2|\vec{q}\,'|\sqrt{s}\right\}\\
&- C_2\,(2M)|\vec{q}\,'|(q_0-|\vec{q}|\cos\theta)(q_0+|\vec{q}\,'|)(1-\cos\theta)\\
&+ C_3\,(2M)|\vec{q}\,'|2\sqrt{s}(|\vec{q}|+|\vec{q}\,'|)(1-\cos\theta)\\
&+ C_4\,(2M\nu)(q_0+|\vec{q}\,'|)(|\vec{q}|-|\vec{q}\,'|)(1-\cos\theta)\,,\\
p^t_{7,\lambda} &= -C_3\,|\vec{q}\,'|^2\sqrt{s}(1-\cos\theta)\,,\\
p^t_{7,\lambda'} &= C_3\,|\vec{q}||\vec{q}\,'|\sqrt{s}(1-\cos\theta)\,,\\
p^t_{7,\lambda\lambda'} &= C_3\,(|\vec{q}|-|\vec{q}\,'|)|\vec{q}\,'|\sqrt{s}(1-\cos\theta)\,,\\
p^t_{8,\lambda} &= 1/4|\vec{q}\,'|\left\{-C_1\left[(-|\vec{q}|+|\vec{q}\,'|)(1-\cos\theta)+2(q_0-|\vec{q}|\cos\theta)\right]\right.\\
&\qquad \left.-\left[C_3\,(2M)-C_4\,(q_0+|\vec{q}\,'|)\right](1-\cos\theta)\right\}\,,\\
p^t_{8,\lambda'} &= 1/4\left\{-C_1\left[|\vec{q}|(|\vec{q}|-|\vec{q}\,'|)(1-\cos\theta)+2|\vec{q}\,'|(q_0-|\vec{q}|\cos\theta)\right]\right.\\
&\qquad \left.+|\vec{q}|\left[C_3\,(2M)-C_4\,(q_0+|\vec{q}\,'|)\right](1-\cos\theta)\right\}\,,\\
p^t_{8,\lambda\lambda'} &= 1/4\left\{-C_1\left[\left((|\vec{q}|-|\vec{q}\,'|)^2+2|\vec{q}\,'|(q_0+|\vec{q}|)\right)(1-\cos\theta)\right]\right.\\
&\qquad \left.+(|\vec{q}|-|\vec{q}\,'|)\left[C_3\,(2M)-C_4\,(q_0+|\vec{q}\,'|)\right](1-\cos\theta)\right\}\,,\\
p^t_{9,\lambda} &= |\vec{q}\,'|^2\sqrt{s}(1-\cos\theta)\left\{C_1(|\vec{q}|-|\vec{q}\,'|)-C_3(2M)+C_4(q_0+|\vec{q}\,'|)\right\}\,,\\
p^t_{9,\lambda'} &= |\vec{q}||\vec{q}\,'|\sqrt{s}(1-\cos\theta)\left\{C_1(|\vec{q}|-|\vec{q}\,'|)+C_3(2M)+C_4(q_0+|\vec{q}\,'|)\right\}\,,\\
p^t_{9,\lambda\lambda'} &= |\vec{q}\,'|\sqrt{s}(1-\cos\theta)\left\{C_1(|\vec{q}|^2-|\vec{q}\,'|^2)+C_3(2M)(|\vec{q}|-|\vec{q}\,'|)\right.\\
&+ \left.C_4(q_0+|\vec{q}\,'|)(|\vec{q}|+|\vec{q}\,'|)\right\}\,,\\
p^t_{10} &= (2M)\left\{-C_1(2\nu)+C_2(q_0+|\vec{q}\,'|)+C_3(|\vec{q}\,'|+|\vec{q}|)\right\}\,,\\
p^t_{10,\lambda} &= |\vec{q}\,'|\left\{-C_1\left[(|\vec{q}\,'|-|\vec{q}|)(1-\cos\theta)+2(q_0-|\vec{q}|\cos\theta)\right]\right.\\
&\qquad \left.+\left[C_3(2M)+C_4(q_0+|\vec{q}\,'|)\right](1-\cos\theta)\right\}\,,\\
p^t_{10,\lambda'} &= -C_1\left\{(|\vec{q}|-|\vec{q}\,'|)|\vec{q}|(1-\cos\theta)+2|\vec{q}\,'|(q_0-|\vec{q}|\cos\theta)\right\}
\end{aligned}
$$

$$
\begin{aligned}
& + \left\{C_3(2M) - C_4(q_0 + |\vec{q}\,'|)\right\} |\vec{q}\,| (1 - \cos\theta)\,, \\
p^t_{10,\lambda\lambda'} &= -C_1 \left\{ 4M\nu\cos\theta + 2|\vec{q}\,||\vec{q}\,'|\sin^2\theta \right. \\
& \qquad \left. + \left[(|\vec{q}\,'| - |\vec{q}\,|)^2 + 2|\vec{q}\,'|(q_0 + |\vec{q}\,|) \right] (1 - \cos\theta) \right\} \\
& + C_2\,(2M)(q_0 + |\vec{q}\,'|)\cos\theta + C_3(2M)(|\vec{q}\,| + |\vec{q}\,'|) \\
& - C_4(q_0 + |\vec{q}\,'|)(|\vec{q}\,| - |\vec{q}\,'|)(1 - \cos\theta)\,, \\
p^t_{11,\lambda} &= 2|\vec{q}\,'| \left\{ -C_2\,(q_0 - |\vec{q}\,|\cos\theta)(q_0 + |\vec{q}\,'|) \right. \\
& \qquad \left. + C_3 \left[2M\nu(1 - \cos\theta) - (q_0 - |\vec{q}\,|\cos\theta)(|\vec{q}\,| + |\vec{q}\,'|\cos\theta) \right] \right\}, \\
p^t_{11,\lambda'} &= 2 \left\{ -C_2\,|\vec{q}\,'|(q_0 - |\vec{q}\,|\cos\theta)(q_0 + |\vec{q}\,'|) \right. \\
& \qquad \left. + C_3 \left[2M\nu|\vec{q}\,|(1 - \cos\theta) - |\vec{q}\,'|(q_0 - |\vec{q}\,|\cos\theta)(|\vec{q}\,'| + |\vec{q}\,|\cos\theta) \right] \right\}, \\
p^t_{11,\lambda\lambda'} &= 2 \left\{ -C_2 \left[(q_0 + |\vec{q}\,'|)|\vec{q}\,||\vec{q}\,'|\sin^2\theta + |\vec{q}\,'|(q_0 - |\vec{q}\,|\cos\theta)(q_0 + |\vec{q}\,'|)(1 - \cos\theta) \right] \right. \\
& \qquad \left. + C_3\,(|\vec{q}\,| + |\vec{q}\,'|) \left[2M\nu(1 - \cos\theta) - |\vec{q}\,||\vec{q}\,'|\sin^2\theta \right] \right\}, \\
p^t_{12,\lambda} &= 1/4 \left\{ C_1 \left[-4M\nu + |\vec{q}\,'|(|\vec{q}\,| - |\vec{q}\,'|)(1 - \cos\theta) \right] + C_2\,(2M)(q_0 + |\vec{q}\,'|) \right. \\
& \qquad + C_3\,(2M) \left[-2|\vec{q}\,'|(1 - \cos\theta) + (|\vec{q}\,| + |\vec{q}\,'|\cos\theta) \right] \\
& \qquad \left. + C_4\,|\vec{q}\,'|(1 - \cos\theta)(q_0 + |\vec{q}\,'|) \right\}, \\
p^t_{12,\lambda'} &= 1/4 \left\{ C_1 \left[-4M\nu + |\vec{q}\,|(|\vec{q}\,| - |\vec{q}\,'|)(1 - \cos\theta) \right] + C_2\,(2M)(q_0 + |\vec{q}\,'|) \right. \\
& \qquad + C_3\,(2M)(|\vec{q}\,'| + |\vec{q}\,|\cos\theta) \\
& \qquad \left. + C_4\,|\vec{q}\,|(1 - \cos\theta)(q_0 + |\vec{q}\,'|) \right\}, \\
p^t_{12,\lambda\lambda'} &= 1/4 \left\{ C_1 \left[2|\vec{q}\,||\vec{q}\,'|\sin^2\theta + \left(|\vec{q}\,|^2 - |\vec{q}\,'|^2 - 4M\nu \right) (1 - \cos\theta) \right] \right. \\
& \qquad + C_2\,(2M)(q_0 + |\vec{q}\,'|)(1 - \cos\theta) - C_3\,(4M)|\vec{q}\,'|(1 - \cos\theta) \\
& \qquad \left. + C_4\,(|\vec{q}\,| + |\vec{q}\,'|)(1 - \cos\theta)(q_0 + |\vec{q}\,'|) \right\}, \qquad \text{(F.2)}
\end{aligned}
$$

where C_1, C_2, C_3, C_4 are defined as

$$
\begin{aligned}
C_1 &= \left[1 - \frac{|\vec{q}\,|}{E + M} \frac{|\vec{q}\,'|}{E' + M} \right], \qquad C_3 = \left[\frac{|\vec{q}\,|}{E + M} + \frac{|\vec{q}\,'|}{E' + M} \right], \\
C_2 &= \left[1 + \frac{|\vec{q}\,|}{E + M} \frac{|\vec{q}\,'|}{E' + M} \right], \qquad C_4 = \left[\frac{|\vec{q}\,|}{E + M} - \frac{|\vec{q}\,'|}{E' + M} \right]. \qquad \text{(F.3)}
\end{aligned}
$$

F.1.2 $T^s_{\lambda'=\pm1\,\lambda'_N=-\frac{1}{2}\,,\,\lambda=\pm1\,\lambda_N=\frac{1}{2}}$

The s-channel helicity amplitudes for the case of transverse polarization of the initial photon and when the nucleons have opposite helicities, are given by :

$$
\begin{aligned}
& T^s_{\lambda'=\pm1\,\lambda'_N=-\frac{1}{2}\,,\,\lambda=\pm1\,\lambda_N=\frac{1}{2}} = \sqrt{E + M}\,\sqrt{E' + M}\,\frac{1}{2}\sin(\theta/2) \\
& \times \left\{ F_1 \left[n^t_1 + n^t_{1,\lambda\lambda'}\,\lambda\lambda' \right] + F_2 \left[n^t_2 + n^t_{2,\lambda\lambda'}\,\lambda\lambda' \right] + F_3\,\nu Q^2 \left[n^t_3 + n^t_{3,\lambda\lambda'}\,\lambda\lambda' \right] \right. \\
& + F_4\,\nu \left[n^t_{4,\lambda}\,(\lambda - \lambda') + n^t_{4,\lambda\lambda'}\,\lambda\lambda' \right] + F_5\,Q^2 \left[n^t_{5,\lambda}\,\lambda + n^t_{5,\lambda'}\,\lambda' + n^t_{5,\lambda\lambda'}\,\lambda\lambda' \right] \\
& + F_6 \left[n^t_{6,\lambda}\,\lambda + n^t_{6,\lambda'}\,\lambda' + n^t_{6,\lambda\lambda'}\,\lambda\lambda' \right] + F_7 \left[n^t_{7,\lambda}\,\lambda + n^t_{7,\lambda'}\,\lambda' + n^t_{7,\lambda\lambda'}\,\lambda\lambda' \right] \\
& \left. + F_8\,\nu Q^2 \left[n^t_{8,\lambda}\,\lambda + n^t_{8,\lambda'}\,\lambda' + n^t_{8,\lambda\lambda'}\,\lambda\lambda' \right] + F_9 \left[n^t_{9,\lambda}\,\lambda + n^t_{9,\lambda'}\,\lambda' + n^t_{9,\lambda\lambda'}\,\lambda\lambda' \right] \right.
\end{aligned}
$$

$$
\begin{aligned}
&+ F_{10}\,\nu\left[n^t_{10} + n^t_{10,\lambda}\,\lambda + n^t_{10,\lambda'}\,\lambda' + n^t_{10,\lambda\lambda'}\,\lambda\lambda'\right] \\
&+ F_{11}\left[n^t_{11,\lambda}\,\lambda + n^t_{11,\lambda'}\,\lambda' + n^t_{11,\lambda\lambda'}\,\lambda\lambda'\right] \\
&+ F_{12}\,Q^2\left[n^t_{12,\lambda}\,\lambda + n^t_{12,\lambda'}\,\lambda' + n^t_{12,\lambda\lambda'}\,\lambda\lambda'\right]\Big\}\,, \qquad \text{(F.4)}
\end{aligned}
$$

where the kinematical factors which appear for the different combinations of photon polarizations in Eq. (F.4) are given by :

$$
\begin{aligned}
n^t_1 &= C_2\,|\vec{q}\,'|\,(q_0 - |\vec{q}|\cos\theta)\,, \\
n^t_{1,\lambda\lambda'} &= C_2\,|\vec{q}\,'|\,(q_0\cos\theta - |\vec{q}|)\,, \\
n^t_2 &= C_2\,(2M\nu)^2\,, \\
n^t_{2,\lambda\lambda'} &= C_2\left\{(2M\nu)^2\cos\theta + |\vec{q}||\vec{q}\,'|\sin^2\theta\left[(4M\nu) + |\vec{q}\,'|(q_0 - |\vec{q}|\cos\theta)\right]\right\}, \\
n^t_3 &= C_2\,(2M\nu)\,, \\
n^t_{3,\lambda\lambda'} &= C_2\left\{2M\nu\cos\theta + |\vec{q}||\vec{q}\,'|\sin^2\theta\right\}, \\
n^t_{4,\lambda} &= \left\{C_1\left(q_0 + |\vec{q}\,'|\right) + C_4\left(|\vec{q}| - |\vec{q}\,'|\right)\right\}(2M\nu)\,, \\
n^t_{4,\lambda\lambda'} &= \left\{-C_1\left(q_0 + |\vec{q}\,'|\right) + C_4\left(|\vec{q}\,'| - |\vec{q}|\right)\right\} \\
&\quad\cdot\left\{|\vec{q}||\vec{q}\,'|\sin^2\theta + (2M\nu)\,(1+\cos\theta)\right\}\,, \\
n^t_{5,\lambda} &= -1/4\left\{C_1\left(q_0 + |\vec{q}\,'|\right) + C_4\left(|\vec{q}| + |\vec{q}\,'| + 2|\vec{q}\,'|\cos\theta\right)\right\}, \\
n^t_{5,\lambda'} &= 1/4\left\{C_1\left(q_0 + |\vec{q}\,'|\right) + C_4\left(|\vec{q}| - |\vec{q}\,'|\right)\right\}, \\
n^t_{5,\lambda\lambda'} &= 1/4\left\{C_1\left(q_0 + |\vec{q}\,'|\right) + C_4\left(|\vec{q}\,'| + |\vec{q}|\right)\right\}(1+\cos\theta)\,, \\
n^t_{6,\lambda} &= |\vec{q}\,'|(2M)\Big\{-C_2\,\nu\left[(|\vec{q}| + |\vec{q}\,'|)(1+\cos\theta) + 2(q_0 - |\vec{q}|\cos\theta)\right] \\
&\qquad + C_4\left[(2M\nu)(1+\cos\theta)\right. \\
&\qquad\quad \left. + (q_0 - |\vec{q}|\cos\theta)(|\vec{q}| + |\vec{q}\,'| + 2|\vec{q}\,'|\cos\theta)\right] \\
&\qquad + C_1\,(q_0 - |\vec{q}|\cos\theta)(q_0 + |\vec{q}\,'|) \\
&\qquad - C_3\,\nu\,(q_0 + |\vec{q}\,'|)(1+\cos\theta)\Big\}\,, \\
n^t_{6,\lambda'} &= (2M)\Big\{C_2\,\nu\left[|\vec{q}|(|\vec{q}| + |\vec{q}\,'|)(1+\cos\theta) + 2|\vec{q}\,'|(q_0 - |\vec{q}|\cos\theta)\right] \\
&\qquad + C_4\left[|\vec{q}|(2M\nu)(1+\cos\theta)\right. \\
&\qquad\quad \left. + |\vec{q}\,'|(q_0 - |\vec{q}|\cos\theta)(|\vec{q}| + |\vec{q}\,'| + 2|\vec{q}|\cos\theta)\right] \\
&\qquad - C_1\,|\vec{q}\,'|(q_0 - |\vec{q}|\cos\theta)(q_0 + |\vec{q}\,'|) \\
&\qquad + C_3\,\nu|\vec{q}\,|(q_0 + |\vec{q}\,'|)(1+\cos\theta)\Big\}\,, \\
n^t_{6,\lambda\lambda'} &= C_2\left\{2M\nu\left[\left(|\vec{q}| + |\vec{q}\,'|\right)^2 + 2|\vec{q}\,'|(q_0 - |\vec{q}|)\right](1+\cos\theta)\right. \\
&\qquad \left. + 2|\vec{q}||\vec{q}\,'|\sin^2\theta\, 2|\vec{q}\,'|\sqrt{s}\right\} \\
&- C_1\,(2M)|\vec{q}\,'|(q_0 - |\vec{q}|\cos\theta)(q_0 + |\vec{q}\,'|)(1+\cos\theta) \\
&+ C_4\,(2M)|\vec{q}\,'|2\sqrt{s}(|\vec{q}| - |\vec{q}\,'|)(1+\cos\theta) \\
&+ C_3\,(2M\nu)(q_0 + |\vec{q}\,'|)(|\vec{q}| + |\vec{q}\,'|)(1+\cos\theta)\,, \\
n^t_{7,\lambda} &= -C_4\,|\vec{q}\,'|^2\sqrt{s}(1+\cos\theta)\,, \\
n^t_{7,\lambda'} &= C_4\,|\vec{q}||\vec{q}\,'|\sqrt{s}(1+\cos\theta)\,, \\
n^t_{7,\lambda\lambda'} &= C_4\,(|\vec{q}| + |\vec{q}\,'|)|\vec{q}\,'|\sqrt{s}(1+\cos\theta)\,, \\
n^t_{8,\lambda} &= 1/4\,|\vec{q}\,'|\left\{C_2\left[(|\vec{q}| + |\vec{q}\,'|)(1+\cos\theta) + 2(q_0 - |\vec{q}|\cos\theta)\right]\right.
\end{aligned}
$$

$$
\begin{aligned}
& - \left[C_4(2M) - C_3(q_0+|\vec{q}\,'|)\right](1+\cos\theta)\Big\}\,, \\
n^t_{8,\lambda'} &= 1/4\,\Big\{-C_2\left[|\vec{q}\,|(|\vec{q}\,|+|\vec{q}\,'|)(1+\cos\theta)+2|\vec{q}\,'|(q_0-|\vec{q}\,|\cos\theta)\right] \\
& \quad +|\vec{q}\,|\left[C_4(2M) - C_3(q_0+|\vec{q}\,'|)\right](1+\cos\theta)\Big\}\,, \\
n^t_{8,\lambda\lambda'} &= 1/4\,\Big\{-C_2\left[\left((|\vec{q}\,|+|\vec{q}\,'|)^2+2|\vec{q}\,'|(q_0-|\vec{q}\,|)\right)(1+\cos\theta)\right] \\
& \quad +(|\vec{q}\,|+|\vec{q}\,'|)\left[C_4(2M) - C_3(q_0+|\vec{q}\,'|)\right](1+\cos\theta)\Big\}\,, \\
n^t_{9,\lambda} &= |\vec{q}\,'|^2\sqrt{s}(1+\cos\theta)\left\{C_2(|\vec{q}\,|+|\vec{q}\,'|) - C_4(2M) + C_3(q_0+|\vec{q}\,'|)\right\}\,, \\
n^t_{9,\lambda'} &= |\vec{q}\,||\vec{q}\,'|\sqrt{s}(1+\cos\theta)\left\{C_2(|\vec{q}\,|+|\vec{q}\,'|) + C_4(2M) + C_3(q_0+|\vec{q}\,'|)\right\}\,, \\
n^t_{9,\lambda\lambda'} &= |\vec{q}\,'|\sqrt{s}(1+\cos\theta)\left\{C_2(|\vec{q}\,|^2-|\vec{q}\,'|^2) + C_4(2M)(|\vec{q}\,|+|\vec{q}\,'|)\right. \\
& \quad \left. +C_3(q_0+|\vec{q}\,'|)(|\vec{q}\,|-|\vec{q}\,'|)\right\}\,, \\
n^t_{10} &= (2M)\left\{C_2(2\nu) - C_1(q_0+|\vec{q}\,'|) + C_4(|\vec{q}\,'|-|\vec{q}\,|)\right\}\,, \\
n^t_{10,\lambda} &= |\vec{q}\,'|\left\{C_2\left[(|\vec{q}\,'|+|\vec{q}\,|)(1+\cos\theta)+2(q_0-|\vec{q}\,|\cos\theta)\right]\right. \\
& \quad \left. +\left[C_4(2M)+C_3(q_0+|\vec{q}\,'|)\right](1+\cos\theta)\right\}\,, \\
n^t_{10,\lambda'} &= -C_2\left\{(|\vec{q}\,|+|\vec{q}\,'|)|\vec{q}\,|(1+\cos\theta)+2|\vec{q}\,'|(q_0-|\vec{q}\,|\cos\theta)\right\} \\
& \quad +\left\{C_4(2M) - C_3(q_0+|\vec{q}\,'|)\right\}|\vec{q}\,|(1+\cos\theta)\,, \\
n^t_{10,\lambda\lambda'} &= C_2\left\{4M\nu\cos\theta+2|\vec{q}\,||\vec{q}\,'|\sin^2\theta\right. \\
& \quad \left. -\left[(|\vec{q}\,'|+|\vec{q}\,|)^2+2|\vec{q}\,'|(q_0-|\vec{q}\,|)\right](1+\cos\theta)\right\} \\
& - C_1(2M)(q_0+|\vec{q}\,'|)\cos\theta + C_4(2M)(|\vec{q}\,|-|\vec{q}\,'|) \\
& - C_3(q_0+|\vec{q}\,'|)(|\vec{q}\,|+|\vec{q}\,'|)(1+\cos\theta)\,, \\
n^t_{11,\lambda} &= 2|\vec{q}\,'|\left\{C_1(q_0-|\vec{q}\,|\cos\theta)(q_0+|\vec{q}\,'|)\right. \\
& \quad \left. +C_4\left[2M\nu(1+\cos\theta)+(q_0-|\vec{q}\,|\cos\theta)(|\vec{q}\,|+|\vec{q}\,'|\cos\theta)\right]\right\}\,, \\
n^t_{11,\lambda'} &= 2\left\{-C_1|\vec{q}\,'|(q_0-|\vec{q}\,|\cos\theta)(q_0+|\vec{q}\,'|)\right. \\
& \quad \left. +C_4\left[2M\nu|\vec{q}\,|(1+\cos\theta)+|\vec{q}\,'|(q_0-|\vec{q}\,|\cos\theta)(|\vec{q}\,'|+|\vec{q}\,|\cos\theta)\right]\right\}\,, \\
n^t_{11,\lambda\lambda'} &= 2\left\{C_1\left[(q_0+|\vec{q}\,'|)|\vec{q}\,||\vec{q}\,'|\sin^2\theta - |\vec{q}\,'|(q_0-|\vec{q}\,|\cos\theta)(q_0+|\vec{q}\,'|)(1+\cos\theta)\right]\right. \\
& \quad \left. +C_4(|\vec{q}\,|-|\vec{q}\,'|)\left[2M\nu(1+\cos\theta)+|\vec{q}\,||\vec{q}\,'|\sin^2\theta\right]\right\}\,, \\
n^t_{12,\lambda} &= 1/4\left\{C_2\left[4M\nu+|\vec{q}\,'|(|\vec{q}\,|+|\vec{q}\,'|)(1+\cos\theta)\right] - C_1(2M)(q_0+|\vec{q}\,'|)\right. \\
& \quad -C_4(2M)\left[2|\vec{q}\,'|(1+\cos\theta)+(|\vec{q}\,|+|\vec{q}\,'|\cos\theta)\right] \\
& \quad \left. +C_3|\vec{q}\,'|(1+\cos\theta)(q_0+|\vec{q}\,'|)\right\}\,, \\
n^t_{12,\lambda'} &= 1/4\left\{C_2\left[-4M\nu+|\vec{q}\,|(|\vec{q}\,|+|\vec{q}\,'|)(1+\cos\theta)\right] + C_1(2M)(q_0+|\vec{q}\,'|)\right. \\
& \quad \left. -C_4(2M)(|\vec{q}\,'|+|\vec{q}\,|\cos\theta)+C_3|\vec{q}\,|(1+\cos\theta)(q_0+|\vec{q}\,'|)\right\}\,, \\
n^t_{12,\lambda\lambda'} &= 1/4\left\{C_2\left[-2|\vec{q}\,||\vec{q}\,'|\sin^2\theta+\left(|\vec{q}\,|^2-|\vec{q}\,'|^2-4M\nu\right)(1+\cos\theta)\right]\right. \\
& \quad +C_1(2M)(q_0+|\vec{q}\,'|)(1+\cos\theta) \\
& \quad \left. +C_4(4M)|\vec{q}\,'|(1+\cos\theta)+C_3(|\vec{q}\,|-|\vec{q}\,'|)(1+\cos\theta)(q_0+|\vec{q}\,'|)\right\}\,. \qquad \text{(F.5)}
\end{aligned}
$$

F.1.3 $T^s_{\lambda'=\pm1\,\lambda'_N=\frac{1}{2}\,,\,\lambda=0\,\lambda_N=\frac{1}{2}}$

The s-channel helicity amplitudes for the case of longitudinal polarization of the initial photon and when both nucleons have the same helicities, are given by :

$$
\begin{aligned}
T^s_{\lambda'=\pm1\,\lambda'_N=\frac{1}{2}\,,\,\lambda=0\,\lambda_N=\frac{1}{2}} &= \sqrt{E+M}\,\sqrt{E'+M}\,\frac{\sqrt{Q^2}}{|\vec{q}|}\,\frac{1}{\sqrt{2}}\,\sin(\theta/2) \\
&\times\Big\{F_1\left[p^l_{1,\lambda'}\,\lambda'\right] + F_2\left[p^l_{2,\lambda'}\,\lambda'\right] + F_3\,\nu\left[p^l_{3,\lambda'}\,\lambda'\right] + F_4\,\nu\left[p^l_4 + p^l_{4,\lambda'}\,\lambda'\right] \\
&+ F_5\left[p^l_5 + p^l_{5,\lambda'}\,\lambda'\right] + F_6\left[p^l_6 + p^l_{6,\lambda'}\,\lambda'\right] + F_7\left[p^l_7 + p^l_{7,\lambda'}\,\lambda'\right] \\
&+ F_8\,\nu\left[p^l_8 + p^l_{8,\lambda'}\,\lambda'\right] + F_9\left[p^l_9 + p^l_{9,\lambda'}\,\lambda'\right] + F_{10}\,\nu\left[p^l_{10} + p^l_{10,\lambda'}\,\lambda'\right] \\
&+ F_{11}\left[p^l_{11} + p^l_{11,\lambda'}\,\lambda'\right] + F_{12}\left[p^l_{12} + p^l_{12,\lambda'}\,\lambda'\right]\Big\}\,, \qquad \text{(F.6)}
\end{aligned}
$$

where the kinematical factors which appear for the different combinations of photon polarizations in Eq. (F.6) are given by:

$$
\begin{aligned}
p^l_{1,\lambda'} &= C_1\,|\vec{q}\,||\vec{q}\,'|(1+\cos\theta)\,, \\
p^l_{2,\lambda'} &= -C_1\,|\vec{q}\,||\vec{q}\,'|(1+\cos\theta)\left[2M\nu - 2\sqrt{s}(2\sqrt{s} - q_0 - |\vec{q}\,'|)\right]\,, \\
p^l_{3,\lambda'} &= -C_1\,|\vec{q}\,||\vec{q}\,'|^2\,2\sqrt{s}(1+\cos\theta)\,, \\
p^l_4 &= (2M\nu)\left\{C_2\,(|\vec{q}\,| - |\vec{q}\,'|) + C_3\,(2\sqrt{s} - q_0 - |\vec{q}\,'|)\right\}\,, \\
p^l_{4,\lambda'} &= C_2\,\Big\{-|\vec{q}\,'|(|\vec{q}\,|\cos\theta + |\vec{q}\,'|)(2\sqrt{s} - q_0 - |\vec{q}\,|) \\
&\qquad - q_0|\vec{q}\,|\,(1+\cos\theta)(2\sqrt{s} - q_0 - |\vec{q}\,'|)\Big\} \\
&+ C_3\,(2\sqrt{s} - q_0 - |\vec{q}\,'|)\left\{|\vec{q}\,'|(2\sqrt{s} - q_0 - |\vec{q}\,|) - (1+\cos\theta)|\vec{q}\,|^2\right\}\,, \\
p^l_5 &= 1/4\left\{-C_2\,Q^2(|\vec{q}\,| - |\vec{q}\,'|) + C_3\left[Q^2(2\sqrt{s} - q_0 - |\vec{q}\,'|) + 4M\nu q_0\right]\right\}\,, \\
p^l_{5,\lambda'} &= C_2/4\left\{Q^2(|\vec{q}\,|\cos\theta + |\vec{q}\,'|) - |\vec{q}\,|(1+\cos\theta)\left(|\vec{q}\,|^2 + q_0|\vec{q}\,'|\right)\right\} \\
&+ C_3/4\left\{Q^2(2\sqrt{s} - q_0 - |\vec{q}\,'|) + 4M\nu q_0 - (1+\cos\theta)q_0|\vec{q}\,|(|\vec{q}\,'| + |\vec{q}\,|)\right\}\,, \\
p^l_6 &= |\vec{q}\,'|(2M)\Big\{-C_1\,\nu(|\vec{q}\,| - |\vec{q}\,'|) + C_2(q_0 - |\vec{q}\,|\cos\theta)(|\vec{q}\,| - |\vec{q}\,'|) \\
&\qquad + C_3\left[2M\nu - (2\sqrt{s} - q_0 - |\vec{q}\,'|)(q_0 - |\vec{q}\,|\cos\theta)\right] \\
&\qquad + C_4\nu(q_0 - |\vec{q}\,'| - 2|\vec{q}\,|\cos\theta)\Big\}\,, \\
p^l_{6,\lambda'} &= C_1\,|\vec{q}\,'|\left\{2M\nu\,(|\vec{q}\,|\cos\theta + |\vec{q}\,'|)\right. \\
&\qquad \left. - |\vec{q}\,|(1+\cos\theta)\left(|\vec{q}\,'|4\sqrt{s} - (2\sqrt{s} - q_0)(2\sqrt{s} + q_0 - |\vec{q}\,|\cos\theta)\right)\right\} \\
&- C_2|\vec{q}\,'|(2M)\left\{(q_0 - |\vec{q}\,|\cos\theta)(|\vec{q}\,|\cos\theta + |\vec{q}\,'|) + |\vec{q}\,|(2\sqrt{s})(1+\cos\theta)\right\} \\
&+ C_3|\vec{q}\,'|(2M)\left\{2M\nu - (2\sqrt{s} - q_0 - |\vec{q}\,'|)(q_0 - |\vec{q}\,|\cos\theta)\right\} \\
&+ C_4(2M\nu)\left\{|\vec{q}\,|(1+\cos\theta)(|\vec{q}\,'| + |\vec{q}\,|) + |\vec{q}\,'|(q_0 - |\vec{q}\,'| - 2|\vec{q}\,|\cos\theta)\right\}\,, \\
p^l_7 &= -C_3/2\,|\vec{q}\,'|\left\{|\vec{q}\,'|2\sqrt{s} - (q_0 - |\vec{q}\,|\cos\theta)(2\sqrt{s} - q_0)\right\}\,, \\
p^l_{7,\lambda'} &= -C_2/4\,|\vec{q}\,|(1+\cos\theta)\left\{2\sqrt{s}(|\vec{q}\,'| - q_0) + q_0(|\vec{q}\,'| + q_0)\right\} \\
&+ C_3/4\left\{-2|\vec{q}\,'|\left[|\vec{q}\,'|2\sqrt{s} - (q_0 - |\vec{q}\,|\cos\theta)(2\sqrt{s} - q_0)\right]\right. \\
&\qquad \left. + |\vec{q}\,|(1+\cos\theta)(2\sqrt{s} - q_0)(|\vec{q}\,'| + |\vec{q}\,|)\right\}, \\
p^l_8 &= |\vec{q}\,'|/2\left\{C_1\,Q^2/2\,(|\vec{q}\,| - |\vec{q}\,'|) - C_3\,M\left[|\vec{q}\,|^2 + q_0^2 - 2q_0|\vec{q}\,|\cos\theta\right]\right. \\
&\qquad \left. - C_4\,Q^2/2\,(q_0 - |\vec{q}\,'| - 2|\vec{q}\,|\cos\theta)\right\}\,, \\
p^l_{8,\lambda'} &= C_1/2\left\{-Q^2/2\,|\vec{q}\,'|(|\vec{q}\,|\cos\theta + |\vec{q}\,'|)\right.
\end{aligned}
$$

$$
\begin{aligned}
& + |\vec{q}|(1+\cos\theta)\left[q_0|\vec{q}\,'|2\sqrt{s}+Q^2/2(2\sqrt{s}-q_0)\right]\Big\} \\
- \; & C_2/2\left\{M|\vec{q}|(1+\cos\theta)\left[|\vec{q}|^2+q_0|\vec{q}\,'|\right]\right\} \\
- \; & C_3 M/2\left\{|\vec{q}\,'|\left[|\vec{q}|^2+q_0^2-2q_0|\vec{q}|\cos\theta\right]+(1+\cos\theta)q_0|\vec{q}|(|\vec{q}\,'|+|\vec{q}|)\right\} \\
- \; & C_4 Q^2/4\left\{|\vec{q}\,'|(q_0-|\vec{q}\,'|-2|\vec{q}|\cos\theta)+(1+\cos\theta)|\vec{q}|(|\vec{q}\,'|+|\vec{q}|)\right\}, \\
p_9^l \;=\; & |\vec{q}\,'|/2\left[2\sqrt{s}|\vec{q}\,'|-(q_0-|\vec{q}|\cos\theta)(2\sqrt{s}-q_0)\right] \\
& \cdot\left\{C_1(|\vec{q}|-|\vec{q}\,'|)-C_3(2M)+C_4(q_0+|\vec{q}\,'|)\right\}, \\
p_{9,\lambda'}^l \;=\; & C_1/2\left\{-|\vec{q}\,'|(|\vec{q}|\cos\theta+|\vec{q}\,'|)\left[2\sqrt{s}|\vec{q}\,'|-(q_0-|\vec{q}|\cos\theta)(2\sqrt{s}-q_0)\right]\right. \\
& \left. +(1+\cos\theta)|\vec{q}|(2\sqrt{s}-q_0)(2M\nu)\right\} \\
- \; & C_2/2(1+\cos\theta)|\vec{q}||\vec{q}\,'|(2M)(2\sqrt{s}) \\
- \; & C_3/2|\vec{q}\,'|(2M)\left[2\sqrt{s}|\vec{q}\,'|-(q_0-|\vec{q}|\cos\theta)(2\sqrt{s}-q_0)\right] \\
+ \; & C_4/2|\vec{q}\,'|\left\{(q_0+|\vec{q}\,'|)\left[2\sqrt{s}|\vec{q}\,'|-(q_0-|\vec{q}|\cos\theta)(2\sqrt{s}-q_0)\right]\right. \\
& \left. +(1+\cos\theta)|\vec{q}|(|\vec{q}|+|\vec{q}\,'|)2\sqrt{s}\right\}, \\
p_{10}^l \;=\; & |\vec{q}\,'|\left\{C_1(|\vec{q}|-|\vec{q}\,'|)+C_3(2M)-C_4(q_0-2|\vec{q}|\cos\theta-|\vec{q}\,'|)\right\}, \\
p_{10,\lambda'}^l \;=\; & C_1\left\{-|\vec{q}\,'|(|\vec{q}|\cos\theta+|\vec{q}\,'|)+|\vec{q}|(1+\cos\theta)(2\sqrt{s}-q_0-2|\vec{q}\,'|)\right\} \\
- \; & C_2(1+\cos\theta)(2M)|\vec{q}|+C_3(2M)|\vec{q}\,'| \\
- \; & C_4\left\{|\vec{q}\,'|(q_0-2|\vec{q}|\cos\theta-|\vec{q}\,'|)+(1+\cos\theta)|\vec{q}|(|\vec{q}\,'|+|\vec{q}|)\right\}, \\
p_{11}^l \;=\; & 2|\vec{q}\,'|\left\{C_2(|\vec{q}|-|\vec{q}\,'|)(q_0-|\vec{q}|\cos\theta)+C_3(2M\nu)\right\}, \\
p_{11,\lambda'}^l \;=\; & -C_2\left\{2|\vec{q}\,'|(q_0-|\vec{q}|\cos\theta)(|\vec{q}|\cos\theta+|\vec{q}\,'|)\right. \\
& \left. +(1+\cos\theta)|\vec{q}|\left[4M\nu-(2\sqrt{s}-q_0-2|\vec{q}\,'|)(q_0+|\vec{q}\,'|)\right]\right\} \\
+ \; & C_3\left\{|\vec{q}\,'|(4M\nu)+(1+\cos\theta)|\vec{q}|(2\sqrt{s}-q_0-2|\vec{q}\,'|)(|\vec{q}\,'|+|\vec{q}|)\right\}, \\
p_{12}^l \;=\; & -C_1/2(|\vec{q}|-|\vec{q}\,'|)\left[Q^2/2(2\sqrt{s}-q_0-|\vec{q}\,'|)+2M\nu q_0\right] \\
- \; & C_2/2(2M)Q^2/2(|\vec{q}|-|\vec{q}\,'|) \\
+ \; & C_3/2(2M)\left[Q^2(2\sqrt{s}-q_0-|\vec{q}\,'|)+q_0(2M\nu)\right] \\
- \; & C_4/2\left[Q^2(2M\nu)+(q_0+|\vec{q}\,'|)\left(Q^2/2(2\sqrt{s}-q_0-|\vec{q}\,'|)+q_0(2M\nu)\right)\right], \\
p_{12,\lambda'}^l \;=\; & C_1/2\left\{\left[Q^2/2(2\sqrt{s}-q_0-|\vec{q}\,'|)+q_0(2M\nu)\right](|\vec{q}\,'|-|\vec{q}|)\right. \\
& \left. -|\vec{q}|(1+\cos\theta)Q^2/2(2\sqrt{s}-q_0-|\vec{q}\,'|)\right\} \\
+ \; & C_2/2(2M)Q^2/2(|\vec{q}|\cos\theta+|\vec{q}\,'|) \\
+ \; & C_3/2(2M)\left[Q^2(2\sqrt{s}-q_0-|\vec{q}\,'|)+q_0(2M\nu)\right] \\
+ \; & C_4/2\left\{-Q^2(2M\nu)-(q_0+|\vec{q}\,'|)\left(Q^2/2(2\sqrt{s}-q_0-|\vec{q}\,'|)+q_0(2M\nu)\right)\right. \\
& \left. +(1+\cos\theta)Q^2/2|\vec{q}|(|\vec{q}\,'|+|\vec{q}|)\right\} \qquad \text{(F.7)}
\end{aligned}
$$

F.1.4 $T^s_{\lambda'=\pm1\,\lambda'_N=-\frac{1}{2}\,,\,\lambda=0\,\lambda_N=\frac{1}{2}}$

The s-channel helicity amplitudes for the case of longitudinal polarization of the initial photon and when the nucleons have opposite helicities, are given by :

$$
T^s_{\lambda'=\pm1\,\lambda'_N=-\frac{1}{2}\,,\,\lambda=0\,\lambda_N=\frac{1}{2}} = \sqrt{E+M}\,\sqrt{E'+M}\,\frac{\sqrt{Q^2}}{|\vec{q}|}\,\frac{1}{\sqrt{2}}\cos(\theta/2)
$$

$$
\begin{aligned}
&\times \Big\{ F_1 \left[n^l_{1,\lambda'}\,\lambda' \right] + F_2 \left[n^l_{2,\lambda'}\,\lambda' \right] + F_3 \nu \left[n^l_{3,\lambda'}\,\lambda' \right] + F_4 \nu \left[n^l_4 + n^l_{4,\lambda'}\,\lambda' \right] \\
&+ F_5 \left[n^l_5 + n^l_{5,\lambda'}\,\lambda' \right] + F_6 \left[n^l_6 + n^l_{6,\lambda'}\,\lambda' \right] + F_7 \left[n^l_7 + n^l_{7,\lambda'}\,\lambda' \right] \\
&+ F_8 \nu \left[n^l_8 + n^l_{8,\lambda'}\,\lambda' \right] + F_9 \left[n^l_9 + n^l_{9,\lambda'}\,\lambda' \right] + F_{10} \nu \left[n^l_{10} + n^l_{10,\lambda'}\,\lambda' \right] \\
&+ F_{11} \left[n^l_{11} + n^l_{11,\lambda'}\,\lambda' \right] + F_{12} \left[n^l_{12} + n^l_{12,\lambda'}\,\lambda' \right] \Big\} \,, \qquad \text{(F.8)}
\end{aligned}
$$

where the kinematical factors which appear for the different combinations of photon polarizations in Eq. (F.8) are given by :

$$
\begin{aligned}
n^l_{1,\lambda'} &= -C_2\,|\vec{q}||\vec{q}\,'|(1-\cos\theta)\,, \\
n^l_{2,\lambda'} &= C_2\,|\vec{q}||\vec{q}\,'|(1-\cos\theta)\left[2M\nu - 2\sqrt{s}(2\sqrt{s}-q_0-|\vec{q}\,'|)\right]\,, \\
n^l_{3,\lambda'} &= C_2\,|\vec{q}||\vec{q}\,'|^2\,2\sqrt{s}(1-\cos\theta)\,, \\
n^l_4 &= (2M\nu)\left\{C_1\,(|\vec{q}|+|\vec{q}\,'|) + C_4\,(2\sqrt{s}-q_0-|\vec{q}\,'|)\right\}\,, \\
n^l_{4,\lambda'} &= C_1\,\Big\{-|\vec{q}\,'|(|\vec{q}\,|\cos\theta+|\vec{q}\,'|)(2\sqrt{s}-q_0+|\vec{q}\,|) \\
&\qquad + q_0|\vec{q}\,|\,(1-\cos\theta)(2\sqrt{s}-q_0-|\vec{q}\,'|)\Big\} \\
&+ C_4\,(2\sqrt{s}-q_0-|\vec{q}\,'|)\left\{-|\vec{q}\,'|(2\sqrt{s}-q_0+|\vec{q}\,|) + (1-\cos\theta)\,|\vec{q}\,|^2\right\}\,, \\
n^l_5 &= 1/4\left\{-C_1\,Q^2(|\vec{q}|+|\vec{q}\,'|) + C_4\,\left[Q^2(2\sqrt{s}-q_0-|\vec{q}\,'|) + 4M\nu q_0\right]\right\}\,, \\
n^l_{5,\lambda'} &= C_1/4\left\{Q^2(|\vec{q}\,|\cos\theta+|\vec{q}\,'|) + |\vec{q}\,|(1-\cos\theta)\,\left(|\vec{q}\,|^2 + q_0|\vec{q}\,'|\right)\right\} \\
&+ C_4/4\left\{-\left[Q^2(2\sqrt{s}-q_0-|\vec{q}\,'|) + 4M\nu q_0\right] - (1-\cos\theta)\,q_0|\vec{q}\,|(|\vec{q}\,'|-|\vec{q}\,|)\right\}\,, \\
n^l_6 &= |\vec{q}\,'|(2M)\left\{-C_2\,\nu(|\vec{q}|+|\vec{q}\,'|) + C_1(q_0-|\vec{q}\,|\cos\theta)(|\vec{q}\,|+|\vec{q}\,'|)\right. \\
&\qquad + C_4\left[2M\nu - (2\sqrt{s}-q_0-|\vec{q}\,'|)(q_0-|\vec{q}\,|\cos\theta)\right] \\
&\qquad \left. + C_3\nu(q_0-|\vec{q}\,'|-2|\vec{q}\,|\cos\theta)\right\}\,, \\
n^l_{6,\lambda'} &= C_2\,|\vec{q}\,'|\left\{2M\nu\,(|\vec{q}\,|\cos\theta+|\vec{q}\,'|)\right. \\
&\qquad \left. + |\vec{q}\,|(1-\cos\theta)\left(|\vec{q}\,'|4\sqrt{s} - (2\sqrt{s}-q_0)(2\sqrt{s}+q_0-|\vec{q}\,|\cos\theta)\right)\right\} \\
&- C_1|\vec{q}\,'|(2M)\left\{(q_0-|\vec{q}\,|\cos\theta)(|\vec{q}\,|\cos\theta+|\vec{q}\,'|) - |\vec{q}\,|(2\sqrt{s})(1-\cos\theta)\right\} \\
&- C_4|\vec{q}\,'|(2M)\left\{2M\nu - (2\sqrt{s}-q_0-|\vec{q}\,'|)(q_0-|\vec{q}\,|\cos\theta)\right\} \\
&+ C_3(2M\nu)\left\{|\vec{q}\,|(1-\cos\theta)(|\vec{q}\,'|-|\vec{q}\,|) - |\vec{q}\,'|(q_0-|\vec{q}\,'|-2|\vec{q}\,|\cos\theta)\right\}\,, \\
n^l_7 &= -C_4/2\,|\vec{q}\,'|\left\{|\vec{q}\,'|2\sqrt{s} - (q_0-|\vec{q}\,|\cos\theta)(2\sqrt{s}-q_0)\right\}\,, \\
n^l_{7,\lambda'} &= C_1/4\,|\vec{q}\,|(1-\cos\theta)\left\{2\sqrt{s}(|\vec{q}\,'|-q_0) + q_0(|\vec{q}\,'|+q_0)\right\} \\
&+ C_4/4\left\{2|\vec{q}\,'|\left[|\vec{q}\,'|2\sqrt{s} - (q_0-|\vec{q}\,|\cos\theta)(2\sqrt{s}-q_0)\right]\right. \\
&\qquad \left. + |\vec{q}\,|(1-\cos\theta)(2\sqrt{s}-q_0)(|\vec{q}\,'|-|\vec{q}\,|)\right\}\,, \\
n^l_8 &= |\vec{q}\,'|/2\left\{C_2\,Q^2/2\,(|\vec{q}|+|\vec{q}\,'|) - C_4\,M\left[|\vec{q}\,|^2 + q_0^2 - 2q_0|\vec{q}\,|\cos\theta\right]\right. \\
&\qquad \left. - C_3\,Q^2/2\,(q_0-|\vec{q}\,'|-2|\vec{q}\,|\cos\theta)\right\}\,, \\
n^l_{8,\lambda'} &= C_2/2\,\Big\{-Q^2/2\,|\vec{q}\,'|(|\vec{q}\,|\cos\theta+|\vec{q}\,'|) \\
&\qquad - |\vec{q}\,|(1-\cos\theta)\left[q_0|\vec{q}\,'|2\sqrt{s} + Q^2/2(2\sqrt{s}-q_0)\right]\Big\} \\
&+ C_1/2\left\{M|\vec{q}\,|(1-\cos\theta)\left[|\vec{q}\,|^2 + q_0|\vec{q}\,'|\right]\right\} \\
&+ C_4 M/2\left\{|\vec{q}\,'|\left[|\vec{q}\,|^2 + q_0^2 - 2q_0|\vec{q}\,|\cos\theta\right] - (1-\cos\theta)q_0|\vec{q}\,|(|\vec{q}\,'|-|\vec{q}\,|)\right\} \\
&- C_3\,Q^2/4\left\{-|\vec{q}\,'|(q_0-|\vec{q}\,'|-2|\vec{q}\,|\cos\theta) + (1-\cos\theta)|\vec{q}\,|(|\vec{q}\,'|-|\vec{q}\,|)\right\}\,,
\end{aligned}
$$

$$
\begin{aligned}
n_9^l &= |\vec{q}\,'|/2\left[2\sqrt{s}|\vec{q}\,'| - (q_0 - |\vec{q}|\cos\theta)(2\sqrt{s} - q_0)\right] \\
&\quad \cdot \left\{C_2(|\vec{q}| + |\vec{q}\,'|) - C_4 2M + C_3(q_0 + |\vec{q}\,'|)\right\}, \\
n_{9,\lambda'}^l &= C_2/2\left\{-|\vec{q}\,'|(|\vec{q}|\cos\theta + |\vec{q}\,'|)\left[2\sqrt{s}|\vec{q}\,'| - (q_0 - |\vec{q}|\cos\theta)(2\sqrt{s} - q_0)\right]\right. \\
&\qquad \left. -(1-\cos\theta)|\vec{q}|(2\sqrt{s} - q_0)(2M\nu)\right\} \\
&+ C_1/2(1-\cos\theta)|\vec{q}||\vec{q}\,'|(2M)(2\sqrt{s}) \\
&+ C_4/2|\vec{q}\,'|(2M)\left[2\sqrt{s}|\vec{q}\,'| - (q_0 - |\vec{q}|\cos\theta)(2\sqrt{s} - q_0)\right] \\
&+ C_3/2|\vec{q}\,'|\left\{-(q_0 + |\vec{q}\,'|)\left[2\sqrt{s}|\vec{q}\,'| - (q_0 - |\vec{q}|\cos\theta)(2\sqrt{s} - q_0)\right]\right. \\
&\qquad \left. +(1-\cos\theta)|\vec{q}|(|\vec{q}\,'| - |\vec{q}|)2\sqrt{s}\right\}, \\
n_{10}^l &= |\vec{q}\,'|\left\{C_2(|\vec{q}| + |\vec{q}\,'|) + C_4(2M) - C_3(q_0 - 2|\vec{q}|\cos\theta - |\vec{q}\,'|)\right\}, \\
n_{10,\lambda'}^l &= C_2\left\{-|\vec{q}\,'|(|\vec{q}|\cos\theta + |\vec{q}\,'|) - |\vec{q}|(1-\cos\theta)(2\sqrt{s} - q_0 - 2|\vec{q}\,'|)\right\} \\
&+ C_1(1-\cos\theta)(2M)|\vec{q}| - C_4(2M)|\vec{q}\,'| \\
&- C_3\left\{-|\vec{q}\,'|(q_0 - 2|\vec{q}|\cos\theta - |\vec{q}\,'|) + (1-\cos\theta)|\vec{q}|(|\vec{q}\,'| - |\vec{q}|)\right\}, \\
n_{11}^l &= 2|\vec{q}\,'|\left\{C_1(|\vec{q}| + |\vec{q}\,'|)(q_0 - |\vec{q}|\cos\theta) + C_4(2M\nu)\right\}, \\
n_{11,\lambda'}^l &= -C_1\left\{2|\vec{q}\,'|(q_0 - |\vec{q}|\cos\theta)(|\vec{q}|\cos\theta + |\vec{q}\,'|)\right. \\
&\qquad \left. -(1-\cos\theta)|\vec{q}|\left[4M\nu - (2\sqrt{s} - q_0 - 2|\vec{q}\,'|)(q_0 + |\vec{q}\,'|)\right]\right\} \\
&+ C_4\left\{-|\vec{q}\,'|(4M\nu) + (1-\cos\theta)|\vec{q}|(2\sqrt{s} - q_0 - 2|\vec{q}\,'|)(|\vec{q}\,'| - |\vec{q}|)\right\}, \\
n_{12}^l &= -C_2/2\left[Q^2/2(2\sqrt{s} - q_0 - |\vec{q}\,'|) + q_0(2M\nu)\right](|\vec{q}| + |\vec{q}\,'|) \\
&- C_1/2(2M)Q^2/2(|\vec{q}| + |\vec{q}\,'|) \\
&+ C_4/2(2M)\left[Q^2(2\sqrt{s} - q_0 - |\vec{q}\,'|) + q_0(2M\nu)\right] \\
&- C_3/2\left[Q^2(2M\nu) + (q_0 + |\vec{q}\,'|)\left(Q^2/2(2\sqrt{s} - q_0 - |\vec{q}\,'|) + q_0(2M\nu)\right)\right], \\
n_{12,\lambda'}^l &= C_2/2\left\{\left[Q^2/2(2\sqrt{s} - q_0 - |\vec{q}\,'|) + q_0(2M\nu)\right](|\vec{q}| + |\vec{q}\,'|)\right. \\
&\qquad \left. +|\vec{q}|(1-\cos\theta)Q^2/2(2\sqrt{s} - q_0 - |\vec{q}\,'|)\right\} \\
&+ C_1/2(2M)Q^2/2(|\vec{q}|\cos\theta + |\vec{q}\,'|) \\
&- C_4/2(2M)\left[Q^2(2\sqrt{s} - q_0 - |\vec{q}\,'|) + q_0(2M\nu)\right] \\
&+ C_3/2\left\{Q^2(2M\nu) + (q_0 + |\vec{q}\,'|)\left(Q^2/2(2\sqrt{s} - q_0 - |\vec{q}\,'|) + q_0(2M\nu)\right)\right. \\
&\qquad \left. +(1-\cos\theta)Q^2/2|\vec{q}|(|\vec{q}\,'| - |\vec{q}|)\right\}
\end{aligned}
\tag{F.9}
$$

Appendix G

G.1 Relations between the invariant amplitudes and the VCS helicity amplitudes.

By inserting the single tensors of Eq.(4.63) into the T-matrix elements

$$T_{\lambda'\lambda'_N;\lambda\lambda_N} \equiv -e^2\varepsilon_\mu(\vec{q},\lambda)\,\varepsilon'^{*}_\nu(\vec{q}\,',\lambda')\,\bar{u}(\vec{p}\,',\lambda'_N)H^{\mu\nu}\,u(\vec{p},\lambda_N)$$

with polarization vectors and helicity spinors defined in Appendix A.1, it is straightforward to express the VCS helicity amplitudes as functions of the amplitudes F_i. These expressions are given in the Appendix F.1.

In the following, we will need the expressions of the invariant amplitudes F_i as functions of the *reduced* helicity amplitudes, defined in Appendix A.3. In order to be applicable for numerical calculations, these expressions should not contain any kinematical singularities.

The direct analytical inversion of Appendix F.1 is cumbersome. We therefore proceed in the following way:

First, the formulas of Appendix F.1 are inverted numerically. Second, the analytical inversion is performed in two steps. As a first step, we obtain the amplitudes of Berg and Lindner B_i as functions of the helicity amplitudes, which are then combined into F_i's, using the relations between the two sets of amplitudes. A numerical comparison of both analytic and numerical inversion procedures serves as a cross check for this complicated calculation.

G.1.1 VCS helicity amplitudes in the invariant basis of Berg and Lindner

We first take into account the photons' polarization. For the longitudinally polarized initial photon, we obtain:

$$\begin{aligned} T_{\lambda'\lambda'_N;0\lambda_N} &= \frac{\lambda'}{\sqrt{2}}\frac{Q\sin\Theta}{q_0-|\vec{q}|\cos\Theta}\left[B_1 - \frac{2}{\sin^2\Theta}\frac{|\vec{q}|-q_0\cos\Theta}{\sqrt{s}|\vec{q}||\vec{q}\,'|}B_9\right] \\ &\cdot\ \bar{u}(\vec{p}\,',\lambda'_N)\,u(\vec{p},\lambda_N) \\ &+ \frac{\lambda'}{\sqrt{2}}\frac{Q\sin\Theta}{q_0-|\vec{q}|\cos\Theta}\left[B_2 - \frac{2}{\sin^2\Theta}\frac{|\vec{q}|-q_0\cos\Theta}{\sqrt{s}|\vec{q}||\vec{q}\,'|}B_{10}\right] \end{aligned}$$

$$
\begin{aligned}
& \cdot \quad \bar{u}(\vec{p}\,',\lambda'_N)\not{K}u(\vec{p},\lambda_N) \\
+ & \quad \frac{Q\sqrt{2}}{s\vec{q}^{\,2}|\vec{q}\,'|\sin\Theta}\left[B_5+B_7+\frac{2\sqrt{s}|\vec{q}|}{|\vec{q}\,'|}\frac{|\vec{q}|-q_0\cos\Theta}{(q_0-|\vec{q}|\cos\Theta)^2}B_{11}\right] \\
& \cdot \quad \bar{u}(\vec{p}\,',\lambda'_N)\gamma_5 u(\vec{p},\lambda_N) \\
- & \quad \frac{Q\sqrt{2}}{s\vec{q}^{\,2}|\vec{q}\,'|\sin\Theta}\left[B_6+B_8+\frac{2\sqrt{s}|\vec{q}|}{|\vec{q}\,'|}\frac{|\vec{q}|-q_0\cos\Theta}{(q_0-|\vec{q}|\cos\Theta)^2}B_{12}\right] \\
& \cdot \quad \bar{u}(\vec{p}\,',\lambda'_N)\,i\not{N}u(\vec{p},\lambda_N)\,. \qquad \text{(G.1)}
\end{aligned}
$$

The transverse polarisation of the initial photon leads to

$$
\begin{aligned}
T_{\lambda'\lambda'_N;\pm1\lambda_N} &= \frac{1}{2}\left[\lambda\lambda'\frac{|\vec{q}|-q_0\cos\Theta}{q_0-|\vec{q}|\cos\Theta}B_1-B_3-\frac{2\lambda\lambda' Q^2}{\sqrt{s}|\vec{q}||\vec{q}\,'|(q_0-|\vec{q}|\cos\Theta)}B_9\right] \\
& \cdot \quad \bar{u}(\vec{p}\,',\lambda'_N)u(\vec{p},\lambda_N) \\
+ & \quad \frac{1}{2}\left[\lambda\lambda'\frac{|\vec{q}|-q_0\cos\Theta}{q_0-|\vec{q}|\cos\Theta}B_2-B_4-\frac{2\lambda\lambda' Q^2}{\sqrt{s}|\vec{q}||\vec{q}\,'|(q_0-|\vec{q}|\cos\Theta)}B_{10}\right] \\
& \cdot \quad \bar{u}(\vec{p}\,',\lambda'_N)\not{K}u(\vec{p},\lambda_N) \\
+ & \quad \left\{\lambda\left[\frac{|\vec{q}|-q_0\cos\Theta}{s\vec{q}^{\,2}|\vec{q}\,'|\sin^2\Theta}(B_5+B_7)+\frac{2Q^2}{\sqrt{s}|\vec{q}|\vec{q}\,'^2(q_0-|\vec{q}|\cos\Theta)^2}B_{11}\right]\right. \\
& \qquad \left. +\,\lambda'\frac{q_0-|\vec{q}|\cos\Theta}{s\vec{q}^{\,2}|\vec{q}\,'|\sin^2\Theta}(B_5-B_7)\right\}\bar{u}(\vec{p}\,',\lambda'_N)\gamma_5 u(\vec{p},\lambda_N) \\
- & \quad \left\{\lambda\left[\frac{|\vec{q}|-q_0\cos\Theta}{s\vec{q}^{\,2}|\vec{q}\,'|\sin^2\Theta}(B_6+B_8)+\frac{2Q^2}{\sqrt{s}|\vec{q}|\vec{q}\,'^2(q_0-|\vec{q}|\cos\Theta)^2}B_{12}\right]\right. \\
& \qquad \left. +\,\lambda'\frac{q_0-|\vec{q}|\cos\Theta}{s\vec{q}^{\,2}|\vec{q}\,'|\sin^2\Theta}(B_6-B_8)\right\}\bar{u}(\vec{p}\,',\lambda'_N)\,i\not{N}u(\vec{p},\lambda_N)\,.
\end{aligned}
\qquad \text{(G.2)}
$$

The matrix elements of the operators in Eqs.(G.2 ,G.1) with the spinors defined in (A.2) are:

$$
\begin{aligned}
\bar{u}(\vec{p}\,',\lambda'_N)u(\vec{p},\lambda_N) &= \sqrt{(E+M)(E'+M)}\left[1-4\lambda_N\lambda'_N\frac{|\vec{q}|}{E+M}\frac{\sqrt{s}-M}{\sqrt{s}+M}\right] \\
& \cdot \quad \left(\sin\frac{\Theta}{2}(\lambda_N-\lambda'_N)-\cos\frac{\Theta}{2}\delta_{\lambda_N\lambda'_N}\right)
\end{aligned}
$$

$$
\begin{aligned}
\bar{u}(\vec{p}\,',\lambda'_N)\not{K}u(\vec{p},\lambda_N) &= \sqrt{(E+M)(E'+M)}\,(\sqrt{s}-M)\left[1+4\lambda_N\lambda'_N\frac{|\vec{q}|}{E+M}\right]\\
&\cdot\quad\left(\sin\frac{\Theta}{2}(\lambda_N-\lambda'_N)-\cos\frac{\Theta}{2}\delta_{\lambda_N\lambda'_N}\right)\\
\bar{u}(\vec{p}\,',\lambda'_N)\gamma_5\,u(\vec{p},\lambda_N) &= 2\sqrt{(E+M)(E'+M)}\left[\lambda_N\frac{|\vec{q}|}{E+M}-\lambda'_N\frac{\sqrt{s}-M}{\sqrt{s}+M}\right]\\
&\cdot\quad\left(\sin\frac{\Theta}{2}(\lambda_N-\lambda'_N)-\cos\frac{\Theta}{2}\delta_{\lambda_N\lambda'_N}\right)\\
\bar{u}(\vec{p}\,',\lambda'_N)\,i\not{N}u(\vec{p},\lambda_N) &= \sqrt{s}|\vec{q}||\vec{q}\,'|\sin\Theta\sqrt{(E+M)(E'+M)}\\
&\cdot\quad\left[\lambda_N\frac{q}{E+M}+\lambda'_N\frac{\sqrt{s}-M}{\sqrt{s}+M}\right]\\
&\cdot\quad\left(\cos\frac{\Theta}{2}(\lambda_N-\lambda'_N)+\sin\frac{\Theta}{2}\delta_{\lambda_N\lambda'_N}\right)
\end{aligned}
$$

By combining now helilcity amplitudes, one can easily invert these relations. With the following abbreviations for kinematical factors,

$$
\begin{aligned}
C_1 &= 1+\frac{|\vec{q}|}{E+M}\,, & C_2 &= 1-\frac{|\vec{q}|}{E+M}\,,\\
C_3 &= 1+\frac{\sqrt{s}-M}{\sqrt{s}+M}\frac{|\vec{q}|}{E+M}\,, & C_4 &= 1-\frac{\sqrt{s}-M}{\sqrt{s}+M}\frac{|\vec{q}|}{E+M}\,,\\
C_5 &= \frac{|\vec{q}|}{E+M}+\frac{|\vec{q}\,'|}{E'+M}\,, & C_6 &= \frac{|\vec{q}|}{E+M}-\frac{|\vec{q}\,'|}{E'+M}\,,
\end{aligned}
$$

we obtain the amplitudes B_i as functions of the reduced helicity amplitudes τ_i:

$$
\begin{aligned}
(-e^2)\,B_1 &= -\frac{\sqrt{(E+M)(E'+M)}}{4\sqrt{s}\,|\vec{q}|}\,(\sqrt{s}-M)\,\frac{|\vec{q}|-q_0\cos\theta}{t+Q^2}\\
&\left\{\;C_2\left[\tau_1+\cos^2\frac{\theta}{2}\tau_2-\sin^2\frac{\theta}{2}\Big(\tau_4+\tau_7\Big)\right.\right.\\
&\qquad\left.-\frac{2\sqrt{2}\,Q}{|\vec{q}|-q_0\cos\theta}\sin^2\frac{\theta}{2}\left(\tau_9-\cos^2\frac{\theta}{2}\tau_{11}\right)\right]\\
&+C_1\left[-\tau_5-\sin^2\frac{\theta}{2}\tau_6+\cos^2\frac{\theta}{2}\Big(\tau_3+\tau_8\Big)\right.\\
&\qquad\left.\left.+\frac{2\sqrt{2}\,Q}{|\vec{q}|-q_0\cos\theta}\cos^2\frac{\theta}{2}\left(\tau_{10}-\sin^2\frac{\theta}{2}\tau_{12}\right)\right]\right\},
\end{aligned}
$$

$$
\begin{aligned}
(-e^2)\,B_2 &= \frac{\sqrt{(E+M)(E'+M)}}{4\sqrt{s}\,|\vec{q}|}\,\frac{|\vec{q}|-q_0\cos\theta}{t+Q^2}\\
&\left\{\;C_3\left[\tau_1+\cos^2\frac{\theta}{2}\tau_2-\sin^2\frac{\theta}{2}\Big(\tau_4+\tau_7\Big)\right.\right.
\end{aligned}
$$

$$
\begin{aligned}
&\quad - \frac{2\sqrt{2}Q}{|\vec{q}\,| - q_0\cos\theta}\sin^2\frac{\theta}{2}\left(\tau_9 - \cos^2\frac{\theta}{2}\tau_{11}\right)\Bigg] \\
&+ C_4\Bigg[-\tau_5 - \sin^2\frac{\theta}{2}\tau_6 + \cos^2\frac{\theta}{2}\left(\tau_3+\tau_8\right) \\
&\quad + \frac{2\sqrt{2}Q}{|\vec{q}\,| - q_0\cos\theta}\cos^2\frac{\theta}{2}\left(\tau_{10} - \sin^2\frac{\theta}{2}\tau_{12}\right)\Bigg]\Bigg\},
\end{aligned}
$$

$$
\begin{aligned}
(-e^2)\,B_3 &= -\frac{\sqrt{(E+M)(E'+M)}}{8\sqrt{s}\,|\vec{q}\,||\vec{q}\,'|}\,(\sqrt{s}-M) \\
&\quad \Bigg\{ C_2\Bigg[\tau_1 + \cos^2\frac{\theta}{2}\tau_2 + \sin^2\frac{\theta}{2}\left(\tau_4+\tau_7\right)\Bigg] \\
&\quad + C_1\Bigg[\tau_5 + \sin^2\frac{\theta}{2}\tau_6 + \cos^2\frac{\theta}{2}\left(\tau_3+\tau_8\right)\Bigg]\Bigg\},
\end{aligned}
$$

$$
\begin{aligned}
(-e^2)\,B_4 &= \frac{\sqrt{(E+M)(E'+M)}}{8\sqrt{s}\,|\vec{q}\,||\vec{q}\,'|} \\
&\quad \Bigg\{ C_3\Bigg[\tau_1 + \cos^2\frac{\theta}{2}\tau_2 + \sin^2\frac{\theta}{2}\left(\tau_4+\tau_7\right)\Bigg] \\
&\quad + C_4\Bigg[\tau_5 + \sin^2\frac{\theta}{2}\tau_6 + \cos^2\frac{\theta}{2}\left(\tau_3+\tau_8\right)\Bigg]\Bigg\},
\end{aligned}
$$

$$
\begin{aligned}
(-e^2)\,B_5 &= -\frac{\sqrt{(E+M)(E'+M)}}{4t}\,\frac{s\,|\vec{q}\,|^2\,|\vec{q}\,'|^3\sin^4\theta}{(t+Q^2)^2} \\
&\quad \Bigg\{ C_5\Bigg[(|\vec{q}\,| - q_0)\left(\tau_5 - \sin^2\frac{\theta}{2}\tau_6\right) \\
&\qquad + (|\vec{q}\,| + q_0)\sin^2\frac{\theta}{2}\left(\tau_3 - \tau_8\right) \\
&\qquad - \sqrt{2}Q\left(\tau_{10} + \sin^2\frac{\theta}{2}\tau_{12}\right)\Bigg] \\
&\quad - C_6\Bigg[(|\vec{q}\,| + q_0)\left(\tau_1 - \cos^2\frac{\theta}{2}\tau_2\right) \\
&\qquad - (|\vec{q}\,| - q_0)\cos^2\frac{\theta}{2}\left(\tau_4 - \tau_7\right) \\
&\qquad - \sqrt{2}Q\left(\tau_9 + \cos^2\frac{\theta}{2}\tau_{11}\right)\Bigg]\Bigg\},
\end{aligned}
$$

$$
\begin{aligned}
(-e^2)\,B_6 \;=\;& \frac{\sqrt{(E+M)(E'+M)}}{t}\,\frac{\sqrt{s}\,|\vec{q}\,|\,|\vec{q}\,'|^2\sin^2\theta}{(t+Q^2)^2} \\
& \Bigg\{\; C_5\sin^2\frac{\theta}{2}\Bigg[(|\vec{q}\,|+q_0)\Big(\tau_1-\cos^2\frac{\theta}{2}\tau_2\Big) \\
& \qquad -(|\vec{q}\,|-q_0)\cos^2\frac{\theta}{2}\Big(\tau_4-\tau_7\Big) \\
& \qquad -\sqrt{2}\,Q\Big(\tau_9+\cos^2\frac{\theta}{2}\tau_{11}\Big)\Bigg] \\
& + C_6\cos^2\frac{\theta}{2}\Bigg[(|\vec{q}\,|-q_0)\Big(\tau_5-\sin^2\frac{\theta}{2}\tau_6\Big) \\
& \qquad +(|\vec{q}\,|+q_0)\sin^2\frac{\theta}{2}\Big(\tau_3-\tau_8\Big) \\
& \qquad -\sqrt{2}\,Q\Big(\tau_{10}+\sin^2\frac{\theta}{2}\tau_{12}\Big)\Bigg]\;\Bigg\},
\end{aligned}
$$

$$
\begin{aligned}
(-e^2)\,B_7 \;=\;& -\frac{\sqrt{(E+M)(E'+M)}}{t}\,\frac{s\,|\vec{q}\,|^2\,|\vec{q}\,'|^3\sin^2\theta}{(t+Q^2)^2} \\
& \Bigg\{\; C_5\sin^2\frac{\theta}{2}\Bigg[(|\vec{q}\,|+q_0)\sin^2\frac{\theta}{2}\Big(\tau_5-\sin^2\frac{\theta}{2}\tau_6\Big) \\
& \qquad +(|\vec{q}\,|-q_0)\cos^4\frac{\theta}{2}\Big(\tau_3-\tau_8\Big) \\
& \qquad -\sqrt{2}\,Q\cos^2\frac{\theta}{2}\Big(\tau_{10}+\sin^2\frac{\theta}{2}\tau_{12}\Big)\Bigg] \\
& - C_6\cos^2\frac{\theta}{2}\Bigg[(|\vec{q}\,|-q_0)\cos^2\frac{\theta}{2}\Big(\tau_1-\cos^2\frac{\theta}{2}\tau_2\Big) \\
& \qquad -(|\vec{q}\,|+q_0)\sin^4\frac{\theta}{2}\Big(\tau_4-\tau_7\Big) \\
& \qquad -\sqrt{2}\,Q\sin^2\frac{\theta}{2}\Big(\tau_9+\cos^2\frac{\theta}{2}\tau_{11}\Big)\Bigg]\;\Bigg\},
\end{aligned}
$$

$$
\begin{aligned}
(-e^2)\,B_8 \;=\;& \frac{\sqrt{(E+M)(E'+M)}}{t}\,\frac{\sqrt{s}\,|\vec{q}\,|\,|\vec{q}\,'|^2\sin^2\theta}{(t+Q^2)^2} \\
& \Bigg\{\; C_5\Bigg[(|\vec{q}\,|-q_0)\cos^2\frac{\theta}{2}\Big(\tau_1-\cos^2\frac{\theta}{2}\tau_2\Big) \\
& \qquad -(|\vec{q}\,|+q_0)\sin^4\frac{\theta}{2}\Big(\tau_4-\tau_7\Big)
\end{aligned}
$$

$$
\begin{aligned}
& -\sqrt{2}\,Q\sin^2\frac{\theta}{2}\left(\tau_9+\cos^2\frac{\theta}{2}\tau_{11}\right)\Bigg] \\
& + C_6\Bigg[\,(|\vec{q}\,|+q_0)\sin^2\frac{\theta}{2}\left(\tau_5-\sin^2\frac{\theta}{2}\tau_6\right) \\
& \quad +(|\vec{q}\,|-q_0)\cos^4\frac{\theta}{2}\left(\tau_3-\tau_8\right) \\
& \quad -\sqrt{2}\,Q\cos^2\frac{\theta}{2}\left(\tau_{10}+\sin^2\frac{\theta}{2}\tau_{12}\right)\Bigg]\Bigg\},
\end{aligned}
$$

$$
\begin{aligned}
(-e^2)\,B_9 \;=\; & -\frac{\sqrt{(E+M)(E'+M)}}{8\,(t+Q^2)}\,(\sqrt{s}-M)\,|\vec{q}\,'|\sin^2\theta \\
& \Bigg\{\;C_2\Bigg[\tau_1+\cos^2\frac{\theta}{2}\tau_2-\sin^2\frac{\theta}{2}\left(\tau_4+\tau_7\right) \\
& \qquad -\frac{|\vec{q}\,|-q_0\cos\theta}{\sqrt{2}\,Q\cos^2\frac{\theta}{2}}\left(\tau_9-\cos^2\frac{\theta}{2}\tau_{11}\right)\Bigg] \\
& + C_1\Bigg[-\tau_5-\sin^2\frac{\theta}{2}\tau_6+\cos^2\frac{\theta}{2}\left(\tau_3+\tau_8\right) \\
& \qquad +\frac{|\vec{q}\,|-q_0\cos\theta}{\sqrt{2}\,Q\sin^2\frac{\theta}{2}}\left(\tau_{10}-\sin^2\frac{\theta}{2}\tau_{12}\right)\Bigg]\Bigg\},
\end{aligned}
$$

$$
\begin{aligned}
(-e^2)\,B_{10} \;=\; & \frac{\sqrt{(E+M)(E'+M)}}{8\,(t+Q^2)}\,|\vec{q}\,'|\sin^2\theta \\
& \Bigg\{\;C_3\Bigg[\tau_1+\cos^2\frac{\theta}{2}\tau_2-\sin^2\frac{\theta}{2}\left(\tau_4+\tau_7\right) \\
& \qquad -\frac{|\vec{q}\,|-q_0\cos\theta}{\sqrt{2}\,Q\cos^2\frac{\theta}{2}}\left(\tau_9-\cos^2\frac{\theta}{2}\tau_{11}\right)\Bigg] \\
& + C_4\Bigg[-\tau_5-\sin^2\frac{\theta}{2}\tau_6+\cos^2\frac{\theta}{2}\left(\tau_3+\tau_8\right) \\
& \qquad +\frac{|\vec{q}\,|-q_0\cos\theta}{\sqrt{2}\,Q\sin^2\frac{\theta}{2}}\left(\tau_{10}-\sin^2\frac{\theta}{2}\tau_{12}\right)\Bigg]\Bigg\},
\end{aligned}
$$

$$
\begin{aligned}
(-e^2)\,B_{11} \;=\; & \frac{\sqrt{(E+M)(E'+M)}}{8t}\,\sqrt{s}\,|\vec{q}\,|\,|\vec{q}\,'|^2\sin^2\theta \\
& \Bigg\{\;C_5\sin^2\frac{\theta}{2}\Bigg[\tau_5-\sin^2\frac{\theta}{2}\tau_6+\cos^2\frac{\theta}{2}\left(\tau_3-\tau_8\right)
\end{aligned}
$$

$$
\left. - \frac{|\vec{q}| - q_0 \cos\theta}{\sqrt{2}\, Q \sin^2\frac{\theta}{2}} \left(\tau_{10} + \sin^2\frac{\theta}{2}\tau_{12} \right) \right]
$$

$$
- C_6 \cos^2\frac{\theta}{2} \left[\tau_1 - \cos^2\frac{\theta}{2}\tau_2 - \sin^2\frac{\theta}{2}\Big(\tau_4 - \tau_7\Big) \right.
$$

$$
\left. \left. - \frac{|\vec{q}| - q_0 \cos\theta}{\sqrt{2}\, Q \cos^2\frac{\theta}{2}} \left(\tau_9 + \cos^2\frac{\theta}{2}\tau_{11} \right) \right] \right\},
$$

$$
\begin{aligned}
(-e^2)\, B_{12} \quad &= - \frac{\sqrt{(E+M)(E'+M)}}{8t} |\vec{q}\,'| \sin^2\theta \\
&\left\{ C_5 \left[\tau_1 - \cos^2\frac{\theta}{2}\tau_2 - \sin^2\frac{\theta}{2}\Big(\tau_4 - \tau_7\Big) \right. \right. \\
&\qquad \left. - \frac{|\vec{q}| - q_0 \cos\theta}{\sqrt{2}\, Q \cos^2\frac{\theta}{2}} \left(\tau_9 + \cos^2\frac{\theta}{2}\tau_{11} \right) \right] \\
&+ C_6 \left[\tau_5 - \sin^2\frac{\theta}{2}\tau_6 + \cos^2\frac{\theta}{2}\Big(\tau_3 - \tau_8\Big) \right. \\
&\qquad \left. \left. - \frac{|\vec{q}| - q_0 \cos\theta}{\sqrt{2}\, Q \sin^2\frac{\theta}{2}} \left(\tau_{10} + \sin^2\frac{\theta}{2}\tau_{12} \right) \right] \right\}.
\end{aligned}
\tag{G.3}
$$

As a cross check for these expressions, the numerical test with the Born amplitude was performed. The Born helicity amplitudes were calculated numerically, combined together into the amplitudes B_i, and compared with the analytic formulas evaluated at the same kinematical points.

G.1.2 Relations $F_i \leftrightarrow \tau_i$

By substituting now the expressions of Eq.(G.3) into the relations between the F_i and B_i of Appendix D.1, we obtain the desired formulae, which do not contain any kinematical singularities:

$$
\begin{aligned}
(-e^2) F_1(Q^2,\nu,t) \quad = \quad & - \frac{\sqrt{(E+M)(E'+M)}}{8\sqrt{s}|\vec{q}\,||\vec{q}\,'|(\sqrt{s}+M)} \\
& \left\{ \left[\frac{\nu}{2\sqrt{s}} \frac{|\vec{q}| + q_0}{|\vec{q}|} C_1 - C_2 \right] \tau_1 + \left[\frac{\nu}{2\sqrt{s}} \frac{|\vec{q}| - q_0}{|\vec{q}|} C_2 - C_1 \right] \tau_5 \right. \\
& + \left[\nu \frac{|\vec{q}| + q_0}{2|\vec{q}|} \left[\frac{|\vec{q}| + q_0}{2\sqrt{s}|\vec{q}|} C_1 + \frac{2M}{s - M^2} \left(1 + \frac{t + Q^2}{4\sqrt{s}|\vec{q}|} \right) C_2 \right] \right. \\
& \qquad \left. \left. - \frac{\sqrt{s} + M}{4M|\vec{q}|} \left[|\vec{q}| + q_0 + 2|\vec{q}| \cos^2\frac{\Theta}{2} \right] C_3 \right] \tau_2 \right. \\
& + \left[\nu \frac{|\vec{q}| + q_0}{2|\vec{q}|} \left[- \frac{|\vec{q}| - q_0}{2\sqrt{s}|\vec{q}|} C_2 + \frac{2M}{s - M^2} \left(1 + \frac{t + Q^2}{4\sqrt{s}|\vec{q}|} \right) C_1 \right] \right.
\end{aligned}
$$

$$
\begin{aligned}
&\qquad\qquad - \frac{s-M^2}{2M|\vec{q}|}\left(C_2 + \frac{t+Q^2}{4|\vec{q}\,'|(\sqrt{s}-M)}C_4\right)\Big]\,\tau_3 \\
&+ \left[\frac{\sqrt{s}}{M}\cos^2\frac{\Theta}{2} + \frac{|\vec{q}|-q_0\cos\Theta}{2M} - \nu\frac{|\vec{q}|-q_0}{2\sqrt{s}|\vec{q}|}\cos^2\frac{\Theta}{2}\right] C_1\,\tau_4 \\
&+ \left[\nu\frac{|\vec{q}|-q_0}{2|\vec{q}|}\left[\frac{|\vec{q}|-q_0}{2\sqrt{s}|\vec{q}|}C_2 + \frac{2M}{s-M^2}\left(1-\frac{t+Q^2}{4\sqrt{s}|\vec{q}|}\right)C_1\right]\right. \\
&\qquad\qquad \left. - \frac{\sqrt{s}+M}{4M|\vec{q}|}\left[|\vec{q}|-q_0+2|\vec{q}|\sin^2\frac{\Theta}{2}\right]C_4\right]\,\tau_6 \\
&+ \left[\nu\frac{|\vec{q}|-q_0}{2|\vec{q}|}\left[-\frac{|\vec{q}|+q_0}{2\sqrt{s}|\vec{q}|}C_1 + \frac{2M}{s-M^2}\left(1-\frac{t+Q^2}{4\sqrt{s}|\vec{q}|}\right)C_2\right]\right. \\
&\qquad\qquad \left. + \frac{s-M^2}{2M|\vec{q}|}\left(C_1 + \frac{t+Q^2}{4|\vec{q}\,'|(\sqrt{s}-M)}C_3\right)\right]\,\tau_7 \\
&+ \left[\frac{\sqrt{s}}{M}\sin^2\frac{\Theta}{2} - \frac{|\vec{q}|-q_0\cos\Theta}{2M} - \nu\frac{|\vec{q}|+q_0}{2\sqrt{s}|\vec{q}|}\sin^2\frac{\Theta}{2}\right] C_2\,\tau_8 \\
&- \frac{\sqrt{2}Q\nu}{2\sqrt{s}|\vec{q}|}\left[C_1\,\tau_9 + C_2\,\tau_{10}\right] \\
&+ \frac{\sqrt{2}Q\nu}{4\sqrt{s}|\vec{q}|^2}\left[(\sqrt{s}+M)C_5 + M\frac{t+Q^2}{s-M^2}C_2\right]\,\tau_{11} \\
&+ \frac{\sqrt{2}Q\nu}{4\sqrt{s}|\vec{q}|^2}\left[(\sqrt{s}+M)C_6 - M\frac{t+Q^2}{s-M^2}C_1\right]\,\tau_{12}\Bigg\}
\end{aligned}
$$

$$
\begin{aligned}
(-e^2)F_2(Q^2,\nu,t) \;=\; & -\frac{\sqrt{(E+M)(E'+M)}}{64Ms\sqrt{s}|\vec{q}|^3|\vec{q}\,'|^2}(\sqrt{s}-M) \\
& \Big\{|\vec{q}|C_1\left[(|\vec{q}|+q_0)\tau_1 - (|\vec{q}|-q_0)\cos^2\frac{\Theta}{2}\tau_4 - \sqrt{2}Q\tau_9\right] \\
& + \left[\frac{\sqrt{s}+M}{2}C_5 + \frac{M}{2}\frac{t+Q^2}{s-M^2}C_2\right] \\
& \cdot\left[(|\vec{q}|+q_0)\tau_2 - (|\vec{q}|-q_0)\tau_7 + \sqrt{2}Q\tau_{11}\right] \\
& + |\vec{q}|C_2\left[(|\vec{q}|-q_0)\tau_5 - (|\vec{q}|+q_0)\sin^2\frac{\Theta}{2}\tau_8 - \sqrt{2}Q\tau_{10}\right] \\
& + \left[-\frac{\sqrt{s}+M}{2}C_6 + \frac{M}{2}\frac{t+Q^2}{s-M^2}C_1\right] \\
& \cdot\left[(|\vec{q}|+q_0)\tau_3 - (|\vec{q}|-q_0)\tau_6 - \sqrt{2}Q\tau_{12}\right]\Big\}
\end{aligned}
$$

$$
\begin{aligned}
(-e^2)F_3(Q^2,\nu,t) \;=\; & -\frac{\sqrt{(E+M)(E'+M)}}{32M\nu s\sqrt{s}|\vec{q}|^3|\vec{q}\,'|^2}(\sqrt{s}-M) \\
& \Big\{|\vec{q}|C_1\left[(\sqrt{s}-\frac{|\vec{q}|+q_0}{2})\tau_1 + (\sqrt{s}+\frac{|\vec{q}|-q_0}{2})\cos^2\frac{\Theta}{2}\tau_4 + \frac{s-M^2}{\sqrt{2}Q}\tau_9\right] \\
& + \frac{1}{2}\left[(\sqrt{s}+M)C_5 + M\frac{t+Q^2}{s-M^2}C_2\right]
\end{aligned}
$$

$$
\begin{aligned}
&\cdot\left[(\sqrt{s}-\frac{|\vec{q}|+q_0}{2})\tau_2+(\sqrt{s}+\frac{|\vec{q}|-q_0}{2})\tau_7-\frac{s-M^2}{\sqrt{2}Q}\tau_{11}\right]\\
&-|\vec{q}|C_2\left[(\sqrt{s}+\frac{|\vec{q}|-q_0}{2})\tau_5+(\sqrt{s}-\frac{|\vec{q}|+q_0}{2})\sin^2\frac{\Theta}{2}\tau_8-\frac{s-M^2}{\sqrt{2}Q}\tau_{10}\right]\\
&+\frac{1}{2}\left[-(\sqrt{s}+M)C_6+M\frac{t+Q^2}{s-M^2}C_1\right]\\
&\cdot\left[(\sqrt{s}-\frac{|\vec{q}|+q_0}{2})\tau_3+(\sqrt{s}+\frac{|\vec{q}|-q_0}{2})\tau_6+\frac{s-M^2}{\sqrt{2}Q}\tau_{12}\right]\Bigg\}
\end{aligned}
$$

$$
\begin{aligned}
(-e^2)F_4(Q^2,\nu,t) &= -\frac{\sqrt{(E+M)(E'+M)}}{32s|\vec{q}|^3|\vec{q}'|\nu(\sqrt{s}+M)}\\
&\Bigg\{|\vec{q}|C_1\left[(|\vec{q}|+q_0)\tau_1-(|\vec{q}|-q_0)\cos^2\frac{\Theta}{2}\tau_4-\sqrt{2}Q\tau_9\right]\\
&-\left[\frac{\sqrt{s}+M}{2}C_3-\frac{2M^2\nu}{s-M^2}C_2\right]\left[(|\vec{q}|+q_0)\tau_2-(|\vec{q}|-q_0)\tau_7+\sqrt{2}Q\tau_{11}\right]\\
&+|\vec{q}|C_2\left[(|\vec{q}|-q_0)\tau_5-(|\vec{q}|+q_0)\sin^2\frac{\Theta}{2}\tau_8-\sqrt{2}Q\tau_{10}\right]\\
&-\left[\frac{\sqrt{s}+M}{2}C_4-\frac{2M^2\nu}{s-M^2}C_1\right]\left[(|\vec{q}|+q_0)\tau_3-(|\vec{q}|-q_0)\tau_6-\sqrt{2}Q\tau_{12}\right]\Bigg\}
\end{aligned}
$$

$$
\begin{aligned}
(-e^2)\tilde{F}_6(Q^2,\nu,t) &= \frac{\sqrt{(E+M)(E'+M)}}{32Ms|\vec{q}|^3|\vec{q}'|(\sqrt{s}+M)}\\
&\Bigg\{|\vec{q}|C_1\left[(|\vec{q}|+q_0)\tau_1-(|\vec{q}|-q_0)\cos^2\frac{\Theta}{2}\tau_4-\sqrt{2}Q\tau_9\right]\\
&+\left[\frac{\sqrt{s}+M}{2}C_3+\frac{2M^2\nu}{s-M^2}C_2\right]\left[(|\vec{q}|+q_0)\tau_2-(|\vec{q}|-q_0)\tau_7+\sqrt{2}Q\tau_{11}\right]\\
&+|\vec{q}|C_2\left[(|\vec{q}|-q_0)\tau_5-(|\vec{q}|+q_0)\sin^2\frac{\Theta}{2}\tau_8-\sqrt{2}Q\tau_{10}\right]\\
&+\left[\frac{\sqrt{s}+M}{2}C_4+\frac{2M^2\nu}{s-M^2}C_1\right]\left[(|\vec{q}|+q_0)\tau_3-(|\vec{q}|-q_0)\tau_6-\sqrt{2}Q\tau_{12}\right]\Bigg\}
\end{aligned}
$$

$$
\begin{aligned}
(-e^2)F_7 &= \frac{\sqrt{(E+M)(E'+M)}}{16s|\vec{q}|^2|\vec{q}'|}\Bigg\{\frac{2\sqrt{s}}{\sqrt{s}+M}\left[C_1\left(\frac{|\vec{q}|}{|\vec{q}'|}\tau_4-\frac{|\vec{q}'|}{|\vec{q}|}\tau_7\right)+C_2\left(\frac{|\vec{q}|}{|\vec{q}'|}\tau_8-\frac{|\vec{q}'|}{|\vec{q}|}\tau_3\right)\right]\\
&+\frac{Q^2}{|\vec{q}||\vec{q}'|}\left[\left(1-\frac{|\vec{q}|+q_0}{2\sqrt{s}}\right)C_3\tau_2+\left(1+\frac{|\vec{q}|-q_0}{2\sqrt{s}}\right)C_4\tau_6\right]\\
&-\frac{\sqrt{2}Q}{|\vec{q}|}\left[C_3\tau_{11}-C_4\tau_{12}\right]\Bigg\}
\end{aligned}
$$

$$
(-e^2)F_8 = -\frac{\sqrt{(E+M)(E'+M)}}{8Mvs|\vec{q}'||\vec{q}|^3(\sqrt{s}+M)}
$$

$$
\begin{aligned}
&\left\{ |\vec{q}|C_1 \left[\left(\sqrt{s} - \frac{|\vec{q}|+q_0}{2} \right) \tau_1 + \left(\sqrt{s} + \frac{|\vec{q}|-q_0}{2} \right) \cos^2\frac{\Theta}{2} \tau_4 + \frac{s-M^2}{\sqrt{2}Q} \tau_9 \right] \right. \\
&+ \left[\frac{\sqrt{s}+M}{2} C_3 + \frac{2M^2\nu}{s-M^2} C_2 \right] \\
&\cdot \left[\left(\sqrt{s} - \frac{|\vec{q}|+q_0}{2} \right) \tau_2 + \left(\sqrt{s} + \frac{|\vec{q}|-q_0}{2} \right) \tau_7 - \frac{s-M^2}{\sqrt{2}Q} \tau_{11} \right] \\
&- |\vec{q}|C_2 \left[\left(\sqrt{s} + \frac{|\vec{q}|-q_0}{2} \right) \tau_5 + \left(\sqrt{s} - \frac{|\vec{q}|+q_0}{2} \right) \sin^2\frac{\Theta}{2} \tau_8 - \frac{s-M^2}{\sqrt{2}Q} \tau_{10} \right] \\
&+ \left[\frac{\sqrt{s}+M}{2} C_4 + \frac{2M^2\nu}{s-M^2} C_1 \right] \\
&\left. \cdot \left[\left(\sqrt{s} - \frac{|\vec{q}|+q_0}{2} \right) \tau_3 + \left(\sqrt{s} + \frac{|\vec{q}|-q_0}{2} \right) \tau_6 + \frac{s-M^2}{\sqrt{2}Q} \tau_{12} \right] \right\}
\end{aligned}
$$

$$
\begin{aligned}
(-e^2)F_9 \;=\; & \frac{\sqrt{(E+M)(E'+M)}}{128M^2\nu s|\vec{q}\,'||\vec{q}|^2} Q^2 \\
& \left\{ C_3 \left[\tau_1 + \left(\frac{2\sqrt{s}|\vec{q}|}{|\vec{q}\,'|(|\vec{q}|+q_0)} - \frac{|\vec{q}|-q_0}{|\vec{q}|+q_0} \cos^2\frac{\Theta}{2} \right) \tau_4 - \frac{\sqrt{2}Q}{|\vec{q}|+q_0} \tau_9 \right] \right. \\
& - C_4 \left[\tau_5 + \left(\frac{2\sqrt{s}|\vec{q}|}{|\vec{q}\,'|(|\vec{q}|-q_0)} - \frac{|\vec{q}|+q_0}{|\vec{q}|-q_0} \sin^2\frac{\Theta}{2} \right) \tau_8 - \frac{\sqrt{2}Q}{|\vec{q}|-q_0} \tau_{10} \right] \\
& + \frac{2\sqrt{s}-|\vec{q}|-q_0}{|\vec{q}|(\sqrt{s}+M)} \left[\left(1 - \frac{2|\vec{q}|}{|\vec{q}\,'|} \right) \frac{\sqrt{s}+M}{2} C_3 - \frac{2M^2\nu}{s-M^2} C_2 \right] \tau_2 \\
& + \frac{2\sqrt{s}+|\vec{q}|-q_0}{|\vec{q}|(\sqrt{s}+M)} \left[\left(1 + \frac{2|\vec{q}|}{|\vec{q}\,'|} \right) \frac{\sqrt{s}+M}{2} C_4 - \frac{2M^2\nu}{s-M^2} C_1 \right] \tau_6 \\
& + \frac{2\sqrt{s}-|\vec{q}|-q_0}{|\vec{q}\,'|(\sqrt{s}+M)} \left[\left(\sqrt{s} - |\vec{q}\,'| \frac{|\vec{q}|-q_0}{2|\vec{q}|} \right) C_1 - M \left(1 - \frac{t+Q^2}{4\sqrt{s}|\vec{q}|} \right) \frac{|\vec{q}|-q_0}{|\vec{q}|+q_0} C_2 \right] \tau_7 \\
& + \frac{2\sqrt{s}+|\vec{q}|-q_0}{|\vec{q}\,'|(\sqrt{s}+M)} \left[- \left(\sqrt{s} - |\vec{q}\,'| \frac{|\vec{q}|+q_0}{2|\vec{q}|} \right) C_2 + M \left(1 + \frac{t+Q^2}{4\sqrt{s}|\vec{q}|} \right) \frac{|\vec{q}|+q_0}{|\vec{q}|-q_0} C_1 \right] \tau_3 \\
& + \frac{2\sqrt{2}}{|\vec{q}|Q} \sqrt{s} \frac{|\vec{q}|-|\vec{q}\,'|}{\sqrt{s}+M} \left[\frac{\sqrt{s}+M}{2} C_3 - \frac{2M^2\nu}{s-M^2} C_2 \right] \tau_{11} \\
& \left. + \frac{2\sqrt{2}}{|\vec{q}|Q} \sqrt{s} \frac{|\vec{q}|+|\vec{q}\,'|}{\sqrt{s}+M} \left[\frac{\sqrt{s}+M}{2} C_4 - \frac{2M^2\nu}{s-M^2} C_1 \right] \tau_{12} \right\}
\end{aligned}
$$

$$
\begin{aligned}
(-e^2)F_{10} \;=\; & \frac{\sqrt{(E+M)(E'+M)}}{32M\sqrt{s}|\vec{q}\,'||\vec{q}|\nu} \qquad \left\{ C_3 \left[\tau_1 + \cos^2\frac{\Theta}{2} \tau_2 + \sin^2\frac{\Theta}{2} (\tau_4 + \tau_7) \right] \right. \\
& \left. + \; C_4 \left[\tau_5 + \sin^2\frac{\Theta}{2} \tau_6 + \cos^2\frac{\Theta}{2} (\tau_3 + \tau_8) \right] \right\},
\end{aligned}
$$

$$
(-e^2)\left(\tilde{F}_{11} + 8M\tilde{F}_6\right) \;=\; \frac{\sqrt{(E+M)(E'+M)}}{4\sqrt{s}|\vec{q}\,'||\vec{q}|^2(\sqrt{s}+M)}
$$

$$
\begin{aligned}
&\left\{ C_1 \left[\tau_1 + \cos^2\frac{\Theta}{2}\left(\tau_4 + \frac{M}{\sqrt{s}}\tau_3\right) - \tau_7 - \frac{M}{\sqrt{s}}\sin^2\frac{\Theta}{2}\tau_6 + \frac{\sqrt{2}q_0}{Q}\tau_9 \right] \right. \\
&- C_2 \left[\tau_5 + \sin^2\frac{\Theta}{2}\left(\tau_8 + \frac{M}{\sqrt{s}}\tau_7\right) - \tau_3 - \frac{M}{\sqrt{s}}\cos^2\frac{\Theta}{2}\tau_2 - \frac{\sqrt{2}q_0}{Q}\tau_{10} \right] \\
&+ \frac{1}{\sqrt{2}Q}\left[(\sqrt{s}+M)C_5 + \frac{M}{\sqrt{s}}(|\vec{q}\,| - q_0\cos\Theta)C_2 \right]\tau_{11} \\
&\left. - \frac{1}{\sqrt{2}Q}\left[(\sqrt{s}+M)C_6 + \frac{M}{\sqrt{s}}(|\vec{q}\,| - q_0\cos\Theta)C_1 \right]\tau_{12} \right\}
\end{aligned}
$$

$$
\begin{aligned}
Q^2F_5 - 8M\nu^2F_9 - (t+Q^2)F_7 \;=\; & -\frac{\sqrt{(E+M)(E'+M)}}{4M\sqrt{s}|\vec{q}\,||\vec{q}\,'|(\sqrt{s}+M)} \\
& \left\{ C_1 \left\{ \frac{Q^2}{\sqrt{s}|\vec{q}\,|}(M^2 - t/8)\left[\tau_5 - \sin^2\frac{\Theta}{2}\tau_6\right] \right.\right. \\
& \left.\left. + \left[(s-M^2)\cos^2\frac{\Theta}{2} + \frac{(|\vec{q}\,|+q_0)^2}{\sqrt{s}|\vec{q}\,|}(M^2 - t/8)\sin^2\frac{\Theta}{2}\right][\tau_3 - \tau_8] \right\} \right. \\
& - C_2 \left\{ \frac{Q^2}{\sqrt{s}|\vec{q}\,|}(M^2 - t/8)\left[\tau_1 - \cos^2\frac{\Theta}{2}\tau_2\right] \right. \\
& \left.\left. - \left[(s-M^2)\sin^2\frac{\Theta}{2} - \frac{(|\vec{q}\,|-q_0)^2}{\sqrt{s}|\vec{q}\,|}(M^2 - t/8)\cos^2\frac{\Theta}{2}\right][\tau_7 - \tau_4] \right\} \right. \\
& + Q\frac{\sqrt{s}+M}{\sqrt{2}}\left[C_3 - \frac{2M^2 - t/4}{\sqrt{s}|\vec{q}\,|}C_5 \right]\left[\tau_{10} + \sin^2\frac{\Theta}{2}\tau_{12}\right] \\
& \left. - Q\frac{\sqrt{s}+M}{\sqrt{2}}\left[C_4 - \frac{2M^2 - t/4}{\sqrt{s}|\vec{q}\,|}C_6 \right]\left[\tau_9 + \cos^2\frac{\Theta}{2}\tau_{11}\right] \right\}
\end{aligned}
$$

$$
\begin{aligned}
(-e^2)F_{12} \;=\; & \frac{t+Q^2}{Q^2}F_9 \;+\; \frac{\sqrt{(E+M)(E'+M)}}{16s|\vec{q}\,|^2|\vec{q}\,'|(\sqrt{s}+M)} \\
& \cdot \left\{ C_1 \left[\tau_5 - \sin^2\frac{\Theta}{2}\tau_6 + \frac{|\vec{q}\,|+q_0}{|\vec{q}\,|-q_0}\sin^2\frac{\Theta}{2}[\tau_3 - \tau_8] \right.\right. \\
& \qquad \left.\left. - \frac{\sqrt{2}Q}{|\vec{q}\,|-q_0}[\tau_{10} + \sin^2\frac{\Theta}{2}\tau_{12}] \right] \right. \\
& - C_2 \left[\tau_1 - \cos^2\frac{\Theta}{2}\tau_2 + \frac{|\vec{q}\,|-q_0}{|\vec{q}\,|+q_0}\cos^2\frac{\Theta}{2}[\tau_7 - \tau_4] \right. \\
& \qquad \left.\left. - \frac{\sqrt{2}Q}{|\vec{q}\,|+q_0}[\tau_9 + \cos^2\frac{\Theta}{2}\tau_{11}] \right] \right\}
\end{aligned}
$$

For compactness, the expressions for the amplitudes F_5, F_{11} and F_{12} are only given as combinations with other, already known amplitudes.

These formulas can now be used for dispersion calculations. The imaginary parts of the reduced helicity amplitudes, given by unitarity in terms of the pion photo- and electroproduction multipoles (see Appendix H.1), define the imaginary parts of the amplitudes F_i. Furthermore, these equations will be used to investigate the high energy

behaviour of the amplitudes F_i and, correspondingly, the convergence of the unsubtracted dispersion integrals.

Appendix H

H.1 VCS reduced helicity amplitudes via pion photo- and electroproduction multipoles

If we write down the unitarity equations for the VCS helicity amplitudes and consider only πN itermediate states, then the imaginary parts of the VCS amplitudes can be expressed in terms of the $\gamma^* N \to \pi N$ times $\gamma N \to \pi N$ multipoles :

$$
\begin{aligned}
\mathrm{Im}\tau_1 &= -8\pi q_\pi \sqrt{s} \sum_l (2l+2) \left[A_{l+}(Q^2) A^*_{l+}(0) + A_{(l+1)-}(Q^2) A^*_{(l+1)-}(0) \right] \\
&\quad \times F(-l; l+2; 1; \sin^2 \frac{\theta}{2}), \\
\mathrm{Im}\tau_2 &= -8\pi q_\pi \sqrt{s} \sum_l \frac{l(l+1)(l+2)}{2} \left[B_{l+}(Q^2) B^*_{l+}(0) + B_{(l+1)-}(Q^2) B^*_{(l+1)-}(0) \right] \\
&\quad \times F(-l+1; l+3; 1; \sin^2 \frac{\theta}{2}), \\
\mathrm{Im}\tau_3 &= -8\pi q_\pi \sqrt{s} \sum_l l(l+1)(l+2) \left[A_{l+}(Q^2) B^*_{l+}(0) + A_{(l+1)-}(Q^2) B^*_{(l+1)-}(0) \right] \\
&\quad \times F(-l+1; l+3; 2; \sin^2 \frac{\theta}{2}), \\
\mathrm{Im}\tau_4 &= -8\pi q_\pi \sqrt{s} \sum_l \frac{l(l+1)^2(l+2)}{2} \left[B_{l+}(Q^2) A^*_{l+}(0) - B_{(l+1)-}(Q^2) A^*_{(l+1)-}(0) \right] \\
&\quad \times F(-l+1; l+3; 3; \sin^2 \frac{\theta}{2}), \\
\mathrm{Im}\tau_5 &= 8\pi q_\pi \sqrt{s} \sum_l 2(l+1)^2 \left[A_{l+}(Q^2) A^*_{l+}(0) - A_{(l+1)-}(Q^2) A^*_{(l+1)-}(0) \right] \\
&\quad \times F(-l; l+2; 2; \sin^2 \frac{\theta}{2}), \\
\mathrm{Im}\tau_6 &= -8\pi q_\pi \sqrt{s} \sum_l \frac{l^2(l+1)^2(l+2)^2}{12} \left[B_{l+}(Q^2) B^*_{l+}(0) - B_{(l+1)-}(Q^2) B^*_{(l+1)-}(0) \right] \\
&\quad \times F(-l+1; l+3; 4; \sin^2 \frac{\theta}{2}), \\
\mathrm{Im}\tau_7 &= -8\pi q_\pi \sqrt{s} \sum_l \frac{l(l+1)^2(l+2)}{2} \left[A_{l+}(Q^2) B^*_{l+}(0) - A_{(l+1)-}(Q^2) B^*_{(l+1)-}(0) \right]
\end{aligned}
$$

$$
\begin{aligned}
& \times F(-l+1;l+3;3;\sin^2\frac{\theta}{2}),\\
\mathrm{Im}\tau_8 &= -8\pi q_\pi\sqrt{s}\sum_l l(l+1)(l+2)\left[B_{l+}(Q^2)A^*_{l+}(0)+B_{(l+1)-}(Q^2)A^*_{(l+1)-}(0)\right]\\
& \times F(-l+1;l+3;2;\sin^2\frac{\theta}{2}),\\
\mathrm{Im}\tau_9 &= 8\pi q_\pi\sqrt{s}\frac{\sqrt{2Q^2}}{q_0}\sum_l (l+1)^3\left[L_{l+}(Q^2)A^*_{l+}(0)+L_{(l+1)-}(Q^2)A^*_{(l+1)-}(0)\right]\\
& \times F(-l;l+2;2;\sin^2\frac{\theta}{2}),\\
\mathrm{Im}\tau_{10} &= 8\pi q_\pi\sqrt{s}\frac{\sqrt{2Q^2}}{q_0}\sum_l (l+1)^2\left[L_{l+}(Q^2)A^*_{l+}(0)-L_{(l+1)-}(Q^2)A^*_{(l+1)-}(0)\right]\\
& \times F(-l;l+2;1;\sin^2\frac{\theta}{2}),\\
\mathrm{Im}\tau_{11} &= -8\pi q_\pi\sqrt{s}\frac{\sqrt{2Q^2}}{q_0}\sum_l \frac{l(l+1)^2(l+2)}{2}\left[L_{l+}(Q^2)B^*_{l+}(0)-L_{(l+1)-}(Q^2)B^*_{(l+1)-}(0)\right]\\
& \times F(-l+1;l+3;2;\sin^2\frac{\theta}{2}),\\
\mathrm{Im}\tau_{12} &= 8\pi q_\pi\sqrt{s}\frac{\sqrt{2Q^2}}{q_0}\sum_l \frac{l(l+1)^3(l+2)}{4}\left[L_{l+}(Q^2)B^*_{l+}(0)+L_{(l+1)-}(Q^2)B^*_{(l+1)-}(0)\right]\\
& \times F(-l+1;l+3;3;\sin^2\frac{\theta}{2}),
\end{aligned}
\tag{H.1}
$$

where τ_i are the reduced helicity amplitudes defined in Eq. (A.10). In Eqs. (H.1), q_π is the pion momentum in the intermediate state and F is a hypergeometric polynomial defined as :

$$F(a;b;c;x) = 1+\frac{ab}{c}\frac{x}{1!}+\frac{a(a+1)b(b+1)}{c(c+1)}\frac{x^2}{2!}+... \tag{H.2}$$

$A_{l\pm}$, $B_{l\pm}$, $L_{l\pm}$ are defined as in Ref.[Wal 69].

Appendix I

I.1 t-channel helicity amplitudes for VCS

In order to calculate the subtraction functions $F_1(Q^2,\nu=0,t)$ and $F_5(Q^2,\nu=0,t)$, one has to relate them to the helicity amplitudes in the t-channel, that is to those for the process $\gamma^\star\gamma\to N\bar{N}$. For this reaction, we choose the kinematics in the c.m. system as follows:

$$\begin{aligned}
q'^{\mu} &= (|\vec{q}'|,0,0,|\vec{q}'|)\\
q^{\mu} &= (q_0,0,0,-|\vec{q}'|)\\
p'^{\mu} &= (E_N,p_N\sin\Theta_t,0,p_N\cos\Theta_t)\\
p^{\mu} &= (E'_N,-p_N\sin\Theta_t,0,-p_N\cos\Theta_t) \qquad \text{(I.1)}\\
&\text{with}\\
|\vec{q}'| &= \frac{t+Q^2}{2\sqrt{t}}\\
q_0 &= \frac{t-Q^2}{2\sqrt{t}}\\
E_N &= E'_N=\frac{\sqrt{t}}{2}\\
p_N &= \sqrt{\frac{t}{4}-M^2}
\end{aligned}$$

With these vectors, we again start by constructing the invariant tensor of Berg and Lindner Eq.(4.72). The definition of the basis vectors in this basis in the t-channel is different from that in the s-channel by the corresponding crossing, $q'\to -q'$, $p'\to -p'$, so that now

$$\begin{aligned}
K_t^{\mu} &= \frac{1}{2}(q-q')^{\mu}=-\frac{1}{2\sqrt{t}}(Q^2,0,0,t+Q^2),\\
L_t^{\mu} &= \frac{1}{2}(-q'-q)^{\mu}=(-\frac{\sqrt{t}}{2},\vec{0})\\
L'^{\mu}_t &= L_t^{\mu}-\frac{L_t\cdot K_t}{K_t^2}K_t^{\mu}=-\frac{t+Q^2}{2\sqrt{t}(t+2Q^2)}(t+Q^2,0,0,Q^2),\\
P_t^{\mu} &= \frac{1}{2}(p-p')^{\mu}
\end{aligned}$$

$$
\begin{aligned}
P'^{\mu}_t &= P^{\mu}_t - \frac{P_t\cdot K_t}{K_t^2}K^{\mu}_t - \frac{P_t\cdot L'_t}{L'^2_t}L'^{\mu}_t = (0,-p_N\sin\Theta_t,0,0)\\
N^{\mu}_t &= \varepsilon^{\mu\nu\alpha\beta}P'_{t\nu}L'_{t\alpha}K_{t\beta} = (0,0,-\frac{t+Q^2}{4}p_N\sin\Theta_t,0)\,,
\end{aligned}
\tag{I.2}
$$

where we fix the phase of the vector N, choosing $\varepsilon_{0123}=+1$. For the polarization vectors we use the Lorentz gauge,

$$
\begin{aligned}
\varepsilon'^{\nu}(\vec{q}',\lambda') &= (0,\frac{\lambda'}{\sqrt{2}},-\frac{i}{\sqrt{2}},0)\\
\varepsilon^{\mu}(-\vec{q}',\lambda=\pm1) &= (0,-\frac{\lambda}{\sqrt{2}},-\frac{i}{\sqrt{2}},0)\\
\varepsilon^{\mu}(-\vec{q}',\lambda=0) &= \frac{1}{2\sqrt{t}Q}(t+Q^2,0,0,t-Q^2)\,.
\end{aligned}
\tag{I.3}
$$

Using these conventions, we can now write down the t-channel helicity amplitudes in the basis of Berg and Lindner (Eq.(4.72)),

$$
\begin{aligned}
T^t_{\lambda'_N\lambda_{\bar N},\lambda'\lambda^{trans}_\gamma} &= \bar u(\lambda'_N)v(\lambda_N)\cdot M_{\mu\nu}\cdot\varepsilon'^{\nu}(\lambda')\varepsilon^{\mu}(\lambda)\\
&= \frac{1}{2}(\lambda'\lambda B_1+B_3)\bar u(\lambda'_N)v(\lambda_N)\\
&+ \frac{1}{2}(\lambda'\lambda B_2+B_4)\bar u(\lambda'_N)\not{K}v(\lambda_N)\\
&- \frac{4}{(t+Q^2)P'^2}\left[\frac{\lambda-\lambda'}{2}B_5+\frac{\lambda+\lambda'}{2}B_7\right]\bar u(\lambda'_N)\gamma_5 v(\lambda_N)\\
&+ \frac{4}{(t+Q^2)P'^2}\left[\frac{\lambda-\lambda'}{2}B_6+\frac{\lambda+\lambda'}{2}B_8\right]\bar u(\lambda'_N)i\not{N}v(\lambda_N)
\end{aligned}
\tag{I.4}
$$

for the transversal polarization of both real and virtual photons and

$$
\begin{aligned}
T^t_{\lambda'_N\lambda_{\bar N},\lambda'\lambda=0} &= -\frac{4Q}{(t+Q^2)p_N\sin\Theta_t}\left\{\frac{\lambda'}{\sqrt{2}}B_9\bar u(\lambda'_N)v(\lambda_N)+\frac{\lambda'}{\sqrt{2}}B_{10}\bar u(\lambda'_N)\not{K}v(\lambda_N)\right.\\
&- \left.\frac{2\sqrt{2}}{t+Q^2}B_{11}\bar u(\lambda'_N)\gamma_5 v(\lambda_N)+\frac{2\sqrt{2}}{t+Q^2}B_{12}\bar u(\lambda'_N)i\not{N}v(\lambda_N)\right\}
\end{aligned}
\tag{I.5}
$$

for the longitudinal polarization of the virtual photon.

The spinors for the outgoing nucleon ($u(\vec{p}',\lambda'_N)$) and antinucleon ($v(-\vec{p}',\lambda_{\bar N})$) are

$$
\begin{aligned}
u(\lambda'_N=+\frac{1}{2}) &= \sqrt{E_N+M}\begin{bmatrix}\chi_{\Uparrow}\\ \frac{p_N}{E_N+M}\chi_{\Uparrow}\end{bmatrix}\\
u(\lambda'_N=-\frac{1}{2}) &= \sqrt{E_N+M}\begin{bmatrix}\chi_{\Downarrow}\\ -\frac{p_N}{E_N+M}\chi_{\Downarrow}\end{bmatrix}
\end{aligned}
$$

$$
\begin{aligned}
v(\lambda_N = +\frac{1}{2}) &= \sqrt{E_N + M} \begin{bmatrix} -\frac{p_N}{E_N+M}\chi_{\Uparrow} \\ \\ \chi_{\Uparrow} \end{bmatrix} \\
v(\lambda_N = -\frac{1}{2}) &= \sqrt{E_N + M} \begin{bmatrix} \frac{p_N}{E_N+M}\chi_{\Downarrow} \\ \\ \chi_{\Downarrow} \end{bmatrix}
\end{aligned}
$$

where

$$
\chi_{\Uparrow} = \begin{bmatrix} \cos\frac{\Theta_t}{2} \\ \\ \sin\frac{\Theta_t}{2} \end{bmatrix} \qquad \chi_{\Downarrow} = \begin{bmatrix} -\sin\frac{\Theta_t}{2} \\ \\ \cos\frac{\Theta_t}{2} \end{bmatrix}, \tag{I.6}
$$

thus giving for the matrix elements

$$
\begin{aligned}
\bar{u}(\lambda'_N)v(\lambda_N) &= -2p_N(-1)^{\frac{1}{2}-\lambda_{\bar{N}}}\delta_{\lambda'_N\lambda_{\bar{N}}} \\
\bar{u}(\lambda'_N)\not{K}v(\lambda_N) &= \frac{t+Q^2}{2\sqrt{t}}\left[2M\cos\Theta_t(-1)^{\frac{1}{2}-\lambda_{\bar{N}}}\delta_{\lambda'_N\lambda_{\bar{N}}} - \sqrt{t}\sin\Theta_t\delta_{\lambda'_N,-\lambda_{\bar{N}}}\right] \\
\bar{u}(\lambda'_N)\gamma_5 v(\lambda_N) &= \sqrt{t}\delta_{\lambda'_N\lambda_{\bar{N}}} \\
\bar{u}(\lambda'_N)i\not{N}v(\lambda_N) &= -\frac{t+Q^2}{4}\sqrt{t}p_N\sin\Theta_t(-1)^{\frac{1}{2}-\lambda_{\bar{N}}}\delta_{\lambda'_N,-\lambda_{\bar{N}}}
\end{aligned}
$$

Finally, substituting these results into the T-matrix elements above, we come to the following expressions for the amplitudes B_i in terms of the t-channel helicity amplitudes:

$$
\begin{aligned}
B_1 + B_3 &= -\frac{1}{2p_N}\left[T^t_{\frac{1}{2}\frac{1}{2},11} + T^t_{\frac{1}{2}\frac{1}{2},-1-1}\right] - \frac{M\cos\Theta_t}{p_N\sqrt{t}\sin\Theta_t}\left[T^t_{-\frac{1}{2}\frac{1}{2},11} + T^t_{-\frac{1}{2}\frac{1}{2},-1-1}\right] \\
B_1 - B_3 &= \frac{1}{2p_N}\left[T^t_{\frac{1}{2}\frac{1}{2},1-1} + T^t_{\frac{1}{2}\frac{1}{2},-11}\right] + \frac{M\cos\Theta_t}{p_N\sqrt{t}\sin\Theta_t}\left[T^t_{-\frac{1}{2}\frac{1}{2},1-1} + T^t_{-\frac{1}{2}\frac{1}{2},-11}\right] \\
B_2 + B_4 &= -\frac{2}{t+Q^2}\frac{1}{\sin\Theta_t}\left[T^t_{-\frac{1}{2}\frac{1}{2},11} + T^t_{-\frac{1}{2}\frac{1}{2},-1-1}\right] \\
B_2 - B_4 &= \frac{2}{t+Q^2}\frac{1}{\sin\Theta_t}\left[T^t_{-\frac{1}{2}\frac{1}{2},1-1} + T^t_{-\frac{1}{2}\frac{1}{2},-11}\right] \\
B_5 &= \frac{(t+Q^2)P'^2}{8\sqrt{t}}\left[T^t_{\frac{1}{2}\frac{1}{2},1-1} - T^t_{\frac{1}{2}\frac{1}{2},-11}\right] \\
B_6 &= \frac{2\sqrt{t}}{p_N\sin\Theta_t}\left[T^t_{-\frac{1}{2}\frac{1}{2},1-1} - T^t_{-\frac{1}{2}\frac{1}{2},-11}\right] \\
B_7 &= -\frac{(t+Q^2)P'^2}{8\sqrt{t}}\left[T^t_{\frac{1}{2}\frac{1}{2},11} - T^t_{\frac{1}{2}\frac{1}{2},-1-1}\right] \\
B_8 &= -\frac{2\sqrt{t}}{p_N\sin\Theta_t}\left[T^t_{-\frac{1}{2}\frac{1}{2},11} - T^t_{-\frac{1}{2}\frac{1}{2},-1-1}\right] \\
B_9 &= \frac{(t+Q^2)\sin\Theta_t}{8\sqrt{2}Q}\left[T^t_{\frac{1}{2}\frac{1}{2},10} - T^t_{\frac{1}{2}\frac{1}{2},-10}\right] \\
&+ \frac{(t+Q^2)M\cos\Theta_t}{8\sqrt{2}Q\sqrt{t}}\left[T^t_{-\frac{1}{2}\frac{1}{2},10} - T^t_{-\frac{1}{2}\frac{1}{2},-10}\right]
\end{aligned}
$$

$$
\begin{aligned}
B_{10} &= \frac{p_N}{2\sqrt{2}Q}\left[T^t_{-\frac{1}{2}\frac{1}{2},10} - T^t_{-\frac{1}{2}\frac{1}{2},-10}\right] \\
B_{11} &= \frac{(t+Q^2)^2 P'^2}{16\sqrt{2}Q\sqrt{t}}\left[T^t_{\frac{1}{2}\frac{1}{2},10} + T^t_{\frac{1}{2}\frac{1}{2},-10}\right] \\
B_{12} &= \frac{(t+Q^2)}{4\sqrt{2}Q\sqrt{t}}\left[T^t_{-\frac{1}{2}\frac{1}{2},10} + T^t_{-\frac{1}{2}\frac{1}{2},-10}\right]
\end{aligned} \tag{I.7}
$$

In the real photon limit, at $Q^2 = 0$, the six non-vanishing amplitudes $B_{1,2,3,4,6,7}$ are related to the invariant amplitudes of Prange $T_{1,2,3,4,5,6}$, as a cross check with the formulas given in Appendix B.1. Note that the longitudinal amplitudes $B_{9,10,11,12}$ are finite but do not contribute to the observables.

Recalling now the relation between the F_1 and B_i amplitudes we obtain at the point $\nu = 0$

$$
\begin{aligned}
F_1(Q^2,\nu=0,t) &= \frac{2}{t+Q^2}B_3 \\
&= -\frac{1}{2(t+Q^2)p_N}\left\{T^t_{\frac{1}{2}\frac{1}{2},11} + T^t_{\frac{1}{2}\frac{1}{2},-1-1} + T^t_{\frac{1}{2}\frac{1}{2},1-1} + T^t_{\frac{1}{2}\frac{1}{2},-11}\right\} .
\end{aligned} \tag{I.8}
$$

To calculate the asymptotic contribution to the amplitude F_1 which is due to intermediate states in the t-channel ($\pi\pi$ and so on), we next generalize the Born amplitude for the process $\gamma\gamma \to \pi\pi$, calculated in Appendix B.1, to the case of the virtual initial photon. With the c.m. kinematics of Eq.(I.2), the Born contribution of the contact, direct and cross diagrams of Fig. 3.10 can be cast into form

$$
\begin{aligned}
\mathcal{M}^{Born} &= 2e^2 F_\pi(Q^2)\,\varepsilon_\mu(\lambda)\varepsilon'_\nu(\lambda') \\
&\quad \left\{ g^{\mu\nu} + \frac{2q^\mu}{t+Q^2}\left[\frac{p^\nu_{\pi^-}}{1-\beta_\pi\cos\Theta_{\pi\pi}} + \frac{p^\nu_{\pi^+}}{1+\beta_\pi\cos\Theta_{\pi\pi}}\right]\right. \\
&\quad \left. - \frac{4}{t+Q^2}\left[\frac{p^\nu_{\pi^-}p^\mu_{\pi^+}}{1-\beta_\pi\cos\Theta_{\pi\pi}} + \frac{p^\nu_{p^\mu_{\pi^-}\pi^+}}{1+\beta_\pi\cos\Theta_{\pi\pi}}\right]\right\} ,
\end{aligned} \tag{I.9}
$$

where $F_\pi(Q^2)$ is the pion form factor taken in the monopole form

$$
F_\pi(Q^2) = \left(1 + \frac{Q^2}{m_\rho^2}\right)^{-1} , \tag{I.10}
$$

with m_ρ the mass of the ρ-meson (vector meson dominance). In the case of the transversely polarized virtual photon, we obtain for the Born helicity amplitudes:

$$
\mathcal{M}^{Born}_{\lambda',\lambda^T} = 2e^2 F_\pi(Q^2)\left\{\delta_{\lambda'\lambda} - \lambda'\lambda\frac{t}{t+Q^2}\frac{\beta^2\sin^2\theta_{\pi\pi}}{1-\beta^2\cos^2\theta_{\pi\pi}}\right\} , \tag{I.11}
$$

whereas the longitudinal polarization results in

$$
\mathcal{M}^{Born}_{\lambda',0} = -2e^2 F_\pi(Q^2)\sqrt{2}\lambda'\frac{Q\sqrt{t}}{t+Q^2}\frac{\beta^2\sin\theta_{\pi\pi}\cos\theta_{\pi\pi}}{1-\beta^2\cos^2\theta_{\pi\pi}} . \tag{I.12}
$$

Expanding now these amplitudes into a partial wave series, as specified in Appendix B.1, we obtain:

$$\begin{aligned}
B_{J=0,\Lambda=0}(t,Q^2) &= 2e^2F_\pi(Q^2)\left\{\frac{Q^2}{t+Q^2}+\frac{t}{t+Q^2}\frac{1-\beta^2}{2\beta}\ln\left(\frac{1+\beta}{1-\beta}\right)\right\}, \\
B_{20}(t,Q^2) &= 2e^2F_\pi(Q^2)\frac{t}{t+Q^2}\frac{\sqrt{5}}{4}\frac{1-\beta^2}{\beta^2} \\
&\quad\cdot\left\{\frac{3-\beta^2}{\beta}\ln\left(\frac{1+\beta}{1-\beta}\right)-6\right\}, \\
B_{21}(t,Q^2) &= 2e^2F_\pi(Q^2)\lambda'\frac{Q\sqrt{t}}{t+Q^2}\frac{\sqrt{15}}{2\beta^2} \\
&\quad\cdot\left\{\frac{1-\beta^2}{\beta}\ln\left(\frac{1+\beta}{1-\beta}\right)-2+\frac{4}{3}\beta^2\right\}, \\
B_{22}(t,Q^2) &= 2e^2F_\pi(Q^2)\frac{t}{t+Q^2}\frac{\sqrt{15}}{4\sqrt{2}} \\
&\quad\cdot\left\{\frac{(1-\beta^2)^2}{\beta^3}\ln\left(\frac{1+\beta}{1-\beta}\right)+\frac{10}{3}-\frac{2}{\beta^2}\right\}. \qquad \text{(I.13)}
\end{aligned}$$

These results can now be used for the unitarization procedure as described in Section 3.4.

Bibliography

[Ahr 93] J. Ahrens et al., MAMI proposal 12/2-93 (1993); H.J. Arends, Proceedings of the 8th International Conference on the Structure of Baryons (Baryons 98), Bonn, Germany, 22-26 Sep. 1998; Eds. D.W. Menze and B. Metsch, World Scientific, Singapore (1999).

[Ahr 02] J. Ahrens, privat communications.

[Akh 81] D. M. Akhmedov and L. V. Fil'kov, Sov. J. Nucl. Phys. **33**, 573 (1981).

[Arn 90] R.A. Arndt, R.L. Workman, Z. Li and L.D. Roper, Phys. Rev. C **42**, 1853 (1990); Phys. Rev. C **42**, 1864 (1990).

[Arn 98] R.A. Arndt, R.L. Workman, I.I. Strakovsky, M.M. Pavan, nucl-th/9807087.

[Arn 01] R.A. Arndt *et al.*, nucl-th/0106059.

[Azn 99] I. G. Aznauryan, S. G. Stepanyan,
Phys. Rev. D **59**, 1(54009) (1999).

[Bab 98] D. Babusci, G. Giordano and G. Matone, Phys. Rev. C **57**, 291 (1998).

[Bab 98b] D. Babusci, G. Giordano, A.I. L'vov, G. Matone and A.M. Nathan, Phys. Rev. C **58**, 1013 (1998).

[Bal 60] A. M. Baldin, Polarizability of the Nucleon,
Nucl. Phys. **18** (1960) 310; L.I. Lapidus, Sov. Phys. JETP **16**, 964 (1963).

[Bar 68] W. A. Bardeen and W. K. Tung, Phys. Rev. **173**, 1423 (1968).

[Ben 92] M. Benmerrouche and N.C. Mukhopadhyay, Phys. Rev. D **46**, 101 (1992).

[Ber 61] R.A. Berg and C.N. Lindner, Nucl. Phys. **26**, 259 (1961).

[Ber 91] V. Bernard, N. Kaiser and U.-G. Meissner, Phys. Rev. Lett. **67**, 1515 (1991).

[Ber 92] V. Bernard, N. Kaiser, J. Kambor and U.-G. Meissner, Nucl. Phys. **B 388**, 315 (1992); Int. J. Mod. Phys. E **4**, 193 (1995).

[Ber 93] V. Bernard, N. Kaiser, A. Schmidt, U.-G. Meissner, Phys. Lett. B **319**, 269 (1993); Z. Phys. A **348**, 317 (1994).

[Ber 93a] P.Y. Bertin, P.A.M. Guichon, C. Hyde-Wright, spokespersons JLab experiment, E-93-050.

[Bjo 64] J.D. Bjorken and S.D. Drell, *Relativistic quantum mechanics*, McGraw-Hill, New York (1964).

[Bjo 65] J.D. Bjorken and S.D. Drell, *Relativistic quantum fields*, McGraw-Hill, New York (1965).

[Bla 97] G. Blanpied et al., Phys. Rev. Lett. **79**, 4337 (1997); Phys. Rev. Lett. **76**, 1023 (1996).

[Bog 56] N.N. Bogoliubov, *report at the International Congress on Theoretical Physics* (Seattle, September 1956);
N.N. Bogoliubov, B.V. Medevedev and M.K. Polivanov, *Problems in the Theory of Dispersion Relations*, Fizmatgiz, Moscow, 1958;
N.N. Bogoliubov, D.V. Shirkov, *Introduction to the Theory of Quantized Fields*, Interscience Publishers, Inc., New York 1959.

[Bos 95] P.E. Bosted, Phys. Rev. C **51**, 409 (1995).

[Bro 81] S.J. Brodsky and G.P. Lepage, Phys. Rev. D **24**, 1808 (1981).

[Cap 56] R. H. Capps, Gyo Takeda, Phys. Pev. **103** N6, 1877 (1956).

[Chew 62] G. Chew, S-matrix theory of strong interaction, W. A. Benjamin, inc., New York 1962

[Caus 73] Causality and Physical Theories, AIP Conference Proceedings N16, Wayne State University, 1973

[Cut 60] R. E. Cutkosky, Journal of Math. Phys. **1** N5, 429 (1960).

[Dam 70] M. Damashek and F.J. Gilman, Phys. Rev. D **1**, 1319 (1970).

[Dav 91] R. M. Davidson, N. C. Mukhopadhyay and R. S. Wittman, Phys. Rev. D **43**, 71 (1991).

[Deg 01] N. Degrande, Ph.D. thesis, University Gent, (2001); Luc Van Hoorebeke, privat communication.

[d'Ho 01] N. d'Hose, H. Merkel, spokespersons MAMI experiment, A1/01-00.

[Dre 97] D. Drechsel, G. Kn¨ochlein, A. Metz and S. Scherer, Phys. Rev. C **55**, 424 (1997).

[Dre 98] D. Drechsel, G. Kn¨ochlein, A.Yu. Korchin, A. Metz and S. Scherer, Phys. Rev. C **57**, 941 (1998).

[Dre 98b] D. Drechsel, G. Kn¨ochlein, A.Yu. Korchin, A. Metz and S. Scherer, Phys. Rev. C **58**, 1751 (1998).

[Dre 98c] D. Drechsel, G. Krein, Phys. Rev. D **58**, 11609 (1998).

[Dre 98d] D. Drechsel, G. Krein and O. Hanstein, Phys. Lett. B **420**, 248 (1998).

[Dre 99] D. Drechsel, M. Gorchtein, B. Pasquini and M. Vanderhaeghen, Phys. Rev. C **61**, 015204 (2000).

[Dre 99b] D. Drechsel, S.S. Kamalov, G. Krein, L. Tiator, Phys. Rev. D **59**, 094021 (1999).

[Dys 58] F. Dyson, Phys. Rev. **110**, 1460 (1958).

[Edm 57] A. Edmonds, Angular momentum in Quantum Mechanics, Princeton University Press, Princeton N.J. (1957).

[Fed 91] F.J. Federspiel, R.A. Eisenstein, M.A. Lucas, B.E. MacGibbon, K. Mellendorf, A.M. Nathan, A. O'Neill, and D.P. Wells, Phys. Rev. Lett. **67**, 1511 (1991).

[Fra 60] W.R. Frazer and J.R. Fulco, Phys. Rev. **117**, 1603 (1960).

[Fro 77] C.D. Froggatt and J.L. Petersen, Nucl. Phys. B **129**, 89 (1977).

[Gal 01] G. Galler et al., Phys. Lett. B **503**, 245-255 (2001).

[Gel 54] M. Gell-Mann, M. L. Goldberger, W. E. Thirring, Use of Causality Conditions in Quantum Theory,
Phys. Rev. **95** (6), 1612 (1954).

[Ger 65] S. Gerasimov, Yad. Fiz. **2**, 598 (1965) [Sov. J. Nucl. Phys. **2**, 430 (1966); S. D. Drell and A. C. Hearn, Phys. Rev. Lett **16**, 908 (1966).

[Gold 55] M. L. Goldberger, Use of Causality Conditions in Quantum Theory,
Phys. Rev. **97** (2), 508 (1955).

[Gold 55a] M. L. Goldberger, Causality Conditions and Dispersion Relations. I. Boson Fields,
Phys. Rev. **99** (3), 979 (1955).

[Gold 55b] M. L. Goldberger, H. Miyazawa and R. Oehme, *ibid.*, p. 986.

[Gui 95] P.A.M. Guichon, G.Q. Liu and A.W. Thomas, Nucl. Phys. **A591**, 606 (1995).

[Gui 98] P.A.M. Guichon and M. Vanderhaeghen, Prog. Part. Nucl. Phys. **41**, 125 (1998).

[Hag 63] R. Hagedorn, Introduction to field theory and dispersion relations, Fortschritte der Physik, Akademie Verlag Berlin, 1963

[Hag 64] R. Hagedorn, Relativistic kinematics, W. A. Benjamin, inc., New York 1964

[Hal 93] E.L. Hallin et al., Phys. Rev. C **48**, 1497 (1993).

[Han 98] O. Hanstein, D. Drechsel, L. Tiator, Nucl. Phys. A **632**, 561 (1998).

[Hei 43] W. Heisenberg, Z. Physik, **120**, 513, 673 (1943)

[Hem 97] T.R. Hemmert, B.R. Holstein and J. Kambor, Phys. Rev. D **55**, 5598 (1997).

[Hem 98] T.R. Hemmert, B.R. Holstein, J. Kambor and G. Kn¨ochlein, Phys. Rev. D **57**, 5746 (1998).

[H¨oh 76] G. H¨ohler et al., Nucl. Phys. B **114**, 505 (1976)

[H¨oh 83] G. H¨ohler, *Pion-Nucleon Scattering*, Landolt-B¨ornstein, Vol.I/9b2, ed. H. Schopper, Springer (1983).

[Hol 94] B.R. Holstein and A. Nathan, Phys. Rev. D **49**, 6101 (1994).

[Hol 97] T.R. Hemmert, B.R. Holstein and J. Kambor, Phys. Lett. B **395**, 89 (1997).

[Jac 83] J. D. Jackson, Klassische Elektrodynamik, 2.verb.Aufl. Berlin; New York: de Gruyter, 1983

[Jaf 92] R. L. Jaffe, P. F. Mende, Nucl. Phys. B **369**, 189 (1992)

[Jam 00] S. Jaminion, Ph.D. thesis, Université Blaise Pascal, Clermont Ferrand, (2000); H. Fonvieille, privat communication.

[Jam 01] S. Jaminion et al., in Proceedings of the Workshop on The Physics of Excited Nucleons (Nstar 2001), Mainz, Germany, (2001), edited by D. Drechsel and L. Tiator (World Scientific, Singapore, 2001)

[Jon 00] M.K. Jones et al., Phys. Rev. Lett. **84**, 1398 (2000).

[Jos 57] R. Jost, H. Lehmann, Nuovo Cimento **5** (1957)

[Kam 99] S. Kamalov and S. N. Yang, Phys. Rev. Lett. **83**, 4494 (1999)

[Kar 55] R. Karplus, M. A. Ruderman, Application of Causality to Scattering, Phys. Rev. **98** (3), 771 (1955).

[Kle 29] O. Klein, Y. Nishina, Zeitschrift f¨ur Physik **52**, 853 (1929).

[Kra 27] H. A. Kramers, Atti. congr. intern. fis. Como **2**, 545 (1927)

[Kro 26] R. Kronig, J. Opt. Soc. Am. **12**, 547 (1926)

[Lan 59] L. D. Landau, Nucl. Phys. **13**, 181 (1959).

[Lav 01] G. Laveissiere et al., in Proceedings of the Workshop on The Physics of Excited Nucleons (Nstar 2001), Mainz, Germany, (2001), edited by D. Drechsel and L. Tiator (World Scientific, Singapore, 2001)

[Low 54] F. E. Low, Scattering of Light of Very Low Frequency by Systems of Spin 1/2, Phys. Rev. **96** number 5, 1428 (1954).

[L'vo 81] A. L'vov, Sov. J. Nucl. Phys. **34**, 597 (1981).

[L'vo 97] A. L'vov, V. A. Petrun'kin and M. Schumacher, Phys. Rev. C **55** 1, 359 (1997).

[L'vo 99] A.I. L'vov and A.M. Nathan, Phys. Rev. C **59**, 1064 (1999).

[L'vo 01] A. L'vov, S. Scherer, B. Pasquini, C. Unkmeir and D. Drechsel Phys. Rev. C **64**, 015203 (2001).

[MAID] D. Drechsel, O. Hanstein, S. Kamalov, L. Tiator, Nucl. Phys. A **645** (1999)

[Man 58] S. Mandelstam, Phys. Rev. **112** N4, 1344 (1958).

[Man 59] S. Mandelstam, Phys. Rev. **115** N6, 1741 (1959).

[McG 95] B.E. MacGibbon, G. Garino, M.A. Lucas, A.M. Nathan, G. Feldman and B. Dolbilkin, Phys. Rev. C **52**, 2097 (1995).

[Met 96] A. Metz, D. Drechsel, Z. Phys. A **356**, 351 (1996), Z. Phys. A **359**, 165 (1997).

[Mol 96] C. Molinari et al., Phys. Lett. B **371**, 181 (1996).

[Mor 88] D. Morgan and M.R. Pennington, Z. Phys. C **37**, 431 (1988).

[Oeh 55] R. Oehme, Phys. Rev. **100**, 1503 (1955), *ibid.*, **102**, 1174 (1956).

[Oeh 95] R. Oehme, Int. J. Phys. A **10**, 1995 (1995).

[Olm 01] V. Olmos de Leon et al., Eur. Phys. J. A **10**, 207-215 (2001).

[Ome 83] A. S. Omelaenko and P. V. Sorokin, Sov. J. Nucl. Phys. **38**, 398 (1983).

[Pas 00] B. Pasquini, D. Drechsel, M. Gorchtein, A. Metz, M. Vanderhaeghen, Phys. Rev. C **62**, 052201 (2000).

[Pas 01a] B. Pasquini, M. Gorchtein, D. Drechsel, A. Metz, M. Vanderhaeghen, Eur. Phys.J. A**11**, 185 (2001).

[Pas 01] B. Pasquini, S. Scherer, D. Drechsel, Phys. Rev. C **63**, 025205 (2001).

[Pav 99] M.M. Pavan, R.A. Arndt, I.I. Strakovsky, R.L. Workman, PiN Newslett. **15**, 171 (1999).

[PDG 98] Particle Data Group, C. Caso et al., Eur. Phys. J. C **3**, 1 (1998).

[PDG 01] Particle Data Group, Eur. Phys. J. **C** (2001)

[Pei 96] J. Peise et al., Phys. Lett. B **384**, 37 (1996).

[Pen 95] M.R. Pennington, in *The Second DaΦne Physics Handbook*, Eds. L. Maiani, G. Pancheri, N. Paver (INFN, Frascati, 1995).

[Pet 61] V. A. Petrun'kin, Sov. Phys. JETP **13**, 808 (1961).

[Pet 81] V. A. Petrun'kin, Sov. J. Part. Nucl. **12**, 278 (1981).

[Pil 79] H. Pilkuhn, *Relativistic Particle Physics* (Springer Verlag, Heidelberg, 1979).

[Pow 49] J. L. Powell, Phys. Rev. **75**, 32 (1949).

[Pra 58] R. E. Prange, Phys. Rev. **110**, 240 (1958).

[Rag 93] S. Ragusa, Phys. Rev. D **47**, 3757 (1993), **49**, 3157 (1994).

[Roc 00] J. Roche et al., Phys. Rev. Lett. **85, 4**, 708-711 (2000).

[SAID] R.A. Arndt, I.I. Strakovsky and R.L. Workman, Phys. Rev. C **53**, 430 (1996).

[Sal 56] A. Salam, Nuovo Cimento **3**, 424 (1956)

[Sal 56a] A. Salam and W. Gilbert, *ibid.*, p. 607.

[San 94] A.M. Sandorfi, C.S. Whisnant and M. Khandaker, Phys. Rev. D **50**, R6681 (1994).

[Sha 97] J. Shaw, R. Miskimen, spokespersons MIT-Bates experiment, 97-03.

[Sie 37] A. J. F. Siegert, Phys. Rev. **52**, 787 (1937).

[Spe 91] D. Spehler and S.F. Novaes, Phys. Rev. D **44**, 3990 (1991).

[Ste 21] O. Stern and W. Gerlach, Z. Physik **7**, 249 (1921), *ibid.* **8**, 110 (1921), *ibid.* **8**, 349 and 353 (1922); R. Frisch and O. Stern, Z. Physik **85**, 4 (1933), I. Estermann and O. Stern, *ibid.* p. 17.

[Tar 75] R. Tarrach, Nuovo Cimento A **28**, 409 (1975).

[Ton 98] J. Tonnison, A.M. Sandorfi, S. Hoblit and A.M. Nathan, Phys. Rev. Lett. **80**, 4382 (1998).

[Vdh 97] Marc Vanderhaeghen, Phys. Lett. B **402**, 243 (1997).

[Wal 69] R. L. Walker, Phys. Rev. **182**, 1729 (1969).

[Zie 92] A. Zieger, R. Van de Vyver, D. Christmann, A. De Graeve, C. Van den Abeele and B. Ziegler, Phys. Lett. B **278**, 34 (1992).

List of Figures

List of Tables